University of Southampton

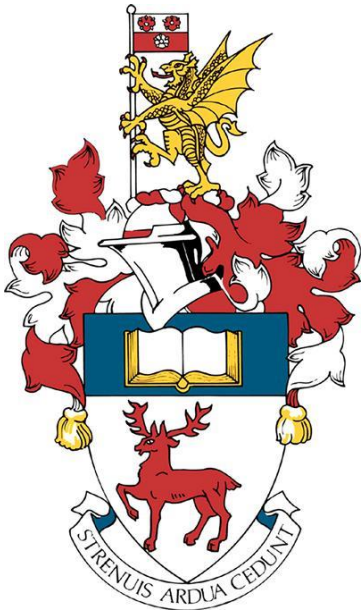

Faculty of Environmental and Life Sciences

School of Biological Sciences

High-Mannose N-Glycans in Breast Cancer: Implications for Targeted Therapies

by

Lydia Kristen Doherty BSc

ORCID ID: 0009-0006-1418-3372

Thesis for the degree of Doctor of Philosophy

February 2024

University of Southampton

Abstract

Faculty of Environmental and Life Sciences

School of Biological Sciences

Doctor of Philosophy

High-Mannose N-Glycans in Breast Cancer: Implications for Targeted Therapies

by

Lydia Kristen Doherty

Breast cancer (BC) is the leading cause of cancer-related deaths in women, responsible for ~685,000 global deaths in 2020. The global incidence of BC continues to rise annually, despite advancements in targeted therapies. These treatments are not universally effective, can be accompanied by drug toxicity, and nearly all patients eventually develop therapeutic resistance. Additionally, therapeutic options for patients with the most aggressive forms of BC, namely triple-negative breast cancer (TNBC) and metastatic disease, are limited with the fewest number and most toxic targeted therapies available. Thus, there is a clear unmet clinical need for new treatment options.

Aberrant glycosylation is considered one of the established hallmarks of cancer. Cancer-associated glycans are recognised for their involvement in various aspects of oncogenesis, including epithelial-mesenchymal transition, invasion, metastasis, and immunosuppression. This research has assisted in identifying glycan serum cancer biomarkers and novel molecular targets which have led to the approval of glycan based-therapeutics in the clinic.

While high-mannose glycans have been associated with many cancers, including BC, previous studies have yielded conflicting results, highlighting the heterogeneity of BC glycosylation. The aim of this thesis was to investigate the potential significance of high-mannose glycans in BC progression and determine whether therapeutically targeting high-mannose antigens could enhance current BC therapeutics.

High-mannose glycans were identified on the cell surface of BC cell lines and within clinical tissues. Cell surface levels of mannose on BC cells were variable, however, levels of high-mannose glycans were higher in non-metastatic BC cell lines compared to metastatic ones. Moreover, we observed that mannose processing enzymes were aberrantly regulated in BC clinical datasets, emphasising the high heterogeneity of expression across samples.

Despite being prevalent in BC, we demonstrated that the induction of high-mannose reduced BC cell migration and invasion *in vitro* and impacted tumour growth *in vivo*. High-mannose glycans were induced by methods of mannosidase inhibition using the inhibitor, Kifunensine, and CRISPR-cas9 targeting of MGAT1. These findings suggest that high-mannose glycans may be critical in modulating cellular behaviours linked to BC progression possibly through complex interactions between high-mannose and highly branched glycoforms. This suggests a potential mechanism for the transition from non-metastatic to metastatic phenotypes.

We also developed three novel bi-specific antibody constructs targeting both HER2 and high-mannose glycans and demonstrated their therapeutic potential. One of these antibodies, 2G12-Hn 2, provided advantages over the standard anti-HER2 therapy, Trastuzumab. To address difficulties in production and increased aggregation faced with larger multitargeting antibodies, such as 2G12-Hn 2, we investigated a novel alternative delivery strategy utilising Replicon RNA. For this, we used Trastuzumab as it is a well-characterised BC mAb of standard format. We established that replicon-produced Trastuzumab retained similar target binding to HER2 and mediated comparable effector functions as traditional recombinant-made Trastuzumab. This paves the way for future experiments to determine the potential of utilising Replicons for the delivery of larger multi-targeting antibodies such as 2G12-Hn 2.

Table of Contents

Table of Tables

Table of Figures

Table of Figures

List of Accompanying Materials

1. Covid-19 Supporting Statement.

Research Thesis: Declaration of Authorship

Print name: Lydia Kristen Doherty

Title of thesis: High-Mannose N-Glycans in Breast Cancer: Implications for Targeted Therapies

I declare that this thesis and the work presented in it are my own and has been generated by me as the result of my own original research.

I confirm that:

1. This work was done wholly or mainly while in candidature for a research degree at this University;
2. Where any part of this thesis has previously been submitted for a degree or any other qualification at this University or any other institution, this has been clearly stated;
3. Where I have consulted the published work of others, this is always clearly attributed;
4. Where I have quoted from the work of others, the source is always given. With the exception of such quotations, this thesis is entirely my own work;
5. I have acknowledged all main sources of help;
6. Where the thesis is based on work done by myself jointly with others, I have made clear exactly what was done by others and what I have contributed myself;
7. None of this work has been published before submission

Signature: ..... Date: 14/02/24

Acknowledgements

This thesis shows a journey of the last four years studying at the University of Southampton. It has been the most challenging, but also the most rewarding task I have ever undertaken. There are many people I would like to acknowledge and express my gratitude to.

Firstly, I would like to thank my primary supervisor, Charlie. I am extremely grateful for all your guidance and patience throughout my PhD, and especially grateful for the support you have provided me with during my thesis write-up. I would like to thank Max for offering me this PhD opportunity while I was a Research Technician, and I would also like to thank Steve for accepting me into his team during the latter part of my PhD. Notable thanks go to Against Breast Cancer for funding my PhD project, for this research would not have been possible without it.

I would like to give thanks to the staff who have supported me at the Centre for Cancer Immunology. This includes to Ian Mockridge for his assistance with affinity purifications, SEC, and SPR experiments, and Patrick Duriez for his assistance with transfections. Additionally, I would like to thank Tatyana Inzhelevskaya for her help with HPLC quality control. I would like to thank Russell Foxall for his assistance with optimising my tissue lectin staining. Many thanks also to Anil Chand and Anna-Liese Silber for conducting the *in vivo* experiments within this work, and to the PCU staff who supported this.

I would like to give special thanks to all my friends and colleagues, both at Building 85 and at the Centre for Cancer Immunology. Honourable mentions go to Himanshi Chawla and Hannah Bauer-Smith, for being great friends and emotional support throughout this PhD. I would also like to thank John Butler, Danielle Tongue, Andy Shapanis, Luis Coy, Chris Barker, Jacob Willcox, Maddy Newby, Joel Allen, Abi Sudol and Alessio D'addabbo for the laughs and support you have provided me with.

I would like to thank my family and close friends for being so incredibly understanding and supportive. Special thanks go to my Mum, Dad, and Grandparents who were always there to

encourage me, giving me the confidence to persist in times of difficulty. I am grateful to my brother, Luke, because I guess I must give him some sort of a mention.

Finally, I would like to thank my fiancé, Sérgio. Thank you for being understanding, and patient, and pushing me when I needed to be pushed. Thank you for consoling me when I was at my lowest and for being there to celebrate my successes with me.

Definitions and Abbreviations

ACN.....Acetonitrile

ADCC.....Antibody-dependent cellular cytotoxicity

ADCP.....Antibody-dependent cellular phagocytosis

Ambic .....Ammonium Bicarbonate

ANOVA.....Analysis of variance

APC .....Antigen-presenting cell

AUC.....Area under the curve

BC .....Breast cancer

CFSE .....Carboxyfluorescein succinimidyl ester

CLR .....C-type lectin receptors

CRDs .....Carbohydrate-recognition domains

DC .....Dendritic cell

DC-SIGN .....C-type lectin receptor dendritic cell-specific intercellular adhesion molecule-3-grabbing non-integrin

DNA .....Deoxyribonucleic acid

DTT .....Dithiothreitol

E:T.....The ratio of effector cells to target cells

ECM .....Extracellular matrix

EDTA .....Ethylenediaminetetraacetic acid

EMT .....Epithelial-to-mesenchymal transition

EGFR .....Epidermal growth factor receptor

ER.....Endoplasmic Reticulum

Fab.....Antigen binding fragment

FACs.....Fluorescence-activated cell sorting

Fc..... Crystallizable fragment

FcγR..... Fcγ receptor

FcRn..... Neonatal Fc receptor

FCS..... Foetal calf serum

FDA..... Food and drug administration

GalNAc ..... N-acetylgalactosamine

GlcNAc..... N-acetylglucosamine

HC..... Heavy chain

HEK cell ..... Human embryonic kidney cell

HER2..... Human epidermal growth factor receptor 2

High-mannose..... N-linked glycoform within the mannose series (Man_5-Man_9)

HIV..... Human immunodeficiency virus

HNF-1 ..... Hepatocyte nuclear factor 1

IAA..... Iodoacetamide

Ig ..... Immunoglobulin

IHC..... Immunohistochemistry

IM ..... Intramuscular

ITAM..... Immunoreceptor tyrosine-based activation motif

ITIM ..... Immunoreceptor tyrosine-based inhibitory motif

IV ..... Intravenous

K_a ..... Association rate

K_d ..... Dissociation rate

K_D..... Dissociation constant

KD ..... Knock-down

Kif ..... Kifunensine

KO..... Knock-out

LC ..... Light chain

M ..... Molar

µM ..... Micromolar

m/z ..... Mass-to-charge ratio

mAb ..... Monoclonal antibody

MCSF ..... Macrophage-colony stimulating factor

MDM ..... Monocyte derived macrophage

MES..... 2-(N-Morpholino) ethane sulfonic acid

MFI ..... Mean fluorescence intensity

MGAT1 ..... Alpha-1,3-mannosyl-glycoprotein 2-beta-N-acetylglucosaminyltransferase

MHC..... Major histocompatibility complex

miRNA..... MicroRNA

mM ..... Millimolar

MOA ..... Mode of action

mRNA ..... Messenger RNA

mTOR..... Mammalian target of rapamycin

MTS..... (3-(4,5-dimethylthiazol-2-yl)-5-(3-carboxymethoxyphenyl)-2-(4-sulfophenyl)-2H-tetrazolium)

NaCl ..... Sodium chloride

NPA..... *Narcissus pseudonarcissus*

OS ..... Overall survival

PBMC..... Peripheral blood mononuclear cells

PBS..... Phosphate-buffered saline

PCR ..... Polymerase chain reaction

PD-1 ..... Programmed death protein 1

PD-L1 ..... Programmed death-ligand 1

PFS..... Progression free survival

PI ..... Propidium iodide

PK ..... Pharmacokinetic

Replicon ..... Self-replicating RNA

RNA ..... Ribonucleic acid

RPMI..... Roswell park memorial institute

RT ..... Room temperature

RU..... Response units

scFv ..... Single-chain variable fragment

SC ..... Subcutaneous

SCID ..... Severe combined immunodeficiency

SEC ..... Size-exclusion chromatography

sgRNA..... Single guide RNA

siRNA..... Small interfering RNA

SPR ..... Surface plasmon resonance

t1/2 ..... Half life

TME ..... Tumour microenvironment

TNBC ..... Triple negative breast cancer

Trast ..... Trastuzumab

Tris-HCl..... Tris(hydroxymethyl)aminomethane hydrochloride

VEEV..... Venezuelan encephalitis virus

WT..... Wild-type

Chapter 1 Introduction

1.1 Breast Cancer

Breast cancer is the most commonly diagnosed cancer among women and accounted for approximately 685,000 deaths globally in 2020 (Bray *et al.*, 2018; WHO, 2023). The global incidence of breast cancer has risen annually (Bray *et al.*, 2015; Giaquinto *et al.*, 2022), and this trend is predicted to continue. Breast cancer is typically distinguished into four molecular subtypes: luminal A, luminal B, human epidermal growth factor receptor 2 ($HER2^+$) and triple-negative breast cancer (TNBC). Clinical management and treatment of breast cancers is guided by the molecular differences of these subtypes. Advances in therapeutics and delivery strategies mean the five-year relative survival for non-metastatic disease is approximately 80% (NIH, 2020b). Despite this, the advancement of metastatic disease and spread to distant organs including the lungs, bone, brain and liver results in a median overall survival of only 3 years (Cardoso *et al.*, 2018), and a five-year relative survival of approximately 25% (NIH, 2020b). Although treatable, metastatic breast cancer is considered incurable and progress in improving patient outcome and quality of life has been slow (Cardoso *et al.*, 2018; Harbeck *et al.*, 2019). Therefore, factors which contribute to tumour progression and metastasis are of interest. Since aberrant glycosylation contributes to immunosuppression and cancer invasiveness, this research aims to investigate the effects of influencing breast cancer glycosylation on the tumour microenvironment and metastasis.

1.2 Epidemiology

Breast cancer incidence and outcome varies depending on the demographic and region. Higher incidences are reported in high-income regions such as New Zealand, Australia, North America, and Europe, relative to low-income regions such as eastern Asia and middle Africa (Allemani *et al.*, 2015). This can be explained by the availability of resources for detection and increased lifestyle and environmental risk factors (Winters *et al.*, 2017). Despite the lower incidence in lower income

regions, breast cancer is associated with higher mortality compared to higher income regions due to late stage diagnoses and limited treatment access (Hossain, Ferdous and Karim-Kos, 2014; Ginsburg *et al.*, 2017). The age of breast cancer presentation also differs with region (Wong *et al.*, 2018); in one study 25% of total diagnoses in developing countries were in patients under 35 years of age, relative to 10% in developed countries (Agarwal *et al.*, 2007). In addition, ethnicity also influences tumour subtype, incidence of metastasis, and five-year survival rates (Kohler *et al.*, 2015; DeSantis *et al.*, 2016). These patterns are likely influenced by genetic predisposition, lifestyle, and environmental factors.

1.3 Genetic predisposition and lifestyle factors

Between 5% and 10% of all breast cancer cases are attributed to inherited genetic mutations (Shiovitz and Korde, 2015). Mutated genes are characterised as either high, moderate, or low penetrance depending on their inherited risk of development. Carriers of highly penetrant genes, namely *BRCA1*, *BRCA2*, *PTEN*, *TP53*, *CDH1* and *STK11* possess an increased lifetime risk of up to 85% of developing breast cancer (Hall *et al.*, 1990; Wooster *et al.*, 1994; FitzGerald *et al.*, 1998; Birch *et al.*, 2001; Pharoah, Guilford and Caldas, 2001; Lim *et al.*, 2004; Tan *et al.*, 2012; Shiovitz and Korde, 2015).

Lifestyle factors also influence the development of breast cancer. Later first pregnancy, lack of breast feeding, early menarche and late menopause have all been documented as risk factors for breast cancer (Althuis *et al.*, 2005; Harbeck *et al.*, 2019). Additionally, modifiable lifestyle risk factors which increase risk include obesity, alcohol consumption, and lack of physical activity (Chen *et al.*, 2011; Picon-Ruiz *et al.*, 2017; Suzuki *et al.*, 2017). Further, the use of hormone contraception, even in low doses, has been linked with increased breast cancer risk (Mørch *et al.*, 2017; Del Pup, Codacci-Pisanelli and Peccatori, 2019). More accessible education and awareness campaigns to promote healthy lifestyles and inform lifestyle decisions could reduce the burden of breast cancer.

1.4 Breast biology

Breasts are comprised of mammary glandular tissue and stroma. The mammary glands consist of lobules containing alveoli composed of an inner lumen surrounded by alveolar cells, myoepithelial cells, and a basement membrane (Harbeck *et al.*, 2019). Connected to the alveolus are milk ducts which lead to the nipple. Most of the breast is comprised of stroma which is adipose tissue.

The cells of the glandular tissue have receptors for oestrogen, progesterone, and prolactin which stimulate the alveolar cells to divide and increase in number, causing the lobule to enlarge (Harbeck *et al.*, 2019). The amounts of hormones released are dependent on menstruation and menopause; each menstruation releases more hormones to promote proliferation. If a genetic mutation occurs when these alveolar cells proliferate tumours may form.

If a mutation occurs the affected cells (usually epithelial cells which line the ducts or lobule), grow uncontrollably forming a tumour/*in-situ* carcinoma (Sgroi, 2010). Tumours begin localised to the basement membrane of alveoli and are classified histologically as either ductal carcinoma in-situ (DCIS) or lobular carcinoma in-situ (LCIS) (Harbeck *et al.*, 2019). Tumour cells of DCIS grow from the wall of the ducts into the lumen and can cross the basement membrane to become invasive ductal carcinoma. Invasive ductal carcinoma typically metastasizes via the lymphatic system and blood. LCIS features clusters of tumour cells growing within the lobules of the breast. These tumours cause the alveoli to enlarge but less commonly invade the ducts or cross the basement membrane to become invasive lobular carcinoma. Cells of invasive lobular carcinoma typically metastasize via viscera.

1.5 Pathophysiology

Breast cancers arise from successive molecular alterations caused by a series of acquired somatic and/or inherited germline mutations (Polyak, 2007). These mutations are dynamic, typically occur at multiple sites within the genome, and can range from point mutations to chromosomal aberrations (Sgroi, 2010). The resulting activation of oncogenes and loss of function of tumour

suppressor genes provides a growth advantage, leading to cellular transformation. This process is further supported by the tumour microenvironment consisting of extracellular matrix, fibroblasts, blood vasculature and inflammatory cells.

All cancers, including breast cancer, share common fundamental traits and hallmarks which facilitate transformation and metastasis. These fundamental traits have been identified as the ability to: sustain chronic proliferation; evade growth suppressors; resist cell death; enable reproductive immortality; induce angiogenesis; activate invasion and metastasis; evade immune destruction; and reprogram energy metabolism (Hanahan and Weinberg, 2000, 2011). Genome instability and inflammation are enabling factors which contribute to many of the hallmarks to support tumorigenesis (Hanahan and Robert A, 2017). Knowledge of these hallmarks and how they drive breast cancer transformation is important to ensure a targeted approach to research and therapeutic development.

1.6 Common somatic mutations

Most genetic alterations in cancer are gene amplification/likely gain-of-function mutations (Koboldt *et al.*, 2012a; Hoadley *et al.*, 2014). Studies have demonstrated the most frequently mutated genes encode cell-cycle modulators (Koboldt *et al.*, 2012b; Nik-Zainal *et al.*, 2016). The most common genes and their reported rate of mutation in breast cancer cells are *TP53* (mutated in ~40% of tumours), *PIK3CA* (30%), *HER2* (30%), *MYC* (20%), *PTEN* (16%), *CCND1* (16%), *FGFR1* (11%), and *GATA3* (10%) (Jeffrey S. Ross *et al.*, 2003; Saal *et al.*, 2005; Koboldt *et al.*, 2012b). These molecular alterations result in (hyper)activation/repression of integral proteins to sustain proliferation and cell growth and inhibit apoptosis. This occurs through the loss of function of inhibitory elements, and both activation and prevention of inhibition of signaling pathways driving cell proliferation and survival (Kolch *et al.*, 1993; Stephens *et al.*, 1997; Holbro *et al.*, 2003). Most breast cancers are driven by multiple low-penetrant mutations which act accumulatively (Harbeck *et al.*, 2019).

1.7 Subtypes

Breast cancers can be classified by histology alone, its intrinsic subtype status, or its surrogate intrinsic subtype status. Common histological subtypes are DCIS, LCIS, or their progressive forms invasive ductal carcinoma and invasive lobular carcinoma, respectively (see Chapter 1.4). The intrinsic subtype method is based on gene expression signatures (PAM-50 (Prediction Analysis of Microarray)) (Perou *et al.*, 2000; Sørlie *et al.*, 2001; Parker *et al.*, 2009). The surrogate intrinsic subtype classification is used routinely in the clinic, which focuses on immunohistochemistry analysis of key proteins and histology. These key proteins are oestrogen receptor (ER), progesterone receptor (PR), human epidermal growth factor 2 receptor (HER2) and Ki67 (**Table 1.1**).

Luminal A-like cancers are the most common breast cancer with the best prognosis. The 5-year relative survival percentage of patients with localised disease is ~100% (NIH, 2020a). Gene expression profiling has identified commonly observed mutations in *PIK3CA*, *MAP3KI*, *ESR1*, *XBP1*, *GATA3* and *FOXA1* (Fragomeni, Sciallis and Jeruss, 2018; Harbeck *et al.*, 2019). The Immunohistochemical profile is $ER^+/PR^+/HER2^-$, and cancers are typically low grade with low proliferation rates (**Table 1.1**).

Luminal B-like cancers have a similar immunohistochemical profile to luminal A-like cancers, but often express lower levels of hormone receptors (**Table 1.1**). It is the second most common breast cancer and offers an intermediate prognosis. The 5-year relative survival percentage for localised disease is ~98% (NIH, 2020a). Gene expression profiling has identified commonly observed mutations in *TP53*, *PIK3CA*, *CCND1*, *ESR1*, *MDM2*, *ATM* and/or *HER2* (Fragomeni, Sciallis and Jeruss, 2018; Harbeck *et al.*, 2019). Tumours are often a higher grade and proliferation rate than Luminal A.

Table 1.1: The surrogate intrinsic subtypes of breast cancers. Immunohistochemical receptor status, proliferation index, histological grade, prognosis, and relative proportion of cases is described for each subtype. The histological grade is given according to the Elston and Ellis modified Scarff-Bloom-Richardson system.

Surrogate intrinsic subtype	Receptor status	Ki67 proliferation index	Grade	Relative proportions of cases	Prognosis
Luminal A-like	$ER^+/PR^+/HER2^-$	Low	Low	60-70%	Good
Luminal B-like	$ER^+/PR^+/HER2^{+/-}$	High	High*	10-20%	Intermediate
HER2-enriched	$ER^-/PR^-/HER2^+$	High	High	10-15%	Intermediate
Triple-negative	$ER^-/PR^-/HER2^-$	High	High	10-15%	Poor

*Higher than Luminal A.

$HER2^+$ cancers have an immunohistochemical profile of hormone receptor negative and HER2 positive (**Table 1.1**). They have a high proliferation index and are considered high grade. The 5-year relative survival percentage for localised disease is ~96% (NIH, 2020a). Gene expression profiling has identified commonly observed mutations in *HER2*, *TP53*, *PIK3CA*, *TOPO2*, *GRB7*, *MYC*, *EGFR, CCND1* and *FGFR4* (Fragomeni, Sciallis and Jeruss, 2018; Harbeck *et al.*, 2019). Although aggressive, cancers respond well to targeted therapies.

Triple negative breast cancers are the most aggressive subtype and have a poor prognosis. The 5-year relative survival percentage for localised disease is ~91% (NIH, 2020b). Its immunohistochemical profile is $ER^-/PR^-/HER2^-$, and tumours are high grade with a high proliferation index (**Table 1.1**). They are morphologically, genetically, and clinically heterogenous. Gene expression profiling has further characterised TNBC into six prognostically significant subtypes. These are: basal-like 1 (BL1), basal-like 2 (BL2), mesenchymal-like (M), mesenchymal-stem-like (MSL), immunomodulatory (IM), and luminal androgen receptor (LAR) (Lehmann *et al.*, 2011). BL1 and BL2 subtypes are classified by a high expression of cell cycle genes and mutations in genes involved in DNA repair mechanisms. M and MSL are classified by an enrichment in genes encoding modulators of cell motility, invasion, and mesenchymal differentiation. IM subtypes are enriched

in genes involved in immune cell processes. The LAR subtype is associated with a higher likelihood of relapse and a higher mutational burden; a high expression of genes encoding regulators of the androgen receptor signaling pathway is observed. These subtypes can be used to inform therapy selection (Lehmann *et al.*, 2011; Harbeck *et al.*, 2019).

1.7.1 Oestrogen receptor (ER) and progesterone receptor (PR)

Hormone exposure plays a stimulatory role in the development and progression of sporadic breast cancer. As described in **Chapter 1.4**, hormones stimulate normal breast development. Imbalances in the release of oestrogen and progesterone during menstrual cycles enhances cell proliferation but may also lead to the accumulation of DNA damage. The combination of repetitive cycles and a defective repair process establishes mutations, leading to pre-malignant and malignant cells.

ER is a nuclear transcription factor encoded by the *ESR1* gene. It is upregulated in the majority of breast cancers, and its function is activated through ligand binding with oestrogen. ER interacts with oestrogen response elements located at the promotor region of certain genes to modulate their expression (Williams and Lin, 2013). ER can also directly interact with cell membrane-associated growth factor receptors and cytoplasmic components of downstream signal transduction pathways, to modulate gene expression (Levin and Pietras, 2008). Oestrogen binding to ER^+ breast cancer cells stimulates proliferation, and therefore drugs blocking the effects or production of oestrogen are regularly administered in the treatment of hormone-sensitive breast cancers (Harbeck *et al.*, 2019).

PR is a ligand-activated nuclear transcription factor encoded by the *PR* gene. Its function is activated through binding with progesterone. Interestingly, PR is a key ER target gene and therefore is a downstream effector of oestrogen action (Daniel, Hagan and Lange, 2011). Despite having a similar function and substantial crosstalk with ER, the mitogenic actions of PR in breast cancer have been overlooked (Daniel, Hagan and Lange, 2011). PR interacts with progesterone response elements or other transcriptional factors to regulate gene expression (Faivre and Lange, 2007). Additionally,

crosstalk between PR and components within signal transduction pathways initiating proliferative effects is enhanced in breast cancers (Faivre *et al.*, 2008).

Endocrine resistance is commonly seen with prolonged exposure to oestrogen blocking therapies. Mediators of this resistance have been found to be signaling components upregulated by PR activation (Ring and Dowsett, 2004; Fan *et al.*, 2009). Therefore, PR blocking therapies should also be employed as a treatment in hormone-sensitive breast cancers (Daniel, Hagan and Lange, 2011).

Dysregulation of ER and PR expression is seen in early breast tumour development. These hormone receptors play diverse roles as transcriptional activators and mediators in signal transduction pathways to stimulate proliferation and are therefore critical therapeutic targets for hormone-sensitive breast cancers.

1.7.2 HER2

HER2 is a receptor tyrosine kinase belonging to the ERBB family. Amplification of the *HER2* gene is the primary reason for HER2 overexpression, occurring in approximately 15-30% of breast cancers and resulting in poor prognosis (King, Kraus and Aaronson, 1985; Slamon *et al.*, 1987; Jeffrey S Ross *et al.*, 2003). HER2 is not self-autonomous, and forms functional heterodimers with other members of the ERBB family (Cho *et al.*, 2003). The HER2-ERBB3 heterodimer is the most transforming complex (Soltoff *et al.*, 1994; Alimandi *et al.*, 1995; Pinkas-Kramarski *et al.*, 1996; Graus-Porta *et al.*, 1997). Once activated, their intrinsic kinase ability acts upon intracellular targets to activate the Ras-MAPK and/or PI3/AKT signaling pathways promoting cell growth, proliferation, and survival (Prigent and Gullick, 1994; Holbro *et al.*, 2003) (**Figure 1.1**). Targeting HER2 in $HER2^{+}$ breast cancers has proven to be an effective therapeutic option.

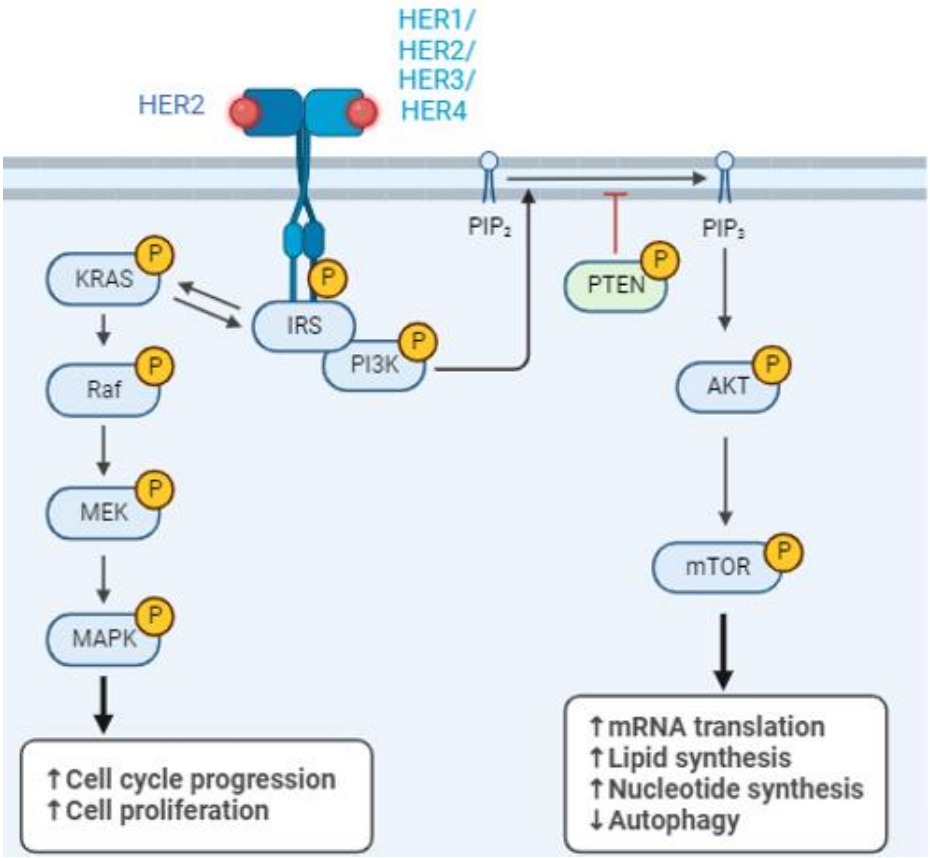

Figure 1.1: HER2 signaling pathway. HER2 is a receptor tyrosine kinase located on the cell membrane which interacts with a variety of ligands. HER2 signaling is activated by the formation of homo or heterodimers with other members of the ERBB family, leading to phosphorylation of intrinsic tyrosine kinase residues. Their intrinsic kinase ability acts upon intracellular targets to activate the Ras-MAPK and/or PI3/AKT signaling pathways promoting cell growth, proliferation, and survival.

1.8 Breast tumour microenvironment

Throughout malignancy the tumour microenvironment (TME) promotes cancer growth and immune evasion. The TME is created and constantly remodelled by the tumour, and consists of a heterogenous pool of tumour cells, cancer-associated fibroblasts, blood vessels, infiltrating inflammatory cells and extracellular matrix (ECM) (Whiteside, 2008; Mittal *et al.*, 2014; Nagarajan and McArdle, 2018; Harbeck *et al.*, 2019).

Immune populations present within the TME can include T cells ($CD8^+$(cytotoxic), $CD4^+$(helper), T regulatory (T_{reg})), dendritic cells, B cells, macrophages, and NK cells. The influence of the immune

system on breast cancer development and the cross talk between the tumour and immune system is dynamic throughout malignancy. Initially, the immune system identifies and recruits immune cells to the tumour site to eliminate the tumour, a process known as immune surveillance (Swann and Smyth, 2007; Mittal *et al.*, 2014). Anti-tumour responses are employed by activated $CD4^+$ and $CD8^+$ T cells to destroy tumour cells which have developed due to failed intrinsic tumour suppressor mechanisms. However, this immune response can be suppressed by breast cancer cells through upregulated immune-checkpoint inhibitors, initiated by T-cell exhaustion (Harbeck *et al.*, 2019). The establishment of a pro-tumour immune response is further supported by the recruitment of immunosuppressive cells, induced by tumour-associated macrophages and tumour- and cancer-associated fibroblast-secreted factors. These tumour-suppressive cells, namely T_{regs} and myeloid-derived stromal cells (MDSCs), prevent an effective immune response and sustain chronic inflammation (Gabrilovich and Nagaraj, 2009). This dynamic progression of immune interactions is known as immunoediting and ultimately establishes a pro-TME to support breast cancer development, immune escape, and metastasis.

During chronic inflammation, the secretome of the pro-tumour microenvironment contributes to tumour survival (Nagarajan and McArdle, 2018). The release of cytokines such as transforming growth factor (TGF-β), interferon γ (IFN-γ), tumour necrosis factor α (TNF-α) stimulates the release of vascular-endothelial growth factor (VEGF) and enzymes such as matrix metalloproteinases (MMPs) immunosuppressive cells, triggering epithelial-mesenchymal transition, angiogenesis, and metastasis (Yang *et al.*, 2008; Kalluri and Weinberg, 2009; Landskron *et al.*, 2014).

The degree of immunogenicity in breast cancer is different between the molecular subtypes: TNBC and $HER2^+$ tumours provoke a higher immune response than luminal A and luminal B (Solinas *et al.*, 2017; Nagarajan and McArdle, 2018). The presence and abundance of immune cells, particularly tumour infiltrating lymphocytes (TIL), within the breast tumour microenvironment is also considered a prognostic factor for response to neoadjuvant treatment and patient survival (Mahmoud *et al.*, 2012; Adams *et al.*, 2014; Loi *et al.*, 2014; Solinas *et al.*, 2017).

The ECM also plays a role in malignancy (Provenzano *et al.*, 2008; Mammoto *et al.*, 2013). It can comprise up to 60% of a tumour mass, and consists of proteoglycans and glycoproteins such as collagens, laminins, fibronectin, and elastin (Kim, Turnbull and Guimond, 2011; Henke, Nandigama and Ergün, 2020). The ECM of the TME is dynamic and varies in composition, organisation and degree of post-translational modifications throughout breast cancer malignancy (Barsky *et al.*, 1982; Xiong *et al.*, 2014). Increased collagen deposition provides a physical context for biochemical signals to support tumour growth and metastasis (Gilkes *et al.*, 2013; Xiong *et al.*, 2014). Upregulated lysyl-oxidases, increases collagen-elastin cross-linking (Peyrol *et al.*, 1997). Increased collagen crosslinking stiffens the ECM forcing focal adhesions, enhancing integrin-mediated growth factor signaling and increasing tumour progression (Levental *et al.*, 2009). Additionally, increased collagen and collagen crosslinking has correlated with increased resistance to chemotherapy and reduced survival in TNBC patients (Rossow *et al.*, 2018; Xiong *et al.*, 2018). Increased levels of hyaluronic acid (HA) in breast cancer facilitates epithelial-mesenchymal transition through ligand binding with CD44 (Heldin *et al.*, 2014). Natively laminins are exclusively expressed in the basement membrane, however their overexpression in breast cancer contributes to reduced adherence to a defined basement membrane and increased invasiveness (Albrechtsen *et al.*, 1981; Alon *et al.*, 1986; Qiu *et al.*, 2018). It is clear the composition and changes to the ECM are critical in breast tumour progression and invasive properties.

1.9 Metastatic disease

Metastasis involves a series of sequential steps. Initially, a loss of adhesive structures (usually through loss of E-cadherin function) on primary tumours occurs to promote epithelial-mesenchymal transition and detachment from the primary site (Chiang and Massagué, 2008). Cancer cells then must translocate into circulation or lymphatic vessels, and subsequently invade, establish and proliferate in distant organs (Bacac and Stamenkovic, 2008; Seyfried and Huysentruyt, 2013). The most common sites for breast cancer metastasis are bone, lung, liver, brain and distant lymph nodes (Harbeck *et al.*, 2019)

The majority of cancer deaths are attributed to metastatic spread, rather than the localised primary cancer (Tarin, 2011; Harbeck *et al.*, 2019). The 5-year survival rate of localised breast tumours is above 90% across all intrinsic subtypes. However, once metastasised, the 5-year relative survival rates drop dramatically. These relative percentages are: ~30% (Luminal A-like), ~43% (Luminal B-like), ~36% ($HER2^+$), and ~11% (TNBC) (NIH, 2020b). It is clear that patient diagnosis and therapy prior to metastasis is vital for patient outcome.

1.10 Glycosylation

Aberrant glycosylation is fundamental in tumour development and progression. Under normal conditions, healthy cells show high heterogeneity of glycosylation patterns depending on numerous factors including cell type and condition, external stimuli, and genetic factors (Zhou *et al.*, 2008; Slade *et al.*, 2016; Zhang *et al.*, 2019). Despite this heterogeneity, aberrant glycosylation relating to cancer biology is recognised as a major focus of research (Pearce and Läubli, 2015; Stowell, Ju and Cummings, 2015; Munkley and Elliott, 2016). Altered glycosylation supports many of the recognised hallmarks of cancer (see Chapter 1.5) in which it sustains proliferation, activates invasion and metastasis, evades immune destruction and stimulates angiogenesis (Fuster and Esko, 2005; Li *et al.*, 2018).

Glycosylation is the ubiquitous and energy-demanding post-translation modification conjugating glycans to proteins and lipids. In eukaryotes, glycoproteins are formed by glycosyltransferases and glycosidases in the ER and Golgi secretory pathway (**Figure 1.2**). The high number of linkage and monosaccharide combinations possible contributes to the high heterogeneity observed in glycan structure and function. Glycosylation is integral to a myriad of biological functions.

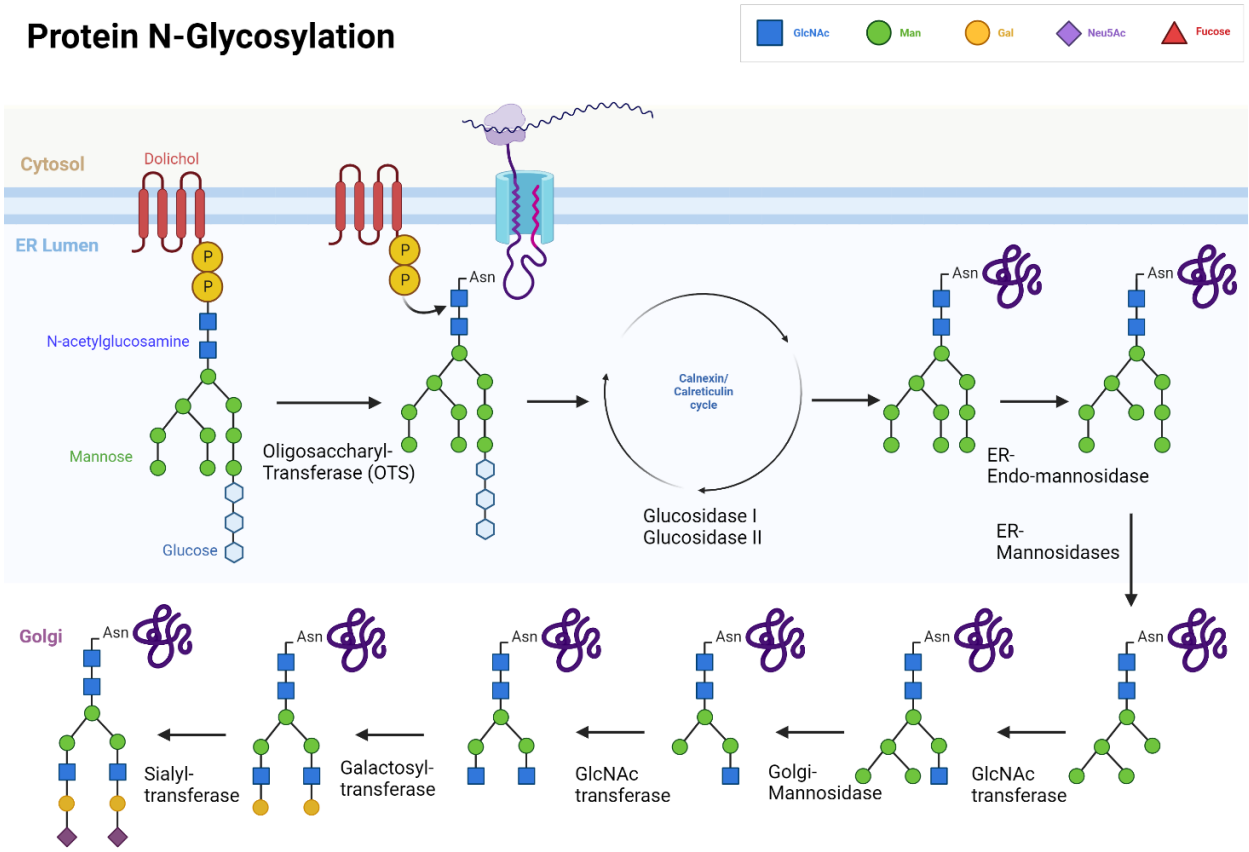

Figure 1.2: A simplified schematic of the biosynthesis of N-linked glycans within the ER and Golgi apparatus. The glycosyltransferases and glycosidases responsible for the catalysis of each reaction are listed between each oligosaccharide chain and the subcellular location of each event is described. O-glycans can also act as acceptor substrates for these enzymes and are modified in this pathway.

1.10.1 Functions

Glycans are integral to biological functions. Their attachment to proteins influences biochemical properties in terms of structure, solubility, activity, protease susceptibility and antigenicity (Varki and E., 2015). Due to their high abundance on the cell surface and influence on hydrophilicity and charge, glycan composition strongly affects the biophysical properties of cellular interactions (Byrne, Donohoe and O'Kennedy, 2007).

Biological functions such as cell-cell signaling and adhesion, protein folding and stability, and reaction specificity between molecules are all dependent on, or influenced by glycan attachment (Varki, 1993; Haltiwanger and Lowe, 2004; Varki and E., 2015; Reily *et al.*, 2019). Additionally,

glycans are integral for regulating immunity and tolerance, in which their signatures trigger tolerogenic or immunogenic signaling pathways (Lübbers, Rodríguez and van Kooyk, 2018).

1.10.1.1 Galectins, C-type lectins and siglecs

The three major families of glycan-binding proteins, known as lectins, are galectins, C-type lectins, and siglecs.

Galectins are soluble glycan-binding proteins, known as lectins, which bind β-galactoside-containing saccharides β-galactoside-containing saccharides (Cerliani et al., 2017). Galectins are classified as prototype, tandem-repeat, or chimera, depending on the structure and number of carbohydrate-recognition domains (CRDs) (Mariño *et al.*, 2023). Galectins can be cytosolic or secreted from cells via a non-canonical pathway independent of the ER and Golgi (Barondes *et al.*, 1994). Soluble galectins crosslink glycosylated cell surface ligands to form multivalent lattices activating signaling pathways. Galectin binding can modulate a myriad of functions such as immune response, receptor kinase signaling, metabolic homeostasis, and induce epithelial-mesenchymal-transition (EMT) and cancer progression (Nabi, Shankar and Dennis, 2015). Galectins are expressed and released by many different cells In the immune system, including activated T and B cells, macrophages and regulatory T cells (Rabinovich and Croci, 2012).

Most C-type lectin receptors (CLR) are calcium-dependent carbohydrate-binding proteins. These can be divided into mannose-specific or galactose-specific, based on the amino acid motif involved in glycan recognition and Ca^{2+} coordination (Brown, Willment and Whitehead, 2018). The type II subfamily of CLRs have a dual function in host-pathogen interactions and immune cell response. These CLRs are expressed on antigen-presenting cells (APCs) such as macrophages and immature dendritic cells (DCs) but have also been found on endothelial cells and NK cells (Rabinovich and Croci, 2012). CLRs such as DC-SIGN, L-SIGN, mannose receptor, macrophage galactose-specific lectin (MGL) and langerin are specific for high-mannose, fucose, GalNAc- or GlcNAc-containing glycans expressed by mammalian cells or pathogens (Apostolopoulos and Mckenzie, 2005; Geurtsen, Driessen and Appelmelk, 2010; Rabinovich and Croci, 2012).

Sialic acid-binding immunoglobulin-like lectins (siglecs) are immunoglobulin type I transmembrane proteins mostly expressed by cells of the immune system, with specificity towards sialic acid-containing glycans (Rabinovich and Croci, 2012). Siglecs comprise of two groups based on sequence similarity and evolutionary relatedness, of which the main group contains the CD33-related subgroup (Crocker, Paulson and Varki, 2007). Many siglecs have tyrosine-binding motifs, particularly immunoreceptor tyrosine-based inhibitory motifs (ITIMS), attenuating tyrosine phosphorylation and eliciting immunomodulatory effects (Crocker, Paulson and Varki, 2007). Siglecs are thought to predominantly contribute to innate immunity. Some siglecs have a restricted expression profile, whereas others are widely expressed on lineages including macrophages, B cells, eosinophils, mast cells, neutrophils, monocytes, and DCs (Von Gunten and Bochner, 2008).

1.11 Glycan biosynthesis

1.11.1 Glycosyltransferases and glycosidases

Glycosyltransferases and glycosidases are enzymes involved in glycan initiation, assembly, processing, and turnover. Glycosyltransferases are generally responsible for elongating glycan chains. This process is often sequential, where the product of one enzyme is the acceptor substrate for another enzyme. Glycan chains are also processed by glycosidases, which are responsible for removing monosaccharides to create intermediates which glycosyltransferases can act on. Collectively, this process creates a linear and/or branched structure of monosaccharides.

1.11.2 N-linked biosynthesis

N-glycans are synthesised from nine monosaccharide precursors connected by glycosidic linkages in differing combinations. Their biosynthesis occurs in two main phases: the synthesis and transfer of the dolichol-linked precursor, and subsequent glycan processing by glycosyltransferases and glycosidases.

1.11.2.1 Synthesis of the dolichol-linked precursor

The synthesis of the N-glycan precursor, Dolichol-P-P-$GlcNAc_2Man_9Glc_3$, occurs across the ER membrane. The process begins on the cytoplasmic side, where GlcNAc-1-P is transferred to the polyisoprenol lipid, dolichol-P, by a GlcNAc-1-phosphotransferase. A further GlcNAc and five Mannose residues are subsequently transferred from UDP-GlcNAc and GDP-Man, respectively, to generate $Man_5GlcNac_2$-P-P-Dol. This molecule is then translocated across the ER membrane to the lumenal side, where four additional Mannose residues and three Glucose residues are transferred from Dol-P-Man and Dol-P-Glc, respectively, to generate the mature N-glycan precursor, Dolichol-P-P-$GlcNAc_2Man_9Glc_3$. Oligosaccharyltransferase (OST) catalyses the transfer of this fourteen-sugar glycan from Dol-P-P to a receptive Asn sidechain within Asn-X-Ser/Thr (where X can be any amino acid except proline) sequons of nascent polypeptides entering the ER through the translocon (**Figure 1.2**).

1.11.2.2 Energy availability

Glycosylation is an energy-demanding post-translational modification. Therefore, monosaccharide availability can be an influential factor or a rate-limiting step contributing to heterogeneity in N-glycosylation. It was demonstrated that reducing glucose availability in cell cultures and supplementing with other monosaccharides could influence glycosylation. For example, both mannose and galactose could effectively be used as glycan precursors, but fucose and fructose could not (Zhang *et al.*, 2019).

Further, previous studies have demonstrated that supplementing cell culture media with D-(+)-mannose increased high-mannose glycoforms and reduced GlcNAc occupancy of recombinantly made IgG (Kildegaard *et al.*, 2016; Slade *et al.*, 2016). The increased mannosylation from 10% to 36% consisted mainly of higher-order mannose glycans (Man_6-Man_9). Interestingly, mannose supplementation did not impair glycolysis or TCA cycle activity of cells, but a notable increase in GDP-Man synthesis (upregulated pathway M6P-M1P-GDPMan) was observed (Slade *et al.*, 2016). As metabolite concentration increased mannosidase concentration decreased (Slade *et al.*, 2016),

and thus expression of alpha-mannosidases was demonstrated to be negatively regulated by mannose-containing metabolites, mannose, M6P, and GDP-mannose.

1.11.2.3 3 Major classes of eukaryotic N-linked glycans

All eukaryotic N-glycans share the core sequence of monosaccharide resides, $Man_3GlcNAc_2$. As such, glycans are classified into three categories based on the residues extending this core. These categories are high-mannose, hybrid and complex (**Figure 1.3**). High-mannose glycans contain only Mannose residues extending the core from both the Manα1-3 and Manα1-6 arm. Hybrid glycans contain only Mannose residues extending from the Manα1-6 arm, and a GlcNAc extending the Manα1-3 arm creating a heterogenous antennae. Complex glycans contain GlcNAc residues extending both the Manα1-3 and Manα1-6 arms, creating up to six heterogenous antennae.

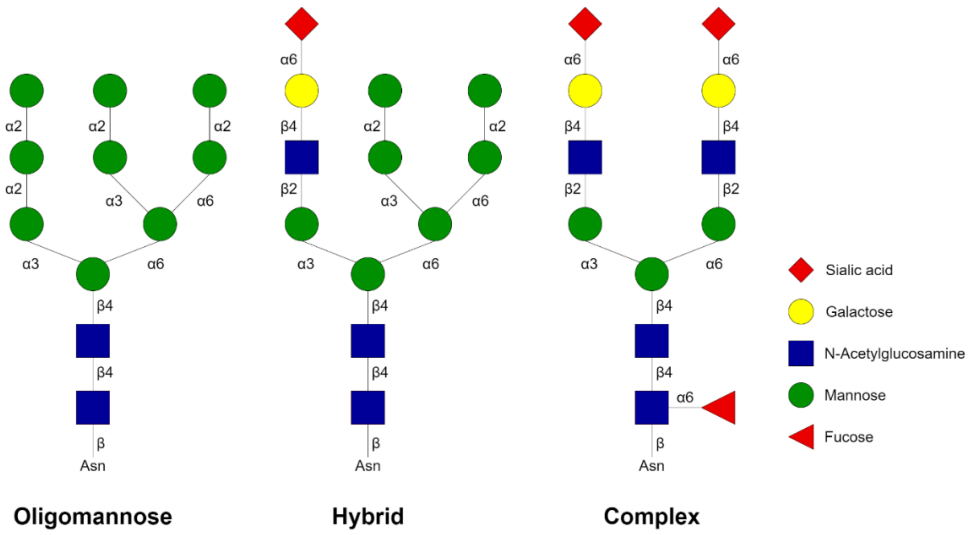

Figure 1.3: Three major classes of eukaryote N-glycans; high-mannose, hybrid and complex. Each glycan shares the common core sequence Manα1-3(Manα1-6)Manβ1-4GlcNAcβ1–4GlcNAcβ1–Asn. The linkage type and position between each monosaccharide is depicted.

1.11.3 O-linked glycan biosynthesis

Many extracellular and secreted proteins are modified by the addition of O-GalNAc to Ser/Thr residues (Bennett *et al.*, 2012; Vasudevan and Haltiwanger, 2014). The addition and modification of O-GalNAc glycans by glycosyltransferases occurs in the Golgi apparatus (**Figure 1.2** and **Table 1.2**)

(Varki and E., 2015). This process is highly heterogenous and the O-glycans synthesised is dependent on the subcellular localisation, substrate specificity and activity levels of glycosyltransferases involved.

1.11.3.1 Polypeptide-N-Acetylgalactosaminyltransferases

Polypeptide GalNAc-transferases (GALNT) are essential to initiate the first step of O-GalNAc glycosylation (Bennett *et al.*, 2012). GALNTs bind UDP-GalNAc as a donor substrate and catalyse the transfer of GalNAc in α-linkage to a peptide acceptor. The peptide acceptor specificity is variable among GALNTs, and most GALNTs can only efficiently transfer GalNAc to Thr rather than Ser (Varki and E., 2015). Despite these slight differences in substrate specificity, most GALNTs can act on most peptides. GALNTs are ubiquitous across all animals and humans have 20 genes encoding different GALNTs (EC 2.4.1.41) (Bennett *et al.*, 2012). The large number of GALNTs, and substantial overlap in GALNTs ability to act on many peptides provides a redundancy and reflects their importance in this process.

O-GalNAc glycosylation is first regulated by the amino acid sequence of the protein acceptor. The lectin domain at the carboxyl terminus of the GALNT recognises remote GalNAc residues and catalyses their transfer to Ser/Thr. The defined acceptor sequon containing Ser/Thr has not yet been defined, but assays have demonstrated Pro residues close to Ser/Thr glycosylation sites promote GalNAc transfer (Murray *et al.*, 2021).

It is extremely difficult to predict the likelihood of O-glycosylation. GALNTs are expressed at differing levels in different tissues which can affect the degree of O-glycosylation. Additionally, the overlapping and dynamic localisation of GALNTs and other glycosyltransferases within the Golgi pathway produces heterogenous mixtures of O-GalNAc glycans attached to all mature glycoproteins. Combined with the limited predictive value of the defined acceptor sequon, the presence and composition of O-GalNAc glycans are often difficult to predict.

Table 1.2: Glycosyltransferases involved exclusively in O-GalNAc glycan biosynthesis, and the common O-GalNAc cores their activity yields (adapted from Varki and E., 2015).

Enzyme	**HUGO Gene Nomenclature Committee**	**O-GalNAc glycan core type**
Polypeptide N-acetylgalactosaminyltransferase	GALNT	**Tn antigen** (GalNAcαSer/Thr)
Core 1 β1-3 galactosyltransferase 1 (C1GalT-1 or T synthase)	C1GALT1	**Core 1/ T antigen** (Galβ1-3GalNAcαSer/Thr)
Essential chaperone for T synthase (COSMC)	C1GALT1C1	**Core 1/ T antigen** (Galβ1-3GalNAcαSer/Thr)
Core 2 β1-6 N-acetylglucosaminyltransferase (C2MGAT1, C2GnT-3)	GCNT1	**Core 2** (GlcNAcβ1-6(Galβ1-3)GalNAcαSer/Thr)
Core 3 β1-3 N-acetylglucosaminyltransferase 6 (C3GnT-6)	B3GNT6	**Core 3** (GlcNAcβ1-3GalNAcαSer/Thr)
Core 2/4 β1-6 N-acetylglucosaminyltransferase 2 (C2GnT-2)	GCNT3	**Core 4** (GlcNAcβ1-6(GlcNAcβ1-3)GalNAcαSer/Thr)
Elongation β1-3 N-acetylglucosaminyltransferase (elongation β3GnT)	B3GNT3	**Poly-N-acetyllactosamine** (GlcNAcβ1-3Gal)$_n$
I branching β1-6 N-acetylglucosaminyltransferase (I GnT)	GCNT2	**I antigen**
β1-3 galactosyltransferase (β3GalT5)	B3GALT5	**Core 3-type** Galβ1-3GlcNAcβ1-3GalNAcαSer/Thr)
Core 1 α2-3 sialyltransferase (ST3Gal I, ST3Gal IV)	ST3GAL1, ST3GAL4	**Sialyated core 1** (Siaα2-6Galβ1-3GalNAcαSer/Thr), **Sialylated core 2** (Siaα2-6GlcNAcβ1-6(Galβ1-3)GalNAcαSer/Thr
α2-6 sialyltransferase (ST6GalNAc I, II, III, or IV)	ST6GALNAC1-4	**Sialyl-Tn antigen** (Siaα2-6GalNAcαSer/Thr), **Sialylated core 1** (Siaα2-6Galβ1-3GalNAcαSer/Thr)
Core 1 3-O-sulfotransferase (Gal3ST4)	GAL3ST4	**Sulfated core 1** (Gal)
α1-2 Fucosyltransferase (FucT-I, FucT-II)	FUT1, FUT2	**Blood group H** (Fucα1-2Gal-)

1.12 Glycosylation in cancer

Aberrant glycosylation in cancer was first described in 1969 (Meezan *et al.*, 1969), and has since been documented as a molecular phenotype of malignant cells (Matsushita *et al.*, 1990; Pancino *et al.*, 1991; Shriver, Raguram and Sasisekharan, 2004; Häuselmann and Borsig, 2014; Munkley and Elliott, 2016). Aberrant glycosylation occurs in a variety of non-random ways. These include the under- and overexpression of glycans, abnormal branching, expression of incomplete/truncated glycans, neoexpression of embryonic glycans, and the presence of novel glycans (Reily *et al.*, 2019). These altered structures arise from multiple factors, including energy availability, the dysregulation of glycosyltransferases and chaperone genes, and epigenetic and genetic mutations (Fuster and Esko, 2005; Potapenko *et al.*, 2015; Stowell, Ju and Cummings, 2015; Dall'Olio and Trinchera, 2017).

Glycan alterations commonly documented in cancer are described in **Table 1.3**. Some of the most prevalent changes include increased β-1,6 branching attributed to increased N-Acetylglucosaminyltransferase-V (MGAT5) activity (Dennis *et al.*, 1987; Lau and Dennis, 2008). This increased branching, in conjunction with an upregulation of sialyltransferases, leads to increased global sialylation by creating additional sites for terminal sialic acid residues (Kim and Varki, 1997). Further, the upregulation of these sialyl- and fucosyltransferases results in altered terminal glycan epitopes commonly found on transformed cells. Common glycan epitopes in cancer include sialyl-Lewis^{x}, sialyl-Lewis^{a}, Thomsen-nouvelle antigen (Tn), sialyl Tn, Globo H, Lewis y, and polysialic acid (Zhang *et al.*, 1997; Häuselmann and Borsig, 2014; Stowell, Ju and Cummings, 2015).

Table 1.3: Common glycan alterations in cancer and their biological effect effect (Adapted from Häuselmann & Borsig, 2014).

Structural Change	Biosynthetic basis of structural change	Lectin binding partners	Cancer hallmark	Reference
Increased β-1,6 branching	Increased MGAT5	Galectins, Siglecs	Sustaining proliferative signaling, activates invasion and metastasis, evade immune destruction	(Varki, 1993; Demetriou *et al.*, 1995; Meany and Chan, 2011)
Aberrant α-2,6 sialylation	Increased ST6Gal1 sialyltransferase	Galectins, Siglecs	Evade immune destruction	(Perdicchio *et al.*, 2016; Stanczak *et al.*, 2018)
Aberrant global sialylation	Increased sialyltransferase activity	Galectins, Siglecs, Selectins	Evade immune destruction	(Perdicchio *et al.*, 2016; Stanczak *et al.*, 2018)
Increased sialyl-Lewis$^{x/a}$	Increased FUT7, FUT3, FUT6, ST3GAL6, B3GNT3	Selectins	Evade immune destruction, activates invasion and metastasis	(Shiraishi *et al.*, 2000; Li *et al.*, 2018)
Decreased disialyl-Lewis$^{x/a}$	Decreased ST6GALNAc6, GlcNAc6ST1	Selectins, Siglecs	Evades immune destruction, correlates with metastasis and poor prognosis	(Tsuchida *et al.*, 2003; Miyazaki *et al.*, 2004)
Increased Tn epitopes	*Cosmc* mutations resulting in reduced T-synthase activity	Galectins	Correlates with metastasis and poor prognosis	(Springer, 1984; Lloyd *et al.*, 1996; Ju *et al.*, 2008; Beatson *et al.*, 2015)
Increased sialyl-Tn epitopes	Increased ST6GalNAc2, ST6GalNAc1	Siglecs, Galectins	Correlates with metastasis and poor prognosis	(Miles *et al.*, 1995; Sewell *et al.*, 2006; Beatson *et al.*, 2015)
Increased T antigen (core 1 structure)	Decreased C2GnT2	Galectins	Correlates with metastasis and poor prognosis	(Springer, 1984; Taylor-Papadimitriou *et al.*, 1999)

Increased sialyl-T antigens	Increased ST3Gal1	Galectins, Siglecs	Correlates with metastasis and poor prognosis	(Lloyd *et al.*, 1996; Burchell *et al.*, 1999)

Glycosylation sustains proliferative signaling, a key hallmark of cancer. Intracellular proteins are subject to O-GlcNAcylation, a modification that competes with phosphorylation during oncogenesis to facilitate cell-cycle progression (Caldwell *et al.*, 2010; Itkonen *et al.*, 2013). Increased N-glycan branching further stimulates the activity of growth factor receptors (Boscher, Dennis and Nabi, 2011). Deregulation of gangliosides, which directly interact with receptor tyrosine kinase and signal transducers, contributes to increased activation of cellular signals and proliferation in cancer (Groux-Degroote *et al.*, 2018). Changes in the extracellular matrix (composed of secreted glycoproteins, glycosaminoglycans, proteoglycans, and collagens) and altered glycosylation of integral membrane proteins can influence signaling functions (English, Lesley and Hyman, 1998; Hallouin *et al.*, 1999; Kim, Turnbull and Guimond, 2011). Increased expression of tumour-associated glycoproteins also supports cell survival by promoting integrin-dependent growth factor signaling (Paszek *et al.*, 2014).

Cell surface glycosylation acts as a mediator of immune inhibition (Li *et al.*, 2018). Increased global sialylation contributes to cancer cell transformation and intensifies with tumour progression (Cohen *et al.*, 2010; Perdicchio *et al.*, 2016; Stanczak *et al.*, 2018). Sialoglycans are considered immunosuppressive, and their presence can influence immune activation by: preventing complement-dependent cytotoxicity (Elward and Gasque, 2003); inhibiting immune-mediated apoptosis by $CD8^+$ cells (Swindall and Bellis, 2011); inhibiting activation of NK cells (Cohen *et al.*, 2010); and acting as immune checkpoint regulators by binding sialic-acid-binding immunoglobulin-like lectins (Siglecs) and stimulating inhibitory signaling pathways and immune suppression (Lübbers, Rodríguez and van Kooyk, 2018).

Cancer cells also mediate immunosuppression through upregulating extracellular galectin release into the TME, and deregulating glycosyltransferase expressions. Complex, branched N-glycans synthesised by MGAT5 are high affinity ligands for galectin-3 (Patnaik *et al.*, 2006; Markowska,

Jefferies and Panjwani, 2011). Both increased expression of galectin-3 and upregulation of MGAT5 are commonly observed in cancers (Varki, 1993; Gordon-Alonso *et al.*, 2017a). Galectin-3 binds extracellular matrix glycoproteins, tumour infiltrating lymphocytes (TIL), and glycans on cytokines such as IFNγ to form glycoprotein-galectin lattices (Gordon-Alonso, Demotte and van der Bruggen, 2014; Gordon-Alonso *et al.*, 2017b). The formation of the glycoprotein/galectin lattices was demonstrated to reduce cytokine diffusion through the tumour matrix (Gordon-Alonso *et al.*, 2017b), inhibiting T-cell tumour infiltration and stimulating angiogenesis (Romagnani *et al.*, 2004; Harlin *et al.*, 2009). In addition, increased galectin-3 binding to glycosylated cell receptors such as T Cell Receptor on $CD8^+$ and VEGF-R2 causes T cell dysfunction and immune suppression (Demotte *et al.*, 2010) and stimulates angiogenesis (Markowska, Jefferies and Panjwani, 2011), respectively. Therefore, increased galectin-3 binding with deregulated N-linked glycans within the tumour microenvironment are strategies employed by cancer cells as a method of immune evasion.

Altered glycosylation activates invasion and metastasis. Increased sialyl $Lewis^{a/x}$ are common epitopes expressed by cancer cells which bind selectins to facilitate hematogenous metastasis. Once cancer cells have infiltrated the bloodstream, sialyl Lewis antigens interact with E-selectins on vascular endothelial cells in the peripheral vessel walls, allowing cancer cells to adhere and invade to other sites (Kannagi *et al.*, 2004). In addition, breast cancer cells highly express underglycosylated MUC1 (Kölbl, Andergassen and Jeschke, 2015). Truncated O-glycans on MUC1 stimulates interactions with extracellular matrix proteins and facilitate attachment of metastasising cancer cells to secondary sites (Ciborowski and Finn, 2002). Additionally, interactions between the underglycosylated MUC1 and CIN85 on cellular invadopodia regulates cancer cell migration and invasion (Cascio *et al.*, 2013). N-glycan composition and branching have also been implicated in driving metastasis. Increased core α1,6-fucosylation of N-glycans, caused by an upregulation of FUT8, has been implicated in epithelial-mesenchymal transition and metastasis of cancerous cells (Chen *et al.*, 2013).

Highly branched N-glycans enhance the metastatic capability of cancerous cells. MGAT5 is involved in the formation of highly branched N-glycans, in which it catalyses the attachment of β1,6-GlcNAc to a α1-3 linked mannose (Brockhausen, Narasimhan and Schachter, 1988). Upregulation of MGAT5 is commonly documented in cancers (Varki, 1993). MGAT5 can act on cell surface receptors, such as cytokine and adhesion receptors, affecting their attenuation at the cell surface and influencing a myriad of functions promoting motility and invasion (Partridge *et al.*, 2004; Guo *et al.*, 2009). In addition, increased β1,6-*N*-linked branched glycans on integrins and cadherin molecules has been demonstrated to attenuate signaling, resulting in reduced cell-cell and cell-matrix interactions and promoting migration (Demetriou *et al.*, 1995). Cancer cells commonly upregulate MGAT5 expression, which results in highly branched N-glycans, impacting cell-cell and cell-matrix adhesion and promoting motility and invasiveness. This is further supported by research exploring the effects of GnT-III. GnT-III catalyses the transfer of GlcNAc to the core β-mannose to create bisecting GlcNAc-type glycans. The overexpression of GnT-III reduced β1,6-GlcNAc branching and suppressed cancer metastasis (Yoshimura *et al.*, 1995).

1.12.1 Sialylation

Aberrant sialylation is recognised as a consistent and prominent change in cancer. One mechanism which leads to increased sialylation is altered sialyltransferase expression. Sialyltransferases catalyse the linkage of sialic acid residues from the donor cytidine-5'-monophosphate-*N*-actylneuraminic acid (CMP-Neu5Ac) to oligosaccharide chains (Szabo and Skropeta, 2017).

1.12.1.1 ST6GAL1

ST6 β-galactosidase alpha-2,6-sialyltransferase I (ST6GAL1) (EC 2.4.99.1) is a type-II membrane protein located in the *trans*-Golgi which catalyses the specific reaction of a sialic acid residue onto the acceptor glycan Galβ1-4GlcNAc via an α2-6 linkage (Hassinen *et al.*, 2010). This protein is encoded by the *ST6GAL1* gene located at 3q27.3 in the human genome (Wang *et al.*, 1993). Upregulated ST6GAL1 has been documented in many cancers and correlates with metastasis and poor prognosis (Perdicchio *et al.*, 2016; Stanczak *et al.*, 2018). Specific immunosuppressive

functions have been directly attributed to the presence of α2-6 linked sialic acid residues on N-linked glycans. The Fas death receptor (CD95) is a substrate for ST6GAL1, and its α2-6 sialylation confers protection against Fas-mediated apoptosis. Therefore, tumours deregulate Fas function by altering sialylation to protect against $CD8^+$ induced apoptosis (Swindall and Bellis, 2011). Additionally, α2-6 sialylation of tumour necrosis factor receptor 1 (TNFR1), caused by upregulated ST6GAL1, was demonstrated to protect tumour cells from TNF-induced apoptosis and anchor TNFR1 to the cell surface promoting cancer cell survival. Therefore, increased ST6GAL1 expression is employed by cancer cells to regulate survival in TNF-rich TME (Holdbrooks, Britain and Bellis, 2018).

Increased ST6GAL1 expression is employed regularly by cancer cells as a method of immunosuppression and transition to a pro-tumour microenvironment. Clonal cancer variants with increased ST6GAL1 expression are therefore selected for during immunoediting, making it a ubiquitous target for therapeutics.

1.12.2 Glycan branching

The increased expression of β 1,6 branched N-linked glycans is an established hallmark of many cancers (Stowell, Ju and Cummings, 2015; Oliveira-Ferrer, Legler and Milde-Langosch, 2017). Branching glycans are significant in contributing to the migratory and invasive phenotype of cancer cells (Guo *et al.*, 2009). Additionally, this increased branching provides more terminal sites for increased global sialylation, galactosylation, and the formation of repeating polylactosamine units bearing fucysoylated- cancer associated $Lewis^{a/x}$ antigens (Pinho and Reis, 2015). Through this process, increased branched glycans can activate invasion and metastasis, sustain proliferative signalling, and assist in immune evasion (Varki, 1993; Meany and Chan, 2011; Ščupáková *et al.*, 2021).

β1,6 branching inhibits contact inhibition (Demetriou *et al.*, 1995), and stimulates cell migration and invasion (Guo *et al.*, 2002, 2009). Increased β1,6 branched glycans modulate integrin clustering and subsequent signal transduction pathways, altering cell-matrix adhesion (Guo *et al.*, 2002).

Further, increased branching has been associated with tumour formation and metastasis (Seberger and Chaney, 1999). BC metastases patients were demonstrated to have increased levels of complex- highly branched glycans, relative to primary BC (Ščupáková *et al.*, 2021). The presence of branched tetra-antennary, sialylated glycans was associated with disease progression in colon carcinoma patients (Boyaval *et al.*, 2022).

Thus, the initiation of the β1,6 branch point, regulation by MGAT5, represents a potential rate-limiting step in cell migration.

1.12.2.1 MGAT5

β1,6-N-acetylglucosaminyltransferase V (MGAT5) (E.C.2.4.1.155) is a Golgi enzyme responsible for the synthesis of tri- and tetra- antennary complex N-glycans. MGAT5 catalyses the addition of N-acetylglucosamine in β 1-6 linkage to the α-linked mannose of biantennary N-linked oligosaccharides.

MGAT5 has been repeatedly implicated in the formation of β1,6-branched glycans and in tumour progression (Dennis *et al.*, 1987; Lau and Dennis, 2008; Häuselmann and Borsig, 2014; Ščupáková *et al.*, 2021). β1,6-branched glycans in BC was found to be an independent risk factor for poor outcome (Handerson *et al.*, 2005). The presence of β1,6-branched glycans was found to be higher in breast invasive carcinoma compared to matched healthy breast tissue (Dennis, Demetrio and Dennis, 1991). An increase in branched glycans initiated by MGAT5, regulated tumour initiation in HER2+ breast cancer, and disruption of MGAT5 resulted significantly delayed onset of mammary carcinoma formation caused by HER2 (Guo *et al.*, 2010).

Additionally, an increased presence of β1,6-branched glycans in breast cancer metastases compared with patient-matched primary tumours (Handerson *et al.*, 2005; Ščupáková *et al.*, 2021).

1.12.3 High-mannose

High-mannose-type glycans are atypical in mammals. Macrophages and dendritic cells of the innate immune system express mannose receptors to distinguish between self- and invading organisms. Binding of these receptors with high-mannose glycoproteins triggers receptor-mediated endocytosis and phagocytosis as part of the host defence (Apostolopoulos and Mckenzie, 2005). Further, soluble mannose-binding lectins in the blood bind to high-mannose glycoproteins found on non-host cells. This binding triggers the complement cascade to initiate an adaptive immune response (Gadjeva, Takahashi and Thiel, 2004).

Despite this, high-mannose glycans have been demonstrated as a pan-cancer feature (Chatterjee, Ugonotti, *et al.*, 2021). Under normal conditions, high-mannose glycans are generally confined to the endoplasmic reticulum (ER) (Loke *et al.*, 2016). However, in cancer, proteins are commonly overexpressed. Increased rates of protein synthesis and cell growth can lead to the saturation of the glycosylation pathway and increased abundance of under-processed high-mannose glycoforms (Johns *et al.*, 2005; Chatterjee, Kawahara, *et al.*, 2021). Aberrant high-mannose glycans have been reported in many cancer entities including blood (Chatterjee, Kawahara, *et al.*, 2021), brain (Park *et al.*, 2020), ovarian (Everest-Dass *et al.*, 2016), breast (Liu *et al.*, 2013; Ščupáková *et al.*, 2021), gastric (Liu *et al.*, 2020), and liver tumours (NUCK *et al.*, 1993; Mendoza *et al.*, 1998).

High-mannose-type glycans have been implicated in crucial recognition events in cancer progression including cell-mediated immune response (Wong *et al.*, 2003), cell adhesion (DW *et al.*, 2012; Alonso-Garcia *et al.*, 2020), migration (Park *et al.*, 2020), and metastasis (Mendoza *et al.*, 1998; Legler, Rosprim, Karius, Eylmann, Rossberg, Ralph M Wirtz, *et al.*, 2018; Ščupáková *et al.*, 2021)

Aberrant regulation of ER mannosidases has been reported to contribute to the creation of this phenotype (Chatterjee, Kawahara, *et al.*, 2021).

1.12.3.1 MANEA

Endo-α-1,2-mannosidase (MANEA) (EC 3.2.1.130) is a type-II membrane protein located in the cis/medial-Golgi (Zuber *et al.*, 2017). MANEA is a glycosidase which catalyses the removal of $Glc_{1-3}Man$ from the immature glycan $Glc_3Man_9GlcNAc_2$ precursor transferred en bloc to nascent polypeptides (see Chapter 1.11.2.1). The protein is encoded by the *MANEA* gene, located at position 6q16.1 in the human genome (Hamilton et al., 2005).

The action of MANEA allows misfolded proteins to bypass the classical N-glycan biosynthesis pathway and ER-degradation cycle (Lubas and Spiro, 1988; Sobala *et al.*, 2020). The glycosylation pathway is a checkpoint route to ensure correct protein folding. In the classical pathway, lectins direct correctly folded glycoproteins to continue through the maturation pathway and identify misfolded glycoproteins and direct them for ER-associated degradation (Shenkman and Lederkremer, 2019). The bypassing of this process by MANEA could allow misfolded proteins to be expressed and secreted, disrupting normal cellular function.

It was found that compartmentalisation of mannosidases within this classical pathway slows down mannose trimming and allows time for nascent polypeptides to fold correctly (Shenkman and Lederkremer, 2019). Therefore, bypassing this classical pathway, which is usually a constraining factor for the rate of glycoprotein trimming and maturation, allows immature glycoproteins to continue through the glycoprotein biosynthesis pathway at a faster rate. The increased substrate available may saturate downstream glycosyltransferases and glycosidases, allowing for immature high-mannose/hybrid-type glycans to escape complete maturation. Further, misfolded proteins with immature N-linked glycans attached (high-mannose), may be sterically unavailable to be worked upon by downstream glycosyltransferases and glycosidases, further increasing the amount of under processed high-mannose/hybrid-type glycoproteins.

1.12.3.2 MAN1B1

ER α-1,2-mannosidase (MAN1B1) (EC 3.2.1.113) is a is a type-II membrane protein located in the ER (Gonzalez *et al.*, 1999). MAN1B1 is part of the glycosyl hydrolase 47 family and is encoded by the *MAN1B1* gene, located at position 9q34.3 in the human genome (Tremblay and Herscovics, 1999).

MAN1B1 is involved in glycoprotein quality control within the endoplasmic-reticulum-associated degradation (ERAD) pathway and catalyses the first mannose trimming step in mammalian N-glycan biosynthesis. MAN1B1 catalyses the removal of a single mannose residue from high-mannose $Man_9GlcNAc_2$ glycan to $Man_8GlcNAc_2$ isomer B (Tremblay and Herscovics, 1999).

Mutations of *MAN1B1* results in autosomal-recessive intellectual disability (Balasubramanian and Johnson, 2019). In addition, is activity can be inhibited with the class I alpha-mannosidase inhibitors, 1-deoxymannojirimycin and Kifunensine (Elbein *et al.*, 1991). Inhibition of this glycosidase with Kifunensine results in a complete shift in cellular N-linked glycans from complex-type to high-mannose-type glycans (**Figure 1.3**). MAN1B1 is therefore, crucial to glycan maturation and the formation of complex- and hybrid-type glycans.

1.12.3.3 MAN1A1, MAN1A2 and MAN1C1

α-1,2-mannosidase I (MAN1A1) (EC 3.2.1.113) is a type-II membrane protein located in the ER/*cis*-Golgi (E *et al.*, 1993). This glycosidase catalyses the removal of mannose residues from the high-mannose $Man_{8-9}GlcNAc_2$ glycan to form $Man_5GlcNAc_2$. The protein is encoded by the *MAN1A1* gene, located at position 6q22.31 in the human genome (Tremblay, Dyke and Herscovics, 1998).

MAN1A1, MAN1A2, MAN1C1 have overlapping substrate specificity (Moremen and Nairn, 2014). MAN1A1, MAN1A2, and MAN1C1 are members of the GH47 Golgi mannosidase I subfamily. These enzymes cleave α-1,2-bound mannose sugars from high-mannose glycans, resulting in the formation of 5-mannose glycans.

Inhibition on MAN1A1, resulting in increased high-mannose-type glycans has been demonstrated to modulate crucial recognition events in cancer progression including cell-mediated immune

response (Wong *et al.*, 2003) and cell adhesion (DW *et al.*, 2012). In breast tumour samples, high *MAN1A1* expression has been associated with longer-recurrence free survival and low *MAN1A1* expression was observed in metastatic phenotypes (Legler, Rosprim, Karius, Eylmann, Rossberg, Ralph M Wirtz, *et al.*, 2018; Park *et al.*, 2020).

Therefore, exploring the effects of MAN1A1 activity and the formation of the high-mannose phenotype and on breast cancer progression and metastasis may be of interest within this project.

1.12.3.4 MGAT1

β-1-2-N-acetylglucosaminyltransferase (MGAT1) (EC 2.4.1.101) is a type-II membrane protein located in the *medial*-Golgi (Hassinen *et al.*, 2010). It catalyses the transfer of a GlcNAc residue via α1-3 linkage to the core Man_5GlcNA_2 glycan structure (Varki and E., 2015). It is encoded by the *MGAT1* gene, and located at position 5q35 in the human genome (Kumar *et al.*, 1990; Tan *et al.*, 2008). It is the initiating step in the formation of hybrid- and complex-type glycans, and in its absence only high-mannose-type glycans are formed (Yip *et al.*, 1997).

As with MAN2A1, MGAT1 activity contributes to the formation of highly branched N-glycans. MGAT1 has also been demonstrated to be upregulated in breast cancer (Potapenko *et al.*, 2015). Therefore, exploring the effects of altered MGAT1 activity on tumour establishment and metastasis may be of interest.

1.12.3.5 MAN2A1

Golgi α-mannosidase II (MAN2A1) (EC 3.2.1.114) is a type-II membrane protein located in the *medial*-Golgi. It is a glycosidase enzyme which catalyses the removal of two mannose units from the $GlcNAcMan_5GlcNAc_2$ intermediate, and is the first step in the formation of complex-type N-glycans (Van Den Elsen, Kuntz and Rose, 2001). The protein is encoded by the *MAN2A1* gene, located at position 5q21.3 in the human genome (Misago et al., 1995). In the absence of MAN2A1 only hybrid glycans are formed (**Figure 1.3**).

MAN2A1 can be inhibited with the selective enzyme inhibitor Swainsonine, preventing the formation of complex and branched N-glycans. Swainsonine has repeatedly been demonstrated to elicit anticancer and antimetastatic effects (Olden *et al.*, 1991; Demetriou *et al.*, 1995; You *et al.*, 2012; Ren *et al.*, 2017). This is mainly attributed to it preventing the expression of β1,6-branched glycans, which are highly implicated in the metastatic capability of cancerous cells (Varki, 1993; Demetriou *et al.*, 1995; Taniguchi and Kizuka, 2015). MGAT5 is responsible for the formation of these highly branched β1,6-GlcNAc glycans, however, the reduction in branching and antimetastatic effects caused by Swainsonine suggests that MAN2A1 also contributes to cancer malignancy.

In addition, the glycosylation pathway has several competition points in which multiple enzymes can act on the same substrates. With regards to glycan branching, GnT-III, which catalyses the formation of GlcNAc bisecting glycans competes with both MAN2A1 and MGAT5 (Taniguchi and Kizuka, 2015). Once GnT-III has catalysed the formation of a GlcNAc bisecting glycan, MAN2A1 can no longer act, and glycans are fixed in a hybrid state (Harpaz and Schachter, 1980). GnT-III activity results in a decrease in N-glycan branching and has been demonstrated to suppress malignancy and metastasis, the opposite effects seen with MGAT5 activity (Yoshimura *et al.*, 1995). Therefore, the interplay between enzymes competing for identical substrates at competition points with the N-linked glycosylation pathway is important to understanding how cancer cells manipulate glycan modifications to progress malignancy.

1.13 Antibodies

To identify and counteract foreign organisms or antigens, B-cells release antibodies. These Abs are glycoproteins classified within the immunoglobulin superfamily, comprised of two heavy chains and two light chains, which define its isotype. In the clinical setting, therapeutic monoclonal antibodies (mAbs) are typically of the γ-immunoglobulin (IgG) isotype due to its high stability and well-studied mechanism of action (MOA) (Muhammed, 2020). The hypervariable regions of the heavy and light chains combine to create the antigen-binding domain, known as the Fab. The four constant domains

collectively serve as the fragment crystallizable (Fc), responsible for initiating Fc-dependent effector functions (Brandsma *et al.*, 2015).

The MOA of mAbs can vary in different applications. For instance, rituximab, an anti-CD20 mAb, induces cell death by binding to surface receptors, triggering a signaling cascade that leads to apoptosis (Alas and Bonavida, 2001). Other mAbs, such as anti-HER2 mAb trastuzumab, inhibit receptor-ligand interactions, and can achieve their desired effects by either blocking the receptor domain or eliminating the soluble ligand from circulation (Nahta and Esteva, 2006). Additionally, mAbs can initiate Fc-dependent effector functions such as antibody-dependent cell-mediated cytotoxicity (ADCC), antibody-dependent cellular phagocytosis (ADCP), and complement-dependent cytotoxicity (CDC). **Figure 1.4** shows a simplified schematic of ADCP activity induced by the clinical anti-HER2 mAb, Trastuzumab.

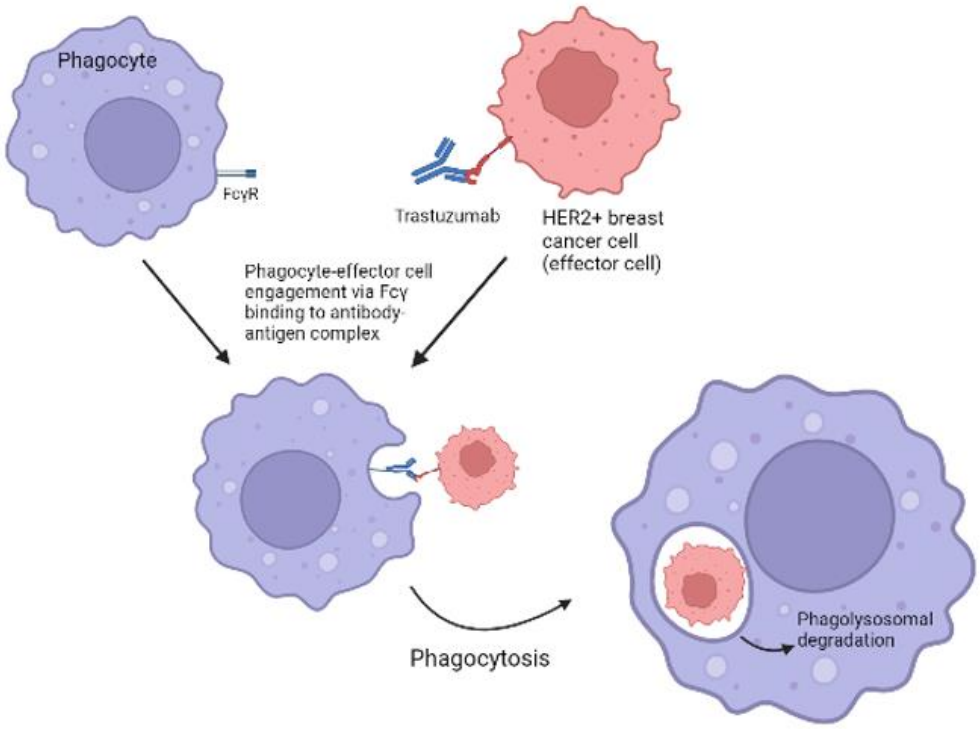

Figure 1.4: Antibody-dependent cellular phagocytosis induced by anti-HER2 mAb Trastuzumab.

1.13.1 Antibody effector functions

Humans express classical FcγR which are termed as activating, inhibitory, and glycosylphosphatidylinositol (GPI)-anchored Fc receptors. FcγRI (CD64), FcγRIIA (CD32A), FcγRIIc

(CD32C), FcγRIIIa (CD16A) are activating (Nimmerjahn and Ravetch, 2006), FcγRIIb is inhibitory (Teige, Mårtensson and Frendéus, 2019), and FcγRIIIb is GPI-anchored (Gogesch *et al.*, 2021). The FcγRs differ in their cellular distribution, where FcγRIIA (CD32A) which mainly mediates ADCP is expressed on monocytes, macrophages, and dendritic cells (DCs) (Gogesch *et al.*, 2021), and FcγRIIIa (CD16A) which mainly mediates ADCC is expressed on macrophages and Natural Killer (NK) cells (Gogesch *et al.*, 2021). FcγRs are mainly expressed on innate immune cells, but can also be expressed on activated T cells (Nimmerjahn and Ravetch, 2006; Chauhan, 2016).

ADCC and ADCP are initiated when antibody-antigen complexes bind the correct balance of activating/inhibitory FcγRs. For example, excess CD16A (FcγRIIIa) binding will initiate ADCC, excess CD32A (FcγRIIA) binding will initiate ADCP, and excess FcγRIIb binding will counteract activating signals and initiate no response (Gogesch *et al.*, 2021). FcγR binding of activating or inhibitory receptors initiates crosslinking and subsequent signaling through immunoreceptor tyrosine-based activation motifs (ITAMS) or immunoreceptor tyrosine-based inhibition motifs (ITIMS) (Brandsma *et al.*, 2015; Teige, Mårtensson and Frendéus, 2019). This cytoplasmic signaling stimulates an intracellular increase in calcium which drives calcineurin/calmodulin-mediated dephosphorylation of nuclear factor activated T cells (NFAT) allowing its nuclear translocation and regulation relevant target genes (Teige, Mårtensson and Frendéus, 2019), mediating cell activation, endocytosis, or phagocytosis (Daëron, 1997).

1.13.2 Clinical mAb production

Originally, mAbs were of murine origin and produced by hybridomas (Köhler and Milstein, 1975). However, drawbacks such as the high immunogenicity, short half-life due to low affinity toward the human neonatal receptor (FcRn), and poor efficacy drove the production of chimeric antibodies (Ober *et al.*, 2001; Pyzik *et al.*, 2015). Chimeric mAbs were developed by fusing the variable antigen-specific region of murine mAb with the constant domains of a human mAb, reducing immunogenicity, extending half-life, and increasing efficacy (Morrison *et al.*, 1984; Presta, 2006). Humanised mAbs were developed to further reduce immunogenicity, in which the murine

complementarity determining regions (CDR) are fused onto human variable heavy and light domains (Jones *et al.*, 1986). Humanised mAbs are approximately 95% human origin by amino acid sequence, and significantly reduce immunogenicity (Jones *et al.*, 1986; Hwang and Foote, 2005). Fully human mAbs can now be produced with advancements in phage display technologies based on human single chain Fv libraries (Vaughan *et al.*, 1996; Winter *et al.*, 2003), and transgenic mouse strains which express human antibody variable domains (Cohenuram and Saif, 2007).

1.13.3 Antibody glycosylation

MAbs are large molecules with requirements of correct assembly and glycosylation. The most common mAbs in the clinic are of IgG1 isotype and have a single N-linked glycan at position N297 in each of the heavy chains (**Figure 1.5**). Glycosylation needs to be carefully monitored, since it is affected by the cell line used, nutrient and supplement availability, pH and cell growth phase (Zhou *et al.*, 2008; Slade *et al.*, 2016; Zhang *et al.*, 2019). Differences in glycosylation can have major implications in antibody function (Roy Jefferis, 2009), immunogenicity (Prabakaran *et al.*, 2012; Zavala-Cerna *et al.*, 2014), and stability (Zheng, Bantog and Bayer, 2011).

Glycan composition has been demonstrated to modulate interactions between the Fc to FcγRs, and in turn impact their ability to initiate antibody effector functions. For example, deglycosylation of IgG1 abolishes its capacity to bind FcγRs and consequently results in loss of effector functions (Tao and Morrison, 1989; Krapp *et al.*, 2003). High-mannose glycans increase binding to FcγRIIIA, enhancing ADCC activity but reducing C1q binding (Zhou *et al.*, 2008; Yu *et al.*, 2012). Afucosylated glycoforms have increased binding to FcγRIIIA and enhanced ADCC potency (Royston Jefferis, 2009). Increased Fc sialylation results in decreased FcγRIIIA engagement and decreased ADCC potency (Raju and Lang, 2014). Terminal galactosylation has been demonstrated to enhance C1q binding, ADCC and ADCP *in vitro* (Tsuchiya *et al.*, 1989; Chung *et al.*, 2014; Peschke *et al.*, 2017), its presence *in vivo* has been suggested to mediate anti-inflammatory activity through FcγRIIB binding (Karsten *et al.*, 2012).

Additionally, the glycoforms can have implications on antibody confirmation, stability, and half-life. For example, deglycosylated antibodies have higher aggregation rates, are less thermally stable, and have increased susceptibility to proteolytic cleavage (Zheng, Bantog and Bayer, 2011). High-mannose glycans have been demonstrated to increase the rate of antibody serum clearance compared to hybrid- or complex-type glycans (Goetze *et al.*, 2011). Increased terminal sialylation improves serum half-life (Raju and Lang, 2014). However, it is suspected that sialylation alters the overall charge of the molecule, impacting cellular antigen binding and increasing susceptibility to proteases (Raju and Lang, 2014).

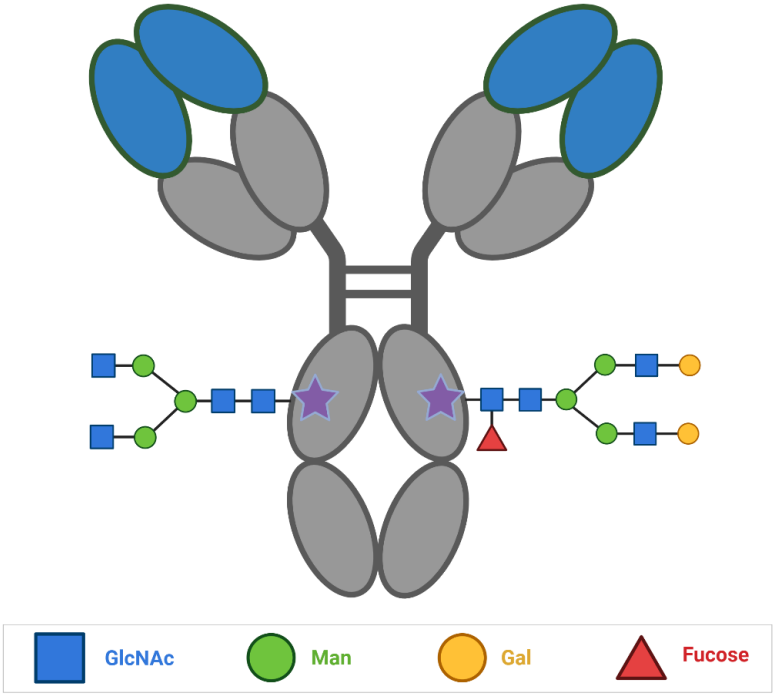

Figure 1.5: IgG1 structure and glycosylation pattern. IgG1 isotype antibody comprising two heavy chains and two light chains, and a hinge region. Variable antigen binding domains are coloured in blue, and constant light and heavy chains are coloured grey. A single N-linked glycan resides at position asparagine 297 of each heavy chain is indicated by a purple star.

1.14 Therapeutic strategies

The development of targeted therapies has revolutionised breast cancer treatment (Schick, Ritchie and Restini, 2021). Traditional cancer management treatment consisted of chemotherapy, radiation therapy and surgery. These methods are indiscriminate and invasive, and often come with significant side effects (Moo *et al.*, 2018). In addition, these treatments are not effective for all cancer types and grades and do not increase overall survival when used as a monotherapy (HB *et al.*, 2009; G *et al.*, 2011). Treatment options now consist of targeted therapies, and many targeted therapies approved for clinical use by the European Medicines Agency (EMA) or Food and Drug Administration (FDA) are immunotherapies. Cancer immunotherapies aim to stimulate and enhance the immune response to effectively destroy cancer cells. There are several types of approved cancer immunotherapies, including direct targeting antibodies, immunomodulation, and cancer vaccines. Advances in targeted therapies mean the five-year relative survival for non-metastatic disease is approximately 80% (NIH, 2020b). However, these therapies are not always appropriate for all individuals, can be accompanied by side effects and drug toxicity, and long-term treatment can lead to therapy resistance (BV, S and R, 2016; Moo *et al.*, 2018; Schick, Ritchie and Restini, 2021). Factors such as tumour heterogeneity and the presence of cancer stem cells are thought to contribute to therapy resistance (F *et al.*, 2017). Therefore, the identification of more reliable targets and the development of targeted therapies is still crucial.

Trastuzumab is a humanised monoclonal antibody and was the first targeted therapeutic against HER2 (Hudziak *et al.*, 1989). It blocks homodimerisation through binding domain IV of HER2 (Hudis, 2007). Treatment with Trastuzumab has shown a significant increase in time to disease progression and improved overall survival for patients (Ennis S Lamon *et al.*, 2001; Marty *et al.*, 2005). Following the success of Trastuzumab, other anti-HER2 mAbs were developed. One such example is Pertuzumab, which blocks heterodimerisation by binding HER2 at domain II (Franklin *et al.*, 2004). **Table 1.4** describes the FDA-approved targeted therapeutics available for breast cancer treatment.

Associations between cardiotoxicity and anti-HER2 treatment (Slamon *et al.*, 2001a) mean these treatments are not always appropriate for all individuals, and regular cardiac screening has to be employed (Seidman *et al.*, 2002). Additionally, around 70% of patients are unresponsive to Trastuzumab treatment, and therapeutic resistance throughout therapy occurs in almost all patients (Valabrega *et al.*, 2005; Gallardo *et al.*, 2012). Developing novel anti-HER2 antibodies to combat these challenges are therefore required.

The use of antibody-drug conjugates has also proved a promising therapeutic approach for breast cancer. Ado-trastuzumab and Sacituzumab have been FDA-approved for use in breast cancer, targeting HER2 or TROP-2, respectively. These molecules deliver cytotoxic chemotherapy drugs which induce apoptosis and inhibit tumour growth (Goldenberg *et al.*, 2015; Pavone *et al.*, 2021). TROP-2 is a glycoprotein commonly expressed on cancers which mediates proliferation and invasion (Goldenberg, Stein and Sharkey, 2018). Anti-TROP-2 therapeutics offer invaluable treatment options for TNBC patients, and clinical trials with Sacituzumab have demonstrated its benefit in increasing progression-free and overall survival (Bardia *et al.*, 2019; Rugo *et al.*, 2020).

Immune checkpoint inhibitors are another valuable therapeutic approach for breast cancer treatment. Cancer cells can upregulate ligands such as PD-L1, which binds self-tolerance receptors on T-cells, such as PD-1, to mediate an immunosuppressive effect and promote T-cell exhaustion (Matikas *et al.*, 2019; Ishida, 2020). Antibody-based therapeutics for breast cancer treatment which disrupt this interaction and stimulate anti-tumour response include Pembrolizumab and Atezolizumab (**Table 1.4**). Clinical trials have demonstrated their efficacy to increase progression-free and overall survival for TNBC patients (Cortes *et al.*, 2020; Schmid *et al.*, 2022), however, they have also highlighted their notable adverse effects and toxicity (Martins *et al.*, 2019).

Therapies which target stromal cells which support and influence the invasive and proliferative nature of tumour cells, may also be of importance to consider (Hofmeister, Schrama and Becker, 2008). Targeted therapies, such as Bevacizumab, are currently approved for use in multiple cancer entities either as a monotherapy or in combination with chemotherapies/targeted

immunotherapies (Xu *et al.*, 2022), however, its approved use in metastatic breast cancer was revoked by the FDA due to safety concerns (Montero *et al.*, 2012). Thus, although tumour stroma targeting may be attractive, it should be pursued with caution (Valkenburg, De Groot and Pienta, 2018; Xu *et al.*, 2022).

Table 1.4: Targeted therapies EMA/FDA approved for Breast Cancer treatment (European Medicines Agency, 2021; National Cancer Institute, 2022; Reichert, 2023). Table adapted from (Reichert, 2023).

Generic name	Brand name	Target/Isotype	Modification	BC treatment option
Pembrolizumab	Keytruda	PD-1; Humanised IgG4	S228P	TNBC. High risk of spread of recurrence. In combination with chemotherapy.
Atezolizumab	Tecentriq	PD-L1; humanised IgG1	aglycosylated N297A	TNBC. High risk of spread of recurrence. In combination with chemotherapy.
Trastuzumab	Herceptin	HER2 / humanised IgG1	-	HER2+ BC
Pertuzumab	Perjeta	HER2; humanised IgG1	-	HER2+ BC
Margetuximab	MARGENZA	HER2; Chimeric IgG1-modified ↑CD16 ↓CD32B	F243L, R292P, Y300L, V305I, P396L	HER2+ metastatic BC
Ado-trastuzumab	Kadcyla	HER2; humanised IgG1; Tubulin Inhibitor	-	HER2+ BC
Sacituzumab govitecan	Trodelvy	TROP-2; humanised IgG1; Topo I Inhibitor	-	Metastatic TNBC
Trastuzumab deruxtecan	Enhertu	HER2; humanised IgG1; Topo I Inhibitor	-	HER2+ Metastatic BC

1.14.1 Carbohydrate-based therapeutics

Aberrant glycosylation is a well-established hallmark of cancer (Fuster and Esko, 2005; Munkley and Elliott, 2016; Gray *et al.*, 2020). Recent advances in understanding the presence and role of aberrant

glycans in cancer have been influential in guiding therapeutic design. Indeed, the glycosylation state of cell surface receptors influences ligand binding and efficacy of target immunotherapies. Therefore, glycan-based therapeutics has become an emerging field, and alterations in glycosylation can therefore be capitalised therapeutically as either biomarkers for cancer detection, or as novel molecular targets for therapy.

Aberrant glycan antigens such as carbohydrate antigen 19-9 (CA 19-9) (sialyl Lewis^{a}), CA 72-4, CA 15-3, and CEA are proving reliable and sensitive serum cancer biomarkers and are starting to be employed clinically (Uehara *et al.*, 2008; UK and RS, 2011; MARIAMPILLAI *et al.*, 2017; Ning *et al.*, 2018). CA 19-9 is a cell surface glycoprotein complex used as a biomarker for pancreatic and bile duct cancer (Lee, Teng and Shelat, 2020). The glycan epitope, Sialyl-Tn have been reported to be overexpressed in ovarian and gastrointestinal cancers (Shimada *et al.*, 2014), and suggested for use as a serum biomarker to assess unfavourable outcome (Takamizawa *et al.*, 2022). Additionally, carcinoembryonic antigen (CEA) and CA 15-3 have been approved by the FDA as diagnostic markers for metastatic breast cancer (Uehara *et al.*, 2008; Fu and Li, 2016). CA 15-3 is one of the products of the Mucin1 (MUC-1) gene; MUC-1 is overexpressed on many cancers including breast cancer (O'Hanlon et al., 1995). CEA is part of the immunoglobulin superfamily, and is comprised of 29 genes, including a pregnancy-specific subgroup (Thompson, Grunert and Zimmermann, 1991).

Therapeutic vaccine development towards tumour-associated carbohydrate antigens is also of interest. Glycans are poorly immunogenic and don't induce a strong T-cell mediated immune response (Wei, Wang and Ye, 2018). Therefore, they are often conjugated to carrier proteins such as keyhole limpet hemocyanin (KLH) and tetanus toxoid (TT) (Kagan *et al.*, 2005; Gaidzik, Westerlind and Kunz, 2013). Vaccines have been developed against ganglioside antigens (e.g. GD2, GD3, and GM3) (Rosenbaum *et al.*, 2022), Mucin-related O glycan antigens (e.g. Tn STn and Tf) (Holmberg and Sandmaier, 2004), blood group Lewis antigens (e.g. sialyl Lewis^{a} sialyl Lewis^{x,} Lewis^{y}) (Buskas, Li and Boons, 2004), and Globo-H series antigens (e.g. Globo-H, Gb3, SSEA-3) (Huang *et al.*, 2013).

Although these monovalent vaccines, gave promising preclinical results, many candidates elicited low immune responses in human clinical trials.

Multivalent vaccines targeting multiple tumour-associated carbohydrate epitopes were also developed in the hope of improving clinical effectiveness (Ragupathi *et al.*, 2006; O'Cearbhaill *et al.*, 2016). Indeed, extensive research into the type of adjuvant, carrier (Richichi *et al.*, 2014; Biswas, Medina and Barchi, 2015; Feng, Shaikh and Wang, 2016), and targeted antigen(s) (Cai *et al.*, 2014; Sun *et al.*, 2016; Kavunja *et al.*, 2017; Yin *et al.*, 2017) is being conducted in the hope to improve immune responses and reduce cross reactivity, to deliver carbohydrate-based vaccines to the market (Wei, Wang and Ye, 2018; Mettu, Chen and Wu, 2020; Anderluh *et al.*, 2022).

Targeted glycan therapies are also being developed to block the interactions of immunosuppressive glycans with inhibitory immune receptors in cancer. Blockade of Gal-1 signalling promoted tumour rejection and enhanced T cell-mediated response tumour immune response (Rubinstein *et al.*, 2016). Palleon Pharmaceuticals have recently launched a Phase 1/2 clinical trial with their Bi-Sialidase therapeutic, E-602 (Sharma *et al.*, 2022). E-602 is a fusion protein comprising engineered human sialidases and the human IgG1 Fc region. The sialidase component of E-602 cleaves terminal sialic acid residues from sialoglycans on both immune cell subsets and tumour cells. Sialoglycans are immunosuppressive across multiple cancers and associated with poor outcomes (see Chapter 1.12.1). Preclinical studies demonstrated that sialidase-mediated cleavage of terminal sialic acids restored the immune function of exhausted-like T cells, and enhanced dendritic cell priming and naïve T cell activation (Peng *et al.*, 2021). E-602 has demonstrated antitumour activity as monotherapy and in combination with PD-1/PD-L1 blockade (Che *et al.*, 2022). Additionally, toxicity studies in non-human primates have demonstrated E-602 to be well tolerated and have a wide safety margin (Cao *et al.*, 2022).

Pairing this technology with tumour-associated antigens (TAA) has seen the production of anti-HER2-Sialidase and anti-PD-L1-Sialidase conjugates. Both constructs desialylated their respective targets, $HER2^{+}$ BC cells or PD-L1 expressing tumour and immune cells, more efficiently than non-

targeted Bi-Sialidase (Che *et al.*, 2022). Anti-PD-L1-Sialidase demonstrated a dose-dependent inhibition of tumour growth, and modulation of immune cell infiltration in the TME of transgenic mouse colon carcinoma models, with improved efficacy relative to PD-1/PD-L1 blockade or Bi-Sialidase alone (Che *et al.*, 2022). Anti-HER2-Sialidase demonstrated effects of delayed tumour growth, enhanced immune infiltration and prolonged survival of mice with low HER2-expressing and Trastazumab-resistance BC (Paszek *et al.*, 2014; Gray *et al.*, 2020). Further, this construct showed increased efficacy when delivered in combination with anti-PD1 or anti-CTLA4 monoclonal antibodies (mAbs) (Xiao *et al.*, 2016; Gray *et al.*, 2020). More recently, the production of an engineered bacterial protease with dual-glycan and peptide affinity towards mucins and HER2 has demonstrated promising results (Pedram *et al.*, 2023). This therapeutic approach enabled the targeted degradation of cancer-associated mucins in murine breast cancer models has demonstrated reduced cancer cell viability, primary tumour burden, and metastatic spread (Pedram *et al.*, 2023).

Passive antitumour immunotherapies targeting glycans are also of interest. Anti-GD2 antibodies were the first glycan-targeting immunotherapeutic drug approved by the European Medicines Agency (Spring and Therapeutics, 2015; European Medicines Agency, 2017). These constructs target disialoganglioside GD2, a sialic acid-containing glycosphingolipid antigen present on neuroblastoma cells (Greenwood and Foster, 2017; Mora, 2018). Since then, antibodies against other targets such as GD3 for treatment of patients with melanoma (Tarhini *et al.*, 2017); Fucosyl-GM1 for treatment in small cell lung carcinoma patients (Chu *et al.*, 2022); Globo-H for treatment in patients with advanced solid tumours (Tsimberidou *et al.*, 2023); Lewis^{y} in ovarian cancer patients (Smaletz *et al.*, 2021); and Sialyl Lewis^{a} for treatment in pancreatic cancer patients (O'Reilly *et al.*, 2018), are undergoing clinical trials.

An alternative carbohydrate approach is to modulate the TME. Galectin antagonists, either as competing sugars of neutralising antibodies are currently being explored for their therapeutic potential in clinical trials (Gordon-Alonso, Demotte and van der Bruggen, 2014; N *et al.*, 2014; NIH,

2018; L *et al.*, 2019). As described in Chapter 1.12, increased extracellular release of galectin-3 forming glycoprotein-galectin lattices contributes to T-cell dysfunction, increased angiogenesis and tumour immune evasion (Gordon-Alonso, Demotte and van der Bruggen, 2014; Gordon-Alonso *et al.*, 2017b, 2017a). Therefore, this avenue could provide a potential route for modulating the TME and increasing immune infiltration.

This recent work has highlighted the potential of carbohydrate-based therapies. Carbohydrate-based therapies may be fundamental to establishing an anti-tumour microenvironment and slowing metastasis, the main reason for breast cancer-related deaths (Harbeck *et al.*, 2019; Gray *et al.*, 2020). Further research to identify novel glycan therapeutic targets and develop efficacious targeted therapies is still required.

1.14.2 Delivery of therapeutics

Currently, most clinically approved drugs for cancer are protein/antibody-based biologics or small molecules. However, nucleic acid drugs are starting to be developed as a novel therapeutic strategy.

Nucleic acid drugs act to control the biological function of the cell by either regulating gene expression or utilising the cell's expression machinery. Targeting occurs based on nucleotide sequence information, and thus drugs can be designed against target molecules regardless of their localisation (Ransohoff, Wei and Khavari, 2017; Fox *et al.*, 2018). Additionally, once the target gene sequence has been identified nucleic acid drugs can be rapidly and efficiently made (Heilbron *et al.*, 2021).

Nucleic acid drugs that work to modify or mediate native gene expression include antisense oligonucleotide (ASO) and small interfering RNAs (siRNAs) which inhibit gene function (Hoy, 2018; Keam, 2018; Hara, Yoshioka and Yokota, 2020), microRNA (miRNA) mimics which restore the function of dysregulated miRNAs (Hosseinahli *et al.*, 2018).

mRNA drugs are directly introduced into the target cell, utilising the cell's expression machinery to produce a therapeutic protein (Sahin, Karikó and Türeci, 2014; Sahin *et al.*, 2017). mRNA drugs

enable the production of therapeutic proteins that retain their native conformations and post-translational modifications, such as glycosylation, which can be challenging to achieve in traditionally produced recombinant proteins (Zhou *et al.*, 2008; Slade *et al.*, 2016; Zhang *et al.*, 2019). Importantly, mRNA-based approaches have no requirement for nuclear delivery therefore there is no risk of chromosome integration.

Self-replicating RNAs (Replicons) are the next generation of mRNA-based drugs. Replicon delivery systems are typically based on positive-strand RNA viruses, encoding non-structural proteins (replicase) and structural proteins (replaced by genes of interest (GOI) (Hikke and Pijlman, 2017; Lundstrom, 2020; Comes, Pijlman and Hick, 2023). Once delivered to the target cell, Replicon mRNA is translated to produce the replicase complex which can efficiently self-amplify the original mRNA (AB *et al.*, 2018). The clear advantage is that Replicons can be administered at lower doses than conventional nucleic acid delivery methods (mRNA and DNA plasmids) (AB *et al.*, 2018). Despite this, research into its use to deliver large therapeutics such as mAb for cancer treatment is limited.

1.15 Aim and Objectives

The aim of this thesis is to investigate the significance of high-mannose N-glycans in breast cancer progression and evaluate their potential as a therapeutic target.

Specifically, this research aims to achieve the following objectives:

1. Characterise High-Mannose Glycans: To investigate the prevalence of high-mannose glycans in clinically relevant breast cancer samples and cell lines, elucidating their presence in the disease context.

   Functional Assessment: To determine the functional implications of high-mannose glycans by employing established migration and invasion assays, providing insights into how these glycans influence key cellular behaviours related to breast cancer progression.

We will also employ *in vivo* techniques to assess the impact of high-mannose glycans on breast cancer growth and metastasis, providing a more comprehensive understanding of their role in the disease.

2. Therapeutic Development: To design and create a novel antibody construct capable of specifically targeting high-mannose glycans and investigate its potential as a novel treatment approach for breast cancer.
3. Manufacturing Solutions: To address manufacturing challenges associated with monoclonal antibody production, and to provide a potential solution to overcome the manufacturing challenges which may impede the clinical application of these constructs.

Thus, this thesis seeks to advance our understanding of high-mannose glycans in breast cancer and potentially contribute to the development of innovative therapeutic strategies for improved breast cancer outcomes.

Chapter 2 Materials and Methods

2.1 Ethics

Ethical approval was obtained by Southampton University Hospitals NHS Trust from the East of Scotland Research Ethics Service for the use of leukocyte cones (16/ES/0048, ERGO 19660.A7). Leukocyte cones were obtained from the National Blood Service, Southampton University Hospital.

C57BL/6 mice for *in vivo* experiments were obtained from Charles River Laboratories. Animal procedures were approved by the University of Southampton Ethical Committee, conducted in accordance with the UK Home Office Animal and Scientific procedures Act 1986, and reviewed and approved by the UK Home Office (project licenses P81E1297 and PP9205656a, ERGO 64937 and 70138).

2.2 Reagents

Stocks of commercial trastuzumab (Herceptin) and rituximab (Rituxan) were generously donated from Southampton General Hospital.

2.3 Cells

The human breast cancer cell line SKBR3 was generously donated from CRUK. MDA-MB-453, MCF7, and EO771 were purchased from ATCC. MDA-MB-231 was purchased from ECACC. HCC1143 was gifted from Luis Coy, University of Southampton. EO771.LG was gifted from Dr Bin-Zhi Qian and Professor Jeffrey W Pollard, University of Edinburgh.

2.4 DNA vectors

pFuse2ss vector was employed for delivery of 2G12 HC and 2G12 LC-Herceptin scFv. cDNA sequences for 2G12 Fab (VH and Cγ1) were joined with hIgG1-Fc region cDNA sequences comprising (Cγ2 and Cγ2 + hinge) to create the 2G12 HC construct. cDNA sequences for 2G12 LC were joined

by a flexible linker to Herceptin variable heavy cDNA sequence, which was joined by a flexible linker to Herceptin variable light cDNA sequence. pFuse2ss vector harboured a human IL2 secretory signal sequence to easily isolate recombinant proteins from supernatant.

For Replicon delivery the VEEV vector was employed. Trastuzumab HC and LC cDNA sequences were encoded, separated by an internal ribosomal entry site sequence. The human IL2 secretory signal sequence was encoded upstream of the construct, to allow for secretion of recombinant Trastuzumab.

2.5 Cell line maintenance

2.5.1 Cell line passaging

Cell line maintenance was conducted using aseptic techniques in a Class II Microbiological Safety Cabinet. Cryopreserved cells were thawed rapidly in a water bath at 37˚C and washed with Dulbecco's Phosphate-Buffered Saline (DPBS), no calcium, no magnesium (Gibco™, Cat: 14190144), to remove residual DMSO. Cells were seeded in a Corning T25 cell culture flask in complete Roswell Park Memorial Institute 1640 Medium (RPMI). Cells were maintained without shaking at 37˚C, 5% CO_2 and passaged at 70% confluency. Cell morphology and viability were observed using a light microscope.

Complete Medium (cRPMI) was made by supplementing 500 mL RPMI (Gibco™, Cat: 21875034) with: 50 mL Fetal Calf Serum (FCS) (Sigma, Cat: F9665); 5 mL Penicillin-Streptomycin (Gibco™, Ref: 15140122); 5 mL Sodium pyruvate 100mM (Gibco™, Cat: 11360039); and 5 mL L-Glutamine 200 mM (Gibco™, Cat: 25030081). For EO771 cells lines 5 mL HEPES 1 M (Gibco™, Cat: 15630080) was additionally added.

Cell density and viability was measured using the Invitrogen Countess II Automated Cell Counter. RPMI medium was removed and cells were washed with DPBS before dissociation. Washing was conducted to remove excess FCS and divalent cations, which both inhibit trypsin and facilitate

cadherins. Cells were dissociated using TrypLE™ Express Enzyme (1X), with EDTA (a divalent chelator) (Gibco™, Cat: 12604013) and incubated at 37˚C, 5% CO_2 for 3 minutes. Cells were observed for detachment and diluted to half the culture flask volume with complete RPMI. Agitated cells were transferred to a sterile conical tube and centrifuged at 200 x g for 5 minutes. The cell pellet was resuspended in complete RPMI, and 10 *µL* of sample was removed for cell count. Equal volumes of sample and Trypan Blue Stain (0.4%) (Invitrogen, Cat: 15250061) were mixed and pipetted into the Countess chamber slide, and cell density and viability were measured. Cells were diluted to seeding density with complete RPMI and returned for culture.

2.5.2 Cryopreservation

2.5 X 10^6 cells were resuspended in 1 mL freezing medium (5% sterile DMSO, 45% FBS, 50% complete medium) and aliquoted into cryovials. Vials were placed in a freezing container at -80˚C overnight, allowing samples to cool at a rate of -1˚C/minute. Vials were transferred to liquid nitrogen for long-term cryopreservation.

2.5.3 Enzyme inhibition

To explore the effects of Kifunensine, cells were seeded in an appropriately sized flask and cultured overnight at 37˚C, 5% CO_2 to allow adhesion to the culture dish. 10 µM Kifunensine was added, and cells were cultured at 37˚C, 5% CO_2 for an additional 48 hours.

2.6 MTS assay

Cell proliferation was tested using the CellTiter 96 Aqueous Assay (Promega, UK), according to the manufacturer's instructions. Cells were plated at 10,000 cells/well in 100 µL of cRPMI and incubated at 37˚C, 5% CO_2 for 24 or 48 hours. Absorbance was measured at 490 nm with a spectrophotometer.

2.7 Transwell assays

Cells (5 X 10^5 cells/300 µL) in serum-free RPMI were applied to the top chamber of the Fibronectin-coated migration chambers (Cytoselect™, Cat: CBA-100-FN) with a pore size of 8 µm. Transwells were placed into a migration plate containing 500 µL complete RPMI containing 10% FBS as a chemo-attractant. Cells were incubated for 4.5 hours at 37˚C, 5% CO_2.

The media was aspirated, and the interior of the inserts were carefully swabbed 2-3 times with damp cotton-tipped swabs to remove non-migratory cells. Care was taken to not puncture the polycarbonate membrane. Inserts were submerged in 100% methanol chilled to -20˚C and incubated at RT for 10 mins to fix cells. Inserts were washed twice with sterile water and allowed to air dry at RT. To stain migratory cells, inserts were submerged in 0.2% crystal violet (Sigma-Aldrich, Cat: 61135) solution and incubated at RT in the dark for 30 mins. Crystal violet stain was removed, and inserts were washed twice with sterile water and allowed to air dry at RT prior to imaging.

Migratory cells were counted using five fields of view per membrane at 20X magnification. Migration assays were run in triplicate. The results represent the mean number of migrated cells +/- SEM of a triplicate experiment. Paired students T-test were employed to explore statistical significance. A simplified schematic of the protocol is described in **Figure 2.1**.

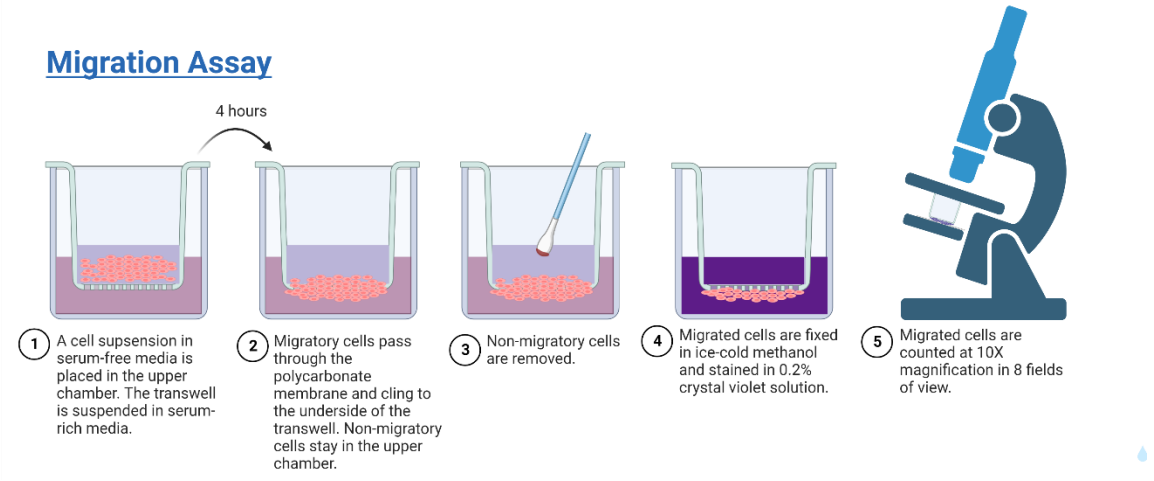

Figure 2.1: Simplified schematic of a migration assay.

2.8 Scratch wound assay

Culture inserts (Thistle Scientific, Cat: 80209-150) were placed in the centre of a 6 well plate, and 0.5 X 10^6 cells/mL were seeded in and around the insert. Plates were incubated for 24 hours at 37˚C, 5% CO_2 to form a confluent monolayer.

Media was aspirated from the wells, and cell inserts were gentle peeled off the plate to mimic a 'scratch'. The scratch was carefully washed with PBS to remove cell debris and fresh media was added to the wells.

Plates were incubated at 37˚C, 5% CO_2 and cells were imaged at 10X magnification at the same intersection of the insert every 24 and 48 hours.

Cell images were analysed using Tscratch, which calculated the percentage of the wound 'open'. The percentage of wound open was plotted across 24 and 48 hours for each condition.

Where possible, scratch wound assays were run in triplicate. The results represent the mean number of migrated cells +/- SEM of a triplicate experiment. Multiple paired T-tests were employed to assess statistical significance. A simplified schematic of the protocol is described in **Figure 2.2**.

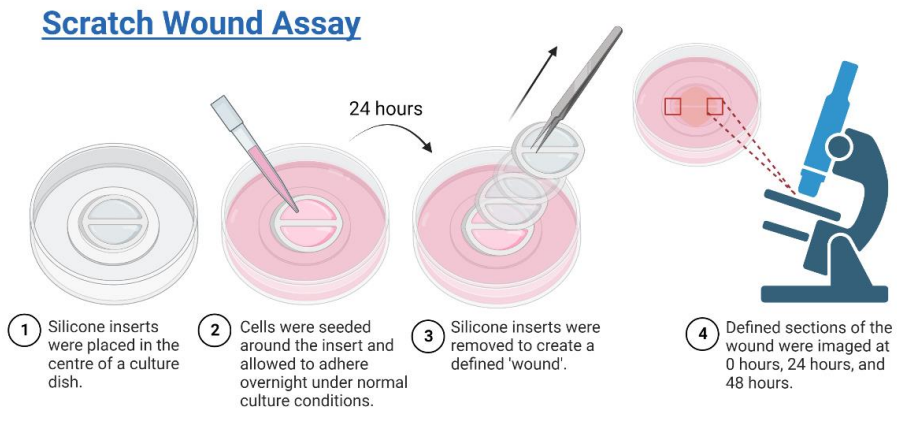

Figure 2.2: Simplified schematic of a scratch wound assay.

2.9 Lectin histochemistry

Human tumour sections were cut from formalin-fixed paraffin embedded tissue and sourced from the University Hospital of Southampton, Histology department. Murine tissue staining was

performed on formalin-fixed paraffin embedded tissue. At humane endpoints, tumours were excised from the primary site of the mammary fat pad. Metastatic tumours were from the metastatic site of the lungs of inoculated mice removed at humane endpoint. *In vivo* procedures were performed by Anil Chand and Anna-Liese Silber. Tissue was harvested and mounted on slides at the University Hospital of Southampton, Histology department. Complementary H&E staining on adjacent tissue slices was performed separately by the University Hospital of Southampton, Histology department, to assist with assigning structures.

Slides were loaded into slide holders and dewaxed as follows: three 7-minute incubations in XTF Clearing Agent, with occasional agitation. Slides were transferred to 100% ethanol and rehydrated with alcohols 100% ethanol, 90%, 80%, and 40% for 2 minutes with gentle agitation. Slides were washed with distilled water for 2 minutes. Antigen retrieval was performed using citrate buffer pH 6.0; slides were emersed in citrate buffer and microwaved on high heat for 10 minutes, and a further 25 minutes on medium heat. Slides were allowed to cool to RT, washed twice with PBS-Tween20 (0.05%) and blocked with PBS-BSA (0.5%) for 20 minutes. Peroxidase suppressor (Vector Laboratories) was added, and slides were incubated for 10 mins at RT.

Primary biotinylated *Narcissus pseudonarcissus* (Vector Laboratories, Cat: B-1375-2) were added to sections at 1:100 and incubated at RT for 30 minutes. Sections were washed three times with PBS-Tween20 (0.05%). Secondary streptavidin Horseradish Peroxidase Antibody Binding Cassette (Vector Laboratories) was applied and incubated for 45 minutes. Sections were washed three times with PBS-Tween20 (0.05%). NovaRed chromogen (Vector Laboratories: SK-4800) was applied and incubated for 10 minutes in the dark. Sections were washed two times with PBS, and once with distilled water. Slides were counter-stained with haematoxylin for 30 seconds. Slides were washed once with distilled water.

Slides were loaded into slide holders and dehydrated as follows: 2 X 10 dips in 90% ethanol, 2 X 10 dips in 100% ethanol, 2 x 10 dips in XTF Clearing Agent. Sections we mounted in XTF mountant and 22x40mm coverslips and dried overnight before imaging.

Slides were imaged with the Olympus CX41 microscope at 10X and 40X magnification. A simplified schematic of the protocol is described in **Figure 2.3**.

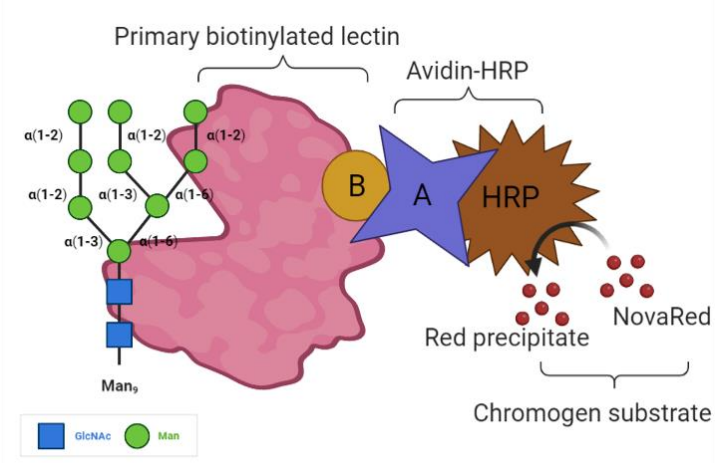

Figure 2.3: Simplified schematic of lectin histochemistry with *Narcissus pseudonarcissus* lectin.

2.10 Flow cytometry

100,000 cells were used for each condition. Cells were washed with blocking buffer ((0.5%) BSA-PBS) and primary biotinylated *Narcissus pseudonarcissus* (Vector Laboratories, Cat: B-1375-2) were added to cells at a dilution of 1:100. Cells were incubated at on ice for 30 minutes. Cells were washed twice with blocking buffer to remove primary lectin. Secondary fluorescein-conjugated streptavidin (Vector Laboratories, Cat: A-5001-1) was added at a dilution of (1:100) and cells were incubated on ice for 30 minutes. Cells were washed twice with blocking buffer to remove secondary antibody and ran on the flow cytometer for a total of 10,000 events (**Figure 2.4**). For each experiment, adsorbed lectin was used as a negative control. Lectin was incubated at RT with 400mM α-methylmannoside hapten sugar (2bsceintific, Cat: S-9005) to adsorb the active site and reduce lectin binding. A simplified schematic of lectin staining for flow cytometry is shown in **Figure 2.4**.

The same protocol was employed for antibody binding assays, in which only the primary and secondary antibodies differed. Primary antibodies employed were the antibody of interest. The secondary antibody employed for detection was the R-Phycoerythrin AffiniPure $F(ab')_2$ Fragment Goat Anti-Human IgG, Fcγ fragment specific (Jackson ImmunoResearch, Cat: 109-116-098).

Samples were analysed using the BD FACSCanto II flow cytometer with FACS DIVA software (BD Biosciences version 8), fitted with lasers with excitation wavelengths of 488nm, 633nm, and 405nm. Fluorescein samples were identified in the FITC channel and PE samples were identified in the PE channel. Unstained cells were run initially to set live cell gates and voltage settings. A total of 10,000 events were recorded for each sample.

Gating and geometric mean fluorescent index (MFI) analyses were performed using FlowJo software (version 10). Data were plotted, and statistical analyses were performed in GraphPad Prism.

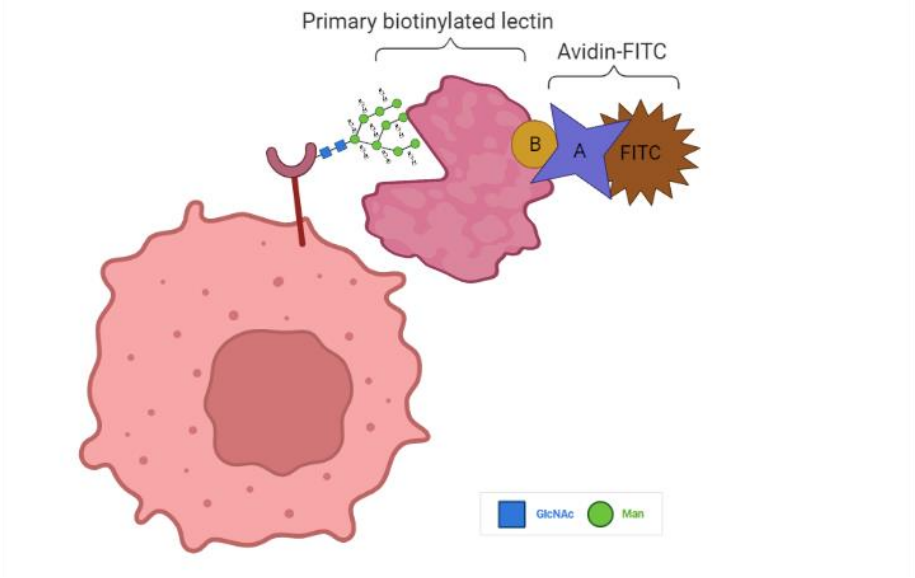

Figure 2.4: Simplified schematic of lectin-based flow cytometry with *Narcissus pseudonarcissus* lectin.

2.11 RNA isolation for transcriptomics

Total RNA was extracted from at least 6 X 10^6 cells using a total RNA Miniprep Kit (Monarch®, Cat: T2010S). To minimise RNA degradation, work areas were treated with RNaseZap™ Rnase Decontamination Solution and all consumables were autoclaved. Reagents were prepared and RNA extraction was performed as per the manufacturer's instructions. Extracted RNA was measured for concentration and purity by spectrophotometric analysis at $A_{260/230}$ and $A_{260/280}$, and samples were placed at -80˚C for storage.

Samples were shipped to GENEWIZ for RNA sequencing and quantitative whole transcriptomics bioinformatics analysis. This included differential expression analysis, gene ontology and splice variant analysis. Three biological replicates were performed for each sample with results showing the mean value.

2.12 Plasmid DNA extraction

Recombinant plasmids were extracted from inoculated overnight *E.coli* cultures using Qiagen Maxiprep kits (Cat: 12162), following manufacturer's instructions. Samples were measured for concentration and purity by spectrophotometric analysis at $A_{280/230}$ and $A_{260/280}$.

2.13 Gel electrophoresis

DNA samples were visualised by agarose gel electrophoresis. A 1.5% agarose gel was made by dissolving 1.5g agarose powder in 100 mL 1X TAE buffer (40 mM tris base, 20 mM acetic acid, 2 mM EDTA). Samples were mixed with 1X GelRed Prestain Loading Buffer (Biotium) and co-electrophoresed alongside a 1 kb Plus DNA ladder for 20 minutes at 125V, 200 mA. Gels were visualised under UV light.

2.14 *In vitro* RNA production and purification

Replicon VEEV plasmid DNA was extracted as described in **Chapter 2.12**. 5 µg DNA was linearised with MluI (Thermo Fisher Scientific, Cat: ER0561), following manufacturer's instructions. DNA was purified using a PCR purification kit (Thermo Fisher Scientific, Cat: K0701), following manufacturer's instructions.

From this point, all work was conducted in a sterile fume cabinet decontaminated with RNaseZap (Thermo Fisher Scientific, Cat: AM9780) to reduce RNA degradation. DNA was *in vitro* transcribed using the mMESSAGE mMACHINE® Kit (Thermo Fisher Scientific, Cat: AM1344), following manufacturer's instructions. RNA was then purified using the MEGAclear transcription clean up kit

(Thermo Fisher Scientific, Cat: AM1908), following manufacturer's instructions. RNA *was* measured for concentration and purity by spectrophotometric analysis at $A_{260/230}$ and $A_{260/280}$, aliquoted, and stored at -80˚C for long-term storage.

2.15 Mammalian cell transfection and purification

Transfections were carried out in HEK293F or MEXi293E suspension cells, according to manufacturer's instructions. Briefly, cells were diluted to 1 X 10^6 viable cells/mL in culture media. 1 µg of plasmid DNA was used per mL of culture volume was used. Cells were incubated at 37°C, 5% CO_2, with shaking for 7 days. Protein-rich supernatant was sterile-filtered and purified by affinity chromatography with a HiTrap™ Protein A (GE Healthcare, Life Sciences). Proteins were further purified by size exclusion chromatography (SEC) (GE Healthcare, Life Sciences: HiLoad™ 16/600 Superdex™ 200 pg column). High performance liquid chromatography was performed to ensure aggregation < 1%.

For DNA-based constructs, heavy chain and light chain vectors were co-transfected at a 1:1 ratio. Some of the later 2G12 constructs were expressed and purified by the antibody production team (Patrick Duriez, Ian Mockridge and Tanya Inzhelevskaya).

2.16 Generation of human monocyte-derived macrophages (MDMs)

Peripheral blood mononuclear cells (PBMC) were isolated from leukocyte cones by density gradient centrifugation. Leukocyte cones were diluted in 2 mM EDTA-PBS, applied to a layer of lymphoprep solution (STEMCELL Technologies), and centrifuged for 20 minutes at 800 x g. The buffy coat was isolated and washed 3X with 2 mM EDTA-PBS for 5 minutes at 300 x g. PBMCs were resuspended in cRPMI and plated at 1 X 10^7 cells/well in a 6-well plate (Corning™). Cells were incubated for 2 hours at 37°C, 5% CO_2 to allow them to adhere before washing with PBS to remove non-adherent cells. Cells were cultured for 7 days in cRPMI + 100 ng/mL macrophage colony stimulating factor (M-CSF). Media was changed on days 1, 3 and 5.

2.17 Antibody-dependent cellular phagocytosis assay

48 hours prior to the ADCP assay, MDMs generated from human donors were harvested and stained after 7 days of culture. Cells were washed 1X with PBS and incubated for 15 minutes in PBS on ice. Cells were harvested with a cell scraper. MDMs were diluted to 1 X 10^7 cells/mL and stained with 1 µM CellTrace Far Red (Thermo Fisher Scientific) at room temperature (RT) for 20 minutes. Stained MDMs were washed and plated at 2 X 10^5 cells/well in cRPMI + 100 ng M-CSF in a flat-bottom 96-well plate (Corning™). Cells were incubated for 48 hours at 37°C, 5% CO_2.

For the ADCP assay, target breast cancer cells were harvested with TrypLE, washed and labelled with 5 µM CFSE (STEMCELL Technologies) for 10 minutes at RT. The stained target cells were opsonised with the antibody constructs on ice for 30 minutes. MDMs were washed with PBS to lose ~50% cells. Opsonised effector cells were added to MDMs for a final effector to target ratio of 1:1, and cocultures were incubated for 1 hour at 37°C, 5% CO_2. Plates were washed with PBS and resuspended in FACs buffer (1% BSA, 0.01 sodium azide). Cells were harvested by scraping.

ADCP activity was detected using the BD FACSCanto II flow cytometer with FACS DIVA software (BD Biosciences version 8), fitted with lasers with excitation wavelengths of 488nm, 633nm, and 405nm. Live cell gating as performed based on forward (FSC) and side scatter (SSC) plots. 10,000 live cell events were collected for each sample.

CellTrace Far Red+ MDMs were identified in the APC channel. CFSE+ target cells were identified in the FITC channel. MDMs were gated as CFSE negative and positive (low and high). Representative dot plots are depicted in results. Data was analysed using FlowJo (version 10). Data were plotted, and statistical analyses were performed in GraphPad Prism.

2.18 Generation of CRISPR guides

Target genes were identified and explored for splice variants and isoforms using Ensembl (genome browser v. 99). Single guide RNAs (sgRNAs) of 20 nucleotides were designed using the Broad

institute GPP sgRNA Designer (CRISPRko). Exons were selected as targets based on their appearance within all splice variants, and their early feature within the gene (**Figure 2.5**). sgRNAs with adjacent PAM sequences were generated using the SpyroCas9 (NGG) setting and scored based on their on- and off-target effects within the Mouse GRCm38 (Ensembl v. 99) genome.

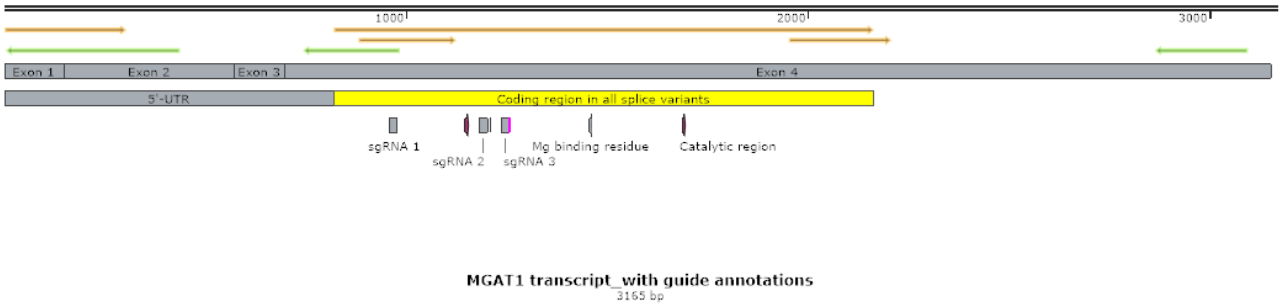

Figure 2.5: Snapgene file of the longest MGAT1 coding transcript. Annotations of note include the coding region across all splice variants, the positions of the single guide RNAs (sgRNAs) designed and site encoding protein catalytic domains. Sequences were obtained from Ensembl (genome browser v. 99), sgRNAs were designed using the Broad institute GPP sgRNA Designer (CRISPRko).

For each KO target, three guide sequences were selected for their diversity within the exon, and low predicted off-target effects. To initiate transcription by the U6 promoter and promote stronger genome annealing, a single guanine was added to the 5' end of sgRNAs that didn't commence with this nucleotide. Tetranucleotide sequences mimicking BsmBI digestion were added to facilitate ligation. Forward and reverse sgRNAs for each sequence position were purchased from Integrated DNA Technologies.

2.19 Cloning into pLentiCRISPR V1

2.19.1 sgRNA annealing

Lyophilized sgRNAs were reconstituted with dH_2O for a final concentration of 100 µM. Any secondary structures which had formed within each guide were denatured, and complimentary forward and reverse sgRNAs were slowly annealed.

1 µL forward sgRNA (100 µM), 1 µL reverse sgRNA (100 µM), 1 µL 10X T4 ligation buffer and 7 µL dH_2O were mixed in a thin-walled PCR tube and annealed by conditions specified in **Table 2.1**. Annealed sgRNAs were diluted 1:250 with dH_2O.

Table 2.1: Conditions for optimal annealing of complimentary sgRNAs.

Stage	Temperature (˚C)	Time (minutes)
1	37	30
2	95	5
3	4*	30

*The temperature was decreased from 95˚C to 4˚C at a rate of 5˚C per minute.

2.19.2 pLentiCRISPR V1 digestion and purification

1 µg pLentiCRISPR V1 vector was digested with BsmBI (**Table 2.2**) and purified by Agarose gel extraction. BsmBI is a type IIS restriction enzyme which cleaves outside of its asymmetric recognition sequences. Thus, a single digestion with BsmBI was adequate for efficient sgRNA cloning. The digested vector was separated by agarose gel electrophoresis. The linearised vector was excised from the agarose gel and purified as per the QIAquick Gel Extraction Kit protocol.

Table 2.2: Digestion of pLentiCRISPR V1 with BsmBI. Reactions were performed at 55˚C for 15 minutes. Components were added sequentially, where BsmBI was added last.

Component	Volume (µL*)*
DNA (1 µg/µL*)*	1
Restriction Enzyme (10 Units/µL*)*	1
10X Buffer	5
dH_2O	to 50

2.19.3 sgRNA ligation

SgRNAs were cloned into the pLentiCRISPR V1 vector. Ligation reactions were set up in 1.5 mL microcentrifuge tubes and incubated at RT for 1 hour **Table 2.3**. A control ligation was performed to assess the efficiency of vector digestion and purification.

Table 2.3: Components of sgRNA ligation into pLentiCRISPR V1. Components were added sequentially where DNA Ligase was added last.

Component	Volume (µL*)*
Digested vector	1
*sgRNA insert	1
10X Buffer	1
T4 DNA ligase (1 Unit/µL)	0.5
dH_2O	to 10

*A control ligation reaction was performed in the absence of a sgRNA insert.

2.19.4 Transformation

Invitrogen™ One Shot™ Stbl3™ chemically competent *E. coli* were transformed with the recombinant pLentiCRISPR V1 vectors by heat shock. All transformation steps were performed on ice to maintain *E. coli* competency.

A transformation control was performed using a control plasmid. 30 µL competent cells were mixed with 2 µL of the ligated sample produced in **Chapter 2.19.3** or 1 µL of control plasmid, and incubated on ice for 30 minutes. Samples were placed in a water bath at 42˚C for 60 seconds and immediately placed on ice for 2 minutes. 200 µL lysogeny broth (LB) was added to each sample, and samples were incubated at 37˚C with shaking for 45 minutes.

100 µL of transformed E. coli was plated onto ampicillin (100 µg/mL) agar plates using a sterile spreading technique. Plates were incubated overnight at 37˚C.

Agar plates were inspected for colony growth. Transformation control plates were inspected to explore E. coli competency was intact. Ligation control plates were inspected to explore pLentiCRISPR V1 digestion efficiency, and thus the proportion of colonies harbouring background vector expected on sample plates. Plates were stored at 4˚C.

2.19.5 Colony selection

Two single colonies were picked for each sgRNA. Sterile conical tubes containing LB ampicillin (100 µg/mL) were inoculated with colonies transferred using a sterile yellow pipette tip. Cultures were explored for the presence of the recombinant plasmid by PCR before subculturing for plasmid extraction.

2.19.6 Plasmid detection

PCR was performed to detect colonies which harboured recombinant sgRNA containing pLentiCRISPR V1 plasmids. 1 µL of the inoculated LB culture was mixed with 19 µL PCR master mix (1X DreamTaq Buffer, 0.1 Units DreamTaq Polymerase, 200 nM U6 Forward primer, 200 nM sgRNA oligonucleotide Reverse primer, 400 µM dNTPs, dH_20) in a thin-walled PCR tube, and PCR was performed using conditions described in **Table 2.4**.

PCR reactions were visualised by agarose gel electrophoresis. Samples which successfully amplified the sgRNA insert were considered positive for the recombinant pLentiCRISPR V1 plasmid. Inoculated cultures corresponding to these positive PCR samples were subcultured overnight at 37˚C with shaking, for plasmid extraction.

Table 2.4: PCR conditions used to screen transformed *E. coli* colonies.

Step	Temperature (˚C)	Time (minutes)
1	95	2
2*	95	0.3
3*	57	0.3
4*	72	0.3
5	72	5

*1 cycle was considered the completion of steps 2 to 4. These steps were consecutively repeated, and 34 cycles were completed before step 5 was performed.

2.20 Lentivirus generation and transduction

All work was conducted in a Class II Microbiological Safety Cabinet. Syringes or needles were not used to mitigate the risk of human infection. Spent media and cells, and contaminated consumables were discarded in 3% Virkon.

Lentivirus was generated in HEK293FT cells. Cells were transfected with three components necessary for viral packaging and downstream transduction: pLentiCRISPR V1/GFP-pLKO control, Packaging plasmid containing Gag and Pol, and Envelope plasmid expressing VSV-G. The transfection plasmid ratio was 4:2:1, respectively.

~1 X 10^6 HEK293FT cells were cultured in complete Dulbecco's modified eagle medium (DMEM) (Gibco™, Cat: 11966025) (10% FBS, 1% Penicillin-Streptomycin) for 2 hours at 37˚C, 5% CO_2. 2 µg total plasmid DNA was mixed and incubated at RT for 10 minutes. 6 µL of polyethyleneimine transfection reagent (PEI) was added and the solution was incubated at RT for 20 minutes. 100 µL DNA-PEI solution was added drop wise and the cells were incubated overnight at 37˚C, 5% CO_2. The supernatant was discarded and replaced with 2 mL complete DMEM. Cells were incubated overnight at 37˚C, 5% CO_2.

The virus-rich supernatant was removed and stored at 4˚C. 2 mL complete DMEM was added and cells were incubated overnight at 37˚C, 5% CO_2. This process was repeated until 6 mL of virus-rich supernatant was harvested. HEK293FT cells were discarded and the virus-rich media was purified using a 0.45 µm filter. Virus aliquots were stored at -80˚C until use.

EO771 cells were transduced with lentivirus generated. A control transduction using lentivirus packaged with GFP-pLKO was performed in tandem to ensure transduction efficiency. WT cells were grown to ensure antibiotic selection efficiency.

~2.5 X 10^6 cells were seeded into a well of a 6-well plate for each transduction. Two control wells were prepared. 0.5 mL of virus was diluted with 1.5 mL complete DMEM and supplemented with polybrene, for a final concentration of 5 µg/mL. The viral solution was applied to KO target cells and transduction control cells. Complete RPMI was added to antibiotic control cells. Cells were incubated overnight at 37˚C, 5% CO_2. Spent media was removed and replaced with 2 mL complete RPMI, and incubated overnight at 37˚C, 5% CO_2.

Spent media was removed and replaced with 2 mL complete RPMI containing 4 µg/mL puromycin to select for transduced cells. Cells were maintained in puromycin until WT cells in the antibiotic control were dead.

2.21 SDS-Page

Sodium Dodecyl Sulfate-polyacrylamide gel electrophoresis (SDS-PAGE) was carried out using precast NuPAGE™ protein gels (4-12% Bis-Tris). For non-reducing conditions, protein was mixed with 1X NuPAGE™ LDS sample buffer before loading. For reducing conditions, 1X NuPAGE™ Sample Reducing Agent was also added before loading. 10 µL Precision Plus Protein Kaleidoscope Prestained Protein Standards (Bio-Rad) was loaded as a molecular weight standard, and protein samples were loaded alongside and electrophoresed at 160V for 45 minutes, in NuPAGE™ MES SDS Running Buffer. Gels were removed from cassettes and stained with Coomassie Brilliant Blue (Thermo Fisher) for 20 minutes at RT, with shaking. Gels were destained in a solution comprising

10% acetic acid, 40% Ethanol, and 50% dH2O for 60 minutes (or longer if needed) at RT, with shaking, before being visualised.

2.22 Glycopeptide LC-MS

Proteins analysed by SDS-PAGE were excised using a scalpel. Gel bands were cut into small pieces and incubated in 100% acetonitrile (ACN) until Coomassie stain was removed. ACN was removed, and gel pieces were resuspended in 50 µL DTT solution (10 mM DTT-100 mM Ammonium Bicarbonate), and incubated at 56˚C for 30 minutes. Gel pieces were cooled to RT and 300 µL ACN was added. After 10 minutes, liquid was removed, and gel pieces were covered in 50 µL IAA solution (55mM IAA-100mM Ammonium Bicarbonate) and incubated in the dark for 10 minutes. 300 µL AmBic was added and bands were incubated 30 minutes at RT with occasional vortexing. Liquid was removed and 500 µL ACN was added. Bands were incubated at RT with occasional vortexing until gel pieces became white and shrank. Liquid was removed, 50 µL trypsin solution was added (13 ng/µL trypsin 10%ACN-10mM AmBic) and bands were incubated on ice for 2 hours. 20 µL 10 mM AmBic was added to solution and samples were incubated overnight at 37˚C.

15uL 25 mM AmBic was added to the bands. Samples were vortexed and incubated at 37˚C for 15 minutes. Liquid was removed and 200 µL ACN was added. Samples were centrifuged at 12,000 x g for 1 minute and supernatant was collected. 100 µL extraction buffer (1:2.5% formic acid:ACN) was added to gel pieces and incubated at 37 ˚C for 10 minutes with shaking. Samples were centrifuged at 12,000 x g for 1 minute and supernatant was collected and pooled with previous harvest. Supernatants were dried in a vacuum centrifuge (Vac-man).

2.23 Released glycan LC-MS

For analysis by LC-MS whole-cell lysate was extracted and glycans were labelled with procainamide. Cells were harvested, washed with PBS, and incubated in 0.25% Trypsin-EDTA at 37˚C for 20 mins. Cells were pelleted and the supernatant was incubated with 700 µL PNGaseF (In-house 0.1 µg/mL) at 37˚C overnight to cleave N-glycans.

Protein was purified from the glycans using a protein-binding Oasis PRiME HLB 96-well µElution Plate (Waters, Cat: 186008052). Wells were washed thrice with 200 µL ACN to condition the plate, and twice with 200 µL 0.1% TFA to equilibrate the plate, each time pulling the liquid through with the vacuum. Samples were collected into a fraction collection 96-well plate (Waters). The wells were then washed twice with 700 µL 0.1% TFA. The flow-through was transferred to a 1.5 mL Eppendorf tubes to be dried in the speed-vac. The resultant sugars were analysed by UPLC in the same way as outlined above.

The lyophilized glycans were then resuspended in 30 uL of MilliQ water and 100 µL of procainamide labelling mixture was added. To make the labelling mixture 60 mg of sodium cyanoborohyride was added to 1ml of buffer (70% DMSO 30% acetic acid) and dissolved. 110 mg of procainamide was then dissolved in this solution. The mixture with the glycans was then incubated at 65 degrees for 4 hours.

The labelled glycans were purified using HyperSep HyperCarb SPE cartridges (Thermo, Cat: 60106-301). The cartridge was conditioned with 1 mL methanol and washed 1 mL MilliQ H_20. Cartridges were equilibrated with 3 X 1 mL ACN-TFA (0.1%), then washed with 1 mL MilliQ H_2O. Cartridges were loaded with the labelled glycan sample. Once loaded the cartridges were washed twice with 1 mL MilliQ H_2O. The loaded samples were eluted from the cartridges with 3X 1 mL 50% ACN-TFA (0.1%). The elution was lyophilised overnight in the speed-vac.

Lyophilised samples were resuspended in 24 µL 50mM ammonium formate. 24 µL of 100% ACN was added to a HILIC-UPLC vial (Waters) followed by 6 µL of the labelled glycan mixture. The samples are then loaded for analysis by LC-MS. The glycans were separated in the column based on their size and as they leave the column the procainamide acted as a fluorophore. The sample is excited at 480nm and emitted at 330nm and the intensity of the emission provides a measure of the glycans that have eluted from the column, providing a spectrum.

2.24 Surface plasmon resonance analysis

HER2 binding was assessed by surface plasmon resonance using the Biacore™ T-100 (Cytiva). Anti-histidine antibody (Cytiva His Capture Kit) was immobilised via amine coupling (Cytiva Amine coupling kit) to 1000 response units (RU) of a CM5 sensor chip, according to manufacturer's instructions. Recombinant his-tagged human HER2 (R&D Systems) was captured on the surface of the chip at 5 or 0.5 µg/mL. Antibody constructs were 5X serially diluted to 100 nM, 20 nM, 4 nM, 0.5 nM, and 0.16 nM in HSB-EP+ pH 7.4 (Cytivia). Constructs were flowed over the chip at 30 µL/min (association; 150 seconds, dissociation; 300 seconds). Sensorgrams were fitted to a 1:1 binding model and affinity, association, and dissociation constants were calculated using the Biacore Bioevaluation Software (Cytiva). Sensorgrams were visualised using GraphPad Prism (version 9).

2.25 *In vivo* experiments

All *In vivo* experiments in this thesis were performed by Anil Chand and Anna-Liese Silber and supported by the PCU staff at the Centre for Cancer Immunology.

2.25.1 Primary tumour growth

2.5 X 10^5 EO771 cells were subcutaneously injected into the mammary fat pad of 11- to 12-week-old female C57BL/6 mice (Charles River Laboratories). Tumour measurements were recorded every two to three days, until humane endpoint.

2.25.2 Metastasis

5 X 10^5 EO771.LG cells were subcutaneously injected into the tail vein of 11- to 12-week-old female C57BL/6 mice (Charles River Laboratories). Metastatic burden was analysed every two to three days using IVIS luminescent imager, until humane endpoint.

2.26 Statistical analysis

All graphs and statistical analyses were produced in GraphPad Prism. Significance was assessed by Students two-tailed unpaired T-test to test the significance of means between two groups. Multiple T-tests were performed to test for significant differences between two groups across multiple time points or cell lines. When more than two groups were present, a one-way ANOVA was used to test the significance of differences between means. A 2-way ANOVA was used to test differences when two independent variables were tested across more than two groups. Significance was assessed with P-values of <0.05 as noted on individual figures (*P<0.05, **p<0.01, ***p<0.001, ****p<0.0001).

2.27 Xena platform

Expression of glycosyltransferases in clinically relevant human datasets was explored using the Xena online platform. Xena contains multiple datasets pulled from online repositories, including Pan Cancer Atlas publication's data site, and TCGA ATAAC-seq publication's data site. Xena applies the same RNA-seq pipeline analysis to raw data allowing expression to be compared across multiple repositories. For example, within the TCGA, TARGET, GTEx data set employed in this thesis, raw data from multiple repositories was re-aligned to hg38 genome and expressions were called using RSEM and Kallisto methods. The Welch's t-test was automatically applied to test statistical significance of between glycosyltransferase expression, with the assumption of unequal variances to adjust for unequal sample sizes.

Chapter 3 The significance of high-mannose N-glycans in Breast Cancer progression

3.1 Introduction

Glycans form the interface between a cell and its environment and mediate a variety of processes, including cell-cell signalling and adhesion, protein folding and stability, and reaction specificity between molecules (Varki, 1993; Haltiwanger and Lowe, 2004; Varki and E., 2015; Reily *et al.*, 2019). Additionally, glycans are integral for regulating immunity and tolerance, in which their signatures trigger tolerogenic or immunogenic signaling pathways (Lübbers, Rodríguez and van Kooyk, 2018). The composition and expression of glycans can change dynamically, depending on the cell type, external stimuli, and genetic factors (Zhou *et al.*, 2008; Slade *et al.*, 2016; Zhang *et al.*, 2019). Additionally, alterations in glycan processing occur throughout oncogenesis, and as such aberrant glycosylation is considered one of the established hallmarks of cancer (Fuster and Esko, 2005; Li *et al.*, 2018) (see Chapter 1.12). An emerging field of interest within this is the presence of high-mannose glycans.

Glycans can become aberrant due to a multitude of reasons. Firstly, due to the over- or under-expression of glycosyltransferases at the transcript level (Buckhaults *et al.*, 1997; Kannagi *et al.*, 2008; Hatano *et al.*, 2011), or the chaperone level (Schietinger *et al.*, 2006; Aryal, Ju and Cummings, 2010). Secondly, due to the mislocalisation of glycosyltransferases in the Golgi (Kellokumpu, Sormunen and Kellokumpu, 2002; Gill *et al.*, 2010). Third, due to changes to the peptide backbone sequence and structure (Pinho and Reis, 2015). Finally, aberrant glycosylation can occur due to the altered availability of sugar-nucleotide substrates and acceptor substrates (Kumamoto *et al.*, 2001).

The most common aberrant glycosylation patterns in cancer are increased complex-type glycans, and feature increased β1,6-*N*-linked branched glycans, sialylation and fucosylation. Increased branched glycans can sustain proliferative signalling, activate invasion and metastasis, and assist cancer cells to evade immune destruction (Varki, 1993; Demetriou *et al.*, 1995; Meany and Chan,

2011; Ščupáková *et al.*, 2021). Increased sialylation is associated with invasiveness and metastasis (Kannagi *et al.*, 2004), and immunosuppression (Cohen *et al.*, 2010; Perdicchio *et al.*, 2016; Stanczak *et al.*, 2018). Indeed, sialoglycans stimulate inhibitory signaling pathways and immune suppression by binding siglecs (Cohen *et al.*, 2010; Perdicchio *et al.*, 2016; Lübbers, Rodríguez and van Kooyk, 2018). Increased core α1,6-fucosylation, caused by an upregulation of FUT8, is implicated in epithelial-mesenchymal transition and metastasis (Chen *et al.*, 2013; Taniguchi and Kizuka, 2015; Tu *et al.*, 2017).

Another emerging glycan phenotype of interest is high-mannose glycans. Under normal conditions, high-mannose glycans are generally confined to the endoplasmic reticulum (ER) (Loke *et al.*, 2016). However, in cancer, proteins are commonly overexpressed. Increased rates of protein synthesis and cell growth can lead to the saturation of the glycosylation pathway and an increased abundance of under-processed high-mannose glycoforms (Johns *et al.*, 2005; Chatterjee, Kawahara, *et al.*, 2021). Aberrant regulation of ER mannosidases has also been reported to contribute to the creation of this phenotype (Chatterjee, Kawahara, *et al.*, 2021). The presence of high-mannose glycans correlates negatively with MAN1A1 MAN1A2 and MAN1B1 expression (Chatterjee, Kawahara, *et al.*, 2021). MAN1A1 expression was significantly reduced in several high-mannose-expressing tumour cells, relative to non-tumour cells (Chatterjee, Kawahara, *et al.*, 2021). Reduced MAN1A1 expression was associated with enhanced cell surface mannose, increased cellular adhesion and reduced sheet migration in BC cells (Legler, Rosprim, Karius, Eylmann, Rossberg, Ralph M Wirtz, *et al.*, 2018). A downregulation of MAN1A1 leading to the elevation of high-mannose glycans was reported in metastatic cholangiocarcinoma cell lines, relative to non-invasive parental lines (Park *et al.*, 2020).

Aberrant high-mannose glycans have been reported in many cancer entities including blood (Chatterjee, Kawahara, *et al.*, 2021), brain (Park *et al.*, 2020), ovarian (Everest-Dass *et al.*, 2016), breast (Liu *et al.*, 2013; Ščupáková *et al.*, 2021), gastric (Liu *et al.*, 2020), and liver tumours (NUCK *et al.*, 1993; Mendoza *et al.*, 1998).

High-mannose glycans have been implicated in mechanisms of cell adhesion, migration, and invasion. The elevation of high-mannose glycans with Kifunensine, a small molecule mannosidase inhibitor, increased cell migration and invasion in cholangiocarcinoma cell lines (Park *et al.*, 2020). In addition, the induction of high-mannose glycans via either mannosidase inhibition or knock-down (KD) of mannosidase enzymes was demonstrated to increase *in vitro* cell adhesion in melanoma cells (Mendoza *et al.*, 1998), and BC cells (Legler, Rosprim, Karius, Eylmann, Rossberg, Ralph M Wirtz, *et al.*, 2018).

The role of high-mannose glycans in metastasis is also of interest. The induction of high-mannose glycans on melanoma cells using small molecule inhibitors was demonstrated to increase *in vivo* liver metastasis (Mendoza *et al.*, 1998). Decreased MAN1A1 protein expression in BC patient tumour samples, which was suspected to increase high-mannose glycans, was significantly correlated with brain metastasis (Legler, Rosprim, Karius, Eylmann, Rossberg, Ralph M Wirtz, *et al.*, 2018). High-mannose glycans were reported upregulated in metastatic BC tissues compared to primary BC tumour tissues within the same patient (Ščupáková *et al.*, 2021). Additionally, the presence of high-mannose glycans on gastric cancer cells in patient tissues with primary advanced gastric adenocarcinoma was correlated with tumour, node, metastasis (TNM) stage (Liu *et al.*, 2020).

In addition, aberrant high-mannose glycans may play a role in immune modulation within the tumour microenvironment (TME). C-type lectins are glycan-binding receptors expressed on macrophages and dendritic cells (DC) to distinguish between self- and invading organisms. The association of elevated high-mannose glycans in cancer with mannose-binding proteins within the TME may be of relevance. Positive staining for $CD206^{+}$ (mannose receptor (MR)) stromal macrophages and for mannose on tumour cells, was reported in gastric tissue samples, and both significantly correlated with tumour, node, metastasis (TNM) stage (Liu *et al.*, 2020). MR^{+} tumour associated macrophages (TAMs) were described as M2-like, and involved in inflammation, chemotaxis and angiogenesis (Movahedi *et al.*, 2010). MR^{+} M2-like macrophages were correlated

with metastatic progression in colorectal cancer patient primary tumours (Ålgars *et al.*, 2012). Engagement of MR on monocyte-derived DCs with anti-MR mAb and natural mannose-based ligands showed increased production of anti-inflammatory cytokines and reduced ability to generate a Th1-polarised immune response (Chieppa *et al.*, 2003). Additionally, the role of the C-type mannose-binding lectin, DC-SIGN is of interest. Native Binding of DC-SIGN to its ligand, ICAM3 expressed on T cells, allows T cell receptor to interact with MHC molecules presenting peptides, facilitating T cell activation (Geijtenbeek *et al.*, 2000; Švajger *et al.*, 2010). Tissue staining in colon cancer patients revealed high DC-SIGN expression within the tumour stroma compared to matched normal control tissue (Yanmei *et al.*, 2014). Interestingly, high tumour DC-SIGN levels negatively correlated with soluble DC-SIGN serum levels within the same patients, and an increased presence of soluble DC-SIGN correlated with long-term survival (Yanmei *et al.*, 2014). Elevated high-mannose glycans within the TME may, therefore, bind C-type lectins and block native ligand interactions, modulating the immune response (Wong *et al.*, 2003). However, it is currently difficult to draw conclusions, since many C-type lectins also bind other cancer-associated glycan phenotypes, including fucosylated Lewis^{a,b,x,y} structures, with high affinity (Appelmelk *et al.*, 2003; Blixt *et al.*, 2004). Indeed, the binding of DC-SIGN with fucosylated glycoforms has been demonstrated to induce a proangiogenic profile promoting tumour progression (Merlotti *et al.*, 2019; Hu *et al.*, 2020). Therefore, the impact of high-mannose glycans and mannose-binding proteins on immune modulation needs further investigation.

Further, the reported presence of high-mannose glycans in cancer is variable and sometimes conflicting, and appears to depend on the cancer type, tumour stage, and the techniques employed to assess (Chatterjee, Kawahara, *et al.*, 2021).

There is evidence to show that the presence of aberrant high-mannose glycans depends on the cancer type. For example, assessment of tumour and matched non-tumour tissue showed no difference in high-mannose glycans present within patients with liver cancer, gastric cancer, prostate cancer, and chronic lymphocytic leukaemia, whereas complex-type glycans were

overexpressed (Chatterjee, Kawahara, *et al.*, 2021). However, significant differences were observed in basal cell carcinoma, squamous cell carcinoma, and colorectal cancer (Chatterjee, Kawahara, *et al.*, 2021).

In addition, the site of cancer metastasis has also been demonstrated to be influential in reported cases of aberrant high-mannose glycans. Metastatic BC patient tissues showed a site-specific upregulation of high-mannose glycans, primarily associated with lung and diaphragm metastasis but not with bone metastasis (Ščupáková et al., 2021). Decreased MAN1A1 protein expression and increased high-mannose glycans were observed specifically in bone-seeking and brain-seeking metastatic BC cell lines, relative to parental cell lines (Legler, Rosprim, Karius, Eylmann, Rossberg, Ralph M Wirtz, *et al.*, 2018). Decreased MAN1A1 protein expression correlated with brain metastasis, but not bone or lung metastasis in clinical BC patient tumours (Legler, Rosprim, Karius, Eylmann, Rossberg, Ralph M Wirtz, *et al.*, 2018).

Further, there is evidence to show that the experimental method used to detect glycans influences results (Chatterjee, Kawahara, *et al.*, 2021). For example, studies which interrogated whole-cell lysate and membrane fractions showed highly elevated high-mannose glycans (Park *et al.*, 2020; Chatterjee, Kawahara, *et al.*, 2021). Incompletely processed glycoproteins which are still trafficking the secretory pathway may contribute to these reported high levels. Studies which interrogated the cell secretome of cultured cells reported only a slight elevation of high-mannose glycans, and a high elevation of complex-type glycans (Zhang *et al.*, 2014).

Despite their low secretion rate, high-mannose glycans have been reported to be elevated in the serum of advanced BC patients (Leoz *et al.*, 2011). Although this supports previous findings that high-mannose glycans are elevated in BC, a separate study which also assessed serum samples from stage 4 advanced metastatic BC patients showed no elevation in high-mannose glycans, relative to healthy individuals (Abd Hamid *et al.*, 2008). Additional authors also reported that serum high-mannose glycans were not elevated in BC patients compared to healthy cancer-free patients, and no trend was observed across BC stage (Vreeker *et al.*, 2021). Conversely, R *et al.*, reported

decreased levels of serum high-mannose glycans in newly diagnosed BC patients, relative to healthy controls (2014). It has been demonstrated that the serum N-glycome of BC patients changes significantly throughout treatment (Saldova *et al.*, 2017). Additionally, stratification of BC patients according to histological subtype (e.g. invasive ductal carcinoma versus invasive lobular carcinoma) revealed clear differences in serum glycomic signatures (Vreeker *et al.*, 2021). Indeed, clinical data within some studies are not always defined, such as the stage of advanced disease progression (Leoz *et al.*, 2011) secondary sites of metastasis (Abd Hamid *et al.*, 2008; Leoz *et al.*, 2011), histological stratification (Abd Hamid *et al.*, 2008; Leoz *et al.*, 2011), and patient treatment regimens (Abd Hamid *et al.*, 2008; Leoz *et al.*, 2011; Vreeker *et al.*, 2021). Therefore, due to the lack of reported clinical data within studies, and the high heterogeneity within BC disease, it is difficult to determine a general N-glycomic signature which distinguishes BC patients from controls.

In addition, glycosylation is a dynamic and heterogenous modification, and there is evidence to suggest that high-mannose glycans may be selected for at different stages of oncogenesis. In colon carcinoma samples it was observed that the relative levels of high-mannose glycans were elevated at the start of oncogenesis, however, as the disease progressed to invasive adenocarcinoma, high-mannose glycans were in relatively low abundance compared to branched tetra-antennary, sialylated glycans (Boyaval *et al.*, 2022). Successive changes in N-glycan repertoire have been reported across BC oncogenesis (Ščupáková et al., 2021). High-mannose glycans were significantly increased in clinical BC tissues across all age and stage groups compared to matched adjacent normal tissue, but also significantly higher in tumours from patients >40 years of age, and in patients in early-stage BC (Liu et al., 2013).

Of interest, several studies which reported an increase in high-mannose glycans also reported a general increase in total glycan abundance, and elevation of other glycans, including complex-type sialylated- and fucosylated- glycans (Liu *et al.*, 2013; Park *et al.*, 2020; Ščupáková *et al.*, 2021).

The clinical significance of high-mannose glycans in BC has also been noted. Reduced MAN1A1 expression correlated with poor prognosis in BC patients (Milde-Langosch *et al.*, 2014). Lower

MAN1A1 expression was observed in TNBC tumours compared with $HER2^+$ or luminal carcinomas, and correlated with shorter disease-free survival (Legler, Rosprim, Karius, Eylmann, Rossberg, Ralph M. Wirtz, *et al.*, 2018). An increase in N-glycan abundance correlated with BC progression, with significant increases in high-mannose, fucosylated and sialylated glycans observed in metastasis (Ščupáková *et al.*, 2021). In several cases high-mannose glycans have been reported expressed on the cell surface of BC cell lines (Liu *et al.*, 2013; Oh *et al.*, 2022), and implicated in increased cell adhesion (Legler, Rosprim, Karius, Eylmann, Rossberg, Ralph M Wirtz, *et al.*, 2018). High-mannose glycans were upregulated on the cell surface of BC tissues, relative to matched adjacent normal tissue (Liu *et al.*, 2013; Ščupáková *et al.*, 2021). Elevated levels of high-mannose glycans in the serum of BC patients relative to healthy controls, have been both reported (Leoz *et al.*, 2011) and disputed (Abd Hamid *et al.*, 2008; Vreeker *et al.*, 2021).

While there is growing evidence for the accumulation of high-mannose glycans in BC, some reports are contradictory. Thus, the role high-mannose glycoproteins play within BC development and progression along with their dynamic regulation still needs to be fully elucidated. Therefore, we aimed to investigate the presence and role of high-mannose glycans in BC progression. To do this, we investigated the regulation of mannose processing enzymes within clinical BC samples. We determined the presence of high-mannose glycans within clinical BC tissues and determined their presence on the cell surface of BC cells. Finally, we aimed to understand their role in BC progression and generated two models in which high-mannose glycans were elevated. We validated these models and evaluated the impact of high-mannose glycans on BC migration and invasion *in vitro* and on tumour growth and metastatic burden *in vivo*.

3.2 Results

3.2.1 Mannose expression in primary clinical samples

Growing evidence suggests that high-mannose glycans may be a feature within the BC microenvironment and during BC tumour development. However, so far, the evidence is variable and has focused on the detection of high-mannose species themselves across both tumours and in serum samples. Therefore, we initially wanted to determine if there was any evidence for the dysregulation of mannose processing enzymes in clinical BC cancer samples compared to healthy normal breast tissue. To do this we analysed TCGA, TARGET, and GTEx RNAseq data deposited in the Xena Browser platform (**see section 2.27**) (**Figure 3.1**).

Overall, there was a statistically significant difference in expression levels of almost all the mannose processing enzymes in invasive breast carcinoma, relative to matched healthy mammary tissue (**Figure 3.1**). In addition, there was a high level of heterogeneity in expression levels across invasive breast carcinoma samples, relative to matched healthy tissue. This can be seen by the lack of block colour within each column representing a specific glycosyltransferase/glycosidase in the breast invasive carcinoma row (**Figure 3.1**). It is important to note that the datasets contain samples from all subtypes and stages of BC, and so this may account for some of the observed variability.

Generally, there was a trend towards an upregulation of glucosidases in carcinoma versus normal tissue, as seen by MOSGS, GANAB and PRKCSH columns (**Figure 3.1**). In cancer progression, including BC, there is a general upregulation of protein expression. As many proteins require glycosylation, there is an increased flow of proteins through the calnexin/calreticulin ER degradation pathway. Thus, the increase in glycosidases here may be explained by the increased requirement for glycosylation machinery.

Further, a trend towards a downregulation in ER and Golgi mannosidases in carcinoma versus normal mammary tissue was observed (**Figure 3.1**). These glycosidases are responsible for glycan trimming and begin N-glycan processing towards hybrid- and complex-type glycans. Therefore,

since there is a trend towards a downregulation of these enzymes in invasive breast carcinoma, less mannose trimming may occur, and this could result in more high-mannose glycans than seen in matched healthy mammary tissue. Overall, despite the heterogeneity, the trends observed in expression of mannose processing enzymes suggest that they may act to increase high-mannose expression in invasive breast carcinoma compared to matched normal tissue.

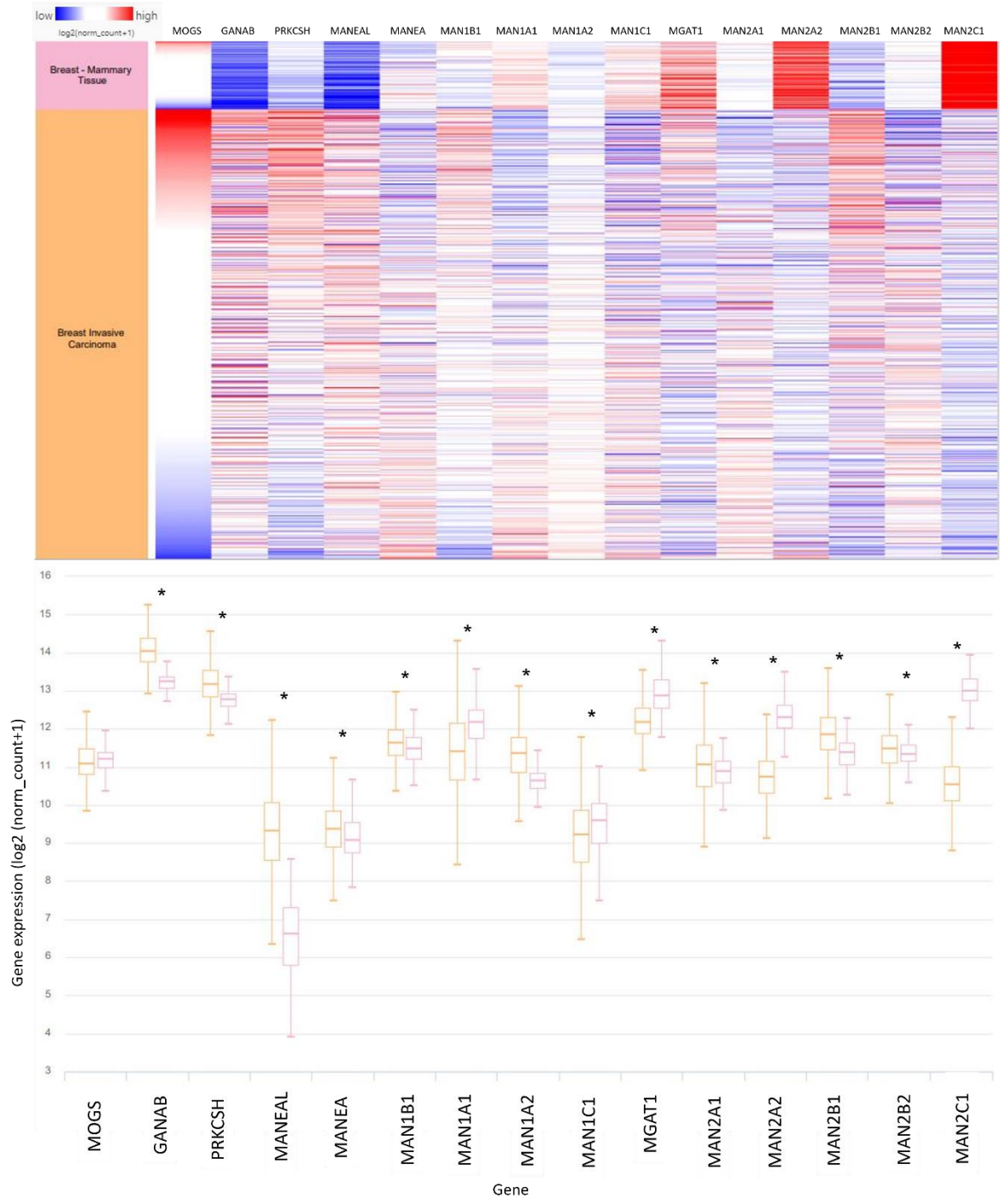

Figure 3.1: Gene expression levels of mannose processing enzymes in invasive breast carcinoma and matched breast mammary tissue. TCGA, TARGET, and GTEx dataset of 1391 samples were re-analyzed (re-aligned to hg38 genome and expressions are called using RSEM and and Kallisto methods) by the same RNA-seq pipeline on the Xena Platform. Welch's t-test. * Represents statistically significant differences, where $P < 0.001$. Default statistics used from Xena Browser platform.

To verify whether these transcriptional changes observed in the RNAseq data translate to increased high-mannose expression, we next wanted to assess the presence of high-mannose glycans within tumour tissues. To do this, lectin staining for the presence of high-mannose N-glycans within breast tissue samples was employed. The lectin, *Narcissus pseudonarcissus* (NPA) binds poly α-mannose structures, specifically binding terminal α-1,6-mannose structures, as well as internal α-1,3- and 1,6-mannose structures. A primary biotinylated lectin was employed with a secondary avidin-HRP antibody, and Novared chromogen.

Before staining clinical samples, we first had to optimise NPA lectin staining. To do this we used OCT frozen sections of EO771 cells. The EO771 cell line is a TNBC cell line established from a spontaneous mammary adenocarcinoma in C57BL/6 mice (Casey, Laster and Ross, 1951). These cells can be chemically/genetically modified before their inoculation into a mouse mammary gland as an allograft. Therefore, these cells are appropriate for *in vitro* and *ex vivo* assays, with the ability to translate directly to *in vivo* projects and were heavily utilised within this chapter. As such, staining was optimised in the murine cell line rather than a human cell line at this stage to establish the robustness of our model cell lines, EO771 and EO771.LG, and translatability between murine and human clinical data.

As a positive control, NPA lectin staining was performed on EO771 cells cultured in the presence of Kifunensine (Kif) (**Figure 3.2**). Kif is a small molecule inhibitor which competitively inhibits MAN1B1, with off-target effects to other α-mannosidases. This blocks N-glycan processing resulting in predominantly high-mannose glycans (Man_9). Therefore, Kif treated cells acted as a positive control for the lectin staining, as a brighter stain was expected with increased high-mannose glycans.

Overall, the lectin staining for OCT frozen sections of EO771 cells was successfully optimised (**Figure 3.2**). The untreated EO771 cells showed weak staining for NPA lectin. As expected, the Kif treated EO771 cells showed much stronger red chromogen staining relative to the untreated EO771 cells. As a further control, there was no chromogen staining observed in the Kif cultured cells when no

primary lectin was present. Together, this suggests that the NPA lectin is binding the expected high mannose epitopes, and there is no non-specific secondary antibody or chromogen.

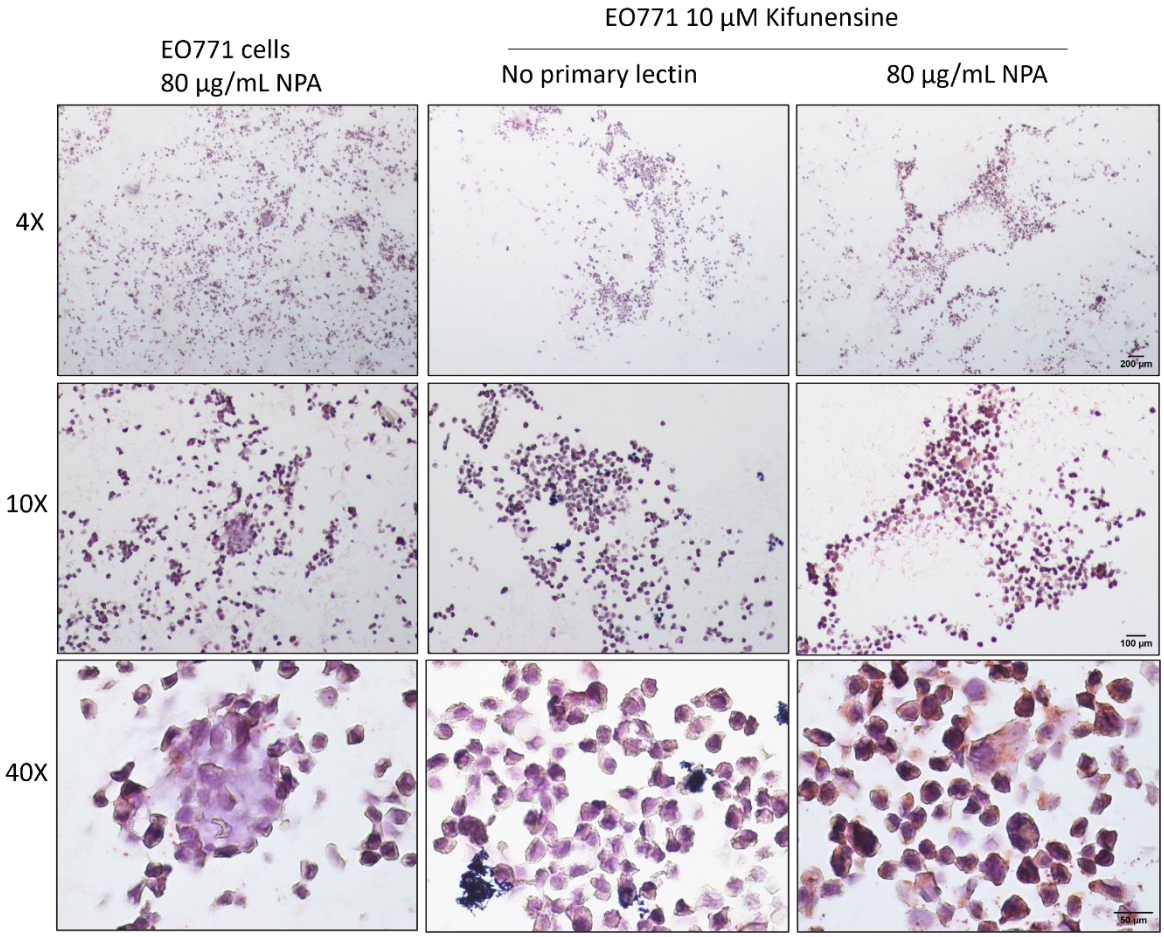

Figure 3.2: Mannose staining of EO771 cell pellets cultured with or without 10 µM Kif. EO771 cells were cultured with or without Kif, pelleted and suspended in OCT. Cell pellets were frozen and sliced using a cryostat prior to being mounted on full-faced slides. Slides were stained with NPA lectin (Red) and haemoxylin counter stain for identification. Slides were imaged at 4X, 10X and 40X magnification.

Human clinical breast tumour samples were then stained with the mannose-binding lectin, NPA. Dual cytokeratin staining was also performed to aid in identifying structures within the tissue. Two TNBC samples and two $HER2^{+}$ BC full-faced sections were stained and imaged. Samples were analysed and assessed with the aid of an in-house consultant pathologist. Representative sections are presented in **Figure 3.3**.

Cytokeratin staining was performed to identify breast tumour cells. Morphologically, invasive BC was identified by the amount of high tubule formation and disorganised structures, and infiltrating

tumour cells in the fibrous tissue. **Figure 3.3** shows these tissues to have areas of disorganisation and large, hyperchromatic nuclei.

Positive mannose staining by the Novared chromogen can be seen within the tumour for $HER2^+$ and TNBC tissues (**Figure 3.3**). NPA staining was granular and dotty in nature. There is delicate yet convincing cytoplasmic staining within the tumour cells. However, despite optimisation, the cytokeratin stain was very strong, therefore, it was difficult to see the NPA staining in the dual-stained images.

Within the TNBC samples, positive NPA staining was seen within solid islands of tumour (**Figure 3.3**). There was focal NPA staining within the cytoplasm and possibly on the cell surface of cancer cells. Much of this staining was within the tumour islands and was luminal in nature. Invasive $HER2^+$ samples showed a positive staining pattern similar to TNBC. The staining appeared weaker than observed in TNBC samples, and more cytoplasmic lectin staining was seen. Additionally, some positive NPA staining was seen for a spindle-shaped intermediate cell type which could be stromal fibroblasts (red arrows) and suspected macrophages (purple arrow). In both tissue subtypes, there was positive staining in areas of debris and inflammation.

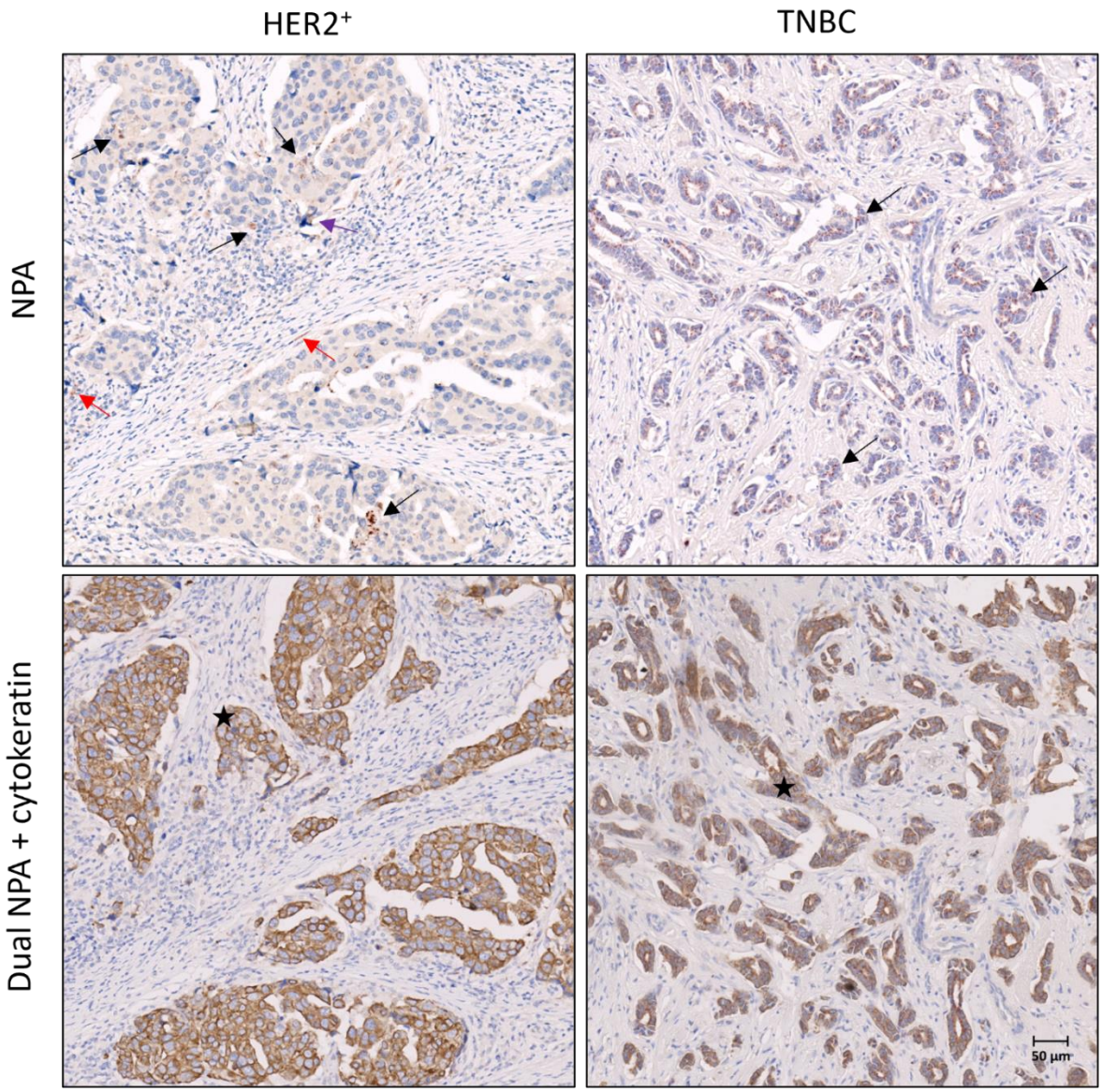

Figure 3.3: Human clinical full-faced breast cancer sections stained with NPA lectin and cytokeratin. Paraffin embedded tissues were stained with NPA lectin and haemoxylin counter-stain, or dual NPA lectin and cytokeratin with haemoxylin counter-stain. Slides were imaged on 10X magnification. NPA lectin staining in NovaRed (red). Cytokeratin staining in DAB (brown). Black arrows show granular lectin staining. Red arrows show fibroblast-like spindle cells. Purple arrow shows inflammatory cell. Black stars show areas defined as tumour by cytokeratin staining.

3.2.2 Mannose expression in metastasis

Studies have suggested that increased high-mannose may also play a role in BC metastasis. Therefore, after confirming the presence of high-mannose in primary tumours, we next wanted to determine if there was a similar pattern observed in metastatic BC.

Gene expression levels of the mannose processing enzymes were explored in metastatic, primary tumour, and solid tissue samples from the breast invasive carcinoma cohort of the TCGA Pan-Cancer dataset (**Figure 3.4**). Overall, there was a statistically significant difference in expression levels of almost all the mannose processing enzymes between metastatic, primary tumour, and normal tissue. The spread of data is larger within primary tumour samples relative to the other conditions. There was a trend towards an upregulation of glucosidases, namely MOSGS, GANAB and PRKCSH throughout BC progression, where expression levels were highest in metastatic samples and lowest in solid normal tissue (**Figure 3.4**). Further, there was a trend towards a downregulation in ER and Golgi mannosidases throughout BC progression (**Figure 3.4**). Indeed, MAN1A1, MAN1A2, and MAN1C1 expression was the lowest in metastatic samples and highest in solid normal tissue (**Figure 3.4**). Conversely, MAN1B1 expression appeared to positively correlate with breast oncogenesis (**Figure 3.4**).

These glycosidases are responsible for glycan trimming and the initiation towards hybrid- and complex- type glycans. Therefore, since there is a trend towards a downregulation of these enzymes could result in more high-mannose glycans. It is important to note that expression data for metastatic BC is represented by only 7 patients, and the site of metastasis was not available to interrogate despite it previously being noted as an important variable.

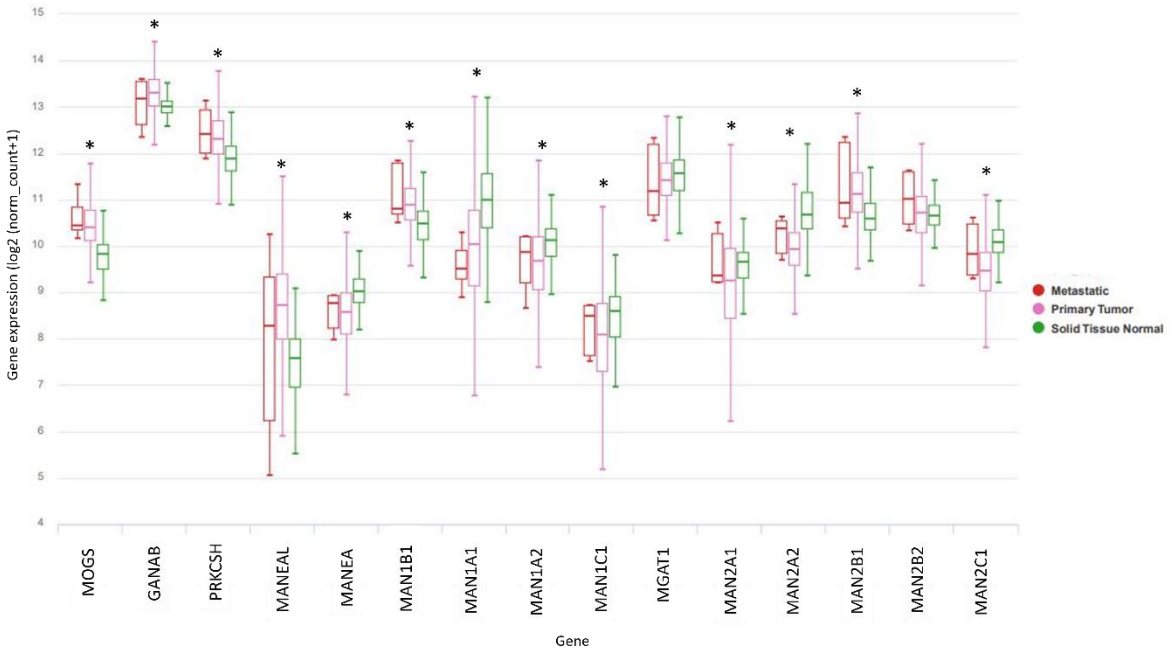

Figure 3.4: Gene expression data of mannose processing enzymes in invasive breast carcinoma samples within TCGA Pan-Cancer cohort on Xena Browser. 1218 samples were reanalysed by Xena using the same RNA-seq pipeline (re-aligned to hg38 genome and expressions are called using RSEM and Kallisto methods). Default statistical significance employed on Xena site, measured by One-way ANOVA * $p < 0.01$.

We next wanted to validate the differences between primary and metastatic tumours in a model system. Therefore, we used EO771 which is a primary murine TNBC cell line established from a spontaneous mammary adenocarcinoma in C57BL/6 mice (Casey, Laster and Ross, 1951), and EO771.LG which is established from parental EO771 mammary tumours which spontaneously metastasised to a lung nodule in C57BL/6 mice (Johnstone *et al.*, 2015a).

Whole cell RNA was isolated from the murine EO771 and EO771.LG model cell lines and sequencing and transcriptomics analyses were performed by GENEWIZ. In a similar fashion, expression levels of mannose processing enzymes were explored (**Figure 3.5**). MANEA was the most upregulated enzyme in EO771.LG, ~9 fold higher relative to EO771 (**Figure 3.5**). Interestingly, this trend was not observed in human samples, where MANEA was upregulated in primary tumour compared to matched normal tissue, but no obvious difference in expression was observed between primary tumour and metastasis (**Figure 3.4**). N-glycan trimming is remarkably conserved between human and mouse (Williams *et al.*, 1993; Helm *et al.*, 2022), therefore observed differences are not

predicted to be due to differences between species. In addition, since the metabolic environments between the EO771 and EO771.LG conditions were similar, comparisons between the cell lines were more controlled than the human clinical data, in which additional variables undoubtedly add further complexity to the results.

Within the murine samples, there was a significant increase in MAN1A1 expression in EO771.LG relative to EO771 (**Figure 3.5**). This is contrary to what was seen in the human clinical data where there was a down-regulation (**Figure 3.4**). MAN1B1 was significantly downregulated in the EO771.LG (**Figure 3.5**), which is also contrary to what was seen within the human clinical dataset where it increased. Since many of these enzymes, such as MAN1A1, MAN1A2, and MAN1C1 have overlapping substrate specificity, it is difficult to draw conclusions from this data.

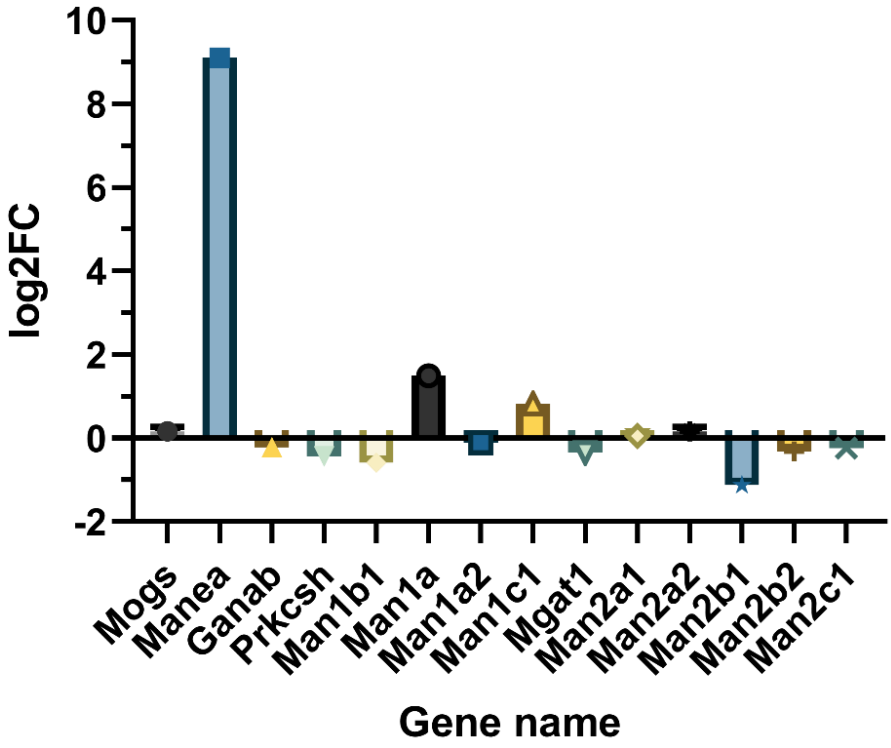

Figure 3.5: Differential expression data from EO771.LG (metastatic) compared to EO771 (primary). The log2 fold change expression of each gene is represented. Whole cell RNA was extracted from cells, and RNA sequencing and differential expression analysis was performed by GENEWIZ.

Expression levels of additional glycosyltransferases and glycosidases regulating N-glycosylation were compared in EO771.LG and EO771 (**Figure 3.6**). Many of the enzymes facilitating β-1,6-

branching were upregulated in EO771.LG; for example, MGAT5 and MGAT4a experienced a 5.8- and 2.3-fold increase in expression, relative to EO771 (**Figure 3.6**). Enzymes which hindered branching were downregulated, for example, MGAT3 expression was 1.7-fold less in EO771.LG, relative to EO771.

Therefore, within the metastatic environment, it appears that there is an upregulation of glycosyltransferases which initiate β1-6 branching and a downregulation of enzymes which interfere with the creation of that phenotype suggesting that high-mannose glycans may not be implicated in metastasis.

Gene name	log2FoldChange						
B3galt4	-2.491949612	St3gal6	-0.404914637	Alg1	0.019056	Dpy19l1	0.385357
St6gal1	-2.191201278	Alg9	-0.388623844	Lman2	0.038021	Lfng	0.388055
Mgat3	-1.785962325	Rft1	-0.347015576	Stt3a	0.043008	Chpf	0.403026
St6galnac2	-1.24156966	Mgat1	-0.343034249	Dpy19l4	0.051298	Alg14	0.411115
B3gnt9	-1.149580407	A4galt	-0.332500232	Man2a1	0.057656	Mgat4b	0.506434
Fut10	-1.129832796	Ost4	-0.332293831	Tmem258	0.083468	Pigm	0.509954
Man2b1	-1.121355699	Lman2l	-0.328848799	Ugcg	0.096397	Xylt2	0.515183
Fut7	-1.040398239	Man2b2	-0.313485587	Stt3b	0.112763	Fktn	0.57542
St6galnac6	-1.036764376	Alg5	-0.276219643	Pigv	0.11323	B3gnt7	0.589047
St3gal1	-1.003760302	Galnt2	-0.258221736	Extl2	0.119469	Galnt4	0.610015
Galnt1	-0.959476261	Poglut1	-0.242947672	Gfpt2	0.120436	Ext1	0.625126
Dpagt1	-0.828066605	Man2c1	-0.230993431	B3galt6	0.133957	Fut8	0.639131
Pomt2	-0.766253344	St3gal3	-0.221268033	Alg3	0.139203	B4galt3	0.741584
Eogt	-0.733795077	Chsy1	-0.203030106	Fkrp	0.14318	B3gat3	0.759641
Pofut2	-0.709441816	Galnt11	-0.177530666	Dpy19l3	0.148839	Man1c1	0.827368
Serp1	-0.68809543	Nus1	-0.173213487	Galnt15	0.16116	Alg13	0.83492
Dad1	-0.661722122	Rpn2	-0.170516968	Man2a2	0.161361	Xylt1	0.888303
B4galt1	-0.655740695	Colgalt1	-0.166464495	Mogs	0.169302	Piga	0.960767
B4galt5	-0.640086117	Dolpp1	-0.162311312	Pigb	0.175743	Csgalnact2	1.209346
Alg11	-0.621285639	B3glct	-0.136576879	Gcnt1	0.182433	Entpd5	1.311049
Dpm1	-0.608839628	Pofut1	-0.128479776	Large1	0.19551	St3gal4	1.370572
Rfng	-0.595310168	Tusc3	-0.112153817	Ddost	0.210253	Man1a	1.498751
Chpf2	-0.595009391	Alg12	-0.111846465	Ostc	0.219484	B3gnt8	1.752772
Man1b1	-0.584483358	Pomgnt2	-0.106755972	Pmm2	0.254511	Mfng	1.905472
Pomt1	-0.569026822	Rpn1	-0.105549974	Gxylt1	0.270154	Galnt3	2.167386
B3gnt3	-0.546881254	Man1a2	-0.105002922	B3gnt2	0.27043	Mgat4a	2.28668
Alg8	-0.528861572	Pigk	-0.104130336	Gcnt2	0.272964	Galnt10	2.817476
Tmtc4	-0.519324064	B4galt7	-0.093352922	Magt1	0.28637	Extl1	2.892326
Extl3	-0.51784308	Galnt7	-0.077723685	Ogt	0.288836	Fut4	2.900312
B4gat1	-0.510095629	Alg6	-0.061215215	Pomgnt1	0.290306	Fut2	3.68019
Ext2	-0.507104449	St3gal2	-0.050586995	St3gal5	0.300841	Large2	4.317688
B3galnt2	-0.502654616	C1galt1c1	-0.049557794	B4galt2	0.327718	Csgalnact1	5.510798
Fut11	-0.473295128	Xxylt1	-0.00779999	Dhdds	0.374802	Mgat5	5.855968
Pmm1	-0.471631444	C1galt1	-0.004922674	Manba	0.379527	B4galt4	8.401188
Tmtc3	-0.428254417	Krtcap2	0.004435785	Gfpt1	0.380066	Manea	9.10225
St6galnac4	-0.425555712	Mgat2	0.012816573	Alg2	0.381156		

Figure 3.6: Fold change data from expression values of glycosyltransferases expressed in EO771.LG (metastatic) relative to EO771 (primary). The most downregulated genes are coloured in green, and the most upregulated genes are coloured in red. Whole cell RNA was extracted from cells, and RNA sequencing and differential expression analysis was performed by GENEWIZ.

To validate the RNAseq data, we performed NPA staining of murine *ex vivo* tissue samples from EO771 primary tumours and EO771.LG lung metastases, to determine the presence of mannose at primary and metastatic lung sites (**Figure 3.7**). NPA staining within the primary tumour tissue from the mammary fat pad revealed weak cytoplasmic staining and more concentrated granular staining on the membrane (**Figure 3.7**). Within the lung tissue, metastatic nodules were identified, and positive granular lectin staining was observed, particularly on the cells lining these metastatic nodules (**Figure 3.7**). There appeared to be less staining within the core of the nodule itself. Staining within the primary tumour was more prevalent across the tissue, compared to the metastatic sample.

Overall, there was staining associated with the tumour cells which was dotty and granular in nature (**Figure 3.7**), similar to what was observed in human clinical samples (**Figure 3.3**). This instilled confidence that this data is translatable and of value to study *in vivo.* Differences in staining patterns between primary tumour and metastatic tumour were observed, and mannose staining did not appear to be stronger in metastatic samples.

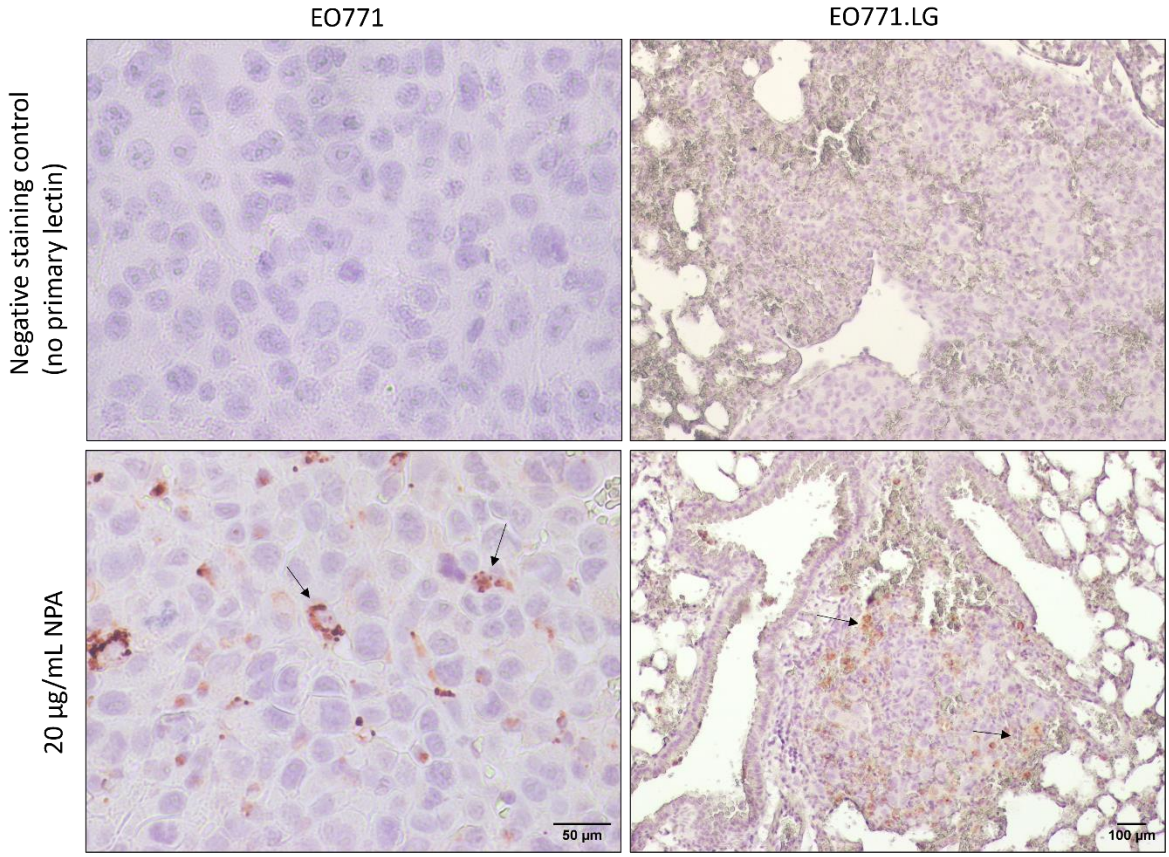

Figure 3.7: *Ex vivo* murine primary tumour (EO771) and lung metastatic nodules (EO771.LG) stained for mannose N-glycans with NPA. EO771 cells were injected subcutaneously into the mammary fat pad of C57BL/6 mice. EO771.LG cells were intravenously injected into the tail vein of C57BL/6 mice. Tissues were harvested and paraffin embedded, and sections were cut for IHC staining. NPA lectin staining and haemoxylin counter-stain was performed. Negative controls where no primary lectin but secondary detection and chromogen staining was performed. NPA lectin staining in NovaRed. Black arrows show representative granular lectin staining. Slides were imaged at 40X magnification for primary tumours and 10X magnification for metastatic nodules.

3.2.3 Cell surface mannose expression

Cell surface high-mannose glycans may directly impact interactions of tumour cells with the extracellular matrix and other cells within the TME. In addition, its presence could serve as a potential therapeutic target. IHC data showed positive staining for mannose, but it was difficult to establish the proximal location, due to difficulties with cytokeratin masking, and since incompletely processed intracellular glycoproteins would have also likely stained positive. Therefore, the

proportion of high-mannose glycans presented on the cell surface of human and murine BC cell lines was next determined.

Since no isotype control is available for lectin flow cytometry, a protocol had to be optimised to assess background binding. NPA lectin was competitively inhibited using its hapten sugar. 400 mM alpha-methylmannoside was incubated with 20 µg/mL NPA for 2 hours at room temperature in either H_2O or blocking buffer (0.5% BSA-PBS) to explore NPA activity and adsorption. To probe for cell surface mannose levels, cells were opsonised with biotinylated NPA and detected with a streptavidin FITC-conjugated secondary antibody (**Figure 3.8**). Cell surface mannose levels were indicated as a measure of fluorescent intensity in the FITC channel.

NPA adsorbed with H_2O inhibited its binding more than lectin adsorbed with 0.5% BSA-PBS. Although NPA binding was not completely abolished, both methods of lectin adsorption reduced cell surface binding. For the remainder of this research, lectins were adsorbed in H_2O, unless otherwise stated.

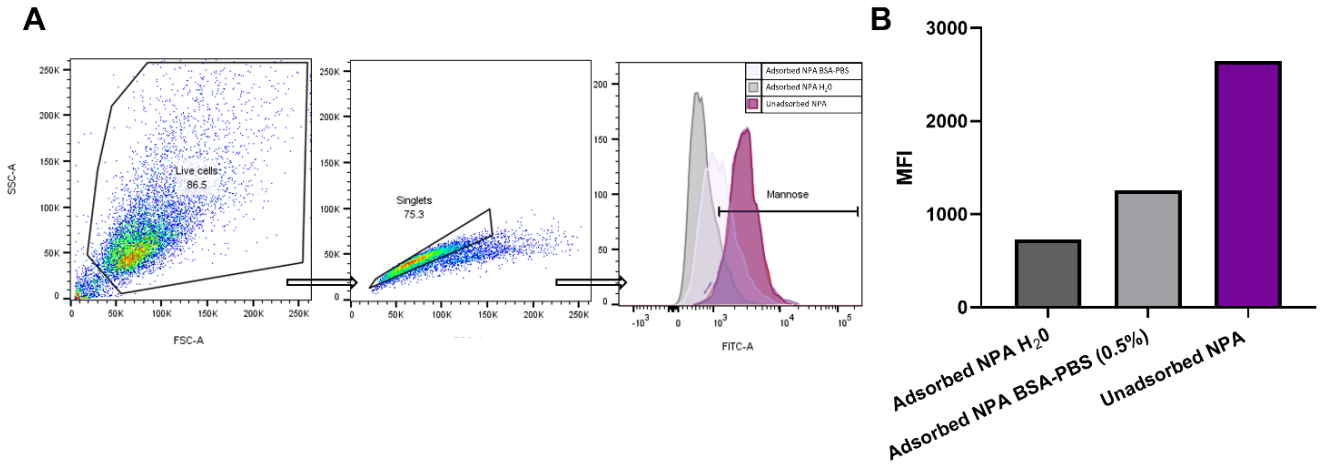

Figure 3.8: Cell surface mannose probing of SKBR3 cells with NPA lectin adsorbed by different methods. (A) Gating strategy for flow cytometry analysis of cell surface glycan epitopes. Live cells were gated prior to single cell gating. Mannose expression was visualised on the FITC channel. (B) Mean fluorescent intensities quantified from the mannose gate.

Once we had optimised NPA labelling for flow cytometry analysis, cell surface mannose expression on human BC cell lines was then determined. Two human TNBC cell lines were used, of which HCC1143 is derived from a primary cancer and MDA-MB-231 is derived from a metastatic cancer. Additionally, three $HER2^+$ BC cell lines were analysed. SKBR3 is a high-expressing HER2 primary BC and MCF7 is a low-expressing HER2 BC. MDA-MB-453 is a metastatic $HER2^+$ BC cell line.

All human cell lines expressed cell surface mannose (**Figure 3.9**). HCC1143 had the highest and most variable expression out of all the cell lines. The average cell surface mannose levels of HCC1143 were twice that of the metastatic TNBC cell line, MDA-MB-231. SKBR3 had the second-highest levels of mannose expression. Similarly, SKBR3 had higher levels of mannose expression than the $HER2^+$ metastatic MDA-MB-453 cell line. MCF7 expressed the lowest levels of mannose but showed the least variability. Overall, $HER2^+$ cell lines appear to express lower levels of mannose than TNBC cells and exhibit less variability in expression. Further, cell lines derived from the primary tumour site appeared to express higher levels of cell surface mannose than the metastatic lines.

Of note is the large range of results within each sample (**Figure 3.9**). Minor differences can impact a cell's glycosylation pattern. To control for variations in glycosylation due to cell growth phase, experiments were consistently performed 48 hours after cell passaging. A one-way ANOVA was performed to explore statistical significance between the means. Presumably, due to the high variability and low number of samples, differences in the mean cell surface mannose levels between the cell lines were not statistically significant. A Shapiro-Wilk test was performed to ensure data fit a normal Gaussian distribution (**Appendix 1**) and appropriate statistics were employed.

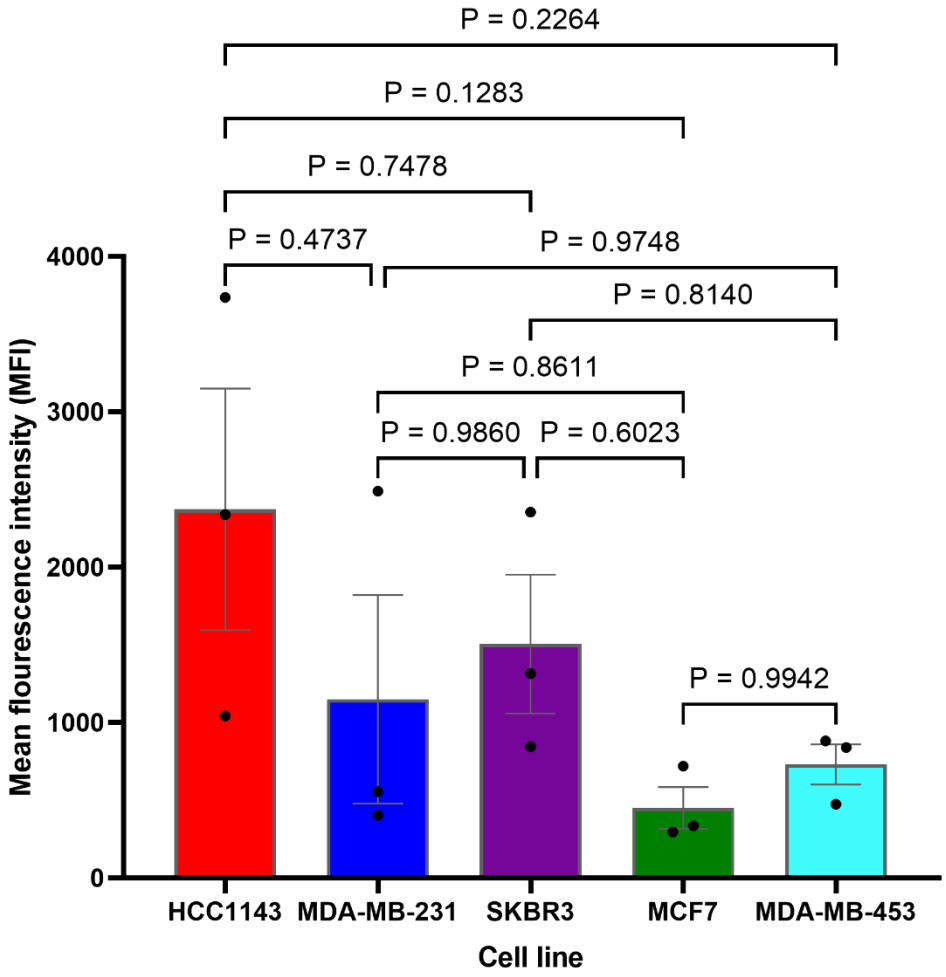

Figure 3.9: Cell surface mannose probing of human breast tumour cell lines with NPA lectin. Cells were cultured and opsonised with the biotin labelled anti-mannose lectin NPA for 30 minutes on ice. Cells were washed with BSA-PBS and a secondary streptavidin-FITC antibody was applied for 30 mins on ice. Adsorbed background lectin binding values were subtracted from test values and plotted. The mean and SEM shown, and a One-way ANOVA was performed.

Cell surface mannose levels were also determined in the murine TNBC model cell lines EO771 and EO771.LG (**Figure 3.10**). EO771 and EO771.LG expressed cell surface mannose at a similar level (**Figure 3.10**). A similar trend towards decreased cell surface mannose was seen in the metastatic versus primary cell line (**Figure 3.10**), as seen with the human cell lines (**Figure 3.9**).

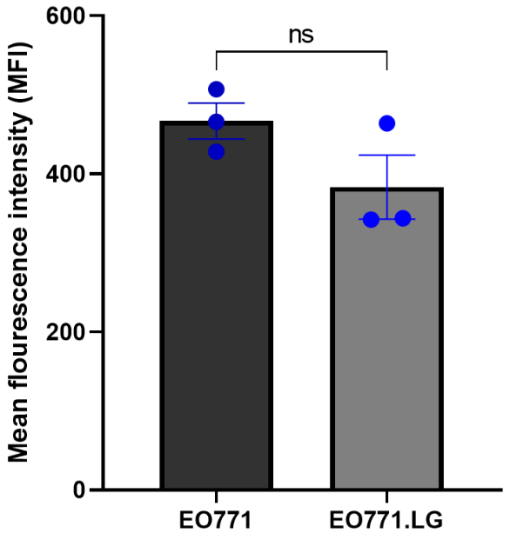

Figure 3.10: Cell surface mannose probing by NPA lectin in murine TNBC EO771 cells and EO771.LG. Cells were cultured and opsonised with the biotin labelled anti-mannose lectin NPA for 30 minutes on ice. Cells were washed with BSA-PBS and a secondary streptavidin-FITC antibody was applied for 30 mins on ice. Adsorbed background lectin binding values were subtracted from test values and plotted. The mean and SEM of triplicate experiments shown. Statistical significance was tested using an unpaired T-test.

3.2.4 Generating high-mannose cell lines using the small molecule inhibitor, Kifunensine

Kifunensine (Kif) is a small molecule inhibitor of alpha-mannosidase enzymes. Treatment of cells with Kif prevents complete glycan processing resulting in under-processed, high-mannose N-linked glycoproteins (**Figure 3.11**). This allows us to utilise it as a tool to transiently investigate the impact of elevated high-mannose glycans on BC phenotypes.

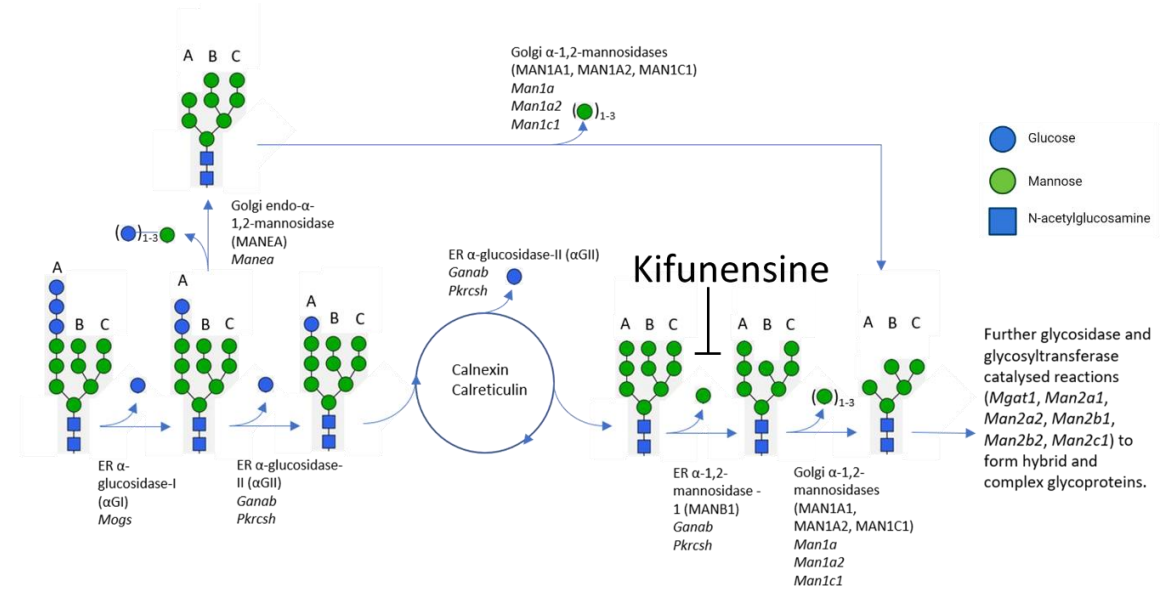

Figure 3.11: Simplified schematic of the N-glycosylation pathway and the effects of Kifunensine on glycan maturation.

First, Kif treatment was optimised using EO771 cells. Cells were titrated with 10 µM, 20 µM, and 30 µM Kif for 48 hours. To confirm the presence of high-mannose glycans, N-glycans were released from whole-cell lysate, and the purified N-linked glycans were subsequently analysed by Ultra-pure liquid chromatography (UPLC) and Mass Spectrometry (MS). Overall, all concentrations of Kif shifted the N-glycan profile towards a predominantly high-mannose phenotype. **Figure 3.12B-D** show the UPLC traces of glycans from cells incubated with 10 µM, 20 µM, and 30 µM Kif to be almost identical, and different to untreated control cells (**Figure 3.12A**). MS was performed to determine these glycan structures. High-mannose, specifically Man_9, structures were responsible for the peak annotated in **Figure 3.12F**. This structure was deduced from its doubly charged negative ion monoisotopic mass. Therefore, 10 µM Kif was used from herein to create a transient high-mannose phenotype.

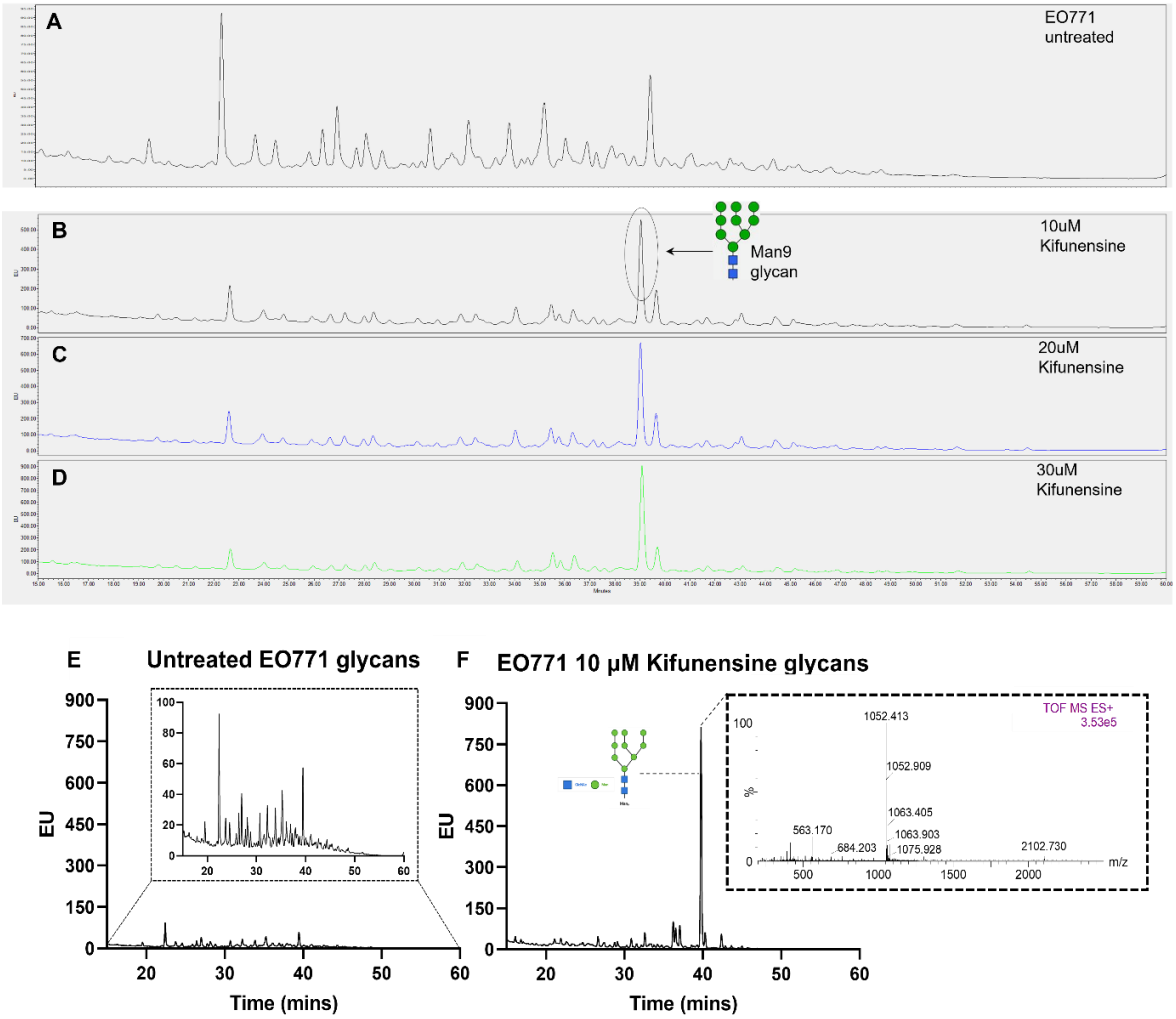

Figure 3.12: Ultra-pure liquid chromatography (UPLC) and Mass Spectrometry analysis of N-linked glycans. EO771 cells were A untreated, or cultured with B 10 µM Kif, C 20 µM Kif, or D 30 µM Kif for 48 hours. Cell lysates were extracted and trypsinised. N-glycans were released in solution from glycopeptides using PNGase F, procainamide-labelled, desalted and purified by carbon column and porous graphite column chromatography. Samples were analysed by HILIC-UPLC [Acquity H-Class UPLC, 2.1 mm × 150 mm Acquity BEH Glycan column (Waters)] (**A**-**D**) and Mass Spectrometry [direct infusion into Synapt G2Si (Waters)] (**E** and **F**) in tandem. **F** shows how high-mannose structures were deduced from their doubly charged negative ion monoisotopic masses.

Once we had established that treatment with Kif could increase Man_9, it was important to determine the potential impact of Kif on cell viability. To maximise the impact of Kif on protein turnover, cells were cultured with 10 µM Kif for 48 and 72 hours, respectively. Cells were imaged and harvested, and viability was measured by trypan blue stain (**Figure 3.13**). Cells treated with Kif

for 48 hours showed no difference in morphology compared to untreated EO771 cells (**Figure 3.13**). EO771 cells exhibit both fibroblast-like and epithelial-like morphologies. **Figure 3.13A** demonstrates that at 48 hours the cells look similar confluency. However, at 72 hours, Kif-treated cells appeared less confluent, became less fibroblast-like and adherent, and exhibited a more epithelial-like morphology. Cell viability was measured by trypan blue staining and revealed cells treated with Kif for 72 hours had dropped by almost half, compared to untreated EO771 cells. Therefore, cells were treated with 10 µM Kif for 48 hours herein to create a transient high-mannose phenotype.

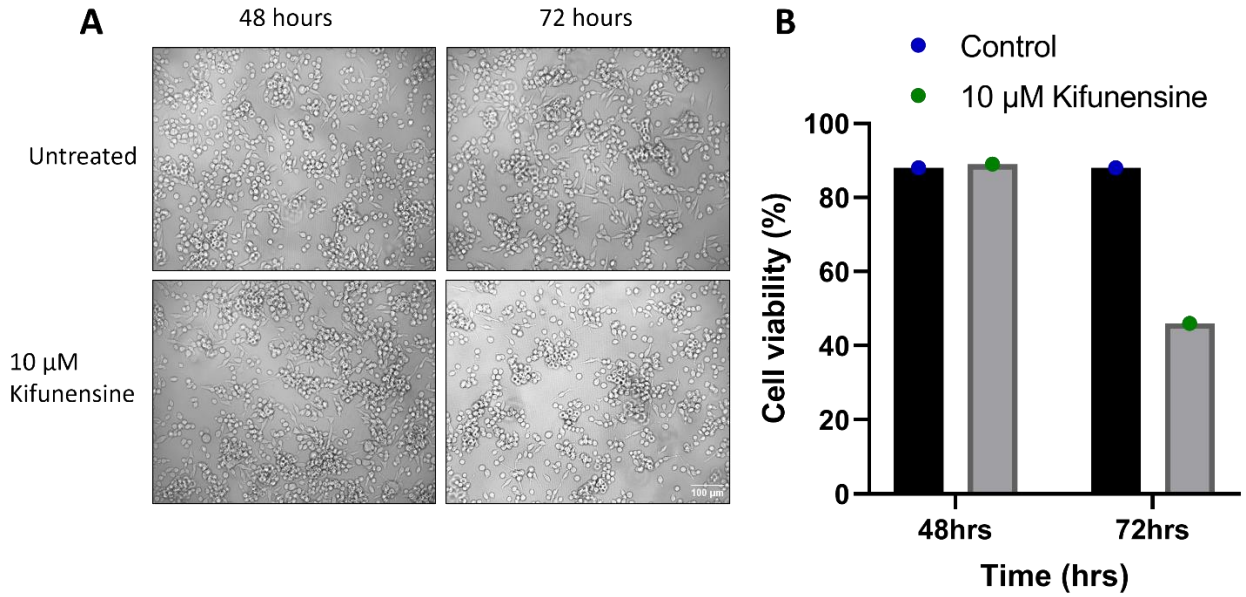

Figure 3.13: Impact of Kifunensine on cell viability. EO771 cells treated with or without 10 µM Kif, incubated for 48 hours and 72 hours, respectively. (A) Images of cells at 10X magnification. (B) Cell viability was measured by trypan blue at 48 and 72 hours.

Cell surface mannose levels of Kif-treated cells were then determined by flow cytometry (**Figure 3.14; Figure 3.15**). As previously described, biotinylated NPA lectin was used to detect cell surface mannose. Mannose levels were determined on the EO771 and EO771.LG murine TNBC cell lines (**Figure 3.14**). Both cell lines had similar levels of baseline mannose expression. When treated with Kif, the average mean fluorescent index (MFI) of EO771 and EO771.LG increased from ~500 to 6000 (**Figure 3.14**). Data are from three independent experiments with the mean + SEM are shown. An unpaired T-test was performed showing there was a statistically significant difference between the MFI of Kif-treated EO771 cells and untreated cells.

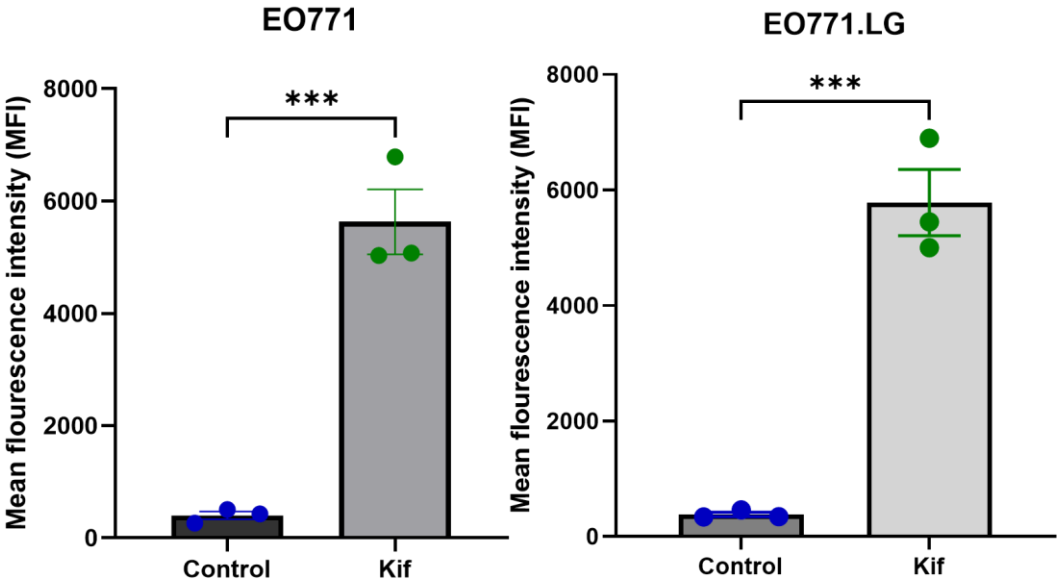

Figure 3.14: Cell surface mannose probing of EO771 and EO771.LG cell lines. Cells were cultured with 10 µM Kifunensine for 48 hours. Cells were opsonised with the biotin labelled anti-mannose lectin NPA for 30 minutes on ice. Cells were washed with BSA-PBS and incubated with a secondary streptavidin-FITC. Data are from three independent experiments with the mean + SEM. *** $p<0.001$ Unpaired T test.

A similar trend was observed when human BC cell lines were cultured with Kif (**Figure 3.15**). Multiple paired T-tests were performed to test for statistical significance. A Shapiro-Wilk test was performed to ensure data fit a normal Gaussian distribution (**Appendix 2**) and appropriate statistics were employed. Although differences were not statistically significant for most cell lines, Kif increased cell surface mannose dramatically across all cell lines. Therefore, culturing cells with 10 µM Kif for 48 hours was used as an extrinsic tool to investigate the effects of high-mannose glycans.

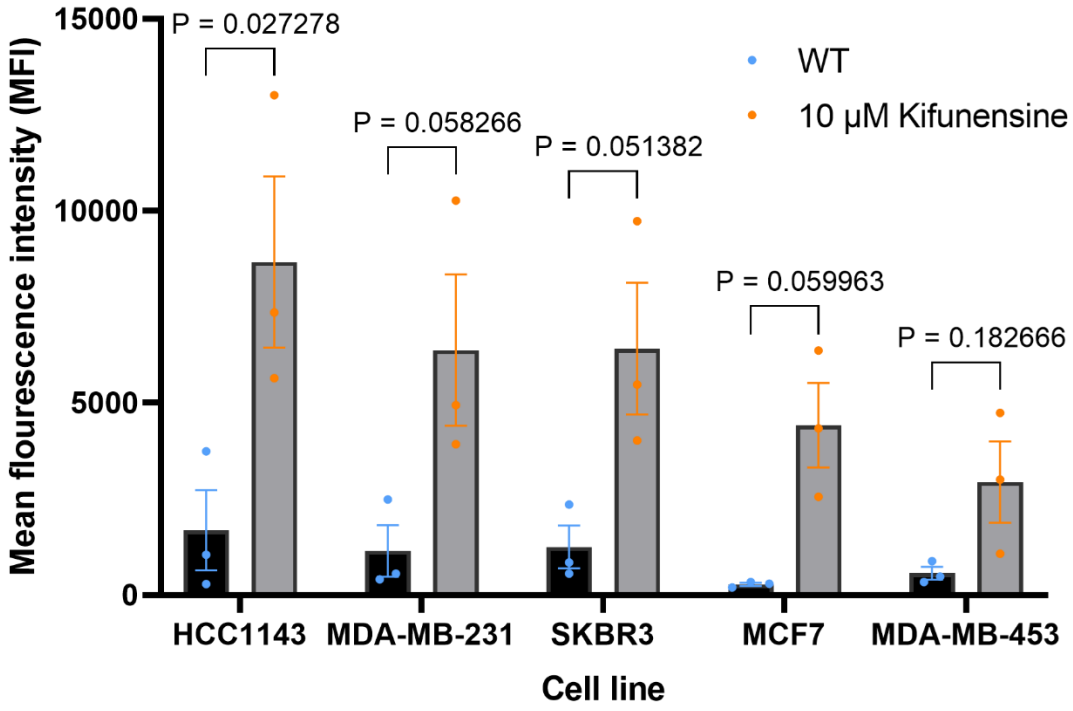

Figure 3.15: Cell surface mannose probing of human breast tumour cell lines treated with Kif with NPA lectin. Cells were cultured with 10 µM Kifunensine for 48 hours. Cells were opsonised with the biotin labelled anti-mannose lectin NPA for 30 minutes on ice. Cells were washed with BSA-PBS and incubated with a secondary streptavidin-FITC. Data are from three independent experiments with the mean + SEM. Multiple paired T-tests were performed to test for statistical significance.

We next wanted to determine whether the transient increase in high-mannose glycans by Kif treatment impacted the phenotypic features of BC cells. EO771 cells were cultured with or without 10 µM Kif for 24 or 48 hours. Cells were harvested and live cell counts were performed (**Figure 3.16**). Overall, Kif treatment did not alter the morphology or rates of proliferation of EO771 cells.

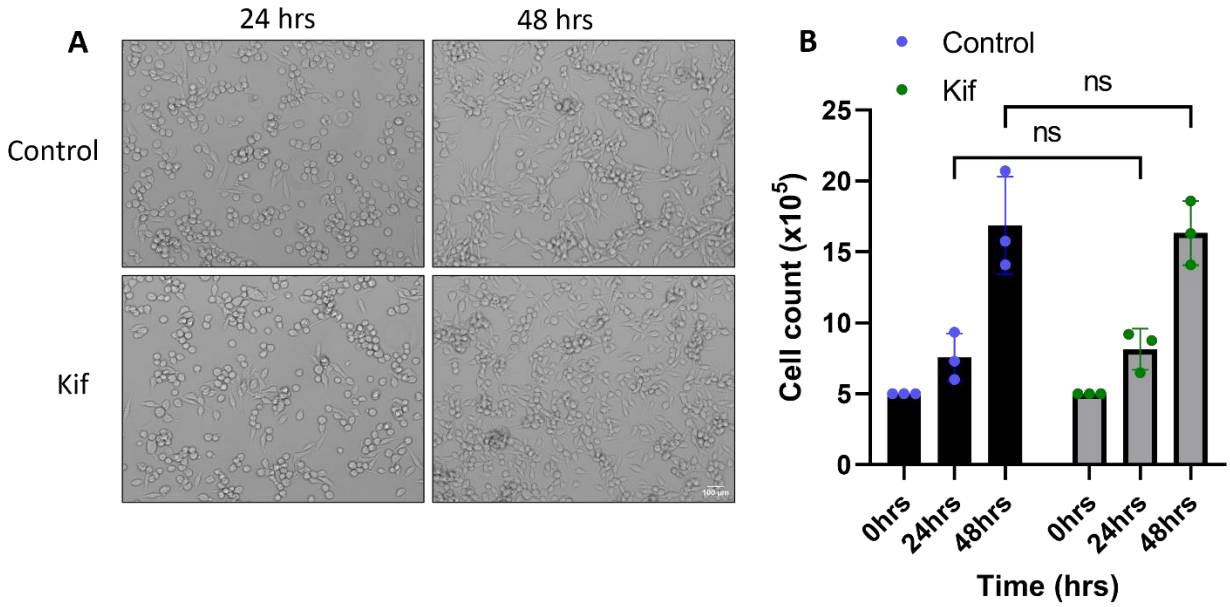

Figure 3.16: Effect of Kifunensine treatment on EO771 cell proliferation. EO771 cells were seeded and cultured with or without 10 µM Kifunensine. (A) Cells were imaged at 10X magnification prior at 24 and 48 hours, respectively. (B) Cells were harvested at the respective time points and viable cells were counted by AO/PI stain. Statistical significance was determined using multiple paired T-tests between Kif treated cells and untreated. Mean and SEM of 3 independent experiments was shown.

The duration in which the high-mannose phenotype induced by Kif was retained by cells was then determined. EO771 cells were cultured with 10 µM Kif for 48 hours. Kif media was removed and replaced with standard media. Cells were harvested at 0 hours, 3 hours, 6 hours, 9 hours, 24 hours, and 72 hours, and whole-cell lysate was extracted. Purified N-linked glycans were analysed by UPLC (**Figure 3.17**). Overall, UPLC traces did not change considerably between the time points 0, 3, 6, 9, and 24 hours. At time 0, the UPLC trace showed the predominant peak to be the Man_9 (**Figure 3.17**), as identified previously in **Figure 3.12F**. The high-mannose peak was maintained for up to 24 hours (**Figure 3.17**). At 72 hours, the high-mannose peak was reduced (**Figure 3.17**), and the glycan profile was similar to untreated cells (**Figure 3.12E**). From this, it can be seen the Kif treatment is a transient modification retained for between 24 and 72 hours.

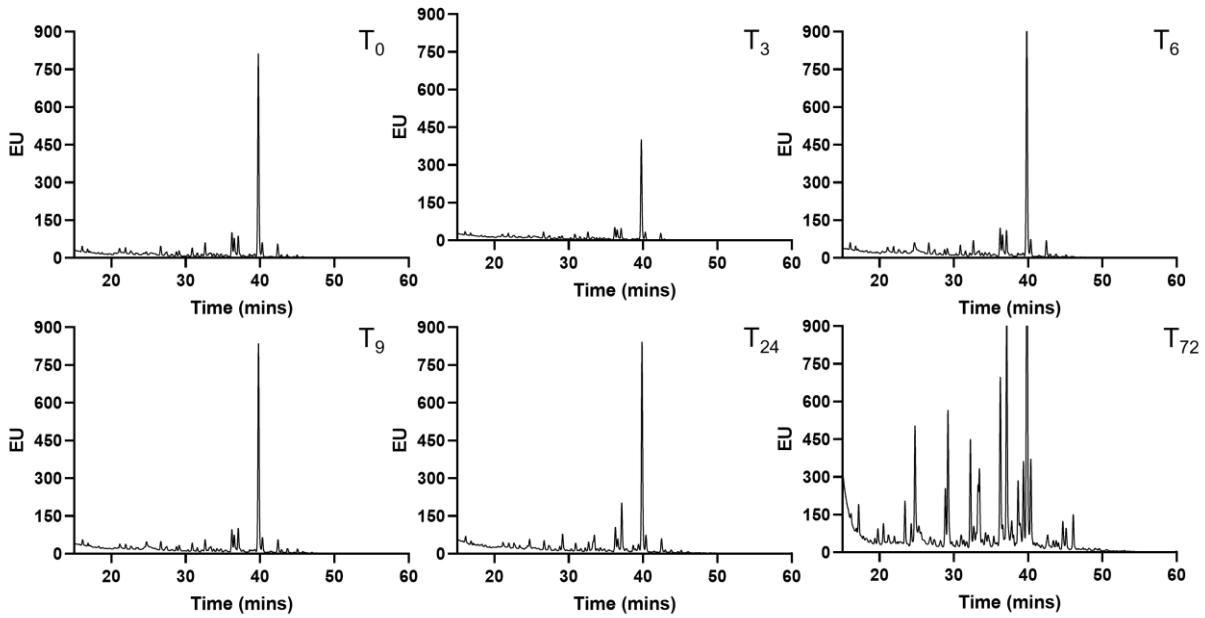

Figure 3.17: Kif time course on glycan repertoire of EO771 cells. EO771 cells were cultured with 10 µM Kif for 48 hours. Cells were washed and re-plated in fresh media in the absence of Kif. Cells were harvested at defined time points, where Tx = x hours. Whole cell lysates were extracted and trypsinised. N-glycans were released in solution from glycopeptides by PNGase F, procainamide-labelled, desalted and purified by carbon column and porous graphite column chromatography. Samples were analysed by HILIC-UPLC [Acquity H-Class UPLC, 2.1 mm × 150 mm Acquity BEH Glycan column (Waters)].

3.2.4.1 The impact of high-mannose glycans by Kifunensine, *in vitro*

After establishing the kinetics of using Kif to generate a high-mannose tumour model, we next wanted to determine if high-mannose glycans impacted the phenotypic features of the BC cells. To do this, we investigated cell migration and invasion using transwell migration and invasion assays, and cell migration by scratch wound assay.

3.2.4.1.1 Cell migration

Transwell migration assays measure the directional migration of individual cells in response to a chemical stimulus. We used FCS to create a chemotaxic gradient, and fibronectin-coated transwells to create a haptotaxic gradient to stimulate directional cell migration. Control wells in the absence of the chemo-attractant, FCS were employed. In this assay, cells were harvested and applied to

fibronectin-coated transwell chambers with a pore size of 8 µm. After 4-5 hours, cells that had migrated through the polycarbonate membrane were fixed, stained, and counted.

First, we established baseline migration rates of EO771 and EO771.LG (**Figure 3.18**). A larger number of EO771.LG cells migrated over time than EO771 cells, suggesting a faster rate of individual cell migration, although this rate was not statistically significant (**Figure 3.18**).

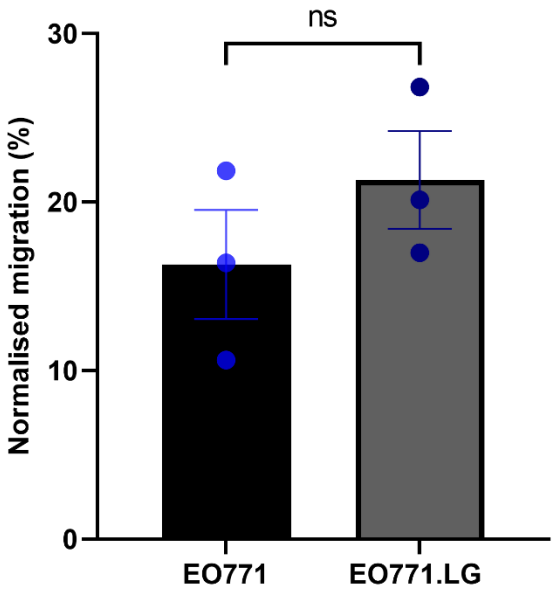

Figure 3.18: Transwell migration assay of EO771 and EO771.LG cells. Cells were applied to fibronectin-coated migration chambers and allowed to migrate through the polycarbonate membrane inserts with 8 µm pores for 4-5 hours. Cells were fixed, stained, and counted with at least 8 fields of view per membrane at 20X magnification. Control wells were performed in the absence of the FCS chemo-attractant. Data was normalised by subtracting control wells and expressed as percentage of migrated cells. Mean and SEM of triplicate experiments are plotted. Statistical significance was tested using unpaired T-test.

Once baseline migration was established, we then established the effects of Kif treatment, and thus high-mannose glycans on cell migration. EO771 and EO771.LG cells were cultured with 10 µM Kif for 48 hours prior to the transwell experiment. Cells were harvested and applied to the fibronectin-coated transwell chambers, as before. For adequate cell migration, migration assays were

performed in the presence of an FCS gradient, and control wells were performed in the absence of an FCS chemo-attractant (0% FCS control) (**Figure 3.19**).

Consistently, the high-mannose phenotype impeded the migration of EO771 cells (**Figure 3.19A**). Fewer Kif-treated cells (EO771.Kif) migrated through the membrane than untreated EO771 cells, when in the presence of the chemo-attractant, FCS. This trend was also true in the absence of the chemotaxic gradient, suggesting Kif treatment impeded the non-directional migration of EO771 cells as well. The lack of statistical significance between EO771.Kif and EO771 were presumably due to the large deviation of data.

A similar trend was observed with the metastatic line. Consistently, Kif treatment impeded cell migration of EO771.LG cells (**Figure 3.19B**). As before, fewer Kif-treated cells (EO771.LG.Kif) migrated through the membrane than untreated EO771.LG cells, in the presence of the chemo-attractant. In the absence of the chemotaxic gradient, there was no difference in the number of cells migrating by chance. This difference between the migration of EO771.LG.Kif and EO771.LG was statistically significant, as measured by an unpaired T-test.

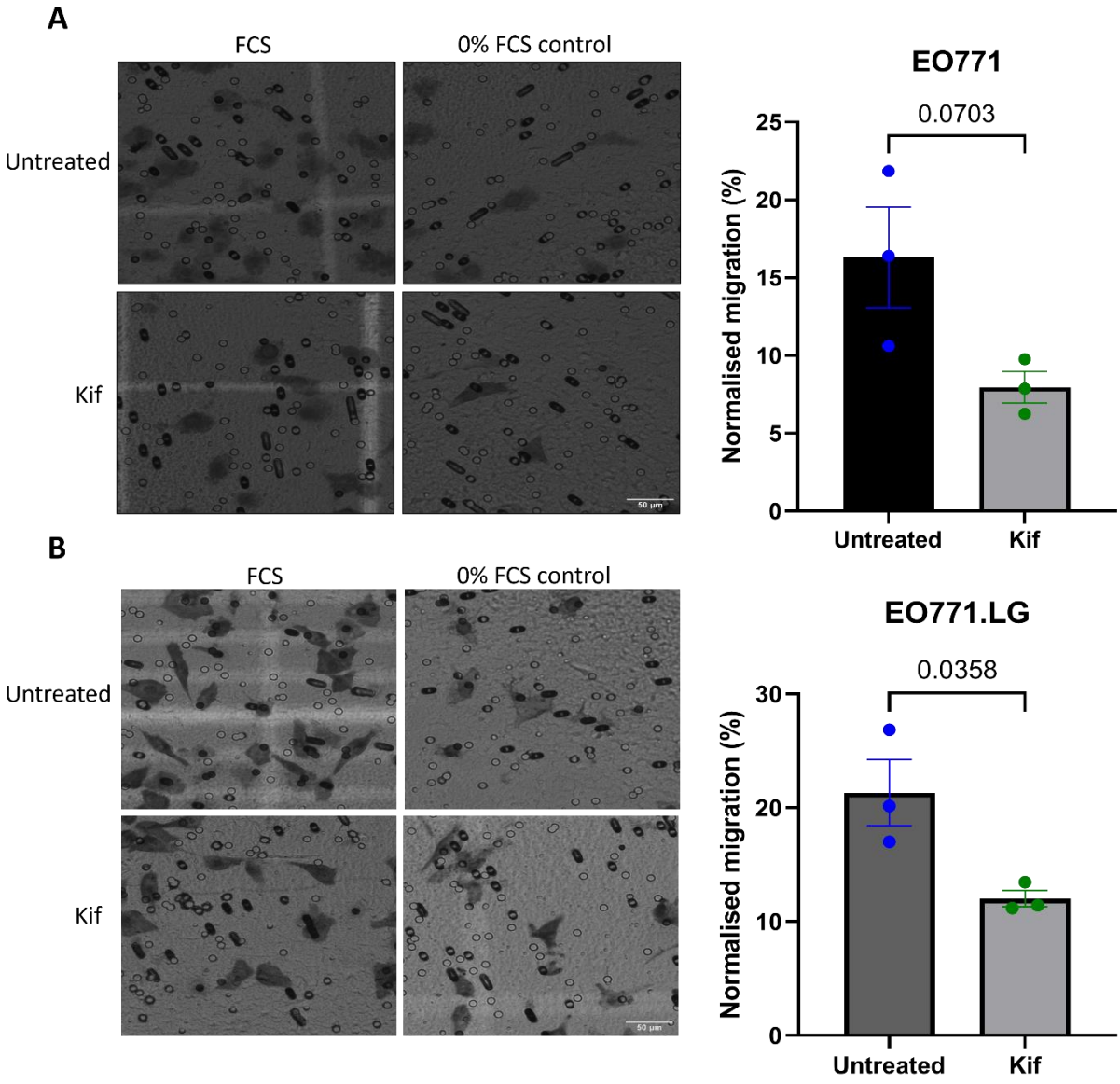

Figure 3.19: Transwell migration assay of Kif treated and untreated EO771 (primary) and EO771.LG (metastatic) cells. Cells were cultured with 10 µM Kif for 48 hours. Cells were applied to fibronectin-coated migration chambers and allowed to migrate through the polycarbonate membrane inserts with 8 µm pores for 4-5 hours. Cells were fixed, stained, and counted with at least 8 fields of view per membrane at 20X magnification. Control wells were performed in the absence of the FBS chemo-attractant. Data was normalised by subtracting control wells and expressed as percentage of migrated cells. (A) EO771 cells. (B) EO771.LG cells. Mean and SEM of triplicate experiments are plotted. Statistical significance was tested using unpaired T-tests analysis.

The effects of Kif on cellular sheet migration were determined using a scratch wound assay. This assay helps to understand the potential impact of high-mannose glycans on the dynamics of collective cell sheet migration. Typically, a scratch is created within a monolayer of cultured cells, and the closure of the gap is observed and analysed over time. Despite best efforts, when performing the scratch the EO771 cell monolayer would lift, preventing consistent results from being obtained. Therefore, we optimised this assay to employ the use of a scratch-wound insert. Silicone inserts of defined size were placed within a culture plate to create a cell-free area, and cells were cultured around the insert. After 24 hours, the insert was carefully peeled off the plate mimicking a 'scratch'. Defined junctions of the insert were imaged over time to observe the gap closure.

Kif treatment impeded cellular sheet migration of EO771 and EO771.LG cells (**Figure 3.20A**). Kif-treated cells did not migrate effectively to close the wound, and by 48 hours cells began to clump and lift from the plate (**Figure 3.20A**). Untreated EO771 cells collectively migrated to close the wound at a faster rate than Kif-treated cells, as seen by the smaller '% open' value (**Figure 3.20B**). This was true at both 24 hours and 48 hours. Similarly, untreated EO771.LG cells collectively migrated at a faster rate than Kif-treated cells (**Figure 3.20C**). This difference became more pronounced over 48 hours.

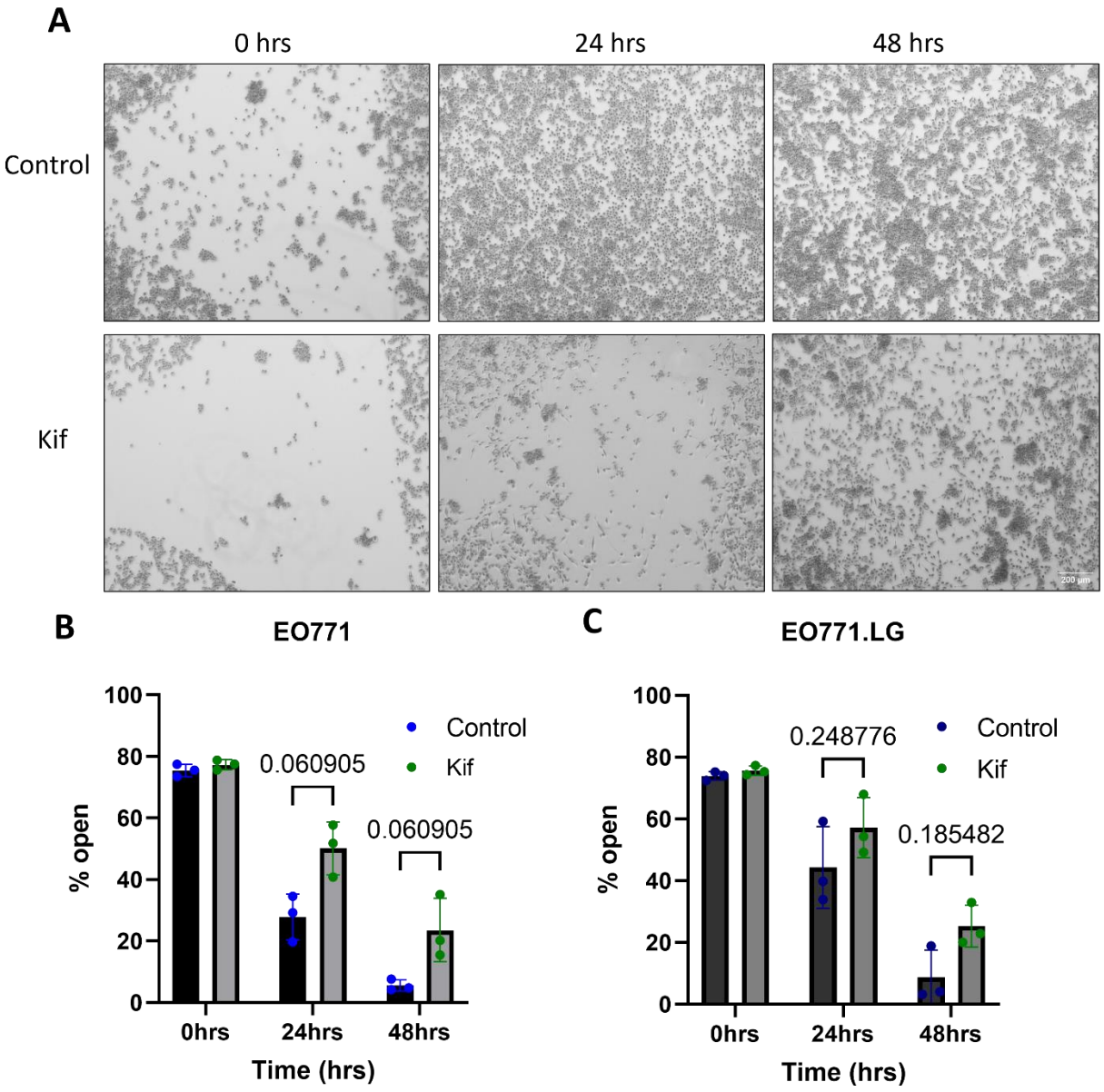

Figure 3.20: Scratch wound assay of Kifunensine treated and untreated EO771 (primary) and EO771.LG (metastatic) cells. Culture inserts were placed in the centre of a 6 well plate. EO771 cells were seeded around a culture insert +/- 10 µM Kifunensine and incubated at 37˚C, 5% CO2 for 24 hours. Media was aspirated, inserts were removed, and wound was washed with PBS to remove debris. Fresh media was added, and plates were incubated for 48 hours. Plates were imaged at 10X magnification at the same intersection of insert at 24 and 48 hours. Images were analysed by Tscratch and results were presented as % open of wound. (A) Representative images of scratch intersection. (B) Data from EO771 cells. (C) Data from EO771.LG cells. Mean and SEM of triplicate experiments are plotted. Statistical significance was tested using multiple paired T-tests analysis.

3.2.4.1.2 Cell invasion

For cells to metastasise, they must first penetrate and invade through the surrounding tissues into circulation. Therefore, transwell invasion assays were employed to investigate the invasive capacity of the cells, which may give some insight into metastatic potential.

Transwell invasion assays measure the directional invasion of individual cells through a collagen matrix in response to a chemical stimulus. As before, we used FCS to create a chemotaxic gradient, and fibronectin-coated transwells to create a haptotaxic gradient to stimulate directional cell invasion. Control wells in the absence of the chemo-attractant, FCS were employed. In this assay, cells were harvested and resuspended in collagen matrix diluted with RPMI to form a collagen-rich suspension. This was placed on top of fibronectin-coated transwell chambers with a pore size of 8 μm. After 24 hours, cells that had invaded through the collagen layer and polycarbonate membrane were fixed, stained, and counted.

First, the concentration of collagen matrix for this assay was optimised, as shown in **Figure 3.21**. At 2 mg/mL collagen, there was not a large difference between cells invading directionally toward a chemotaxic gradient and non-specific invasion. At 0.5 mg/mL, there was a large enough difference to observe directional invasion compared to the no-chemotaxic gradient control. However, the variability in the raw number of cells invading at 0.5 mg/mL collagen was large. This variability was reduced at 1 mg/mL collagen, therefore this concentration was employed for transwell invasion assays from hereon in.

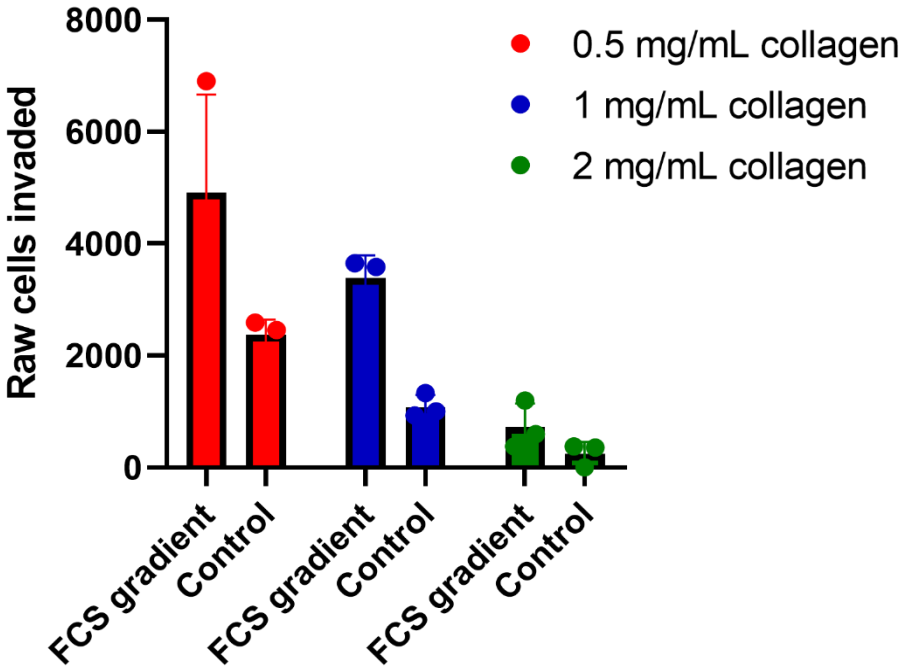

Figure 3.21: Optimisation of collagen concentration to use for transwell invasion assay. Cells were suspended in a collagen-rich suspension (0.5 mg/mL, 1 mg/mL, 2 mg/mL collagen) and applied to fibronectin-coated migration chambers and allowed to invade through the polycarbonate membrane insert for 24 hours. Cells were fixed, stained, and counted with at least 8 fields of view per membrane at 20X magnification. Control wells were performed in the absence of the FCS chemo-attractant. Raw cells invaded was plotted.

Once optimised, baseline invasion rates of untreated EO771 and EO771.LG cells were determined. Cells were harvested, suspended in collagen-rich RPMI, and applied to the fibronectin-coated transwell chambers, as before. Invasion assays were performed in the presence of an FCS gradient, and control wells were performed in the absence of an FCS chemo-attractant. **Figure 3.22** shows the normalised percentage of invaded cells. Overall, there was relatively little difference between the number of invading cells between the EO771 and EO771.LG cell lines.

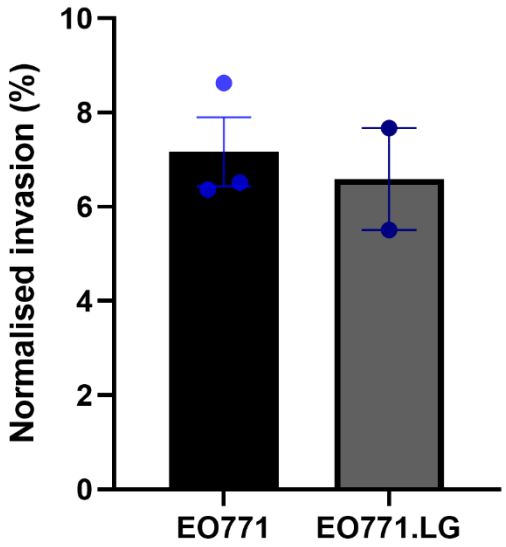

Figure 3.22: Transwell invasion assay of EO771 and EO771.LG cells. Cells were suspended in 1 mg/ml collagen-rich suspension and applied to fibronectin-coated migration chambers and allowed to invade through the polycarbonate membrane insert for 24 hours. Cells were fixed, stained, and counted with at least 8 fields of view per membrane at 20X magnification. Control wells were performed in the absence of the FCS chemo-attractant. Data was normalised by subtracting control wells and expressed as percentage of invaded cells. Mean and SEM of triplicate or duplicate experiments are plotted.

Next, the impact of high-mannose glycans on cell invasion was determined using Kif treatment. Increased high-mannose glycans significantly reduced cell invasion of EO771 and EO771.LG cells (**Figure 3.23**). Normalised cell invasion dropped from ~7% in untreated EO771 cells, to ~1% with Kif treatment (**Figure 3.23A**). There was little difference between cells invading through in the presence or absence of a chemotaxic gradient in EO771.Kif cells (**Figure 3.23A**). This trend was also observed with EO771.LG cells, in which invasion rates dropped from ~7% in untreated EO771.LG cells to ~2% with Kif treatment (**Figure 3.23B**).

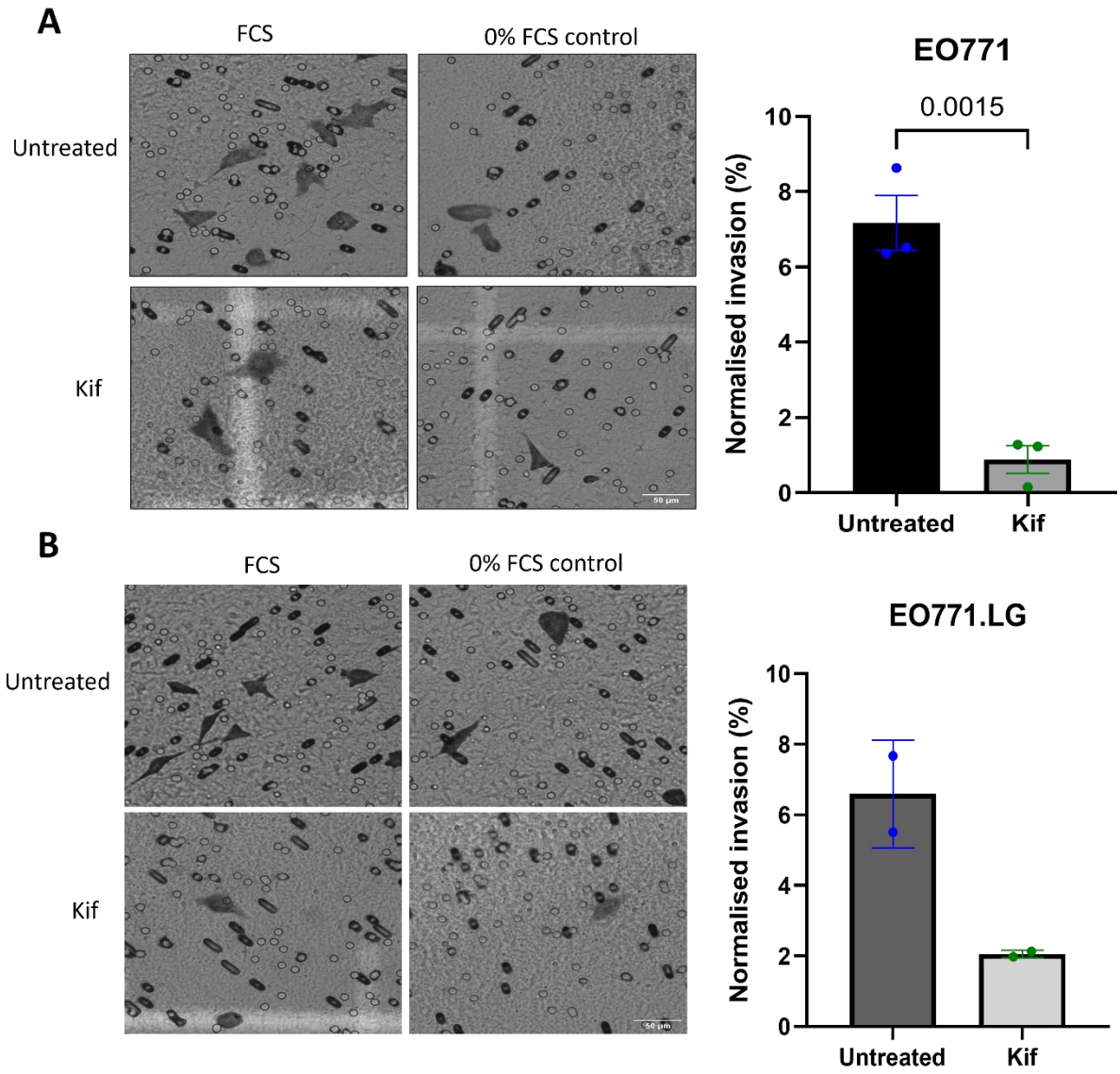

Figure 3.23: Transwell invasion assay of Kif treated and untreated EO771 (primary) and EO771.LG (metastatic) cells. Cells were suspended in a collagen-rich suspension and applied to fibronectin-coated migration chambers and allowed to invade through the polycarbonate membrane insert for 24 hours. Cells were fixed, stained, and counted with at least 8 fields of view per membrane at 20X magnification. Control wells were performed in the absence of the FCS chemo-attractant. Data was normalised by subtracting control wells and expressed as percentage of invaded cells. (A) Data from EO771 cells. (B) Data from EO771.LG cells. Mean and SEM of triplicate or duplicate experiments are plotted. Statistical significance was tested using unpaired T-tests analysis for triplicate experiments.

3.2.4.2 The impact of high-mannose glycans by Kifunensine, *in vivo*

In vitro assays showed that high-mannose impacted cancer cell phenotypes, such as individual cell migration and invasion, and collective sheet migration. However, while informative, *in vitro* assays don't reflect physiological conditions, therefore we moved *in vivo* to test if this was recapitulated in a more physiological setting.

3.2.4.2.1 Rates of primary tumour establishment

Since cell surface mannose may impact interactions with immune cells, we wanted to perform *in vivo* experiments in immunocompetent mice. Therefore, since EO771 cells are derived from C57BL/6 mice we used this as a syngeneic model. In this model, EO771 cells were cultured with 10 µM Kif for 48 hours. Cells were washed 3X with PBS to remove Kif before 2.5 X 10^5 cells were injected subcutaneously into the mammary fat pad of each C57BL/6 mouse. **Figure 3.24A** outlines the experimental timeline, where tumour sizes were measured every 2-3 days. A subset of tumours were harvested at days 6, 11, and 18 for immunohistochemical analyses.

Overall, tumours established from Kif-treated cells grew slower than untreated cells *in vivo* (**Figure 3.24**). This difference was observed from the initial tumour measurements on day 3 and increased throughout the course of the experiment until day 24. At day 17, the difference in mean tumour size between Kif-treated and untreated cells reached statistical significance, and this difference was maintained until the humane endpoint (**Figure 3.24**). This was of interest since we demonstrated *in vitro* that cells removed from Kif-rich media began to lose their high-mannose phenotype after 72 hours (**Figure 3.17**). Indeed, once the Kif-treated cells were injected they were no longer in the presence of the small molecule inhibitor. Therefore, differences in tumour growth kinetics observed were attributed to cellular glycan changes at engraftment and the initial days of the experiment. Importantly we have also shown that Kif treatment doesn't affect cell proliferation *in vitro* (**Figure 3.16**), and so this reduced tumour growth is likely due to mechanisms impacting engraftment/possible immune control, rather than intrinsic effects on cell proliferation.

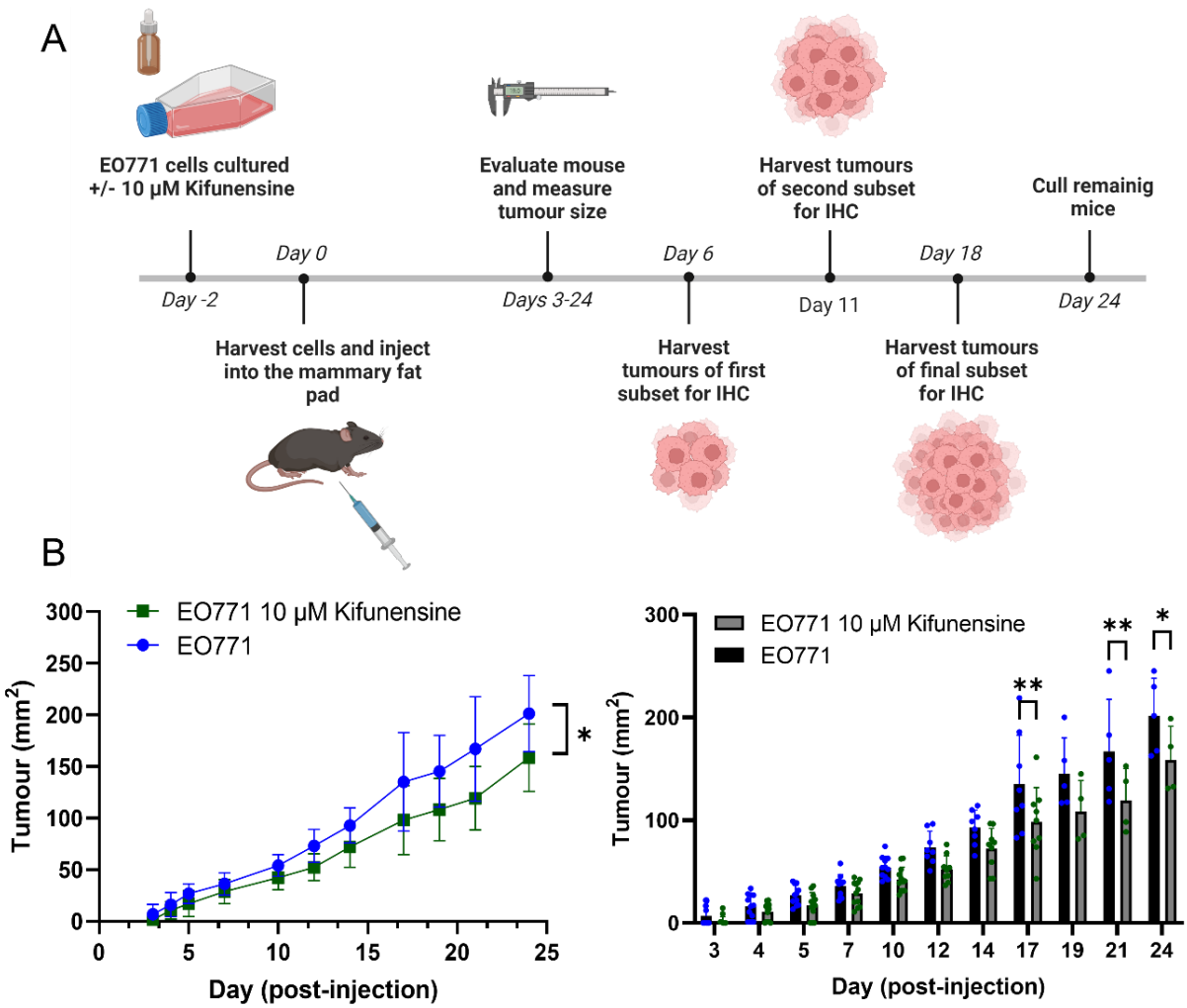

Figure 3.24: Tumour growth kinetics of EO771 cells and EO771 Kif treated cells. (A) Schematic timeline of events for in vivo experiment. EO771 cells were cultured in the absence or presence of 10 µM Kif for 48 hours. Cells were subcutaneously injected into the mammary fat pad of C57BL/6 mice. (B) Data pooled from two independent experiments. Tumour size was measured at defined time points post-injection. n = 16 mice per group. The area under the curve was calculated (left) and assessed for statistical significance by an unpaired T-test. Differences between tumour sizes at each time point was plotted (right) and assessed for statistical significance by 2-way ANOVA. **P< 0.01, * P<0.05.

3.2.4.2.2 Rates of metastatic tumour growth

There is evidence in the literature to suggest high-mannose glycans may play a role in metastasis, and we have shown *in vitro* that high-mannose glycans impact metastatic features such as invasion and migration. Therefore, we used a model of BC metastasis to determine the impact of high-mannose glycans on metastasis.

In this model, the metastatic cell line EO771.LG were injected into the tail vein of C57BL/6 mice. The EO771.LG cell line have been transduced to express the bioluminescent luciferase reporter enzyme, allowing the tracking of metastatic tumour growth using the IVIS *in vivo* imaging system. The luciferase reporter vector also contains a hygromycin selection marker, therefore prior to injection, cells were treated with hygromycin to select for EO771.LG cells which strongly expressed luciferase.

To optimise the correct hygromycin concentration, an antibiotic kill curve with EO771 and EO771.LG cells was performed (**Appendix 3**). For 11 days prior to the experiment, EO771.LG cells were grown in 50 µg/mL hygromycin. Subsequently, the hygromycin was removed and cells were cultured with 10 µM Kif for a further 48 hours. Cells were washed 3X with PBS and 5 X 10^5 cells were injected intravenously (IV) into the tail vein of C57BL/6 mice. The metastatic spread was measured by bioluminescent signal based on the administration of luciferin substrate and cleavage by luciferase reporter protein. Bioluminescence was measured every 2-3 days to determine metastatic burden. After IV injection one of the treatment mice had to be immediately culled due to welfare concerns, reducing this group to n = 2.

For both EO771.LG and EO771.LG.Kif, no metastatic cell growth was detected in the first 14 days as the signal was essentially at background levels (**Figure 3.25**). Metastatic burden was first at detectable limits by approximately day 17 for both untreated and Kif-treated EO771.LG cells (**Figure 3.25**). From this point, the metastatic foci in the lungs grew at a much slower rate in the Kif-treated cells until the humane endpoint at day 21 (**Figure 3.25C**). At day 21, all three mice within the untreated group had metastatic burden, however only one of the two mice in the Kif-treated group presented a bioluminescent signal (**Figure 3.25A;B**).

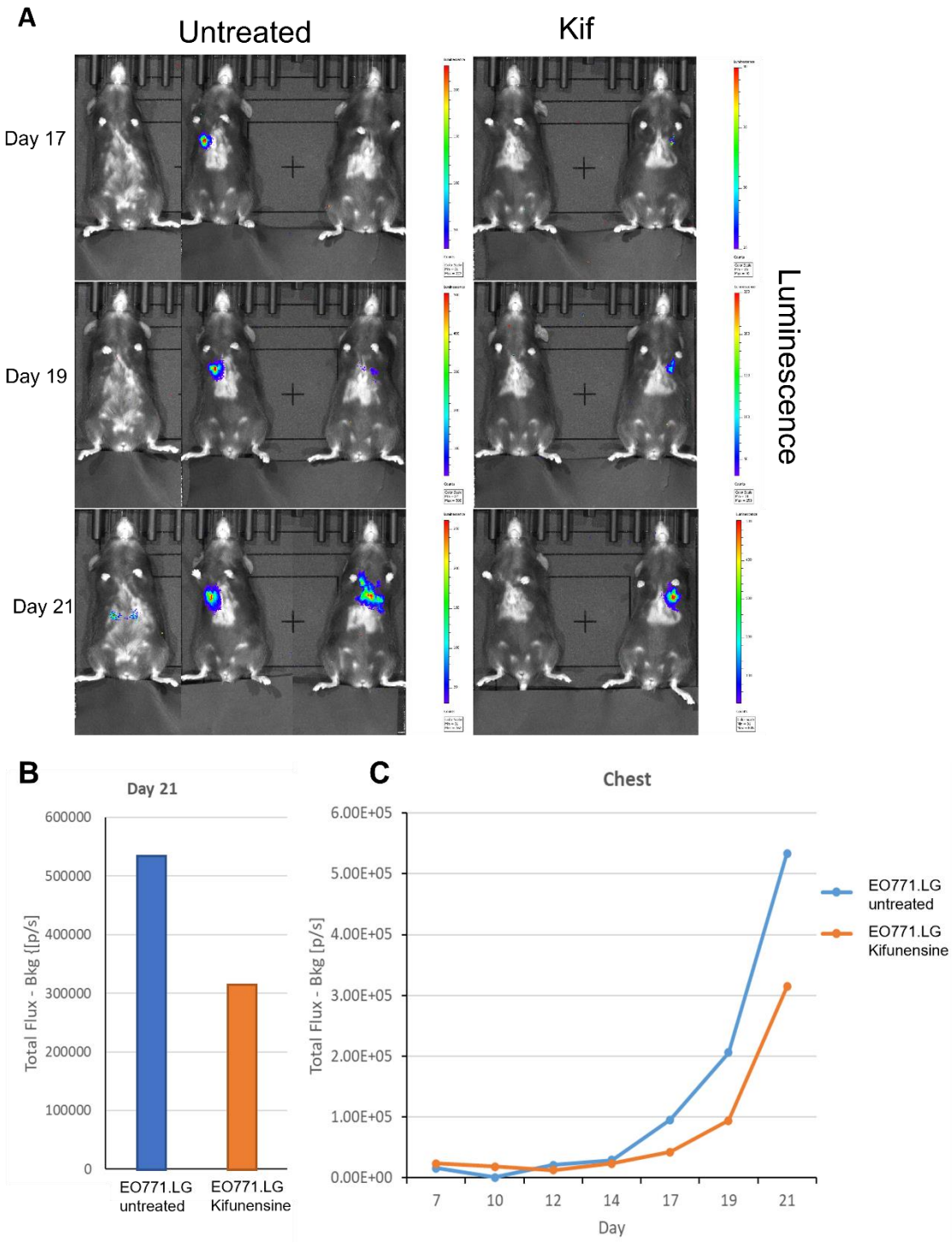

Figure 3.25: Measured bioluminescence of EO771.LG cells and EO771.LG Kif treated cells. EO771 cells were cultured +/- 10 µM Kif for 48 hours. Cells were intravenously injected into the tail vein of C57BL/6 mice. Metastatic spread was measured by bioluminescent signal based on the substrate luciferin cleavage by luciferase reporter protein. (A) Luminescence signal measured across the whole body. The colour bar indicates luminescent signal intensity, in which red is high and blue is low. (B) Total bioluminescence plotted of signal across whole body. (C) Total bioluminescence

plotted of signal across the chest cavity. n = 2 mice for Kif group. n = 3 mice for untreated group.

3.2.5 Generating a stable high-mannose cell line

Although utilising Kif provided valuable insight, its transient nature made it difficult to fully interpret the role of high-mannose glycans *in vivo*, as glycans revert to normal after 48-72 hours. Therefore, we wanted to create a stably elevated high-mannose cellular phenotype. To do this, we targeted MGAT1 using the CRISPR-cas9 system. MGAT1 is the enzyme initiating the formation of hybrid- and complex-type glycans. Therefore, disruption of MGAT1 would produce Man_5-Man_9 high-mannose glycoforms. MGAT1 was targeted since the presence of all the glycoforms within the mannose series (Man_5-Man_9) has been reported within the literature (Leoz *et al.*, 2011).

3.2.5.1 The creation and screening of a stable high-mannose cell line

Three separate sgRNAs were designed to target MGAT1 by CRISPR-cas9. sgRNAs were cloned into the pLentiCRISPR V1 vector (**Figure 3.26**). The pLentiCRISPR V1 vector was successfully digested with BsmBI as verified by agarose gel electrophoresis, and excised by gel extraction. sgRNAs were ligated into the digested vectors, and chemically competent *E. coli* were transformed with the recombinant plasmid and selected for on ampicillin agar plates. Two single colonies were selected for each sgRNA construct and purified recombinant plasmids were screened by PCR using guide primers to confirm correct cloning (**Figure 3.26B**).

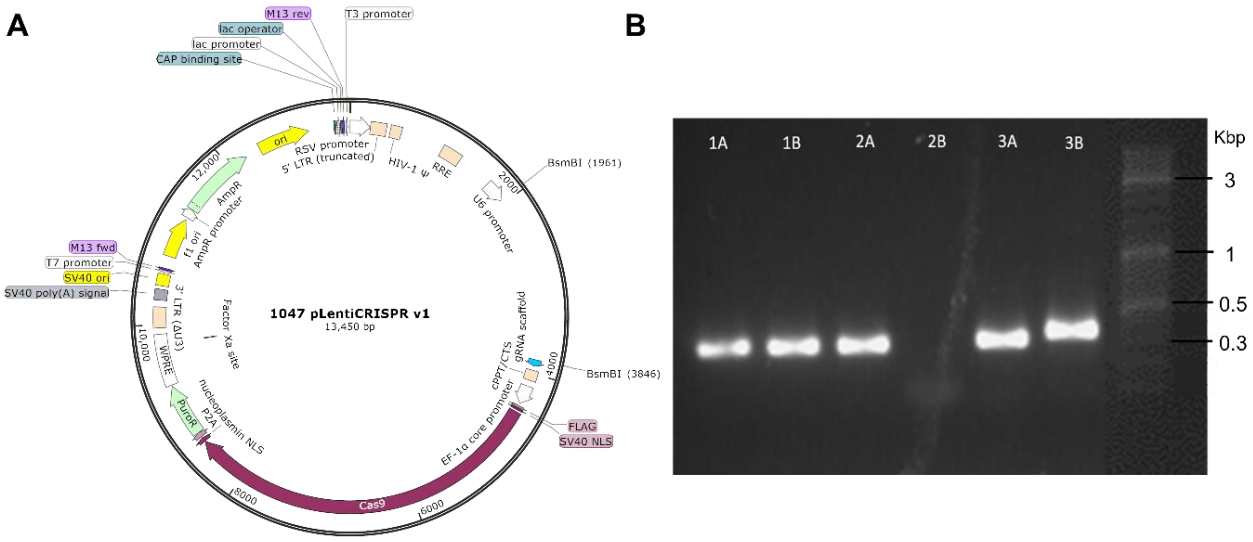

Figure 3.26: sgRNA cloning into pLentiCRISPR vector. (A) The vector map of pLentiCRISPR vector. (B) Agarose gel electrophoresis showing PCR screening results of purified recombinant pLentiCRISPR vector amplified using the sgRNA primers.

EO771 cells were transduced using lentivirus with either pLentiCRISPR V1 vectors containing sgRNAs or an empty vector control and selected for with 4 µg/mL puromycin. A puromycin titration was performed prior to transduction to find the optimal concentration required to kill WT EO771 cells which do not harbour the pLentiCRISPR V1 vector providing puromycin resistance (**Figure 3.27**).

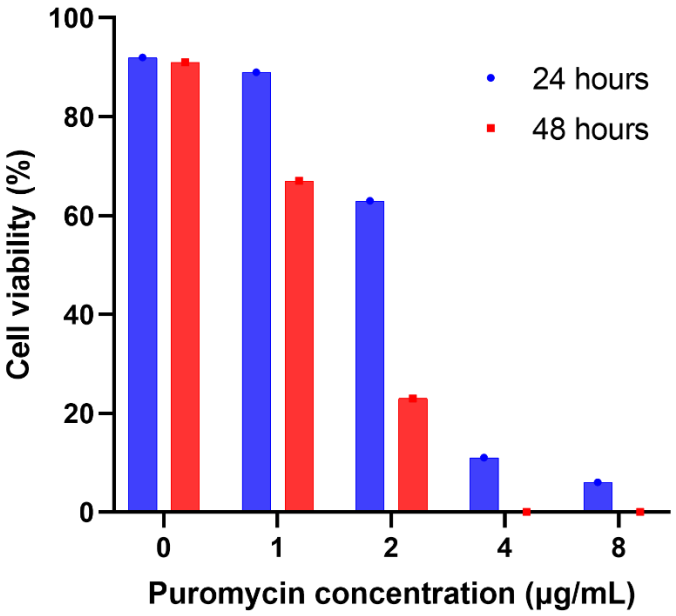

Figure 3.27: Puromycin titration EO771 WT cells. Cells were cultured in 0, 1, 2, 4, or 8 µg/mL puromycin rich media. Cells were harvested and viability was measured by trypan blue at 24 and 48 hours, respectively.

Puromycin-selected EO771 MGAT1 KO cells were grown and observed for differences in cell morphology (**Figure 3.28**). Overall, there was no difference in cell morphology between Kif-treated EO771 cells and the Empty vector control, MGAT1 KO Guide 1, or MGAT1 KO Guide 2, respectively (**Figure 3.28**). All cells retained the mixed epithelial- and fibroblast-like morphology which was seen previously within this work. Interestingly, MGAT1 KO Guide 3 cells largely took on a spindle-shaped, more fibroblast-like morphology. Cells were more elongated than all other cell lines. MGAT1 KO Guide 3 cells appeared to be of similar confluency to the EO771 Empty vector control and Kif-treated EO771 cells. However, MGAT1 KO Guide 1, and MGAT1 KO Guide 2 cells appeared to have been of lower confluency than the other cell lines, despite being seeded at the same number of cells.

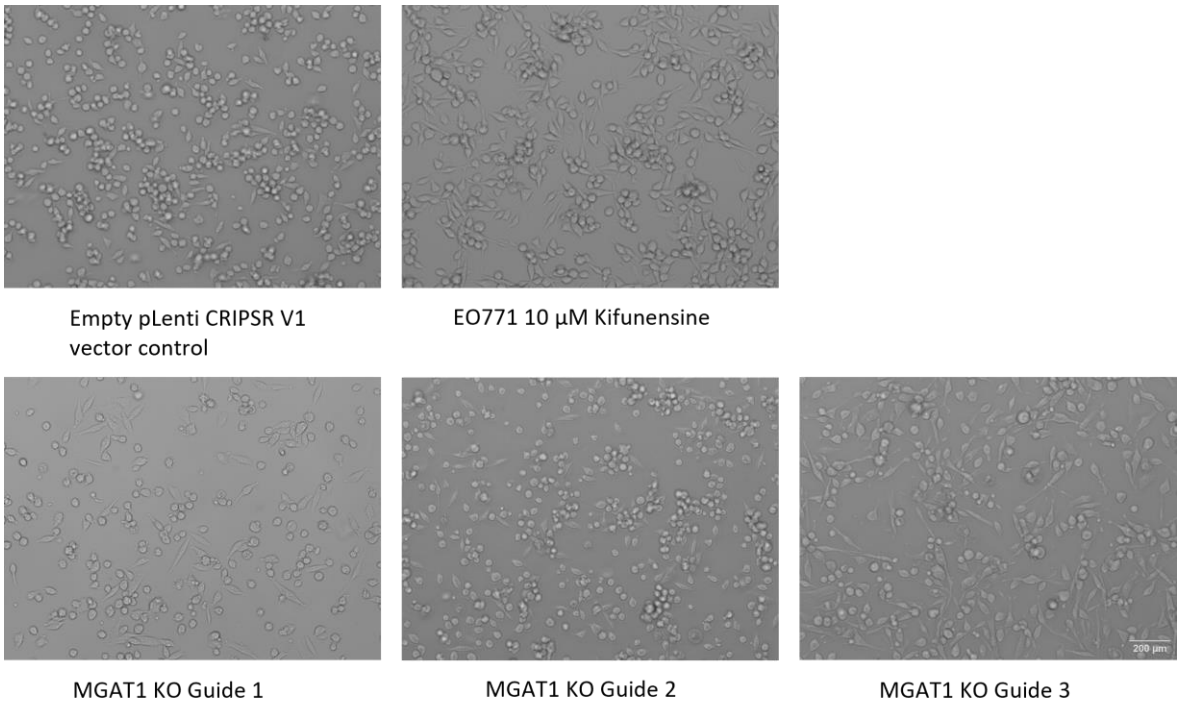

Figure 3.28: Morphology of CRIPSR-cas9 edited cell lines. Cells were seeded and grown in complete media for 48 hours prior to being imaged at 10X magnification. EO771 cells were treated with 10 µM Kifunensine and incubated for 48 hours, for comparison.

Cells were screened for cell surface mannose levels using the NPA lectin-based flow cytometry optimised in **Chapter 3.2.3** (**Figure 3.29**). Cell surface mannose levels of EO771 and EO771 Empty vector control were of similar MFI, suggesting similar cell surface mannose levels. No difference in cell surface mannose levels was seen between the EO771 controls and EO771 MGAT1 KO Guide 1 or EO771 MGAT1 KO Guide 2. Kif-treated cells maintained a higher MFI than EO771 controls, EO771 MGAT1 KO Guide 1, and EO771 MGAT1 KO Guide 2 cells, indicating higher levels of cell surface mannose. Of note, EO771 MGAT1 KO Guide 3 presented an increased MFI, relative to both EO771 controls and Kif-treated cells. This difference was maintained over biological replicates. Overall, these results suggested that the EO771 MGAT1 KO Guide 3 produced a stable high-mannose phenotype, likely due to the disruption of MGAT1, preventing N-glycan processing. It is of note that the KO/KD of MGAT1 was not confirmed as the cause of this stable high-mannose phenotype, since commercially available monoclonal antibodies for western blot against murine MGAT1 were not available for purchase at the time of this research.

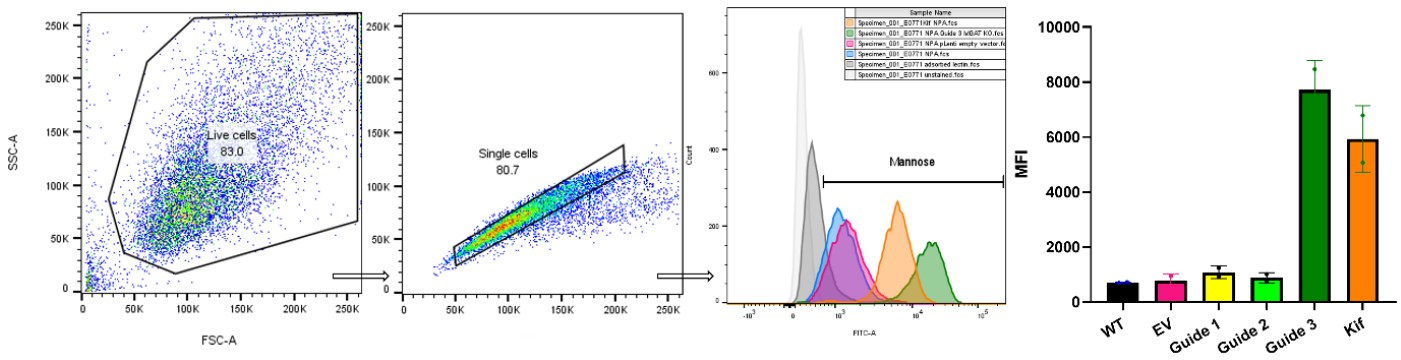

Figure 3.29: Cell surface mannose probing of EO771 WT, EO771 Kifunensine treated, and CRISPR EO771 MGAT1 KO cells. EO771 cells were cultured with 10 µM Kif for 48 hours. Cells were opsonised with the biotin labelled anti-mannose lectin NPA for 30 minutes on ice. Cells were washed with BSA-PBS and a secondary streptavidin. Data are from two independent experiments with the SEM plotted.

Next, we wanted to confirm that the increased NPA lectin binding observed for EO771 MGAT1 KO Guide 3 was due to increased cell surface mannose and investigate which mannose species were present. Thus, glycan analysis was performed using LC-MS (**Figure 3.30**). Whole-cell lysate was extracted and N-glycans were purified and procainamide labelled. Glycans were analysed by LC-MS, and chromatogram peaks belonging to the mannose series (Man_5-Man_9) were identified from the M2 spectra by their doubly charged negative ion monoisotopic masses (**Figure 3.30**; **Appendix 5**; **Appendix 4**).

All species within the mannose series were identified in both cell lines (**Figure 3.30**). The UPLC chromatogram shows that although the mannose series was relatively more pronounced in the EO771 MGAT1 KO Guide 3 cells, some undefined, presumably complex-type, glycans present were still present. Of note, the Man_5 peak in the chromatogram of EO771 MGAT1 KO Guide 3 was most obviously enhanced relative to the other peaks present, compared to the EO771 Empty vector. This data overall suggests that while MGAT1 may be disrupted, the EO771 MGAT1 KO Guide 3 cell line is not a complete MGAT1 KO.

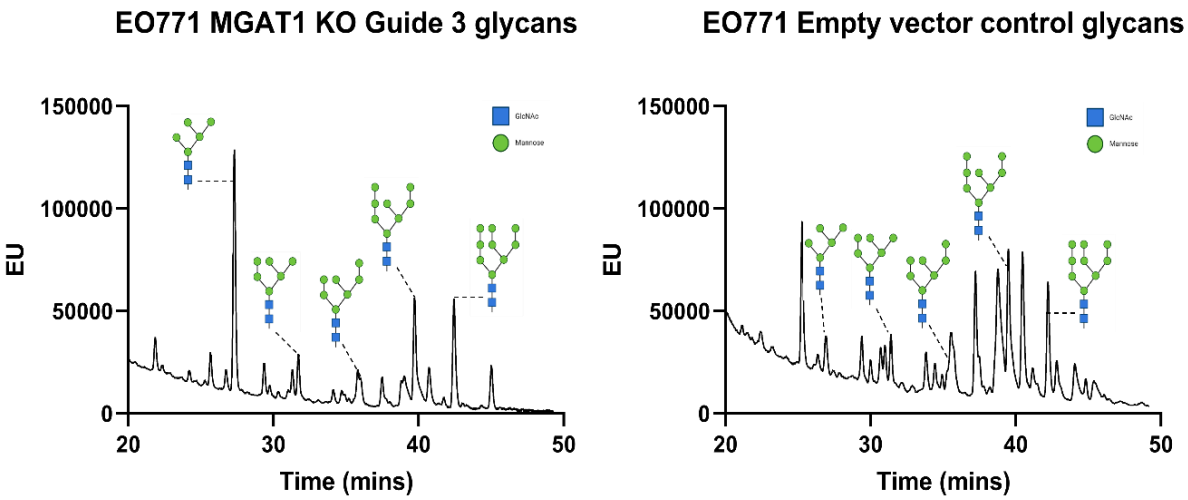

Figure 3.30: LC-MS data of PNGaseF released procainamide labelled glycans from EO771 MGAT1 KO Guide 3 and Empty Vector control. N-glycans were released in solution from glycopeptides using PNGase F, procainamide-labelled, desalted and purified by carbon column and porous graphite column chromatography. Samples were analysed by HILIC-UPLC [Acquity H-Class UPLC, 2.1 mm × 150 mm Acquity BEH Glycan column (Waters)] and Mass Spectrometry [direct infusion into Synapt G2Si (Waters)] in tandem. High-mannose structures were deduced from their doubly charged negative ion monoisotopic masses.

EO771 MGAT1 KO Guide 3 cells presented a stable high-mannose phenotype, therefore, differences in rates of proliferation were next explored. An MTS assay was employed to determine rates of cell proliferation between untreated EO771, EO771 Empty vector control (EO771 EV) and EO771 MGAT1 KO Guide 3 cells (herein known as EO771 Mannose-high (**Figure 3.31**). The MTS assay is a sensitive colorimetric method which quantifies the reduction of MTS tetrazolium by metabolically viable cells, and thus can be used to assess cell proliferation over time.

Overall, there was no difference in observed cellular proliferation between the cell lines (**Figure 3.31**). The quantified absorbance, indicating the number of viable cells, doubled from 24 hours to 48 hours for all cell lines, suggesting normal cell growth patterns.

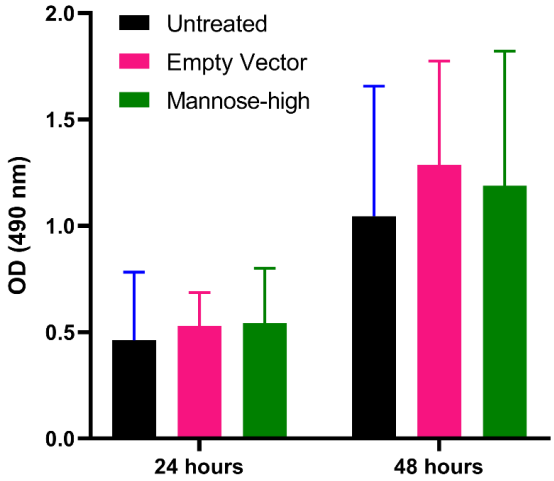

Figure 3.31: MTS assay to explore the effects of CRISPR-cas9 modification on cellular metabolism and proliferation. 10,000 cells were seeded, and the relative absorbance was measured at 24 and 48 hours, respectively. The mean and SEM of duplicate experiments is plotted.

3.2.5.2 EO771 Mannose-high cells *in vitro*

We have now observed that EO771 Mannose-high cells have similar rates of cell proliferation and increased stable cell surface mannose levels (particularly Man_5 species), compared to EO771 EV. Therefore, we were then able to investigate the more permanent effects of high-mannose glycans on *in vivo* tumour growth.

First, EO771 Mannose-high cells were employed within the previously described *in vitro* cell migration and invasion assays, to establish whether the disrupted migrative and invasive abilities observed with Kif-treatment were retained with EO771 Mannose-high cells.

3.2.5.2.1 Cell migration

The impact of high-mannose glycans on cell migration was assessed using the stable EO771 Mannose-high cell line. As before, transwell migration assays were employed to measure the directional migration of individual cells in response to a chemical stimulus. FCS was used to create a chemotaxic gradient, and fibronectin-coated transwells to create a haptotaxic gradient. Control wells in the absence of the chemo-attractant, FCS were employed. Cells were harvested and placed

on top of fibronectin-coated transwell chambers with a pore size of 8 µm. After 4-5 hours, cells that had migrated through the polycarbonate membrane were fixed, stained, and counted.

The EO771 Mannose-high cells had reduced migrative capabilities compared to both EO771 EV and EO771 (**Figure 3.32**). Around 2-fold less EO771 Mannose-high cells migrated through the polycarbonate membrane compared to EO771 untreated cells. These results were similar to the observed effects of Kif-treatment, where half the amount of EO771.Kif cells migrated, compared to EO771 (**Figure 3.19**). Of note, fewer EO771 EV cells migrated through than untreated EO771 cells, which may suggest some off-target effects from CRISPR-cas9 gene editing (**Figure 3.32**).

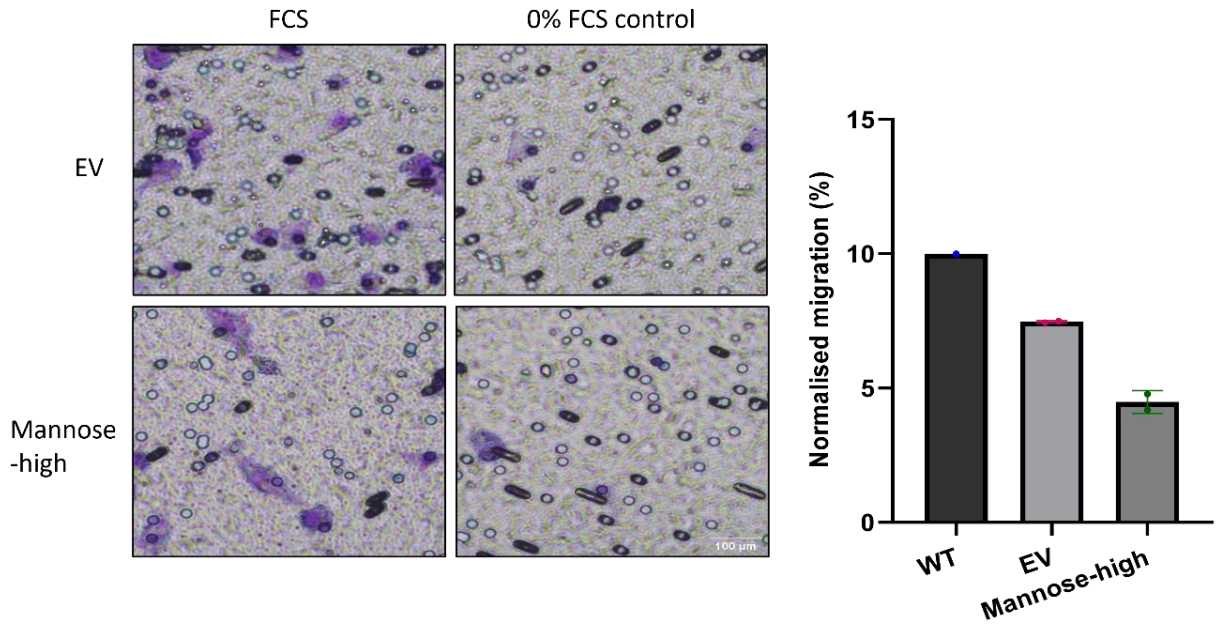

Figure 3.32: Transwell migration assay of EO771 Mannose-high and EO771 Empty Vector control cells. Cells were applied to fibronectin-coated migration chambers and allowed to migrate through the polycarbonate membrane insert for 4-5 hours. Cells were fixed, stained, and counted with at least 8 fields of view per membrane at 10X magnification. Control wells were performed in the absence of the FCS chemo-attractant. Data was normalised by subtracting control wells and expressed as percentage of migrated cells. Mean and SEM of duplicate experiments are plotted.

We next wanted to determine the effects of high-mannose glycans on cellular sheet migration, therefore EO771 Mannose-high cells were employed in a scratch wound assay. As before, silicone

inserts were placed within a culture plate to create a cell-free area, and cells were cultured around the insert. After 24 hours, the insert was carefully peeled off the plate mimicking a 'scratch'. Defined junctions of the insert were imaged over time to observe the gap closure.

EO771 Mannose-high cells had reduced collective sheet migration capabilities compared to the EO771 EV cells (**Figure 3.33**). At both 24 hours and 48 hours, the % open value for EO771 EV was around half that of EO771 Mannose-high cells (**Figure 3.33**). These results followed a similar trend to what was observed previously with Kif-treatment, where the % open value for EO771 cells was half that of EO771.Kif cells (**Figure 3.20**).

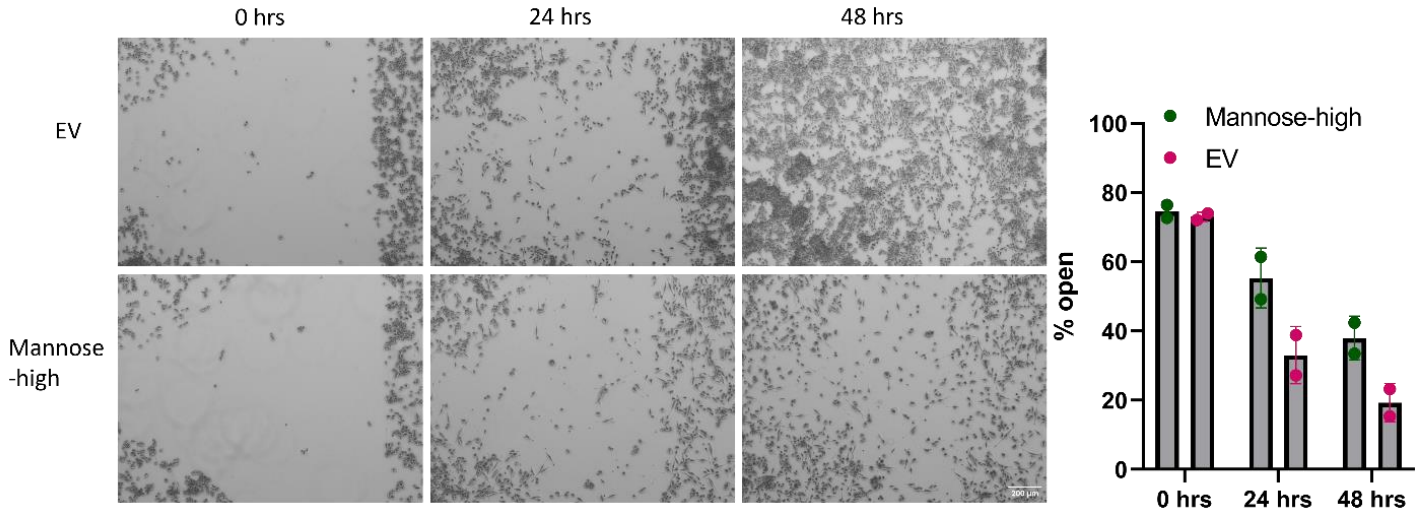

Figure 3.33: Scratch wound assay of EO771 Mannose-high and EO771 Empty Vector control cells. Culture inserts were placed in the centre of a 6 well plate. Cells were seeded around a culture insert and incubated at 37˚C, 5% CO2 for 48 hours. Media was aspirated, inserts were removed, and wound was washed with PBS to remove debris. Fresh media was added, and plates were incubated for 48 hours. Plates were imaged at 10X magnification at the same intersection of insert at 24 and 48 hours. Images were analysed by Tscratch and results were presented as % open of wound. Mean and SEM of duplicate experiments are plotted.

3.2.5.2.2 Cell Invasion

Next, the effects of high-mannose glycans on cell invasion were determined. As before, transwell invasion assays were employed to measure the directional invasion of individual cells through a collagen matrix in response to a chemical stimulus. FCS was employed to create a chemotaxic

gradient, and fibronectin-coated transwells to create a haptotaxic gradient. Control wells in the absence of the chemo-attractant, FCS were employed. Cells were harvested and resuspended in collagen matrix diluted with RPMI to form a collagen-rich suspension. This was placed on top of fibronectin-coated transwell chambers with a pore size of 8 μm. After 24 hours, cells that had invaded through the collagen layer and polycarbonate membrane were fixed, stained, and counted.

The EO771 Mannose-high cells had reduced invasive capabilities compared to both EO771 EV and EO771 (**Figure 3.34**). Around 4-fold less EO771 Mannose-high cells invaded compared to EO771 EV and EO771 untreated cells (**Figure 3.34**). This followed the same trend as what was observed with Kif treatment; around 4-fold less EO771.Kif cells invaded through than EO771 cells (**Figure 3.23**). No difference was observed in the number of invaded EO771 EV cells and untreated EO771 cells (**Figure 3.34**).

Of note, fewer control EO771 cells invaded in this EO771 Mannose-high invasion assay (**Figure 3.34**) compared to what was observed for the EO771.Kif invasion assay (**Figure 3.23**). Since this experiment was only performed once, more replicate experiments should be employed.

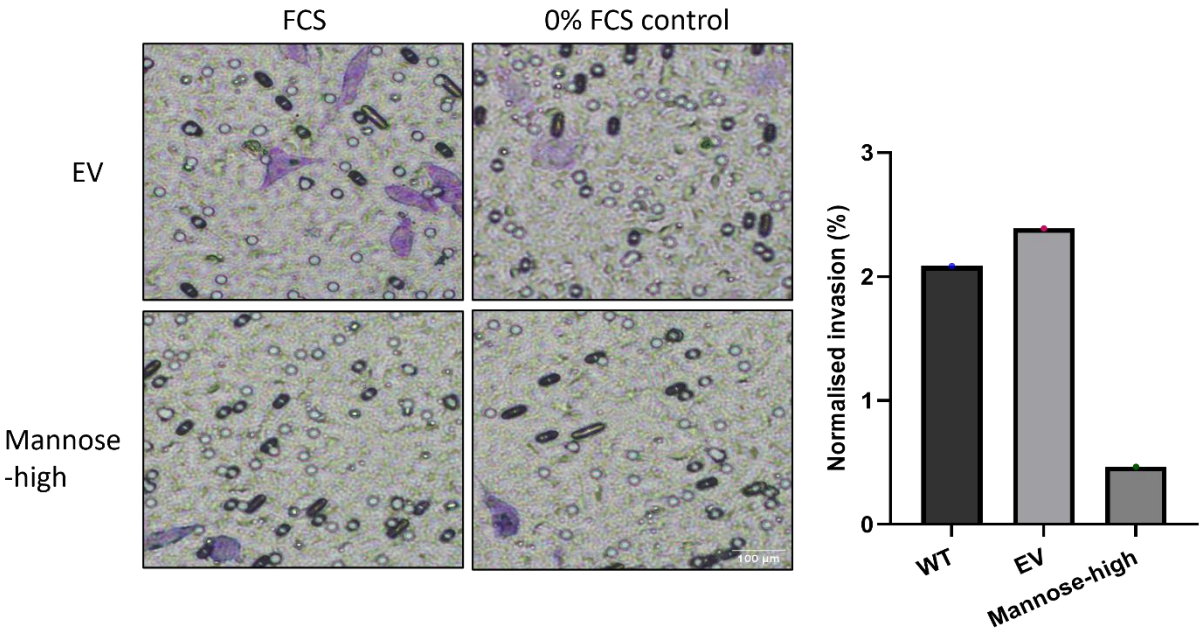

Figure 3.34: Transwell invasion assay of EO771 Mannose-high and EO771 Empty Vector control cells. Cells were suspended in a collagen-rich suspension and applied to fibronectin-coated migration chambers and allowed to invade through the polycarbonate membrane insert for 24 hours. Cells were fixed, stained, and counted with at least 8 fields of view per membrane at 10X magnification. Control wells were performed in the absence of the FCS chemo-attractant. Data was normalised by subtracting control wells and expressed as percentage of invaded cells. n = 1.

3.2.5.3 EO771 Mannose-high cells *in vivo*

We have shown that the stable high-mannose expressing EO771 Mannose-high cells had a similar phenotype in terms of individual cell migration and invasion and collective sheet migration to the Kif-treated cells. Therefore, we next wanted to investigate the effects *in vivo* to determine if having a stable high-mannose phenotype had similar effects.

3.2.5.3.1 Rates of primary TNBC tumour establishment

The effects of a stable high-mannose phenotype on tumour establishment and growth were determined using the C57BL/6 syngeneic *in vivo* model as before, and the EO771 Mannose-high cells. As these CRISPR-modified cells hadn't been utilised *in vivo* before, these cells first had to go

through a process of quarantine to ensure no pathogens were introduced from lentiviral transduction.

Cells were washed 3X with PBS before 3.5 X 10^5 cells were injected subcutaneously into the mammary fat pad of each C57BL/6 mouse. Tumour sizes were measured every 2-3 days, and the quarantine end-point was either when tumour sizes reached 9x9 mm^2 or 27 days. At the end of quarantine, sentient mice sharing the bedding were culled and their serum was analysed for pathogens. These results showed that the EO771 Mannose-high cells were pathogen free therefore, they could be utilised for further *in vivo* analysis.

Tumour measurements from the quarantine screening revealed that EO771 Mannose-high cells had considerably impeded tumour growth compared to EO771 EV (**Figure 3.35**). Both mice injected with EO771 EV cells established tumours which reached the terminal end-point of 9x9 mm^2 by day 16 (**Figure 3.35**). However, one of the mice injected with EO771 Mannose-high cells had complete tumour regression within the first week, while the other mouse had substantially reduced tumour growth, which never reached the size terminal end-point of this screening (**Figure 3.35**).

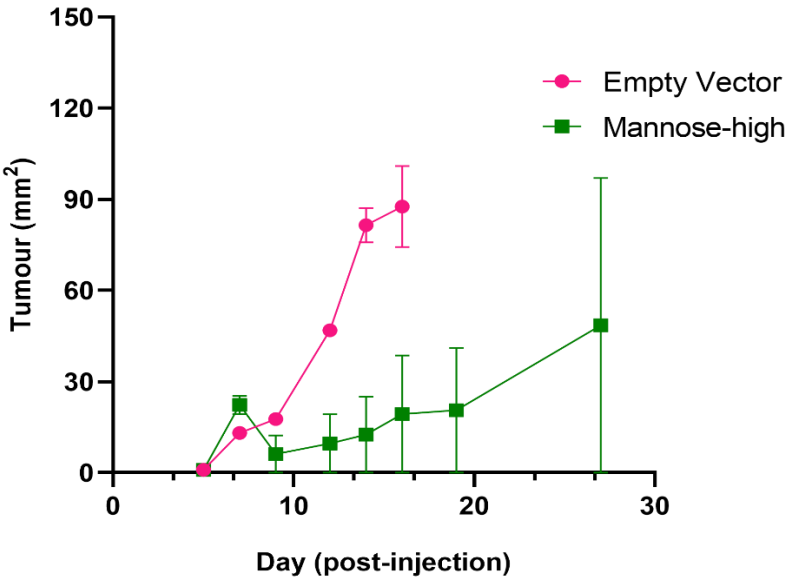

Figure 3.35: Tumour growth kinetics of EO771 Mannose-high cells and EO771 Empty Vector control cells from preliminary quarantine screening. 3.5 X 10^5 EO771 Mannose-high

cells were subcutaneously injected into the mammary fat pad of C57BL/6 mice. Tumour size was measured at defined time points post-injection. n = 2 mice per group.

To confirm the observations from the initial quarantine screening, this experiment was next repeated with a larger number of mice (n = 22) (**Figure 3.36**). As before, cells were washed 3X with PBS before 3.5 X 10^5 cells were injected subcutaneously into the mammary fat pad of each C57BL/6 mouse. Tumour sizes were measured every 2-3 days up to the humane end-point (**Appendix 11**).

Similar to the quarantine experiment, tumour measurements revealed EO771 Mannose-high cells had considerably impeded tumour growth, compared to EO771 EV (**Figure 3.36**). By day 13, all of the tumours within the EV group had reached 5x5 mm^2, whereas only one mouse within the EO771 Mannose-high group bore a 5x5 mm^2 tumour. By day 14, all mice within the EV group had tumours of at least 8x8 mm^2, and by day 17 tumours were at humane end-point.

Within the Mannose-high group, tumours did not reach 8x8 mm^2 until day 17, and one mouse did not reach the humane end-point of 10x10 mm^2 until day 20. Additionally, three mice injected with EO771 Mannose-high cells had complete spontaneous regression of established tumours. Of note, from each group, one mouse did not establish tumour at all. This may have been an artifact of administration, whereby there can be leakage of the cell suspension from the injection site thus impacting the number of seeded cells and in turn, tumour establishment.

As expected, the impact of stable EO771 Mannose-high cells on tumour growth was greater than Kif-treated cells. At day 14, tumours established from EO771 Mannose-high cells were ~2.8-fold smaller than those from control EO771 EV cells (**Figure 3.36**). In the Kif experiment, tumours established from EO771.Kif cells were ~1.3-fold smaller than EO771 WT cells at the same time-point (**Figure 3.24**). This was further exemplified by the complete tumour regression of 3 of 11 mice injected with EO771 Mannose-high cells (**Figure 3.36**).

A subset of tumours were harvested at 5x5 mm^2, 8x8 mm^2 and 10x10 mm^2 for immunohistochemical (IHC) analysis. This was firstly to establish that the high-mannose phenotype was retained throughout the course of the experiment. Secondly, to investigate differences in

immune cell populations which had infiltrated into the tumour between EO771 Mannose-high cells and EV cells. This may give some indication as to whether the impeded tumour growth observed with EO771 Mannose-high cells was a result of an enhanced immune response. Unfortunately, due to time constraints, the IHC results were not analysed within the scope of this thesis.

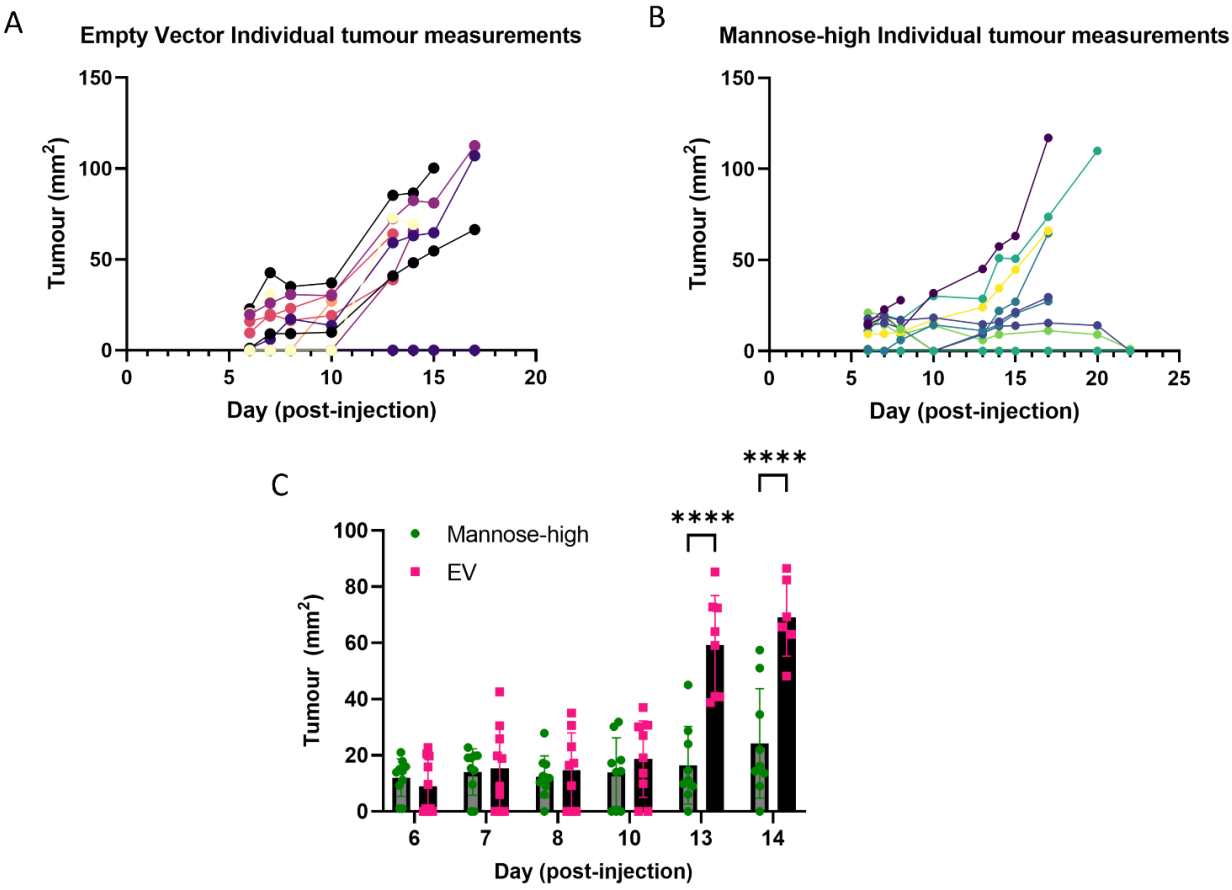

Figure 3.36: Tumour growth kinetics of EO771 Mannose-high cells and EO771 Empty Vector control cells. 3.5 X 10^5 EO771 Mannose-high cells were subcutaneously injected into the mammary fat pad of C57BL/6 mice. Tumour size was measured at defined time points post-injection. n = 11 mice per group. Individual tumour measurements from (A) mice injected with Empty vector cells (B) mice injected with Mannose-high cells. (C) Average tumour measurements up until day 14. A subset of tumours were harvested from each group when they reached 5x5 mm^2, 8x8 mm^2 or 10x10 mm^2 for IHC analysis. Day 14 was the final timepoint where there were enough mice in each group for statistical analyses and a 2-way ANOVA was performed on GraphPad Prism. ****p<0.0001.

3.3 Discussion

Aberrant glycosylation is an established hallmark of cancer. While there is growing evidence for the accumulation of high-mannose glycans in BC, some reports are contradictory (Legler, Rosprim, Karius, Eylmann, Rossberg, Ralph M. Wirtz, *et al.*, 2018; Chatterjee, Kawahara, *et al.*, 2021; Ščupáková *et al.*, 2021). Several factors, such as the stage of cancer, secondary site of metastasis, histology, sample type, and patient treatment regimen have been suggested to influence reports of high-mannose glycans in BC (Abd Hamid *et al.*, 2008; Leoz *et al.*, 2011; Saldova *et al.*, 2017; Vreeker *et al.*, 2021). Thus, the role high-mannose glycans play within BC development and progression, along with their dynamic regulation, still needs to be fully elucidated. Within this chapter, we investigated the presence of high-mannose glycans in BC cells and clinical tissues, and the regulation of this phenotype through gene expression data. Further, we generated and validated two models of elevated high-mannose glycans to determine the impact of high-mannose glycans on *in vitro* cancer phenotypes and *in vivo* tumour growth. This chapter aimed to investigate the potential significance of high-mannose glycans in BC progression.

We have observed positive mannose staining with clinical tissues using the lectin, NPA (**Figure 3.3**). NPA staining was optimised using sections of OCT frozen EO771.Kif cell pellets which acted as a positive stain control (**Figure 3.2**). Typically, lectins can only detect a partial source of a glycan chain, usually the terminus. NPA preferentially binds poly a-mannose structures, specifically binding terminal α-1,6-mannose structures, as well as internal α 1-3 and 1-6 mannose structures (Kaku et al., 1990). Unlike other mannose-binding lectins such as ConA, NPA does not bind glucose. The granular staining pattern of NPA was similar between the EO771.Kif cell pellets and clinical patient samples, and aligns well with staining patterns reported previously within the literature (Liu *et al.*, 2020), giving confidence in the results.

Positive staining for mannose was observed in invasive $HER2^{+}$ and TNBC clinical patient samples (**Figure 3.3**). Positive staining was observed on tumour cells and some unidentified stromal and inflammatory cells. From our current samples, it is unclear whether the staining is present within

the cytoplasm and/or the cell membrane. Since incompletely processed intracellular glycoproteins trafficking through the secretory pathway would have also likely stained positive. However, mannose staining with NPA lectin in gastric cancer patient tissue has previously reported similar staining patterns and revealed that mannose staining was localised to the cell membrane and cytoplasm (Liu *et al.*, 2020).

Difficulties were encountered with dual cytokeratin and lectin staining, as the strength of the cytokeratin staining masked the weaker NPA lectin staining. It is known that dual staining with cytokeratin can produce a 'masking effect', where cytokeratin can saturate epitopes and prevent other reagents from binding. However, since NPA staining was performed before cytokeratin staining, this is not the explanation for these difficulties. Instead, it may be due to the close colours of the brown DAB chromogen used for cytokeratin staining and the red Novared chromogen used for the NPA staining. In future, the use of different coloured chromogens may improve dual staining to assist in identifying where the lectin was specifically staining.

It was important to assess the presence of high-mannose glycans within murine BC models to establish the translatability of this research *in vivo*. High-mannose glycans were identified by NPA staining within murine *ex vivo* TNBC primary and metastatic tissues (**Figure 3.7**). This staining followed a similar granular staining as seen in human clinical samples, providing confidence in the suitability of this model for future use *in vivo*. Within the primary tumour, staining was ubiquitous and associated with tumour cells (**Figure 3.7**). Within the lung metastases, staining was less prevalent, and associated with tumour cells surrounding the outside of the metastatic nodule.

Cell surface probing for mannose via flow cytometry with NPA further validated the presence of cell surface high-mannose glycans (**Figure 3.9**). Cell surface mannose was found to be present on both $HER2^+$ and TNBC cell lines. Of note, metastatic cell lines had less mannose than non-metastatic cell lines (**Figure 3.9**), which correlates with what was observed with mannose staining within *ex vivo* tissue (**Figure 3.7**).

Previous studies have reported elevated high-mannose glycans in BC cell lines, compared to normal breast epithelial cell lines (JA *et al.*, 2009; Liu *et al.*, 2013). In agreement with the results presented here, previous studies also reported that non-invasive cells expressed higher levels of high-mannose glycans than invasive cell lines (JA *et al.*, 2009; Liu *et al.*, 2013). Of note, these data were pooled from TNBC, $HER2^+$, and HR^+ cell lines. The data presented within this thesis further explored differences between molecular subtypes. Overall, TNBC cells expressed more mannose on the cell surface compared to $HER2^+$ cells (**Figure 3.9**). To support this data and confirm differences between tumour and normal, future experiments should be repeated alongside a cell line representing a normal breast cell such as MCF10A.

To validate this data, we investigated whether a dysregulation of glycan processing enzymes in BC cells could explain the high-mannose phenotype. TCGA clinical datasets were first interrogated for mannose processing enzyme expression within breast invasive carcinoma and matched healthy tissue (**Figure 3.1**). The results show that expression patterns of mannose processing enzymes between healthy mammary tissue and invasive breast carcinoma were very different. There was a large variability in expression levels of all enzymes between individual invasive breast samples (**Figure 3.1**). In comparison, there was much less variability between samples in the healthy mammary tissue (**Figure 3.1**). However, despite this variability, the boxplot demonstrates that differences between matched healthy tissue and invasive breast carcinoma across almost all enzymes were statistically significant (**Figure 3.1**). This strongly suggests that the expression of these enzymes is aberrant in invasive breast carcinoma.

A key enzyme required to produce high mannose N-glycans is MAN1A1 and as such its role has been of interest. The presence of high-mannose glycans correlates negatively with MAN1A1 expression (Chatterjee, Kawahara, *et al.*, 2021). Overexpression of MAN1A1 was demonstrated to decrease the global abundance of high-mannose glycans (Park *et al.*, 2020), whereas MAN1A1 knock down (KD) enhanced cell surface mannose (Legler, Rosprim, Karius, Eylmann, Rossberg, Ralph M Wirtz, *et al.*, 2018). The reduced expression of MAN1A1 has been reported in BC patients, and correlated

with poor prognosis and shorter disease-free survival (Milde-Langosch *et al.*, 2014; Legler, Rosprim, Karius, Eylmann, Rossberg, Ralph M. Wirtz, *et al.*, 2018).

We observed lower MAN1A1 expression in invasive breast carcinoma patients compared to normal mammary tissue, and this was statistically significant (**Figure 3.1**), aligning with the previous literature. The impact of MAN1A1 expression on overall survival (OS) was explored via Kaplan Meier plot from the same TCGA datasets (**Appendix 6**). Overall, reduced MAN1A1 expression correlated with better OS, but this was not significant. This contradicts what was reported previously in the literature (Legler, Rosprim, Karius, Eylmann, Rossberg, Ralph M. Wirtz, *et al.*, 2018). Despite the large sample size of the assessed TCGA dataset providing robustness to results (n = 1391), other clinical factors such as molecular subtypes and metastatic progression were not interrogated. Indeed, MAN1A1 expression in invasive breast carcinoma patients showed large variability (**Figure 3.1**). Therefore, observed discrepancies could be due to differences between subtypes and this should be investigated in future.

Previous findings have reported a dysregulation of mannose processing enzymes and BC metastasis. Reduced MAN1A1 expression was reported in metastatic BC compared to parental primary BC cell lines (Legler, Rosprim, Karius, Eylmann, Rossberg, Ralph M. Wirtz, *et al.*, 2018). Additionally, lower expression of mannosidase enzymes in clinical patient tissues correlated with metastasis (Ščupáková *et al.*, 2021), and decreased MAN1A1 protein expression was observed in brain metastases samples from BC patients (Legler, Rosprim, Karius, Eylmann, Rossberg, Ralph M Wirtz, *et al.*, 2018).

Therefore, we interrogated the expression levels of mannose processing enzymes in invasive breast carcinoma patients within the TCGA pan-cancer clinical dataset (**Figure 3.4**). Differences in expression levels were statistically significant for almost all mannose processing enzymes between metastatic, primary tumour, and healthy tissue samples, demonstrating the importance of regulation of upstream mannosidases in BC progression. Only MGAT1 and MAN2B2 were not statistically significant. A significant reduction in MAN1A1 expression was observed during breast

oncogenesis (**Figure 3.4**). Surprisingly, there were no notable differences in the expression levels of MAN1A2 and MAN1C1 between metastatic and primary tumours (**Figure 3.4**), despite these enzymes sharing substrate specificity with MAN1A1. Further investigations are required to understand the extent and stages at which this aberration occurs during BC progression. Additionally, it is essential to highlight that the metastatic expression data is based on a limited sample size of only 7 patients. Consequently, this small sample may not accurately represent the entire population, and a larger sample size is necessary to gain a comprehensive understanding. Moreover, exploring differences between molecular subtypes, metastatic sites, and grades will provide valuable insights into the role of glycosyltransferase regulation in high-mannose glycan expression and its impact on breast cancer progression. Such additional information is crucial for unravelling the complexities of this process.

To determine the translatability of our model murine cancer cell lines, transcriptomics data of glycan processing enzymes were investigated in EO771.LG and EO771 (**Figure 3.5**). In addition, since these cell lines were within metabolically controlled conditions there are fewer external variables to influence glycosylation patterns. Thereby providing a simpler model to assess the dysregulation of the glycan pathway in BC metastasis. The most upregulated enzyme in the metastatic TNBC cell line, EO771.LG, was MANEA. MANEA is an endo-mannosidase which allows glycoproteins to bypass the classical N-glycosylation pathway and provides Man_8 substrates for the mannosidases, MAN1A1, MAN1A2, MAN1C1 (see Chapter 1.12.3.1). MANEA expression was not upregulated in human clinical metastatic samples (**Figure 3.4**). EO771.LG showed downregulation of MAN1B1 and PRKCSH, which is expected considering the substantial upregulation of MANEA. Surprisingly, MAN1A1 was significantly upregulated in EO771.LG, contrary to observations in human clinical datasets. However, this upregulation might be a compensatory response to the increased substrate availability facilitated by MANEA. Notably, despite these alterations in glycan processing enzymes, cell surface mannose levels on EO771 and EO771.LG were not significantly different (**Figure 3.10**). This suggests that these changes in enzyme expression may not be directly contributing to a high-mannose glycan phenotype in these cells.

Within the murine metastatic cells, the regulation of glycan processing enzymes appears to facilitate increased branching. Increased expression of MGAT5 and MGAT4a and decreased expression of MGAT3 was observed in EO771.LG (**Figure 3.5**). MGAT3 catalyses the addition of a bisecting GlcNAc to N-glycans, sterically hindering the formation of branched glycans. Additionally, increases in the expression of FUT4, FUT2, B4GALT4 and ST3Gal4, were observed in EO771.LG, relative to EO771. Therefore, the higher MANEA expression may be a secondary factor to compensate for protein upregulation and saturated glycosylation machinery, rather than contributing to a high-mannose phenotype.

The observed changes in glycan patterns align well with existing literature, as highly branched fucosylated and sialylated N-glycans have been linked to metastasis (see Chapter 1.12). Ščupáková et al. previously reported that clinical BC metastases samples exhibited an increase in highly branched glycans, along with an upregulation of glycosyltransferases involved in the formation of complex, highly branched glycans (2021). Remarkably, similar to what was observed in EO771.LG, an increased expression of MGAT5, B3GALNT2, B4GALNT2, B3GALT3, B3GNT3, B4GALT3, and ST6GALNAC6 was also detected in human clinical BC metastasis compared to primary tumours (Ščupáková et al. 2021). This convergence between murine and human clinical data underscores the robustness and translatability of our model cell lines, EO771 and EO771.LG.

Furthermore, previous studies have highlighted the significant impact of glycosyltransferases on tumour initiation and metastasis. For instance, MGAT5-mediated increased branched glycans have been implicated in regulating tumour initiation in $HER2^{+}$ breast cancer, with the disruption of MGAT5 resulting in a delayed onset of mammary carcinoma formation caused by HER2 (Guo *et al.*, 2010). Similarly, increased expression of FUT1 and B3GNT4 has been associated with metastasis and worse overall survival (Milde-Langosch *et al.*, 2014), while fucosyltransferases have been implicated in promoting metastasis (Julien *et al.*, 2011). The consistent agreement between our findings and the existing literature strengthens our confidence in the relevance and reliability of

our research model using EO771 and EO771.LG cell lines, providing valuable insights into the complex relationship between glycan processing enzymes and breast cancer metastasis.

Overall, the regulation of mannose processing enzymes is aberrant in invasive breast carcinoma. We found the most prominent differences were observed when comparing matched normal to primary breast cancer samples in the clinical human datasets. Additionally, enzymes responsible for the initiation and production of highly branched, complex-type glycans are highly upregulated in the murine models, which correlates with existing literature.

Most research in the literature has focused on the downstream effects of aberrant glycosyltransferase expression, and little is known about the upstream events leading to the dysregulation of glycosyltransferases. However, evidence points to a multifactorial approach of genetic, epigenetic, transcriptional and posttranslational regulation (Dorsett *et al.*, 2021; Pucci *et al.*, 2022). Many of the glycosyltransferase genes are so-called 'house-keeping genes' which are regulated developmentally (Bessler *et al.*, 1995) or in a tissue-specific manner (Dorsett *et al.*, 2021). However, aberrant regulation has been documented for some glycosyltransferases in cancer (Pucci *et al.*, 2022). Such examples include aberrant promotor methylation of FUT7, leading to the progression of lung and bladder cancer through activation of the EGFR/AKT/mTOR pathway (Liang, Gao and Cai, 2017; Liu *et al.*, 2021). Altered MicroRNA-149-5p activity which typically negatively regulates B3GNT3 expression, resulting in lung and breast cancer progression via regulation of EGF/PD1-PD-L1 (Li *et al.*, 2018; Sun *et al.*, 2020). Further, transcription factors such as Sox2 (Dorsett *et al.*, 2019) and HNF-1 (Dorsett *et al.*, 2021) aberrantly regulate ST6GAL1 transcription in ovarian and colon cancers, respectively. More research is required to understand the upstream molecular mechanisms regulating the expression of additional glycosyltransferases in BC progression.

Aberrant glycosylation can mediate invasive phenotypes such as cell adhesion, motility, migration, and invasion (Kölbl, Andergassen and Jeschke, 2015). Previous studies have repeatedly implicated aberrant β1,6 branched glycans in epithelial-mesenchymal transition (EMT) processes such as reduced cell adhesion and increased migration and invasion abilities (Dennis, Demetrio and Dennis,

1991; Demetriou *et al.*, 1995; Taniguchi and Kizuka, 2015), by mechanisms of impeding α5β1 integrin clustering (Guo *et al.*, 2002). In addition, the elevation of high-mannose glycans with Kifunensine was demonstrated to increase cell migration and invasion in cholangiocarcinoma cell lines (Park *et al.*, 2020).

To investigate whether high-mannose glycans affect BC cell migrative and invasive phenotypes, we employed two widely used methods; the scratch wound assay and the transwell migration/invasion assay. Single cell directional migration can be measured via the transwell assay, while collective sheet migration can be analysed via the scratch wound assay. To model elevated cell surface high-mannose glycans in these assays, we utilised the small molecule inhibitor of ER alpha-mannosidase enzymes, kifunensine (Kif). While Kif treatment of murine and human BC cell lines significantly increased cell surface mannose levels, it had no impact on cell proliferation, viability, or morphology (**Figure 3.13; Figure 3.16**). Although the effects of Kif treatment were transient, they were prolonged enough for these assays (**Figure 3.17**).

The use of relevant preclinical models is critical for translating BC research and developing novel therapeutic treatments. Syngeneic mouse models in BC allow for intrinsic cellular events to be assessed, as well as allowing for species-matched tumour interactions with its microenvironment and the effects of a functional immune system to be explored. In this chapter, we utilised the murine BC cell lines EO771 and its metastatic derivative EO771.LG. The EO771 cell line is a TNBC cell line established from a spontaneous mammary adenocarcinoma in C57BL/6 mice (Casey, Laster and Ross, 1951). The EO771.LG line is established from parental EO771 mammary tumours which spontaneously metastasised to a lung nodule in C57BL/6 mice (Johnstone *et al.*, 2015a). These cells can be chemically/genetically modified before their inoculation into a mouse mammary gland as an allograft. Therefore, these cells are appropriate for *in vitro* and *ex vivo* assays, with the ability to translate directly to *in vivo* projects.

The induction of high-mannose glycans on EO771 and EO771.LG cells with Kif reduced individual directional cell migration and invasion, and collective sheet migration *in vitro* (**Figure 3.19; Figure**

3.20; Figure 3.23). Previous findings have demonstrated that inducing high-mannose glycans in BC cells reduced sheet migration (Legler, Rosprim, Karius, Eylmann, Rossberg, Ralph M. Wirtz, *et al.*, 2018). Generally, the impact of this reduction was a similar magnitude between the metastatic and primary BC cell lines. This was likely to be because there was not a significant difference in baseline cell migration and invasion between EO771 and EO771.LG. EO771.LG was isolated from a spontaneous metastasis of the parental EO771 cell line, and thus they are molecularly similar (Johnstone *et al.*, 2015b).

Tumours established from EO771.Kif cells exhibited significantly slower initial growth rates than control EO771 cells and maintained this difference in tumour growth over time (**Figure 3.24**). This intriguing observation is particularly noteworthy as we demonstrated the effects of Kif-induced high-mannose glycans to be transient and lost after 72 hours *in vitro* (**Figure 3.17**). However, in the *in vivo* setting, we observed the impact of Kif-induced high-mannose glycans lasting up to 24 days (**Figure 3.24**). One plausible hypothesis is that the shift to high-mannose glycans disrupts the engraftment and initial growth phase of the tumour, causing a profound effect that prevents the tumour from fully recovering. This could explain the increasing difference in tumour sizes throughout the experiment, even though high-mannose glycans are presumed to be lost after the initial period (**Figure 3.24**). Alternatively, high-mannose glycans may make these cells initially more susceptible to immune control mediated through mannose receptors such as DC-SIGN. C-type lectins which bind high-mannose and branched-fucosylated antigens are expressed on macrophages and dendritic cells (DC) to distinguish between self- and invading organisms (Geurtsen, Driessen and Appelmelk, 2010). DCs recognise many pathogens as foreign through DC-SIGN binding high-mannose glycans, initiating DC maturation and migration to secondary lymphoid organs and initiating an adaptive immune response (Geurtsen, Driessen and Appelmelk, 2010). Therefore, the disrupted tumour growth of high-mannose BC cells may be due to an adaptive immune response initiated through DC-SIGN binding. After the glycan phenotype has reverted, the remaining cells may develop into a tumour. Previous studies have demonstrated that the number of cells which manage to initially engraft is critical for tumour growth (Hoffmann *et al.*, 2020),

thereby explaining how the impact of this transient modification on engraftment could be retained across the course of the experiment.

Furthermore, the metastatic burden of Kif-treated cells was significantly lower than that of the control cells (**Figure 3.25**). The difference in metastatic burden was evident from day 14 and persisted until the end of the experiment. These findings align with our earlier hypothesis, suggesting that the initial shift to high-mannose glycans has a substantial impact on downstream metastatic potential, despite the presumed loss of the altered glycan repertoire. Of note, data from this metastatic burden study is from one biological experiment, in which there were only three control mice and two treatment mice. This experiment was performed as a pilot experiment, and therefore small numbers were used. One of the treatment mice had to be culled immediately after IV administration of Kif-treated cells, reducing this to n = 2. Therefore, this experiment should be repeated to validate these results and explore statistical significance.

Taken together, our results indicate that the induction of high-mannose glycans by Kif treatment leads to a prolonged and meaningful disruption of tumour growth and metastatic progression. The persistence of these effects beyond the presumed loss of high-mannose glycans highlights the potential significance of glycan modifications in influencing tumour behaviour and metastatic outcomes. Further investigation into the underlying mechanisms of this phenomenon may offer valuable insights into novel therapeutic approaches targeting glycosylation pathways in BC treatment.

To overcome the limitations of transient effects, we set out to make a cell line that stably expresses a high-mannose phenotype. For this, MGAT1 was targeted as it represents the bottleneck in the formation of hybrid- or complex- glycans within the N-glycosylation pathway. Although there is much evidence to suggest MAN1A1 is a prognostic factor in high-mannose glycan production, other mannosidases share overlapping substrate specificity. Therefore, targeting MAN1A1 may not result in the high-mannose phenotype due to other compensatory mannosidases. Additionally, previous

studies have identified glycoforms from the whole mannose series (Man_5-Man_9) in BC clinical samples (Ščupáková *et al.*, 2021), thus targeting MGAT1 seemed the most appropriate choice.

Using a CRISPR approach, we produced a stable high-mannose version of EO771 (EO771 Mannose-high). No differences in cellular proliferation, or growth rates were seen as a possible off-target effect of the CRISPR-cas9 editing (**Figure 3.31**). A significant increase in cell surface mannose levels was observed in the EO771 Mannose-high cells, in which the MFI was higher than EO771.Kif (**Figure 3.29**). To verify lectin flow cytometric data, the mannose series glycoforms were identified by LC-MS, showing a dramatic increase in the Man_5 glycoform (**Figure 3.30**). This is to be expected from targeting MGAT1 since MGAT1 catalyses the addition of the first GlcNAc to the Man_5 glycan.

EO771 Mannose-high cells generally experience reduced directional cell migration and invasion, and reduced collective sheet migration, *in vitro* (**Figure 3.32; Figure 3.33; Figure 3.34**). This was in agreement with the previous observations where Kif was used to increase cell surface mannose. Thus, this provided confidence that high-mannose glycans are at least in part responsible for this altered phenotype. Of note, the transwell invasion assay for EO771 Mannose-high was only performed once and should repeated to validate results.

The *in vitro* migratory and invasive capabilities of EO771 Mannose-high cells were not as profoundly affected as those observed with Kif treatment. Although MGAT1 CRISPR targeting created a stable elevated high-mannose cell line, it did not create a complete KO, as evident from the unidentified peaks representing complex-type glycans (**Figure 3.30**). Despite this, this finding also aligns with previous studies in the literature, which have shown that treatment with small molecule inhibitors produces more dramatic results compared to targeting a specific gene (Legler, Rosprim, Karius, Eylmann, Rossberg, Ralph M. Wirtz, *et al.*, 2018). This suggests that the high-mannose phenotype cannot be solely attributed to changes in one glycosyltransferase alone.

EO771 EV had reduced migrative capabilities compared to EO771 (**Figure 3.32**), suggesting potential off-target effects from CRISPR-cas9. However, no difference in cell invasion was observed between

EO771 EV and EO771 cells within the transwell invasion assay (**Figure 3.34**). The effect on sheet migration between EO771 untreated cells and EO771 EV was not assessed. Future work could employ multiple Empty Vector clones to assess whether this same reduction in migrative capabilities was observed, and further determine the cause of any off-target effects resulting from CRISPR-cas9 editing.

The impact of EO771 Mannose-high cells on tumour growth followed a similar trend as Kif-treated cells. Overall, EO771 Mannose-high cells had reduced tumour growth *in vivo* (**Figure 3.35; Figure 3.36**). This was seen independently in two biological repeats. An initial quarantine screening was performed to ensure that the lentiviral transduction used in CRISPR-cas9 editing did not introduce any murine pathogens (**Figure 3.35**). EO771 Mannose-high tumours grew much slower over time compared to tumours established from EV cells. In addition, one of the two mice within the EO771 Mannose-high group experienced complete regression of tumour. To validate this, this experiment was then repeated with greater numbers (**Figure 3.36**). Both the EV control and EO771 Mannose-high group each had one mouse which did not establish tumour. However, within the EO771 Mannose-high group, three mice had spontaneous tumour regression. Additionally, this difference in tumour growth became more significant over time. The interplay between high-mannose glycans and the immune system is still of interest, and IHC analysis of the immune infiltrate within the BC tumours from our *in vivo* experiments may be able to shed light on this. Collectively, these findings suggest that high-mannose glycans may play a critical role in modulating cellular behaviours associated with BC progression.

The syngeneic EO771 model offered a valuable platform to investigate the impact of high-mannose glycans both *in vitro* and *in vivo*. While translating data from murine models to human clinical data can be challenging, the presence of overlapping glycosyltransferase expression data instilled confidence in the validity of our findings. Moreover, the ability to study the effects *in vitro* within a single cell line and then successfully translate these effects *in vivo* proved to be particularly advantageous. However, it is important to note that we observed no difference in baseline cell

migration and invasion between the cell lines, suggesting that they may not be the most impactful models for studying the effects of metastases. To gain a more comprehensive understanding of metastatic processes, it would be prudent to explore and consider other metastatic models for future research.

Overall, we suspect there is a dynamic interplay between high-mannose glycoforms and highly branched glycoforms, and this may potentially be contributing to the complex nature of BC development and metastasis. It was previously demonstrated that the heterogeneity of glycans contributed to BC invasive phenotype (Pally *et al.*, 2021). Therefore, inducing a predominantly high-mannose phenotype may have reduced the invasive capabilities of BC cells by mechanisms of reduced glycan heterogeneity.

Moreover, the regulation of high-mannose glycans appears to be dynamic, and high-mannose glycans may be selected for at different stages of oncogenesis. It was previously demonstrated in colon carcinoma samples that the relative distribution of high-mannose glycans were elevated at the start of oncogenesis, however, as the disease progressed to invasive adenocarcinoma, high-mannose glycans were in relatively low abundance compared to branched tetra-antennary, sialylated glycans (Boyaval *et al.*, 2022). Successive changes in N-glycan repertoire have been reported across BC oncogenesis (Ščupáková et al., 2021). High-mannose glycans were significantly increased in clinical BC tumour tissues across all age and stage groups compared to matched adjacent normal tissue, but also significantly higher in tumours from patients >40 years of age, and in patients in early-stage BC (Liu et al., 2013). Therefore, glycan heterogeneity and the ability of tumour cells to regulate this at different stages of progression may be of importance. A deeper understanding of these dynamic interactions may offer valuable insights for the development of targeted therapies tailored to specific pathological conditions in BC and other diseases where glycosylation plays a pivotal role.

It is important to consider that the presence of high-mannose glycans may be a by-standing artifact of tumour progression. Throughout oncogenesis, proteins are commonly overexpressed. This

overexpression was demonstrated to saturate the glycosylation pathway, resulting in a mixed pool of aberrant high-mannose and native glycoproteins (Johns *et al.*, 2005). Generally, an overall increase in glycan abundance, and significant increases in high-mannose, fucosylated and sialylated glycans were observed in metastasis (Park *et al.*, 2020). It is suspected that high-mannose structures arise as local environmental accessibility prevents further processing (Park *et al.*, 2020). Therefore, a feedback loop could be proposed whereby the process of oncogenesis leads to gain-of-function mutations and increased abundance of all N-glycans leading to the saturation of N-glycosylation machinery. High-mannose glycoproteins experience the highest turnover rates (Xu *et al.*, 2019), leading to increased protein recycling. This further saturates glycosylation machinery, which creates substrates sterically inaccessible for downstream glycosyltransferases, in turn producing more high-mannose glycoproteins. At the same time, other glycan phenotypes such as highly branched fucosylated and sialylated glycans are present. This dynamic instability of glycoprotein production may create a platform to acquire and select for metastatic phenotypes.

In conclusion, we have provided compelling evidence of the association between high-mannose glycans and BC cells within clinical tissues. We observed aberrant regulation of mannose processing enzymes in invasive breast carcinoma samples, indicating their potential significance in BC progression. Interestingly, when we artificially increased cell surface high-mannose glycans using intrinsic and extrinsic methods, we observed a reduction in cellular migration, invasion, and tumour growth. This manipulation also led to a decrease in glycan heterogeneity and the proportion of highly branched, fucosylated, and sialylated glycans. These findings suggest that high-mannose glycans may play a critical role in modulating cellular behaviours associated with BC progression. Possible explanations for the presence of high-mannose glycans in BC progression have been discussed, offering valuable insights into the underlying mechanisms. Moreover, we suspect a dynamic interplay between high-mannose glycoforms and highly branched glycoforms, potentially contributing to the complex nature of BC development and metastasis. Moving forward, future research efforts should focus on exploring the expression of high-mannose glycans at different stages of BC progression and within distinct molecular subtypes. This approach will shed light on

the specific contexts in which high-mannose glycans exert their influence and provide a deeper understanding of their functional significance in BC pathobiology. Overall, our study adds to the growing body of knowledge surrounding the role of high-mannose glycans in BC, and it opens up new avenues for further investigation into potential therapeutic targets and diagnostic markers for this prevalent and devastating disease.

Chapter 4 Targeting high-mannose N-glycans to enhance anti-HER2 therapy

4.1 Introduction

Aberrant glycosylation is an established hallmark of cancer (Fuster and Esko, 2005; Munkley and Elliott, 2016; Gray *et al.*, 2020). Advances in understanding the presence and role of aberrant glycans in cancer has been influential in guiding therapeutic design. Indeed, the glycosylation state of cell surface receptors influences ligand binding and efficacy of target immunotherapies. Therefore, glycan-based therapeutics has become an emerging field.

Carbohydrate-based antitumour vaccines have been developed against ganglioside antigens (e.g. GD2, GD3, and GM3) (Rosenbaum *et al.*, 2022), Mucin-related O glycan antigens (e.g. Tn STn and Tf) (Holmberg and Sandmaier, 2004), blood group Lewis antigens (e.g. sialyl Lewis^{a} sialyl Lewis^{x,} Lewis^{y}) (Buskas, Li and Boons, 2004), and Globo-H series antigens (e.g. Globo-H, Gb3, SSEA-3) (Huang *et al.*, 2013). However, many candidates elicited low immune responses in human clinical trials (Wei, Wang and Ye, 2018). As such, extensive research into the type of adjuvant, carrier (Richichi *et al.*, 2014; Biswas, Medina and Barchi, 2015; Feng, Shaikh and Wang, 2016), and targeted antigen(s) (Cai *et al.*, 2014; Sun *et al.*, 2016; Kavunja *et al.*, 2017; Yin *et al.*, 2017) is being conducted in the hope to improve immune responses and reduce cross-reactivity (Wei, Wang and Ye, 2018; Mettu, Chen and Wu, 2020; Anderluh *et al.*, 2022).

Targeted glycan therapies are also being developed to block the interactions of immunosuppressive glycans with inhibitory immune receptors in cancer. For example, blockade of Gal-1 signaling promoted tumour rejection and enhanced T cell-mediated response in a melanoma model (Rubinstein *et al.*, 2016). The production of sialidase conjugates to tumour-targeting antibodies to target increased global sialoglycans, which are immunosuppressive and associated with poor outcomes across multiple cancers (see Chapter 1.12.1), showed suppressed tumour growth due to

tumour target desialylation (Che *et al.*, 2022). Anti-PD-L1-Sialidase dose-dependently inhibited tumour growth, and modulated immune cell infiltration in colon carcinoma models with improved efficacy relative to PD-1/PD-L1 blockade or Bi-Sialidase alone (Che *et al.*, 2022). Anti-HER2-Sialidase delayed tumour growth, enhanced immune infiltration and prolonged survival of mice with low HER2-expressing and Trastazumab-resistance BC, more than anti-HER2 therapy or Bi-Sialidase alone (Paszek *et al.*, 2014; Gray *et al.*, 2020). Further, delivery of anti-HER2-Sialidase in combination with anti-PD1 or anti-CTLA4 mAbs showed increased efficacy over anti-HER2-Sialidase alone (Xiao *et al.*, 2016; Gray *et al.*, 2020).

Antibodies that directly target the tumour-associated glycans themselves are also of interest. An anti-GD2 antibody was the first glycan-targeting immunotherapeutic drug approved by the European Medicines Agency (Spring and Therapeutics, 2015; European Medicines Agency, 2017). This construct targets disialoganglioside GD2, a sialic acid-containing glycosphingolipid antigen present on neuroblastoma cells (Greenwood and Foster, 2017; Mora, 2018). Since then, antibodies against other targets are undergoing clinical trials and include: anti-GD3 for the treatment of patients with melanoma (Tarhini *et al.*, 2017); anti-Fucosyl-GM1 for treatment in small cell lung carcinoma patients (Chu *et al.*, 2022); anti-Globo-H for treatment in patients with advanced solid tumours (Tsimberidou *et al.*, 2023); anti-Lewis^{y} for treatment in ovarian cancer patients (Smaletz *et al.*, 2021); and anti-Sialyl Lewis^{a} for treatment in pancreatic cancer patients (O'Reilly *et al.*, 2018).

In cancer, proteins are commonly overexpressed. This can lead to the saturation of the glycosylation pathway and the increased abundance of high-mannose glycoforms (Johns *et al.*, 2005). Under normal conditions, high-mannose glycans are generally confined to the endoplasmic reticulum (Loke *et al.*, 2016). However, cancer cells have been shown to aberrantly express high-mannose glycans on the cell surface, in blood, brain, ovarian, gastric, and liver tumours (Mendoza *et al.*, 1998; Liu *et al.*, 2013; Everest-Dass *et al.*, 2016; Park *et al.*, 2020; Chatterjee, Kawahara, *et al.*, 2021; Oh *et al.*, 2022). The clinical significance of high-mannose glycans in breast cancer (BC) has also been noted. In several cases they have been found expressed on the cell surface of BC cells (Liu *et al.*,

2013; Ščupáková *et al.*, 2021; Oh *et al.*, 2022), but also in the serum of BC patients (Leoz *et al.*, 2011). We have additionally reported the presence of high-mannose glycans on the cell surface of BC cell lines, and within clinical human BC tissues (see Chapter 3). These findings present high-mannose glycans as a tumour-associated marker and potential therapeutic target.

Strategies to target high-mannose glycans are emerging. For example, Oh *et al.,* (2022) recently synthesised a 'lectibody', comprised of a high-mannose targeting lectin domain attached to a hIgG Fc domain (AvFc), and demonstrated its use in a non-small cell lung carcinoma (NSCLC) model. AvFc demonstrated selective binding to tumour cells over healthy cells, an ability to elicit ADCC response through FcγRIIIa, and anti-tumour activity in SCID mice (Oh *et al.*, 2022). Further, EGFR and IGF1R were identified as two AvFc targets and suggested inhibition of these receptors was an additional mechanism of action (Oh *et al.*, 2022). This supports previous findings where mAb 806, which specifically binds high-mannose glycoforms of EGFR, prevented the formation of EGRF signaling dimers and generated an antitumor effect in a similar fashion (Hills, Rowlinson-Busza and Gullick, 1995; Johns *et al.*, 2005).

Although targeting high-mannose glycans in this way shows promise, lectin-based drugs show increased aggregation and immunogenicity (Matoba *et al.*, 2010). Engineering AvFc by fusion of the lectin domain to an IgG1 Fc domain increased solubility and stability relative to lectin alone (Hamorsky *et al.*, 2019). However, manufacturing AvFc for clinical use would present challenges; plant-viral-vector-based expression as suggested would produce non-mammalian glycosylation patterns. Differences in glycosylation can have major implications for antibody function (Roy Jefferis, 2009), immunogenicity (Prabakaran *et al.*, 2012; Zavala-Cerna *et al.*, 2014), and stability (Zheng, Bantog and Bayer, 2011). Indeed, reduced FcRn binding was observed with AvFc compared to IgG1, leading to a reduced half-life *in vivo* (Hamorsky *et al.*, 2019). Although an ability to induce ADCC was observed, the potency compared to clinically relevant controls for the same pathology was not established (Oh *et al.*, 2022). Fc glycosylation patterns have not been determined for AvFc, which may have implications for Fc-mediated functions. Additionally, a significant increase in liver

and spleen weights of BALB/C mice receiving twice-weekly doses of AvFc, compared to buffer control was observed (Hamorsky *et al.*, 2019). As no distinct pathologies were observed, this was a suspected immune reaction towards AvFc (Hamorsky *et al.*, 2019), and could be towards the lectin domain or due to abnormal glycosylation profiles.

AvFc has low affinity for individual glycans, and can only demonstrate meaningful binding for clusters of high-mannose glycans (Oh *et al.*, 2022). This suggests that the AvFc may struggle to bind heterogenous high-mannose glycans below a certain proximal threshold.

Glycans are highly heterogenous. In colon carcinoma samples it was observed that the relative levels of high-mannose glycans were elevated during different stages of oncogenesis (Boyaval *et al.*, 2022). High-mannose glycans were elevated at the start of oncogenesis, however, as the disease progressed to invasive adenocarcinoma, high-mannose glycans were in relatively low abundance compared to branched tetra-antennary, sialylated glycans. Successive changes in N-glycans have been reported across BC oncogenesis (Ščupáková *et al.*, 2021). Since glycan expression is heterogenous and is suspected to be dynamic throughout BC oncogenesis, this could potentially limit the efficacy of a high-mannose targeting therapeutic.

Current therapeutics for $HER2^+$ BC include anti-HER2 targeting mAbs such as Trastuzumab. Although Trastuzumab has shown a significant increase in time to disease progression and improved overall survival for $HER2^+$ BC patients (Ennis S Lamon *et al.*, 2001; Marty *et al.*, 2005), it is associated with increased risk of cardiotoxicity (Slamon *et al.*, 2001b; Seidman *et al.*, 2002). Additionally, around 70% of patients are unresponsive to Trastuzumab treatment, and therapeutic resistance throughout therapy occurs in almost all patients (Valabrega *et al.*, 2005; Gallardo *et al.*, 2012). Developing novel anti-HER2 antibodies to combat these challenges is therefore required.

To address the potential limitations of targeting high-mannose glycans alone and the current challenges faced by Trastuzumab, we aimed to create an antibody construct which targets both high-mannose glycans and HER2.

Within this chapter, we designed and generated a multivalent anti-HER2 and anti-high-mannose glycan antibody construct, and derivatives, based on the mAb, 2G12. We aimed to establish construct characteristics advised within the European Medicines Agency published guidelines (Medicines Agency, 2008). These include physiochemical properties, immunochemical properties, and biological function. The physiochemical properties assessed were amino acid sequence, glycosylation status and expression characteristics; The immunochemical properties assessed were cellular binding assays, and epitope binding kinetics and affinity; The biological function was assessed by functional antibody-dependent phagocytosis assays.

4.2 Results

4.2.1 The expression of HER2 and mannose in Breast Cancer

Breast cancer (BC) tumours which are not classified as $HER2^+$ may still express HER2, and thus be susceptible to targeted HER2 therapy. Due to cardiac toxicity caused by HER2 expression on cardiac cells, BC is defined as $HER2^+$ only if it has an immunohistochemistry score of 3+ (where 1 = weak, 2 = moderate and 3 = high), HER2/CEP17 ratio ≥2, or an average HER2 copy number ≥ 6.0 signals per cell (Ahn *et al.*, 2020). Therefore, we initially wanted to verify HER2 expression in clinical BC patients which would not ordinarily be classed as $HER2^+$.

Gene expression levels of HER2 in the TCGA Breast Cancer cohort were determined using the open-source Xena Browser platform (**Figure 4.1**). As expected, HER2 is most highly expressed in $HER2^+$ BC subtypes. Despite not being characterised as overexpressed in other subtypes, HER2 expression can be demonstrated in Luminal A, Luminal B, and Basal subtypes (**Figure 4.1**). Additionally, there is increased expression relative to normal breast tissue in Luminal A, Luminal B, and $HER2^+$ subtypes (**Figure 4.1**). Basal BC has a similar amount of HER2 expression, relative to normal breast. This determines that although HER2 targeting therapeutics are delivered mainly for $HER2^+$ BC, HER2 is still present in all other subtypes. This supported our rationale for developing a multivalent antibody construct targeting HER2 in tandem with other BC-specific markers, such as high-mannose glycans.

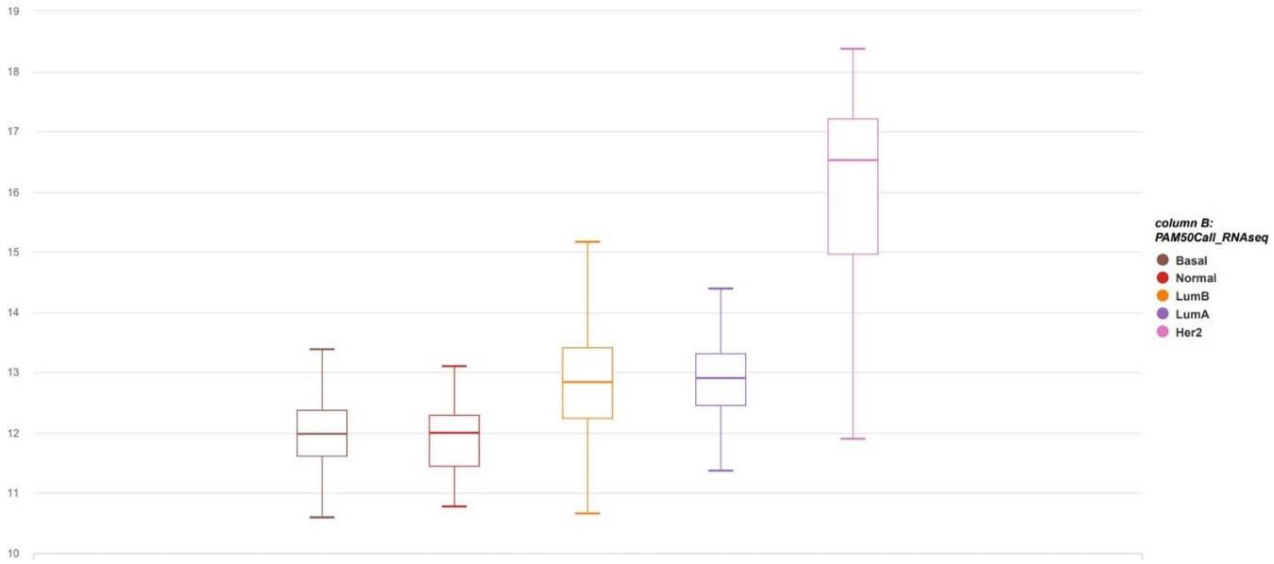

Figure 4.1: HER2 expression in different molecular subtypes of TCGA Breast Cancer (BRCA) cohort. TCGA dataset was analysed using the open-source Xena Browser platform. 508 samples were filtered by their PAM50 status. Illumina HiSeq 2000 RNA Sequencing reads RSEM normalised and log2 (norm_count+1) transformed. Human Genes were mapped onto human genome coordinates using UCSC Xena HUGO probeMap on the Xena Platform.

We next wanted to ensure that HER2 was expressed across human BC cell lines. $HER2^+$ cells SKBR3 ($HER2^+$-high) and MCF7 ($HER2^+$-low), and TNBC cells MDA-MB-231 were harvested and opsonised with 1 µg/mL commercial Herceptin or Rituximab primary antibodies and detected with a PE-conjugated anti-Fc secondary antibody (**Figure 4.2**). **Figure 4.2A-C** shows representative dot plots of the gating strategies used. **Figure 4.2D** shows that SKBR3 cells expressed the highest levels of HER2, ~25-fold higher than MCF7 and MDA-MB-231. While low, this also suggests that BC cell lines traditionally thought of as being HER2 negative do actually express HER2.

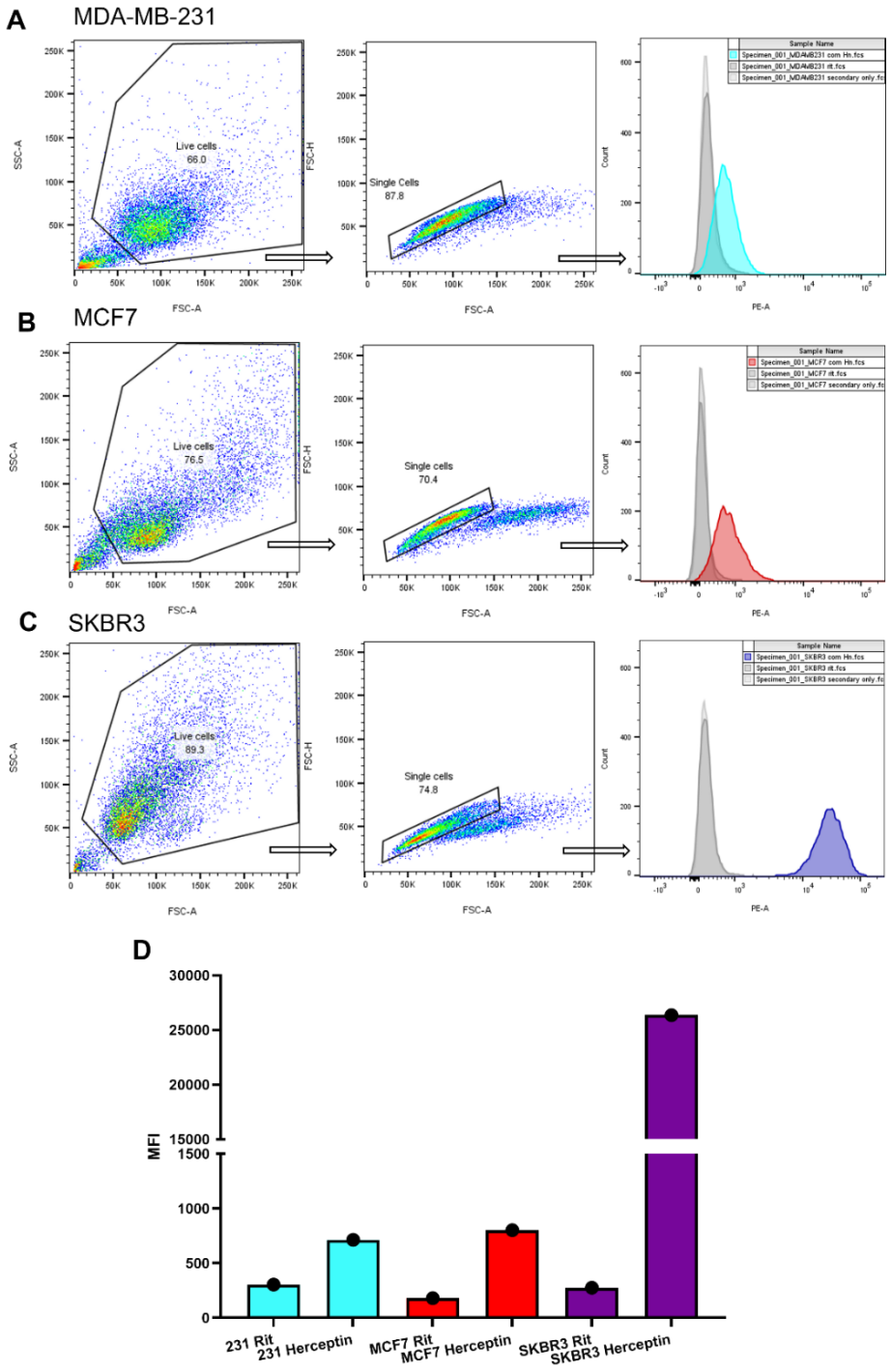

Figure 4.2: anti-HER2 staining of human breast tumour cell lines. Live cell gating was performed for each cell line. Primary unlabelled antibody and anti-Fc PE labelled secondary was used, and cells were imaged using the 488nm wavelength laser employed in the PE channel. HER2 expression was measured by Commercial Herceptin and Commercial Rituximab was an irrelevant isotype control. (A) Representative dot-plots and histogram analysis of TNBC MDA-MB-231 cells. (B) Dot-plot and histogram analysis of HER2^{+}-low, MCF7 cells. (C) Dot-plot and histogram analysis of HER2^{+}-high, SKBR3 cells. (D) Data presented as a bar graph. Abbreviations; 231 = MDA-MB-231. Rit = rituximab isotype control.

We previously determined that high-mannose glycans were present on the cell surface of BC cells (**Figure 3.9**) Additionally, we observed that TNBC cells had higher levels of high-mannose glycans than $HER2^+$ BC cells. Therefore, since TNBC cells do express HER2 at low levels, dual targeting with anti-high-mannose epitopes may reduce the impact of cardiac toxicity, which currently prevents low $HER2^+$ BC patients from receiving anti-HER2 therapy.

4.2.2 2G12-Hn 1 construct design and generation

Based on this evidence, we decided to engineer a multivalent antibody targeting both mannose residues and HER2. A novel 2G12-based construct with single chain variable fragments (scFv) arranged off the light chain was designed and developed, named 2G12-Herceptin (2G12-Hn 1) (**Figure 4.3**). The 2G12 mAb backbone targets high-mannose glycans, and the HER2-targeting scFvs have the amino acid sequence of Herceptin variable fragment domains. Since 2G12 requires a domain exchange of its variable heavy fragments to facilitate mannose-binding, Herceptin scFvs were arranged off the bottom of the light chain to not interfere with this. A flexible amino acid linker of three repeating polyglycine and serine $(Glyc_4Ser_1)_3$ units were designed between the variable fragments of each Herceptin scFv. The same linker was used to connect each scFv with the constant light domain of 2G12.

To produce the 2G12-Hn 1 antibody, gene synthesis and molecular cloning into the pfuse2ss expression vector was performed by NBS Biologicals. Once the construct was received, competent *E. coli* were transformed with 2G12-Hn 1 DNA and bacterial cultures were grown at 37˚C overnight, with shaking. At this point, glycerol stocks were made for long-term storage. Heavy chain (HC) and Light chain (LC) plasmid DNA was purified and HEK293F cells were transfected using PEI-max transfection reagent at a HC:LC ratio of 1:1. Transfections of Trastuzumab DNA within the same expression vector (pfuse2ss) were performed alongside 2G12-Hn expressions, to provide an appropriate control. From herein in-house Trast refers to recombinantly expressed Trastuzumab within the same cell line, whereas Herceptin refers to the commercial, clinical-grade therapeutic.

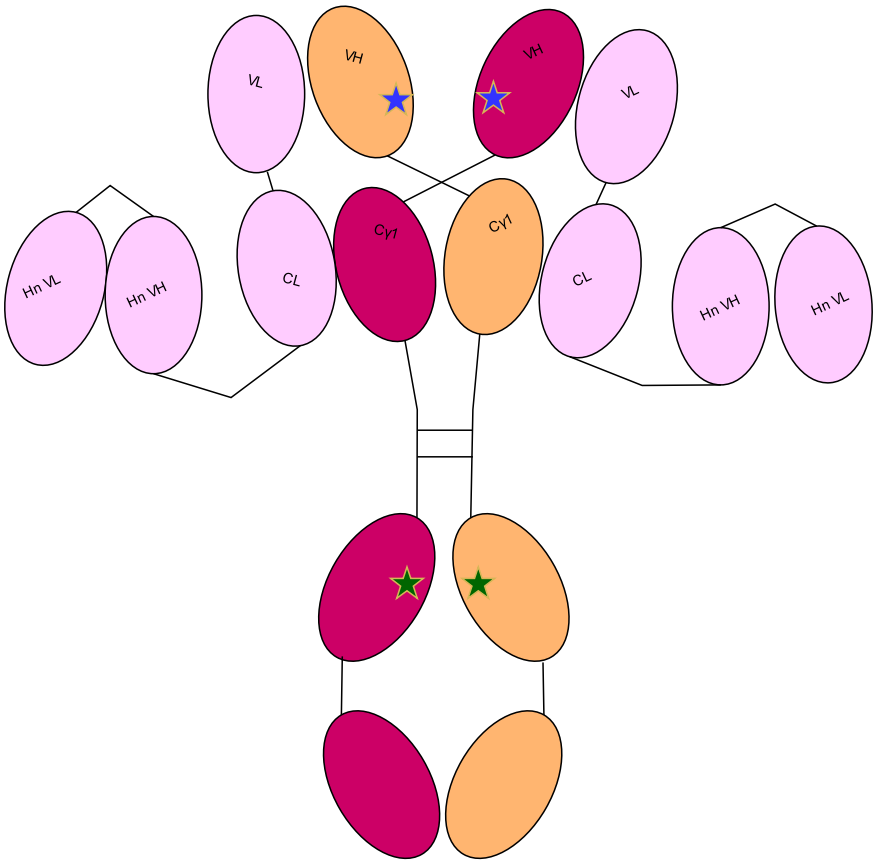

Figure 4.3: 2G12-Hn 1 multivalent antibody targeting mannose glycans and HER2. IgG1 isotype based on 2G12 mannose-targeting antibody and incorporating Herceptin ScFVs. A single N-linked glycan resides at position asparagine 297 of each heavy chain (green star). Domain exchange of the variable heavy domains of 2G12 is indicated by the blue star.

Protein was purified from the supernatant by affinity (protein A) and size exclusion chromatography after 7 days. Protein size and assembly was visualised by non-reducing SDS-PAGE (**Figure 4.4**). Overall, 2G12-Hn 1 expressed and produced a protein at the correct size, as seen by the most prominent band at the predicted size of ~200 kDa. Small bands can be seen at 100 kDa and 50 kDa for 2G12-Hn 1, showing the disruption of non-covalent bonds. The 50 kDa band is likely LC-scFv units. A similar band at 100 kDa can be observed in the Herceptin and In-house Trast, suggesting this species could be HC dimer. The 250 KDa band in Herceptin is predicted to be aggregate, from multiple freeze-thaw cycles.

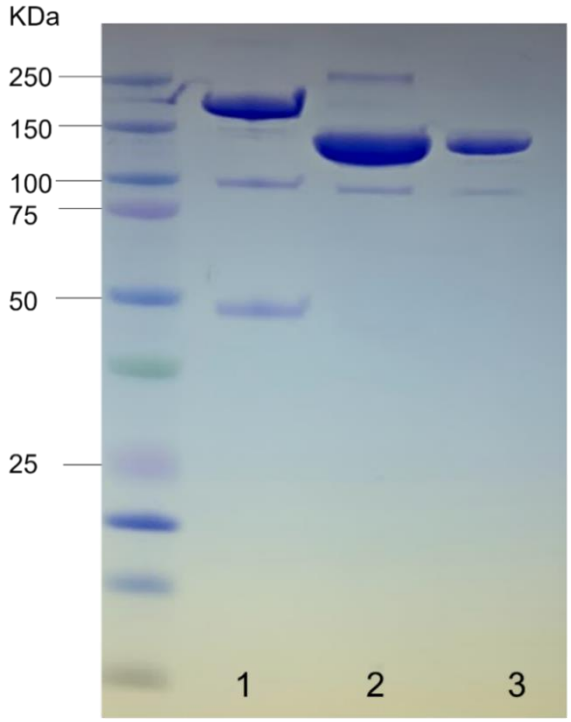

Figure 4.4: SDS-PAGE analysis of SEC purified 2G12-Hn 1. NuPAGE 4-12% Bis-Tris gradient gel ran in MES buffer. 15 µg sample was mixed with 4X loading buffer and electrophoresed at 160 volts for 40 minutes. Kaleidoscope protein ladder was loaded alongside to establish molecular weights. Lane 1; 2G12-Hn 1. Lane 2; Commercial Herceptin. Lane 3; In-house Trastuzumab.

4.2.3 Glycopeptide analysis of 2G12-Hn 1

Antibody glycosylation can influence binding capabilities and biological function, therefore patterns in Fc glycosylation of 2G12-Hn 1 and In-house Trast was investigated. Briefly, SDS-PAGE gel bands from **Figure 4.4** were excised and an in-gel reduction, alkylation, and digestion with trypsin was performed. Peptides were extracted and analysed by liquid chromatography-mass spectrometry (LC-MS).

Overall, the presence of 20 unique glycoforms was determined for each construct, of which the most prominent glycoform is G0F, **Figure 4.5A**. Minor differences can be seen between 2G12-Hn 1 compared to In-house Trast where there was a slight increase in high-mannose type glycans and a decrease in fucosylated glycans. In-house Trast harboured more galactosylated glycoforms. Little

difference was seen in terminal sialic acid residues. Overall, similar glycosylation profiles were observed between the two constructs, suggesting a limited impact on biological function.

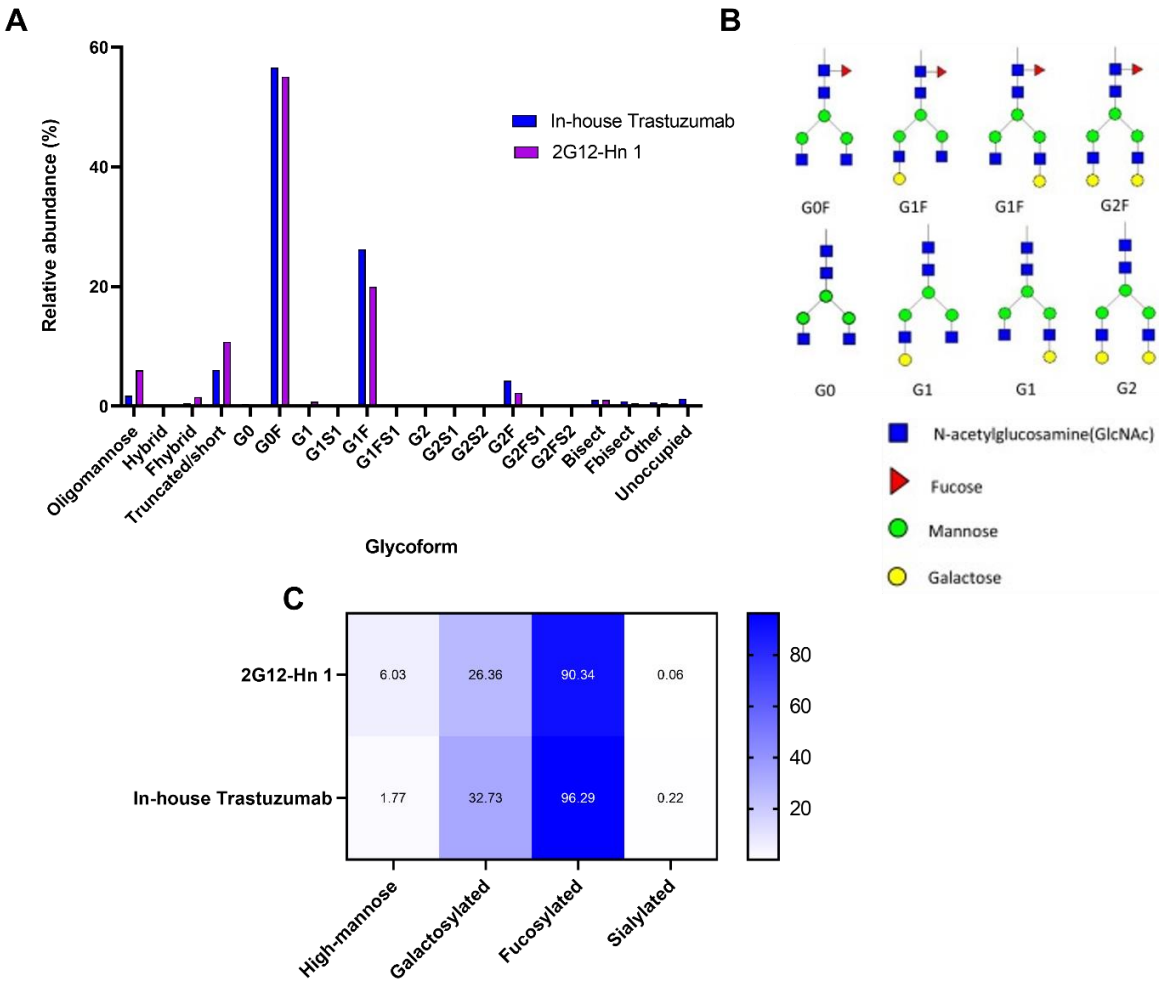

Figure 4.5: Analysis of Fc glycosylation of 2G12-Hn constructs. (A) Categorisation of the relative abundance of glycoforms detected by LC-MS. (B) Schematic of glycan nomenclature. (C) Table of the relative abundance of high-mannose-type, galactosylated, fucosylated, and sialylated glycans for each construct.

4.2.4 Surface plasmon resonance of 2G12-Hn 1

To determine 2G12-Hn 1 HER2 ligand binding capability and affinity, surface plasmon resonance (SPR) was utilised. Commercially available his-tagged HER2 was purchased and captured on a CM5 sensor chip immobilised with anti-His antibody to 1000 RU. The captured HER2 was exposed to 5-fold dilutions of Herceptin, In-house Trast, or 2G12-Hn 1. Sensorgrams of HER2 binding were fitted to the 1:1 binding model using the Biacore Bioevalutation software and plotted in GraphPad prism

9 (**Figure 4.6**). Analysis of the sensorgrams revealed that the 1:1 binding model provided an appropriate fit for the construct binding.

All constructs reached saturation at 100 nM. Herceptin reached saturation at all concentrations tested, suggesting high binding affinity. In-house Trast reached saturation at all but the lowest concentration. However, 2G12-Hn 1 only reached saturation at the highest three concentrations, suggesting a lower HER2 affinity at lower concentrations.

Analysis of the association, dissociation, and equilibrium constants are shown in **Table 4.1**. The association constant (k_a) represents the initial binding affinity to HER2. Herceptin has the highest K_a value, followed by In-house Trast, and then 2G12-Hn 1. This is also reflected in the sensorgrams, where 2G12-Hn 1 binding curve is less exponential (**Figure 4.6**). K_d is the dissociation constant, representing how quickly the interaction between HER2 and the antibody decays. The smaller this value, the slower the dissociation. The calculated K_d values show that In-house Trast had the highest K_d (**Table 4.1**). However, when observing the sensorgrams, none of the constructs dissociated once bound.

The equilibrium constant, KD, is inversely proportional to affinity, therefore the lower the KD the higher the construct affinity for HER2. Herceptin had the lowest KD value overall, followed by In-house Trast, and 2G12-Hn 1 (**Table 4.1**). This is reflected in (**Figure 4.6**), where the curves of Herceptin reached saturation the fastest across all concentrations. 2G12-Hn 1 had a similar KD value to In-house Trast.

The maximal response signal (Rmax) at 100 nM of Herceptin and In-house Trast were both around 100 RU. Of interest, the Rmax of 2G12-Hn 1 at 100 nM reached approximately 170 RU. The density of HER2 on the chip was constant between experiments, and construct concentrations were proportional. Therefore, a greater Rmax could suggest a greater binding affinity of 2G12-Hn 1 at 100 nM.

Overall, 2G12-Hn 1 had the smallest K_a revealing it bound at a slower rate than Herceptin and In-house Trast. In addition, 2G12-Hn 1 showed reduced binding capability at lower concentrations (**Figure 4.6**). Binding affinity was comparable at higher concentrations. This suggests difficulties of 2G12-Hn 1 binding to HER2 at lower concentrations but shows that it can be overcome at higher concentrations.

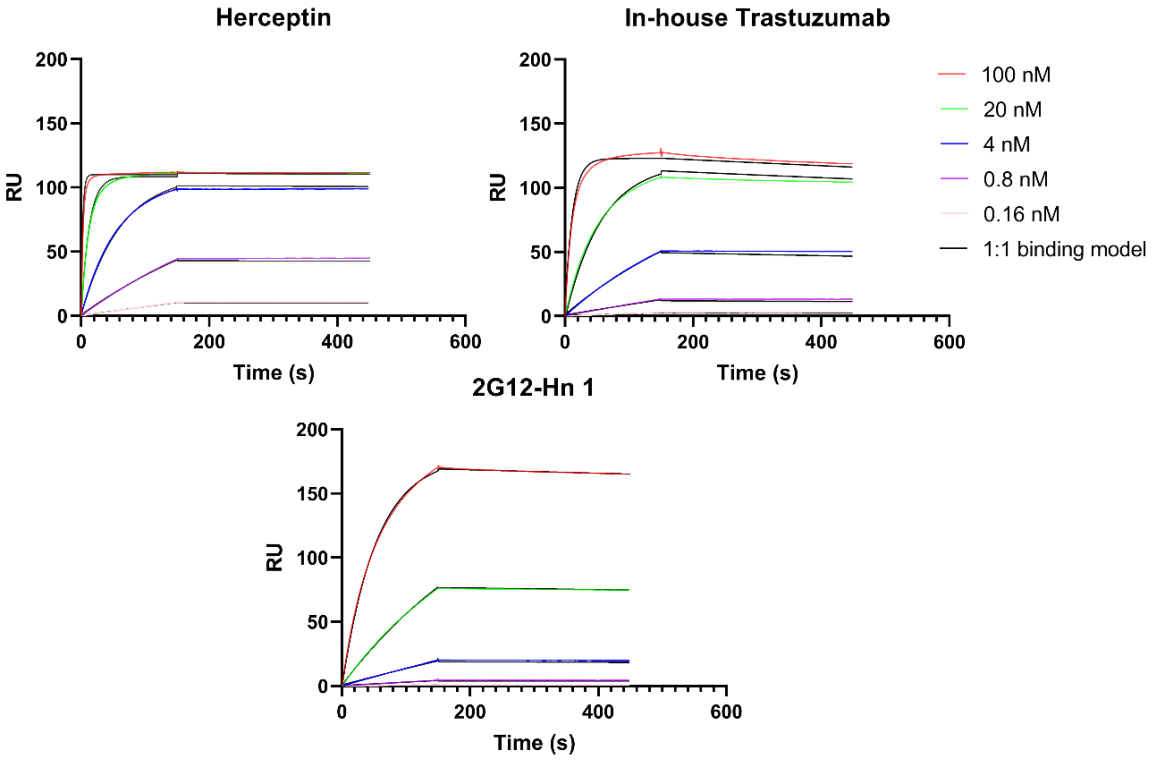

Figure 4.6: SPR analysis of 2G12-Hn 1 mAb binding to HER2 ligand. Sensorgrams of Herceptin, in-house Trastuzumab, and 2G12-Hn 1 for the HER2 ligand. HER2 was immobilised on a chip (5 µg/mL) and antibody constructs were flowed over in 150 second associations and 300 second dissociations on a Cytiva Biacore T200. 5-fold dilution series were performed.

Table 4.1: SPR binding kinetics data for 2G12-Hn 1 mAb against HER2 ligand.

Construct	k_a (1/Ms)	k_d (1/s)	KD (M)
Herceptin	4.08E+06	1.69E-05	4.14E-12
In-house Trastuzumab	8.69E+05	1.93E-04	2.22E-10
2G12-Hn 1	1.85E+05	7.99E-05	4.32E-10

4.2.5 Cell surface binding of 2G12-Hn 1

We next wanted to determine the cell surface binding efficacy of 2G12-Hn 1. $HER2^{+}$-high human BC cell line, SKBR3 cells were employed in this assay. Cells were cultured +/- 10 μM Kifunensine (Kif) for 48 hours, to determine the impact of increasing the mannose epitopes on construct binding efficacy. SKBR3 cells were opsonised with 1 μg/mL primary antibody and detected with a PE-conjugated anti-Fc secondary antibody by flow cytometry. Since only 2G12 and 2G12-Hn 1 have mannose binding capabilities, binding efficacy to Kif-treated cells was initially investigated for these constructs (**Figure 4.7C**).

Figure 4.7 represents cell surface antibody binding of Rituximab, 2G12, In-house Trast, Herceptin, and 2G12-Hn 1. **Figure 4.7A** depicts the gating strategy for live and single cells. Rituximab and 2G12 showed similar low levels of cell surface binding. When cells were treated with Kif, 2G12 binding increased by 60-fold (**Figure 4.7B**).

In-house Trast and Herceptin showed comparably high levels of binding to SKBR3 (**Figure 4.7B**) compared to 2G12 constructs. 2G12-Hn 1 bound 14-fold less to SKBR3 cells than In-house Trast or Herceptin (**Figure 4.7B**). However, when cells were treated with Kif 2G12-Hn 1 binding levels increased by 14-fold, and 2G12-Hn 1 bound comparably with the strongest binders, In-house Trast and Herceptin.

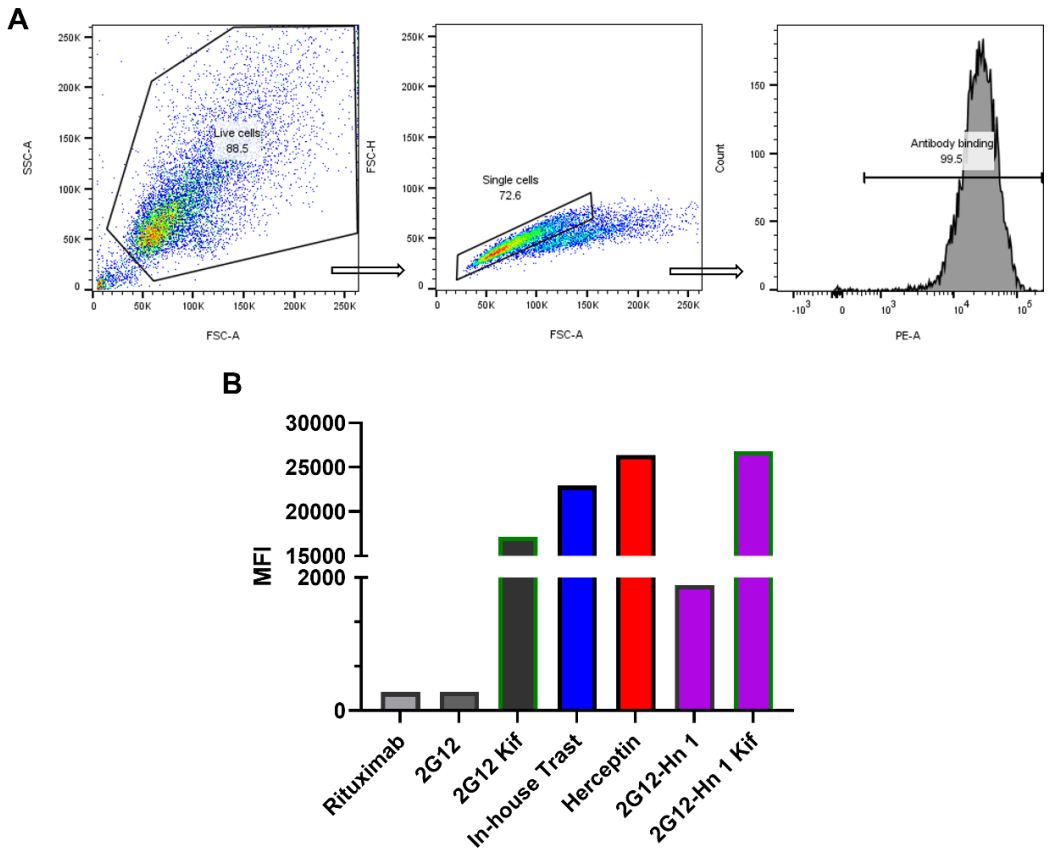

Figure 4.7: 2G12-Hn 1 binding to HER2$^+$ human breast cancer cell line, SKBR3, +/- Kifunensine treatment. SKBR3 cells were cultured with 10 µM Kifunensine for 48 hours. SKBR3 cells were opsonised with 1 µg/mL primary antibody constructs for 30 minutes on ice. PE-labelled anti-Fc secondary antibodies were used to detect primary antibodies. (A) shows representative dot-plots of live and single cell gating strategy. (B) shows the MFI for the binding of antibody constructs to SKBR3 cells. 10,000 events were recorded in the PE channel using the BD FACSCanto II. Analysis was performed using FlowJo software where the geometric mean of the area under the curve for each sample was calculated.

Kif treatment perturbs glycosylation but also interferes with ERAD degradation (Wang *et al.*, 2011). This may elevate cell surface protein expression, which could contribute to the observed increase in 2G12-Hn 1 binding (**Figure 4.7**). Therefore, we investigated the impact of Kif on HER2 epitope expression and stability (**Figure 4.8**). Human BC cells, HER2$^+$-high (SKBR3), HER2$^+$-low (MCF7), and TNBC (MDA-MB-231) cells were cultured +/- Kif, as described previously. Cells were opsonised with 10 µg/mL Herceptin and detected with a PE-conjugated anti-Fc secondary antibody by flow cytometry (**Figure 4.8**). **Figure 4.8A** depicts the gating strategy for live and single cells; treatment

with Kif did not impact cell viability or single cell gating. Across all cell lines, Kif treatment increased Herceptin binding as shown by an increased MFI (**Figure 4.8B**). Cell surface binding was elevated 10-15%, suggesting increased HER2 expression. However, this does not account for the large increase in 2G12-Hn 1 binding observed for Kif-treated SKBR3 cells (**Figure 4.7**B). Nonetheless, the potential for Kif treatment to modestly elevate cell surface receptor expression was considered for future experiments.

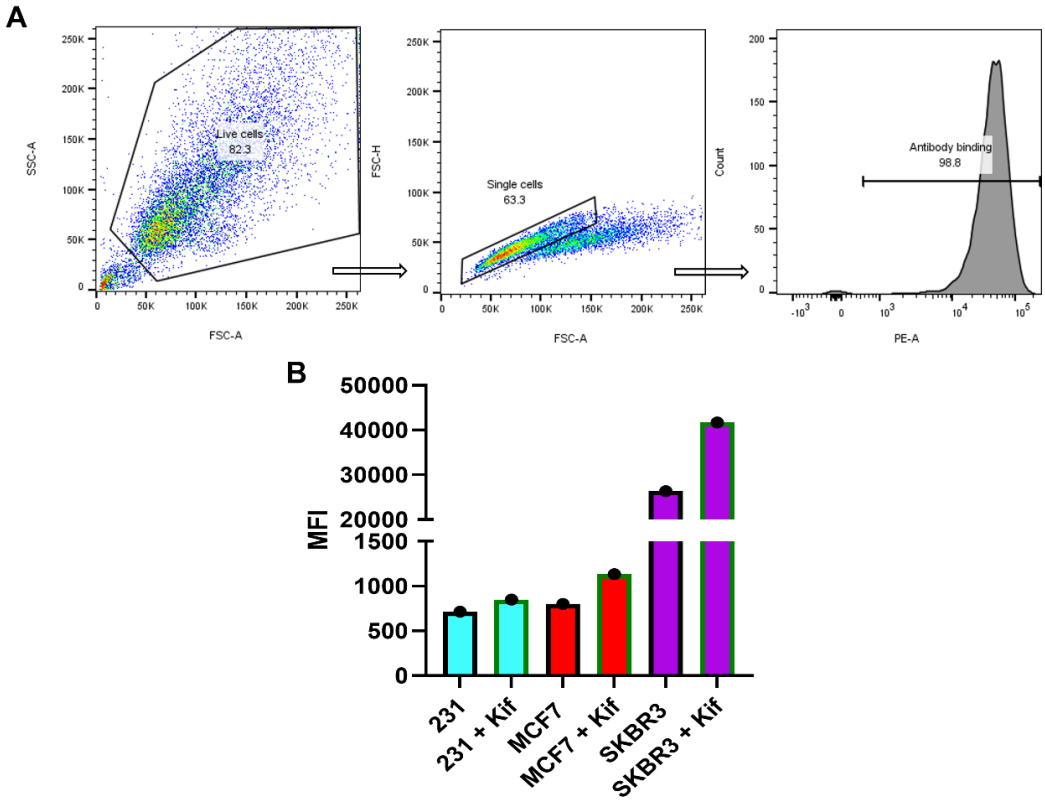

Figure 4.8: The impact of Kifunensine treatment on Herceptin binding to human breast cancer cells. Cells were cultured with 10 µM Kifunensine for 48 hours prior to being harvested and opsonised with Herceptin for 30 minutes on ice. PE-labelled anti-Fc secondary antibodies were used to detect primary antibodies. (A) shows representative dot-plots of live and single cell gating strategy, in which Herceptin binding to SKBR3 cells is depicted. (B) shows the MFI values for Herceptin binding to: TNBC MDA-MB-231 (231) cells +/- Kifunensine, HER2^{+}-low MCF7 cells +/- Kifunensine, and HER2^{+}-high SKBR3 cells +/- Kifunensine. 10,000 events were recorded in the PE channel using the BD FACSCanto II. Analysis was performed using FlowJo software where the geometric mean of the area under the curve for each sample was calculated.

Taken together, these results suggest that the mannose-targeting domain of 2G12-Hn 1 is functional, however, does not provide enough avidity alone. In addition, 2G12-Hn 1 has an impaired ability to bind $HER2^+$ cells as effectively as In-house Trast or Herceptin, without the additional valency provided by mannose binding.

4.2.6 Biological activity of 2G12-Hn 1

Next, we aimed to explore the biological activity of 2G12-Hn 1 by *in vitro* antibody-dependent cellular phagocytosis (ADCP) assay. Briefly, peripheral blood mononuclear cells (PBMCs) were isolated from the blood of healthy human donors and differentiated into M0 macrophages (MDMs). Target BC cells were labelled with CFSE and then opsonised with 1 µg/mL of antibody and cocultured with MDMs. Live cell gating of effector cells was initially examined by flow cytometry to ensure cell viability was maintained and efferocytosis was not influencing phagocytosis levels (**Figure 4.9A**). Cell trace far red (CTFR) stained MDMs were gated as CFSE negative or CFSE positive which represents phagocytic MDMs (**Figure 4.9B**). Phagocytosis levels were plotted as a percentage of total macrophages (**Figure 4.9C**).

Three different human cell lines were used as BC target cells: SKBR3 ($HER2^+$-high), MCF7 ($HER2^+$-low) and MDA-MB-231 (TNBC) (**Figure 4.9C**). SKBR3 cells had the highest level of ADCP of all three cell lines. This was unsurprising since expression levels of HER2 on its cell surface is much higher than MCF7 or MDA-MB-231. Herceptin and In-house Trast induced a similar level of ADCP within each donor, ranging from 20-55%. Although offering some advantage over 2G12 alone, 2G12-Hn 1 induced less ADCP in SKBR3 cells than Herceptin or In-house Trast (**Figure 4.9C**). This finding was consistent across three donors.

MCF7 had the next highest level of ADCP. Herceptin and In-house Trast induced similar levels of ADCP across two out of the three donors. In donor 2, Herceptin offered an advantage over In-house Trast. Contrary to SKBR3, 2G12-Hn 1 induced similar, or better levels of ADCP activity, than In-house Trast with MCF7 cells. ADCP levels in MCF7 cells of donor 1 were ~7% for 2G12-Hn 1, and ~4% for

Herceptin and In-house Trast (**Figure 4.9C**). This suggests dual targeting of HER2 in combination with mannose may have an advantage over targeting HER2 alone, when HER2 expression is low. ADCP levels were very low when using the 2G12 antibody, suggesting that targeting 2G12 alone is not sufficient to induce ADCP.

MDA-MB-231 generally had the lowest levels of ADCP, with donors 1 and 2 being unresponsive to most constructs (**Figure 4.9C**). 2G12-Hn 1 induced the highest levels of ADCP across all three donors. Although ADCP levels of donors 1 and 2 were marginal, 2G12-Hn 1 induced greater levels than all other constructs. Donor 3 was more responsive, with Herceptin and In-house Trast inducing ~4% ADCP (**Figure 4.9C**). 2G12-Hn 1 induced the highest levels of ADCP, ~15% in donor 3 (**Figure 4.9C**). This was >3-fold increase. 2G12-Hn 1 ADCP levels were greater than 2G12 alone, with 2G12 unresponsive across all donors. MDA-MB-231 express the lowest levels of cell surface HER2 (**Figure 4.2**), and the highest levels of cell surface mannose (**Figure 3.9**), relative to SKBR3 and MCF7.

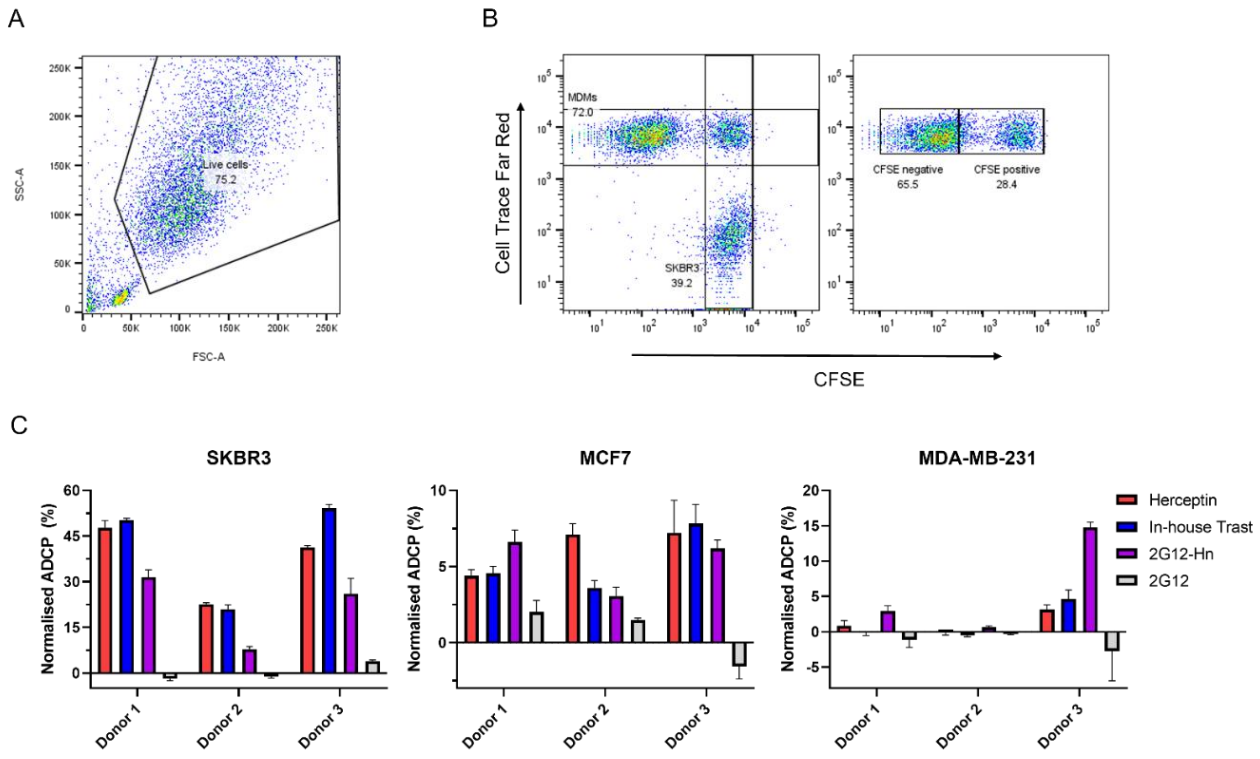

Figure 4.9: Antibody dependent phagocytosis of breast cancer target cells elicited by 2G12-Hn 1.

(A) Representative flow cytometry plot of the live cell gating strategy employed, in which SKBR3 effector cells are depicted. (B) Representative flow cytometry plots to show SKBR3 and MDM populations. MDMs were further gated into CFSE negative and CFSE positive populations. (C) The normalised percentage of ADCP was calculated by subtracting background activity (control wells absent of mAb).

Overall, these results suggest that 2G12-Hn 1 can successfully be expressed with little differences in glycosylation. Cell surface binding and ADCP data suggest that 2G12-Hn 1 can target both mannose and HER2. At low levels of HER2 expression, the 2G12-mannose binding may be acting to increase overall avidity. However, as HER2 expression increased, cellular binding and biological activity induced by the 2G12-Hn 1 antibody decreased in comparison to the antibodies targeting HER2 alone. This suggests that the interaction between HER2 and the anti-HER2 scFv domains of the 2G12-Hn 1 construct may be being impeded, potentially through steric hindrance.

4.2.7 Re-design and generation of new multivalent constructs

Based on this evidence, we next set out to generate further derivatives of the multivalent 2G12-Hn construct with differing placement of the HER2-scFv domains to determine if this could further improve binding. 2G12 requires a domain exchange of its variable heavy fragments to facilitate mannose binding, therefore these domains were not altered. Initially, Herceptin scFvs were arranged off the bottom of the light chain to not interfere with this, **Figure 4.10A**. In the new derivatives, Herceptin scFvs were arranged off the top of the light chain (2G12-Hn 2), or off the top and bottom of the light chain (2G12-Hn 3) as shown in **Figure 4.10B-C**. As before, a flexible amino acid linker of three repeating polyglycine and serine $(Glyc_4Ser_1)_3$ units were designed between the variable fragments of each Herceptin scFv. The same linker was used to connect each scFv with the constant light domain of 2G12.

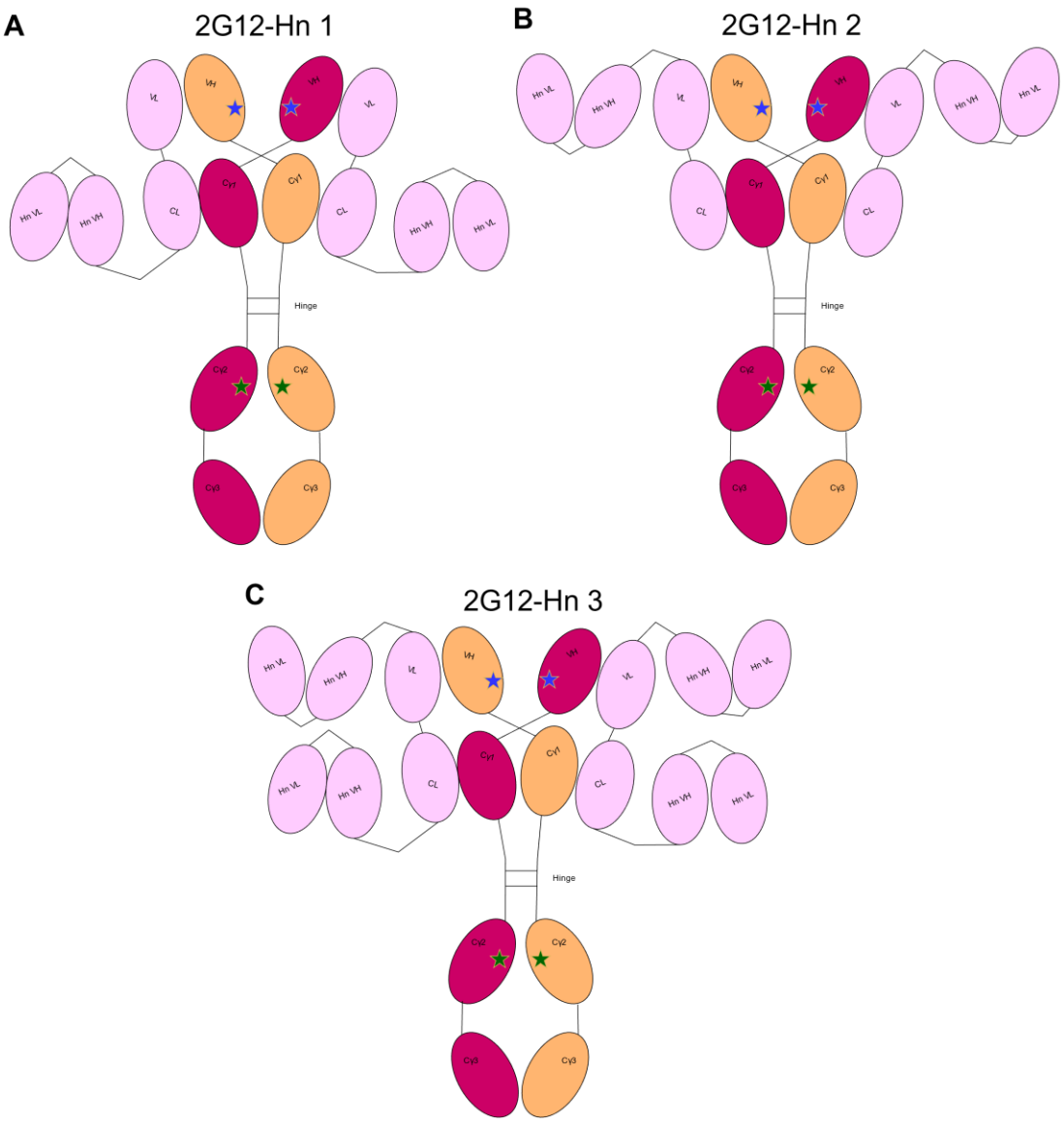

Figure 4.10: Schematic of 2G12-Hn constructs. IgG1 2G12 backbone was used. Light chain domains are indicated in pink. Heavy chain domains are distinguished to visualise domain exchange, and are indicated in orange and magenta, respectively. Blue stars indicate the site of domain exchange which occurs at the variable heavy domains to allow epitope binding. Green stars represent the N-glycosylation site at N297, and hinge region is indicated. (A) 2G12-Hn 1, with ScFvs hanging off the 2G12 constant light domain. (B) 2G12-Hn 2, with ScFvs hanging off the 2G12 variable light domain. (C) 2G12-Hn 3, with ScFvs hanging off both the 2G12 constant and variable light domains.

4.2.8 Expression and assembly of multivalent constructs

To increase yields, all constructs were further expressed in the high-throughput MEXi293E cell line. MEXi293E cells were transfected using PEI-max transfection reagent at a HC:LC ratio of 1:1. In-

house Trastuzumab (in-house Trast) transfections were performed alongside, to provide an appropriate control.

Protein was purified from the supernatant by affinity (protein A) after 7 days. Aggregation was determined via HPLC (**Appendix 8**; **Appendix 9**) and size exclusion chromatography was performed. Protein size and assembly was visualised by SDS-PAGE (**Figure 4.11**). Samples were analysed under non-reducing and reducing conditions.

In-house Trast expressed as expected, with an intact molecular weight of 150 kDa (**Figure 4.11**). Under reducing conditions, HC and LC monomers are seen at the expected band sizes at 50 kDa and 25 kDa respectively. 2G12-Hn 1 and 2G12-Hn 2 both ran intact at ~200 kDa and a single band of 50 kDa under reducing conditions. This is expected since the HC and modified LC are of equal molecular weight in both constructs. 2G12-Hn 3 ran at a higher intact molecular weight of 250 kDa. When reduced to monomers, two prominent bands were observed at 75 kDa and 50 kDa representing modified LC and HC, respectively.

Of note, faint bands can be seen under non-reducing conditions for 2G12-Hn 1 and 2G12-Hn 2 at ~150 kDa and ~50 kDa, and 2G12-Hn 3 at 200 kDa and ~75 kDa, respectively (**Figure 4.11**). These likely represent a construct missing one of the modified LC domains, showing the disruption of non-covalent bonds. Similarly, faint bands can be observed for 2G12-Hn 1 and 2G12-Hn 3 under reducing conditions at ~100 kDa and ~150 kDa, respectively. This suggests an incomplete disruption of interactions, possibly associated with the positioning of ScFVs.

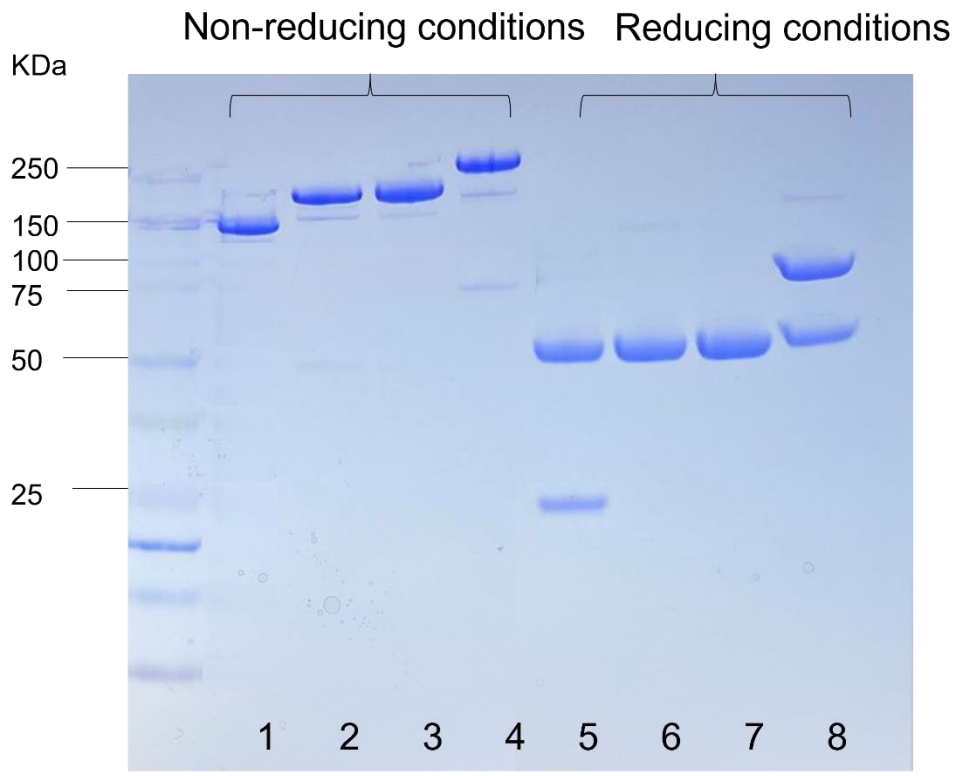

Figure 4.11: SDS-PAGE analysis of SEC purified 2G12-Hn constructs. NuPAGE 4-12% Bis-Tris gradient gel ran in MES buffer. 10 µg sample was mixed with 4X loading buffer and electrophoresed at 160 volts for 40 minutes. Kaleidoscope protein ladder was loaded alongside to establish molecular weights. Lanes 1-4 ran in non-reducing conditions. Lanes 5-6 ran in reducing conditions: Samples were mixed with reducing agent and boiled for 10 minutes prior to loading. Lanes 1 and 5; In-house trastuzumab. Lanes 2 and 6; 2G12-Hn 1. Lanes 3 and 7; 2G12-Hn 2. Lanes 4 and 8; 2G12-Hn 3.

4.2.9 Glycopeptide analysis of multivalent constructs

Since the cell line employed for recombinant protein expression was changed from HEK293F to MEXi293E cells, it was first important to determine any differences in glycosylation. Glycopeptide analysis of HEK293F and MEXi293E expressed In-house Trast was performed, as before. SDS-PAGE gel bands were excised and an in-gel reduction, alkylation, and digestion with trypsin was performed.

Peptides were extracted and analysed by liquid chromatography-mass spectrometry (LC-MS). Overall, the presence of 20 unique glycoforms was determined, of which the most prominent glycoforms were G0F and G1F for HEK293F and MEXi293E expressed In-house Trast, respectively

(**Figure 4.12A**). HEK293F expressed In-house Trast harboured less galactosylated glycoforms than MEXi293E (**Figure 4.12C**). Additionally, HEK293F expressed In-house Trast had less high-mannose and more fucosylated glycoforms. Slight differences in relative glycoform abundances were observed between the different host cell lines.

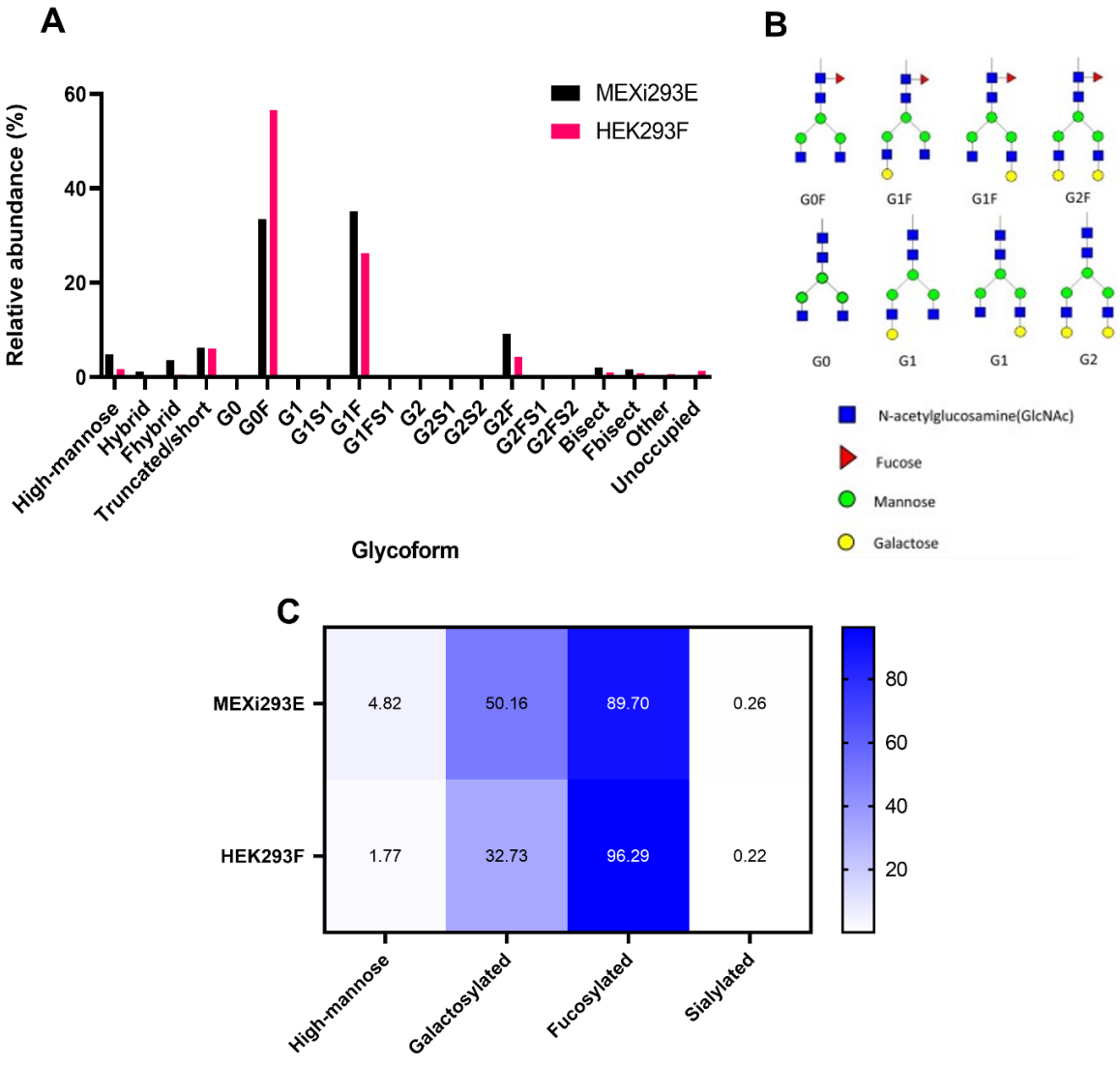

Figure 4.12: Analysis of Fc glycosylation of In-house Trastuzumab expressed in MEXi293E vs HEK293F cells. (A) Categorisation of the relative abundance of glycoforms detected by LC-MS. (B) Schematic of glycan nomenclature. (C) Table of the relative abundance of high-mannose-type, galactosylated, fucosylated, and sialylated glycans for each construct.

Glycopeptide analysis was next performed to characterise 2G12-Hn constructs. SDS-PAGE gel bands from **Figure 4.11** were excised and an in-gel reduction, alkylation, and digestion with trypsin was performed.

Peptides were extracted and analysed by liquid chromatography-mass spectrometry (LC-MS). Overall, the presence of 20 unique glycoforms was determined for each construct, of which the most prominent glycoforms were G0F and G1F (**Figure 4.13A**). Minor differences can be seen across all constructs (**Figure 4.13C**). As before, a slight increase in high-mannose glycans and a decrease in fucosylated glycans was observed for 2G12-Hn 1 compared to all other constructs (**Figure 4.13C**).

Relative levels of each glycoform were most similar between 2G12-Hn 2 and In-house Trast, and 2G12-Hn 1 and 2G12-Hn 3, respectively (**Figure 4.13A**). 2G12-Hn 2 and In-house Trast had higher overall levels of galactosylated glycoforms than 2G12-Hn 1 and 2G12-Hn 3 (**Figure 4.13C**). 2G12-Hn 2 had the lowest levels of high-mannose glycans and the highest levels of fucosylated, galactosylated, and sialylated glycans (**Figure 4.13C**). Despite these modest differences, overall glycosylation profiles were similar across all constructs, suggesting a limited impact on biological function.

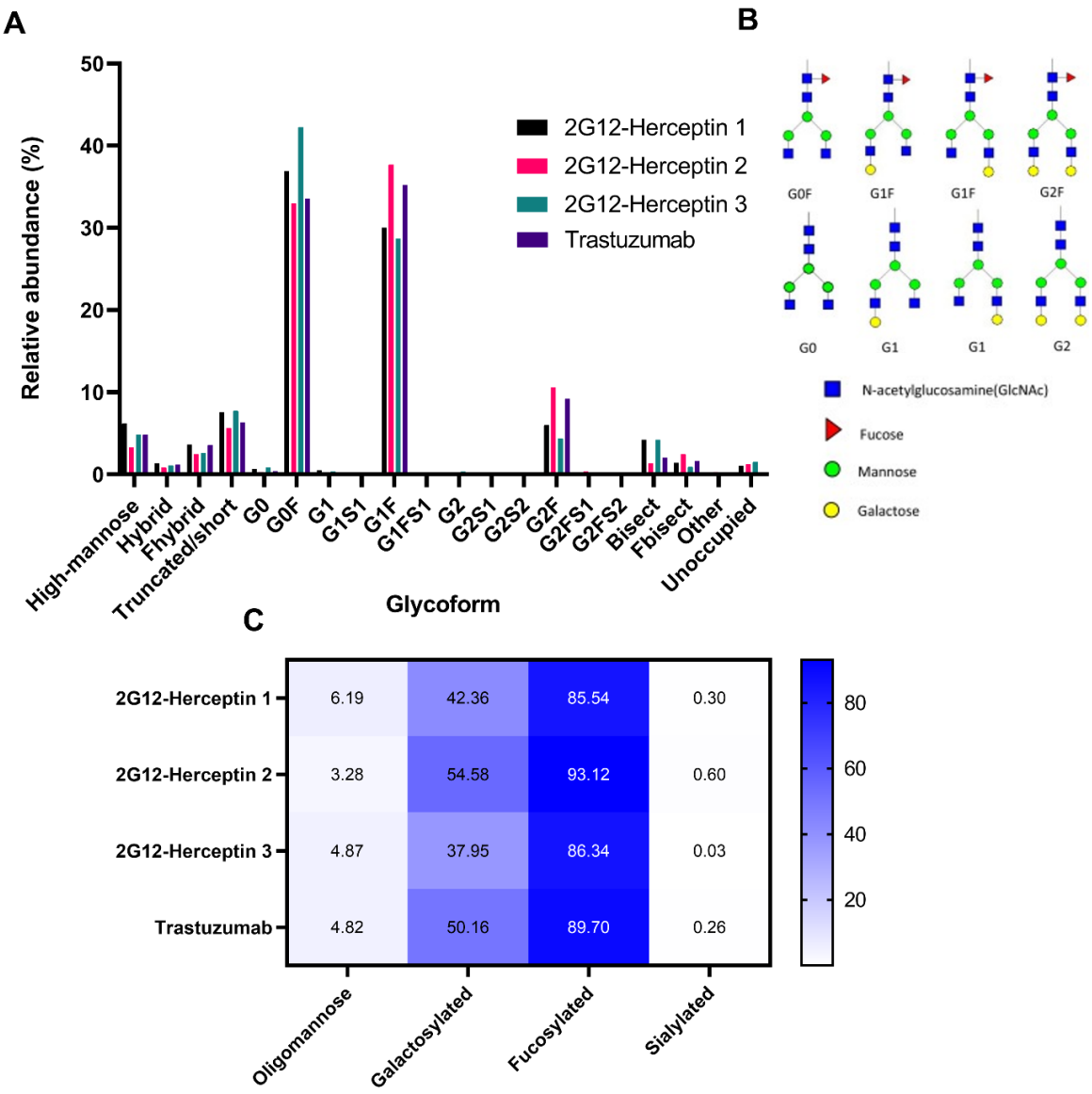

Figure 4.13: Analysis of Fc glycosylation of 2G12-Hn constructs. (A) Categorisation of the relative abundance of glycoforms detected by LC-MS. (B) Schematic of glycan nomenclature. (C) Table of the relative abundance of high-mannose-type, galactosylated, fucosylated, and sialylated glycans for each construct.

4.2.10 Surface plasmon resonance of multivalent constructs

It was suggested in **Chapter 4.2.4** that 2G12-Hn 1 had impaired binding capabilities to HER2 at lower antibody concentrations. To determine the HER2 ligand binding capabilities of the new 2G12-Hn constructs SPR was utilised. His-tagged HER2 was captured on a CM5 sensor chip immobilised with anti-His antibody to 1000 RU. The captured HER2 was exposed to 5-fold dilutions of Herceptin, In-house Trast, 2G12-Hn 1, 2G12-Hn 2, and 2G12-Hn 3.

Sensorgrams of HER2 binding were fitted to the 1:1 binding model using the Biacore Bioevalutation software and plotted in GraphPad prism 9 (**Figure 4.14**). Analysis of the sensorgrams revealed that the 1:1 binding model provided an appropriate fit for the construct binding. The dip in the middle of the sensorgrams shows a bulk shift, which is suggestive of slight differences in analyte running buffer and sample buffer. Indeed, fresh sample buffer was made for samples which was prepared separately to the stock running buffer.

All constructs reached saturation at 100 nM (**Figure 4.14**). Sensorgrams for Herceptin and In-house Trast were similar suggesting similar binding affinities and kinetics. Both constructs reached saturation at all concentrations tested, suggesting high binding affinity. As before, 2G12-Hn 1 only reached saturation at the highest three concentrations, suggesting a lower HER2 affinity at lower concentrations. 2G12-Hn 2 and 2G12-Hn 3 reached saturation at all concentrations, apart from the lowest concentration.

Analysis of the association, dissociation, and equilibrium constants are shown in **Table 4.2**. As before, Herceptin had the highest K_a, followed by In-house Trast, 2G12-Hn 3, 2G12-Hn 2, and 2G12-Hn 1, respectively (**Table 4.2**). This is reflected in the sensorgrams, where the 2G12-Hn 1 binding curve is less exponential (**Figure 4.14**). The calculated K_d values show that 2G12-Hn 2 had the highest K_d so it dissociated the fastest (**Table 4.2**). However, when looking at the sensorgrams, none of the constructs dissociated once bound (**Figure 4.14**). Herceptin had the lowest KD value overall, followed by In-house Trast, 2G12-Hn 3, 2G12-Hn 1, and 2G12-Hn 2, respectively (**Table 4.2**).

The Rmax at 100 nM of Herceptin and In-house Trast were both similar at approximately 60 RU (**Figure 4.14**). This Rmax was similar to 2G12-Hn 1 (**Figure 4.14**), which was ~3-fold lower than what was observed previously (**Figure 4.6**). Of interest, the Rmax of 2G12-Hn 2 and 2G12-Hn 3 at 100 nM reached approximately 70 RU. The density of HER2 on the chip was constant between experiments, and the construct concentration was proportional. Therefore, a greater Rmax could suggest a greater binding affinity of 2G12-Hn 2 and 2G12-Hn 3 at 100 nM.

Overall, 2G12-Hn 2 and 2G12-Hn 3 had similar patterns of binding to each other, and a higher Rmax and faster association rate than 2G12-Hn 1 (**Figure 4.14**; **Table 4.2**). This suggests that these constructs bind the HER2 ligand more effectively than 2G12-Hn 1.

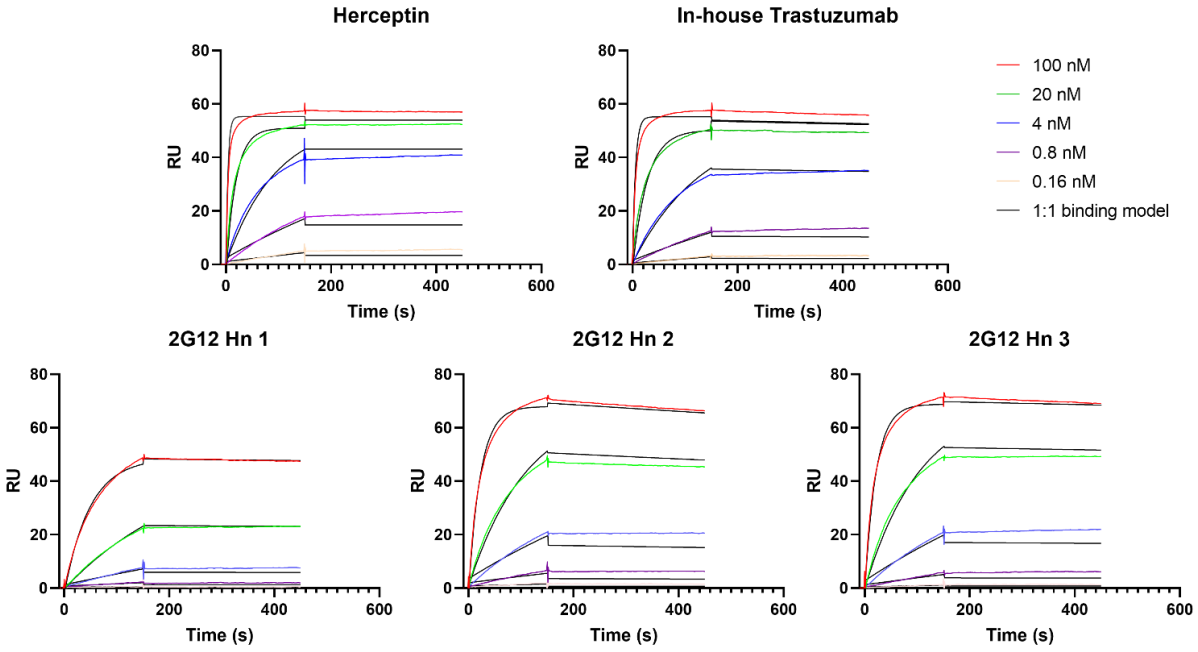

Figure 4.14: SPR analysis of 2G12-Hn constructs binding to HER2 ligand. Avidity to HER2 was assessed by SPR. Antibodies were diluted 5-fold to the concentrations indicated in the legend and analysed with the Biacore™ T-100. The dissociation model was fitted at 150-300 seconds in GraphPad.

Table 4.2: SPR binding kinetics data for 2G12-Hn constructs against HER2 ligand.

Construct	k_a (1/Ms)	k_d (1/s)	KD (M)
Herceptin	4.69E+06	1.10E-06	4.13E-13
In-house Trastuzumab	1.82E+06	8.43E-05	4.64E-11
2G12-Hn 1	2.07E+05	4.23E-05	2.04E-10
2G12-Hn 2	4.42E+05	1.84E-04	4.15E-10
2G12-Hn 3	4.69E+05	6.13E-05	1.31E-10

4.2.11 Cell surface binding of multivalent constructs

We next wanted to determine the cell surface binding efficacy of the new multivalent constructs. $HER2^+$-high (SKBR3), $HER2^+$-low (MCF7), and TNBC (MDA-MB-231) cells were employed in this assay. Cells were opsonised with 1 µg/mL primary antibodies and detected with a PE-conjugated anti-Fc secondary antibody by flow cytometry.

Figure 4.15 represents cell surface antibody binding of Rituximab, 2G12, In-house Trast, Herceptin, and 2G12-Hn 1, 2G12-Hn 2, and 2G12-Hn 3. The gating strategy for live and single cells was the same as previously shown in **Figure 4.7A**.

Figure 4.15A shows construct binding to SKBR3 cells. As before, Rituximab and 2G12 showed similar and low levels of avidity. In-house Trast and Herceptin showed high and comparable avidity. 2G12-Hn 1 still retained difficulty in binding the $HER2^+$-high SKBR3 cells. Interestingly, 2G12-Hn 2 bound SKBR3 cells as strongly as In-house Trast or Herceptin. 2G12-Hn 3 had impaired cell binding relative to 2G12-Hn 2, despite possessing similar structural domains, whereas increased binding capability relative to 2G12-Hn 1.

Similar binding patterns were observed for the other two cell lines (**Figure 4.15B-C**). Rituximab, 2G12, and 2G12-Hn 1 showed similar and low levels of cell surface binding. However, In-house Trast, Herceptin, and 2G12-Hn 2 all possessed high and comparable avidity. 2G12-Hn 3 bound MCF7 and MDA-MB-231 cells marginally stronger than 2G12-Hn 1, however MFI levels were 2-fold less than 2G12-Hn 2. Of note, since the HER2 expression levels of MCF7 were so low, observed antibody cell binding levels were almost identical between MCF7 and MDA-MB-231.

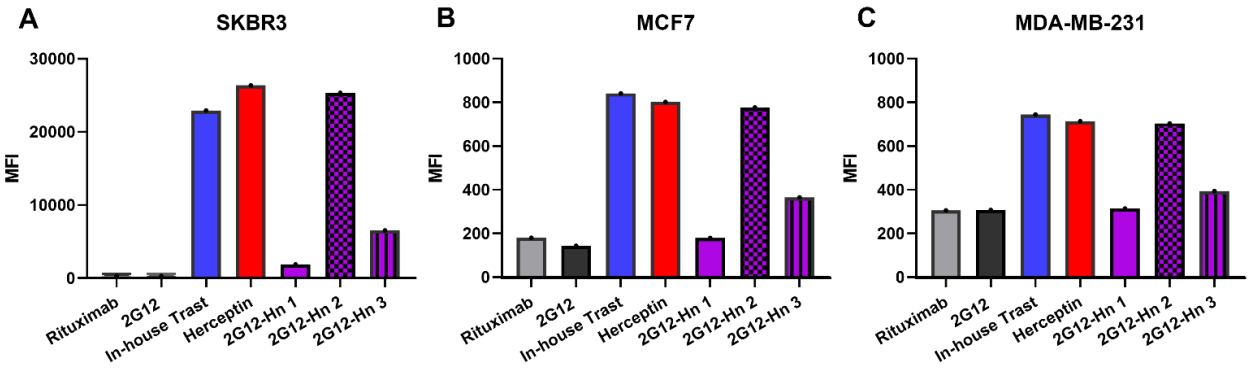

Figure 4.15: Antibody binding to human BC cell lines. Cells were opsonised with 1 µg/mL antibody for 30 minutes on ice. PE-labelled anti-Fc secondary antibodies were used to detect primary antibodies. (A) shows antibody binding levels to SKBR3 cells (B) shows antibody binding levels to MCF7 cells. (C) shows antibody binding levels to MDA-MB-231 cells. 10,000 events were recorded in the PE channel using the BD FACSCanto II. Analysis was performed using FlowJo software where the geometric mean of the area under the curve for each sample was calculated.

2G12-Hn 2 appears to have comparable HER2-binding capabilities to In-house Trast and Herceptin. We next wanted to determine the mannose-binding capabilities. **Figure 4.16** represents cell surface antibody binding of Rituximab, 2G12, In-house Trast, Herceptin, and 2G12-Hn 1, 2G12-Hn 2, and 2G12-Hn 3 to Kif-treated cells. As before, the gating strategy for live and single cells was the same as previously shown in **Figure 4.7A**.

Figure 4.16A shows construct binding to Kif-treated SKBR3 (SKBR3.Kif) cells. As before, Rituximab showed low binding, whereas In-house Trast and Herceptin maintained high and comparable binding. The MFI of 2G12, 2G12-Hn 1, and 2G12-Hn 3 were increased in SKBR3.Kif (**Figure 4.16A**) relative to SKBR3 cells (**Figure 4.15A**). Despite this increased binding, MFI values were lower for most 2G12 constructs, compared to In-house Trast or Herceptin (**Figure 4.16A**). However, increased binding to SKBR3.Kif relative to SKBR3 was observed for 2G12-Hn 2, and this MFI was greater than In-house Trast or Herceptin (**Figure 4.16A**)

The increased binding to Kif-treated cells observed for 2G12 constructs was more prominent in MCF7 (MCF7.Kif) and MDA-MB-231 (MDA-MB-231.Kif) (**Figure 4.16B-C**). The MFI values for 2G12, 2G12-Hn 2, 2G12-Hn 3, 2G12-Hn 1 were 20-fold, 2-fold, 5-fold, and 40-fold higher, respectively, in

MCF7.Kif, relative to MCF7 (**Figure 4.16B**; **Figure 4.15B**). Binding to MCF7.Kif for all 2G12-based constructs was greater than In-house Trast or Herceptin. Kif-treatment did not impede MCF7 cell binding of Rituximab, In-house Trast and Herceptin.

A similar, but more pronounced trend was observed for MDA-MB-231.Kif cells. The MFI values for 2G12, 2G12-Hn 2, 2G12-Hn 3, 2G12-Hn 1 were 30-fold, 3-fold, 10-fold, and 50-fold higher, respectively, in MDA-MB-231.Kif cells, relative to MDA-MB-231 cells (**Figure 4.16A**; **Figure 4.15C**). Binding of all 2G12-based constructs to MDA-MB-231.Kif cells was greater than In-house Trast or Herceptin. Kif-treatment did not impede MDA-MB-231 cell binding of Rituximab, In-house Trast and Herceptin, and their observed MFI values for MCF7.Kif and MDA-MB-231.Kif cells were similar.

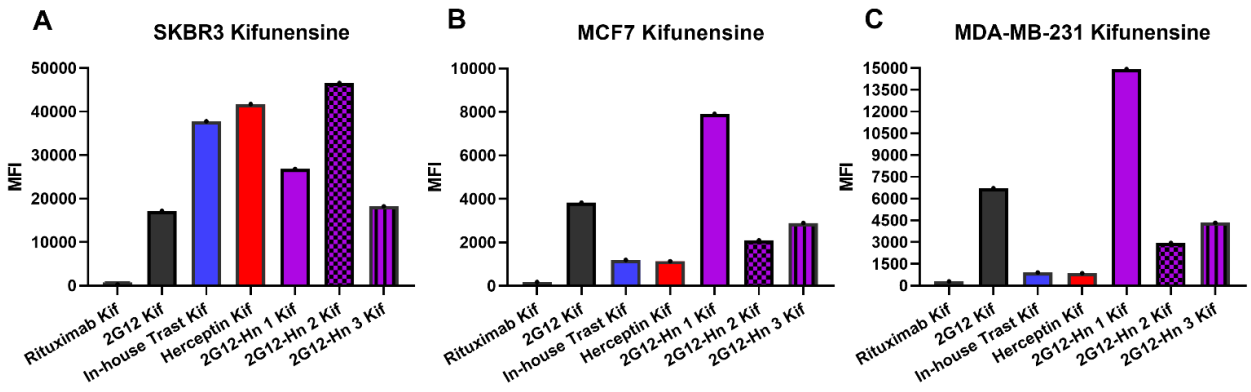

Figure 4.16: Antibody binding to Kifunensine treated human BC cell lines. Cells were cultured with 10 µM Kifunensine for 48 hours. Cells were opsonised with 1 µg/mL antibody for 30 minutes on ice. PE-labelled anti-Fc secondary antibodies were used to detect primary antibodies. (A) shows antibody binding levels to SKBR3 cells (B) shows antibody binding levels to MCF7 cells. (C) shows antibody binding levels to MDA-MB-231 cells. 10,000 events were recorded in the PE channel using the BD FACSCanto II. Analysis was performed using FlowJo software where the geometric mean of the area under the curve for each sample was calculated.

To further characterise the binding of constructs to mannose and HER2, antibody binding titration assays were performed. Antibodies were titred against $HER2^{+}$-high (SKBR3) and $HER2^{+}$-low (MCF7) cell lines. Cells were opsonised with 0.01, 0.1, 1, and 10 µg/mL primary antibodies and detected with a PE-conjugated anti-Fc secondary antibody by flow cytometry.

Figure 4.17 shows construct binding across different concentrations to SKBR3 cells. Binding of Rituximab and 2G12 to SKBR3 did not change as antibody concentration was increased (**Figure 4.17A**). As the concentration of 2G12-Hn 1, 2G12-Hn 2, and 2G12-Hn 3 increased, MFI values increased in a linear fashion (**Figure 4.17B**). This was true for In-house Trast until 1 μg/mL, however, at 10 μg/mL the MFI decreased. 2G12-Hn 2 had a similar binding profile to SKBR3 cells as In-house Trast across 0.01, 0.1, and 1 μg/mL. However, at 10 μg/mL 2G12-Hn 2 binding to SKBR3 cells was 4-fold greater than In-house Trast.

A similar profile was observed for SKBR3.Kif (**Figure 4.18**). As before, binding of Rituximab to SKBR3.Kif did not change as antibody concentration was increased (**Figure 4.18A**). 2G12, 2G12-Hn 1, 2G12-Hn 2, and 2G12-Hn 3 binding to SKBR3.Kif titred with antibody concentration. In-house Trast binding capabilities were reduced at the highest concentration of 10 μg/mL. 2G12-Hn 2 had a similar binding profile to SKBR3.Kif cells as In-house Trast across 0.01, 0.1, and 1 μg/mL (**Figure 4.18B**). As before, at 10 μg/mL binding of 2G12-Hn 2 to SKBR3.Kif cells was 2-fold greater than In-house Trast. Interestingly, Kif-treatment of SKBR3 cells appeared to stabilise In-house Trast binding at 10 μg/mL, as this drop off in MFI was less pronounced.

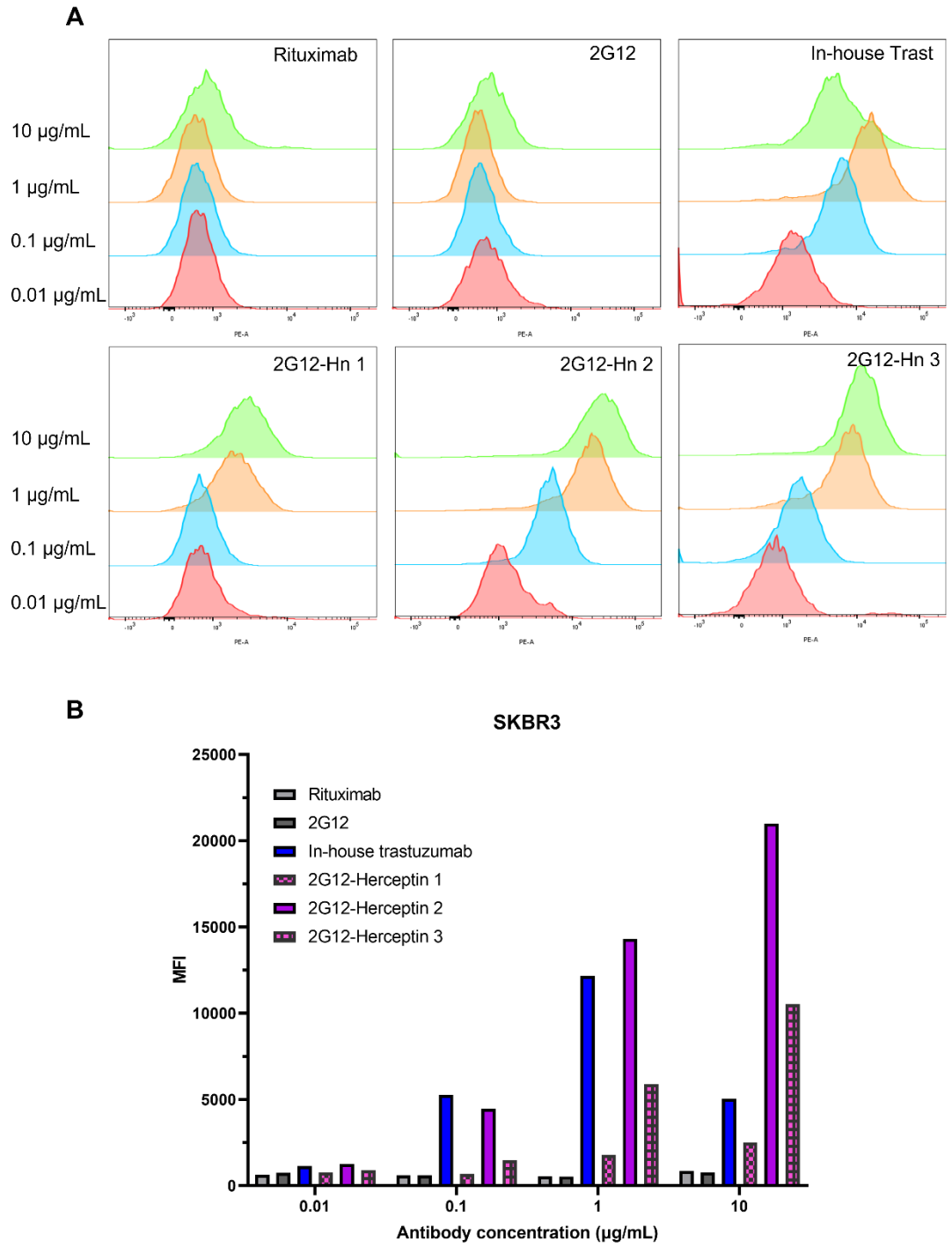

Figure 4.17: Antibody binding titration to SKBR3 cells. Cells were opsonised with antibody constructs for 30 minutes on ice. PE-labelled anti-Fc secondary antibodies were used to detect primary antibodies. (A) Antibody binding histograms of raw flow cytometry data. (B) Antibody binding to SKBR3 cells. 10,000 events were recorded in the PE channel using the BD FACSCanto II. Analysis was performed using FlowJo software where the geometric mean of the area under the curve for each sample was calculated.

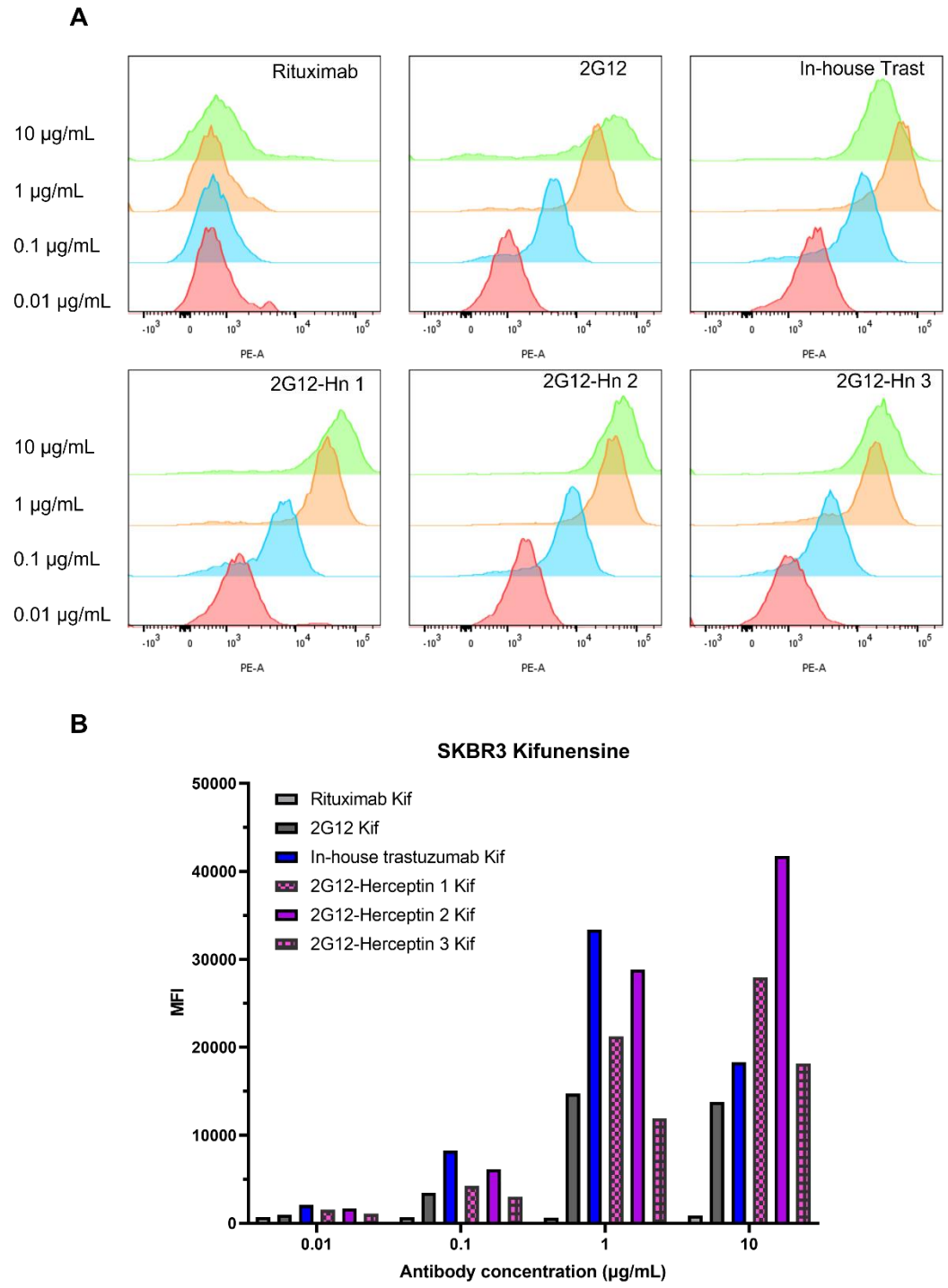

Figure 4.18: Antibody binding titration to Kifunensine treated SKBR3 cells. Cells were cultured with 10 µM Kifunensine for 48 hours. Cells were opsonised with antibody constructs for 30 minutes on ice. PE-labelled anti-Fc secondary antibodies were used to detect primary antibodies. (A) Antibody binding histograms of raw flow cytometry data. (B) Antibody binding to SKBR3.Kif cells. 10,000 events were recorded in the PE channel using the BD FACSCanto II. Analysis was performed using FlowJo software where the geometric mean of the area under the curve for each sample was calculated.

Figure 4.19 shows antibody binding across different concentrations to MCF7 cells. Binding of Rituximab, 2G12, 2G12-Hn 1 and 2G12-Hn 3 to MCF7 cells did not change as antibody concentration was increased (**Figure 4.19A**). A similar binding profile to MCF7 cells was observed between In-house Trast and 2G12-Hn 2 across 0.01, 0.1, and 1 μg/mL (**Figure 4.19B**). As the concentration of In-house Trast and 2G12-Hn 2 increased, MFI values increased until 1 μg/mL, however, at 10 μg/mL the MFI value of both constructs decreased (**Figure 4.19B**). At 10 μg/mL, the MFI of 2G12-Hn 2 and 2G12-Hn 3 was greater than In-house Trast, offering a modest increase in binding and suggesting a more stable interaction at higher concentrations (**Figure 4.19B**).

Binding to MCF7.Kif cells was next assessed (**Figure 4.20**). Binding of Rituximab to MCF7.Kif did not change as antibody concentration was increased (**Figure 4.20A**). 2G12, 2G12-Hn 1, 2G12-Hn 2, and 2G12-Hn 3 binding to MCF7.Kif titred with antibody concentration. In-house Trast binding was reduced at the highest concentration of 10 μg/mL (**Figure 4.20B**). 2G12-Hn 2 had a similar binding profile to MCF7.Kif cells as In-house Trast at 0.01 and 0.1 μg/mL (**Figure 4.20B**). At 10 μg/mL, binding of 2G12-Hn 2 to MCF7.Kif was 4-fold greater than In-house Trast. Similar to SKBR3 (**Figure 4.18**), Kif-treatment of MCF7 cells appeared to stabilise In-house Trast binding at 10 μg/mL, as the drop off in MFI was less pronounced (**Figure 4.20B**). 2G12 and 2G12-Hn 1 were the strongest binders to MCF7.Kif cells at 1 and 10 μg/mL. Indeed, at 10 μg/mL the MFIs of 2G12 and 2G12-Hn 1 were ~6-fold higher than 2G12-Hn 2 (**Figure 4.20B**), further suggesting the position of the HER2 scFv domains on 2G12-Hn 2 may impact mannose targeting.

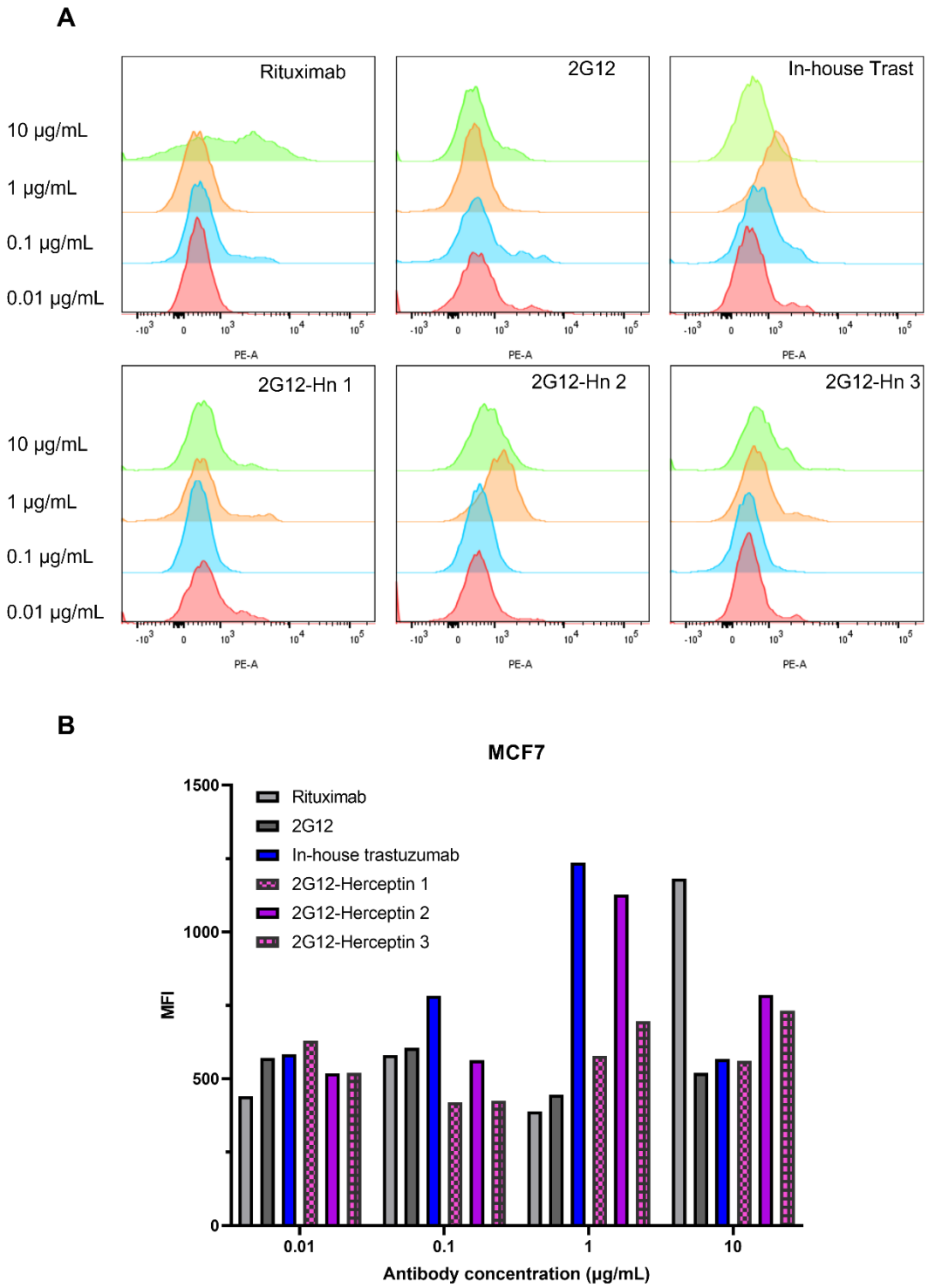

Figure 4.19: Antibody binding titration to MCF7 cells. Cells were opsonised with antibody constructs for 30 minutes on ice. PE-labelled anti-Fc secondary antibodies were used to detect primary antibodies. (A) Antibody binding histograms of raw flow cytometry data. (B) Antibody binding to MCF7 cells. 10,000 events were recorded in the PE channel using the BD FACSCanto II. Analysis was performed using FlowJo software where the geometric mean of the area under the curve for each sample was calculated.

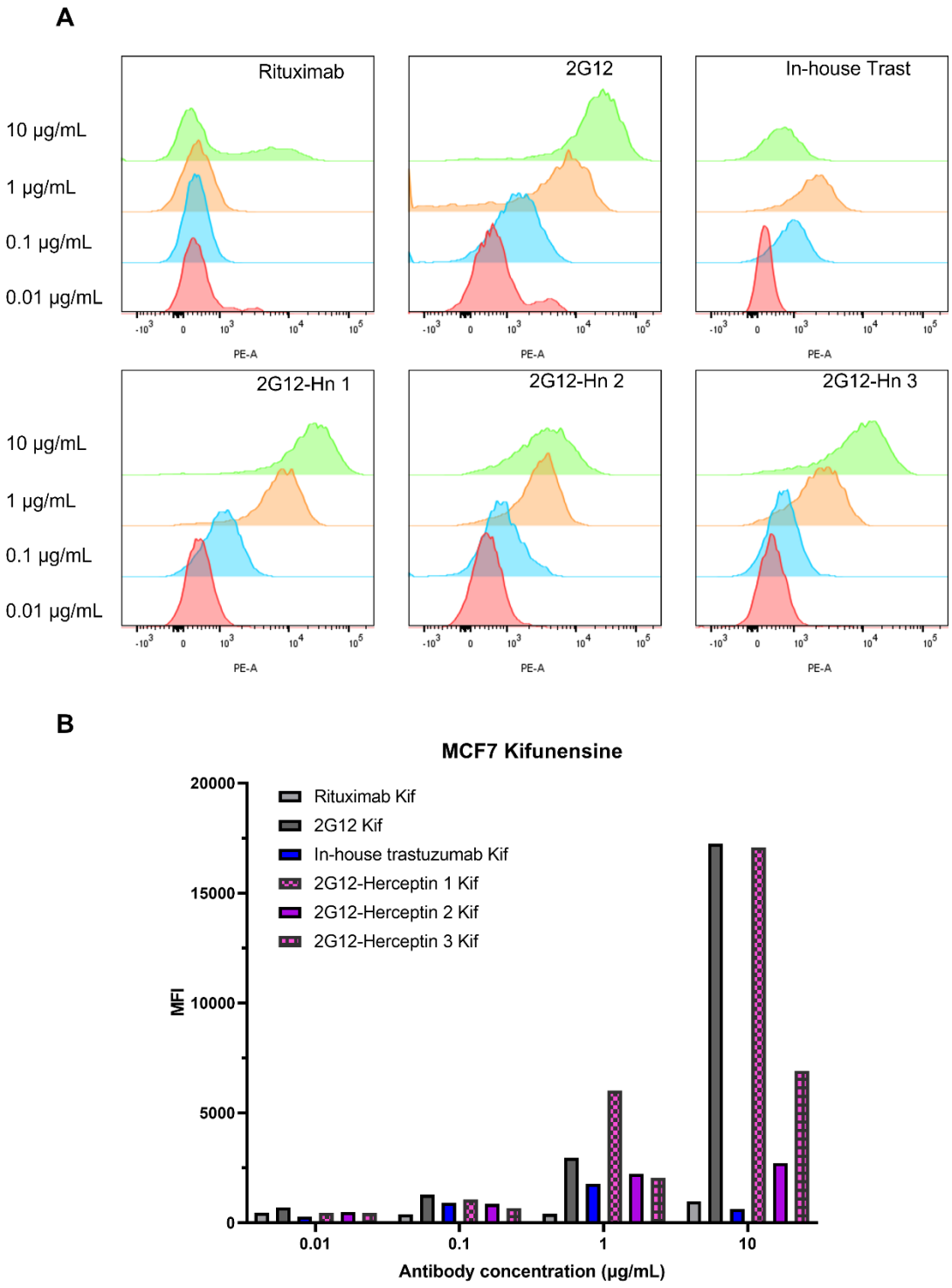

Figure 4.20: Antibody binding titration to Kifunensine treated MCF7 cells. Cells were cultured with 10 µM Kifunensine for 48 hours. Cells were opsonised with antibody constructs for 30 minutes on ice. PE-labelled anti-Fc secondary antibodies were used to detect primary antibodies. (A) Antibody binding histograms of raw flow cytometry dat. (B) Antibody binding to MCF7.Kif cells. 10,000 events were recorded in the PE channel using the BD FACSCanto II. Analysis was performed using FlowJo software where the geometric mean of the area under the curve for each sample was calculated.

4.2.12 Biological function

The biological activity of these constructs was investigated using *in vitro* antibody-dependent cellular phagocytosis (ADCP) assay. For this assay, peripheral blood mononuclear cells (PBMCs) were isolated from the blood of healthy human donors and differentiated into M0 macrophages (MDMs).

A titration was initially performed to determine the most appropriate antibody concentrations for mediating ADCP against the target cells, $HER2^{+}$-high (SKBR3) +/- Kif or $HER2^{+}$-low (MCF7) +/- Kif. Target cells were opsonised with 0.01, 0.1, 1, or 10 µg/mL primary antibody and cocultured with MDMs. ADCP activity was examined by flow cytometry.

We demonstrated in **Chapter 4.2.11** that only 2G12-Hn 2 showed comparable binding to both HER2 and mannose epitopes, as In-house Trast. Therefore, for simplicity, only 2G12-Hn 2 was taken forward for initial ADCP titration analyses, in which In-house Trast and 2G12 were employed as controls.

Figure 4.21A; Figure 4.22A show representative dot-plots of the strategy for live cell gating. Cell trace far red (CTFR) stained MDMs were gated as CFSE negative or CFSE positive, which represents phagocytic MDMs (**Figure 4.21B; Figure 4.22B**). For each antibody concentration, the total area under the curve (AUC) was calculated and plotted (**Figure 4.21C-D; Figure 4.22C-D**).

ADCP levels of SKBR3 cells titred with all constructs (**Figure 4.21C**). Although some variability was observed at each antibody concentration, 2G12-Hn 2 and In-house Trast induced similar levels of ADCP in SKBR3 (**Figure 4.21C**). 2G12-Hn 2 induced more ADCP than In-house Trast at 0.1, 1, and 10 µg/mL. In-house Trast induced more ADCP than 2G12-Hn 2 at 1 µg/mL. Differences were marginal between the antibodies, and overall AUC values were similar. Both In-house Trast and 2G12-Hn 2 induced higher levels of ADCP than 2G12. 2G12 induced less ADCP than the isotype control at concentrations less than 10 µg/mL.

A similar pattern was observed for SKBR3.Kif cells (**Figure 4.21D**). ADCP levels of SKBR3.Kif cells titred with all antibodies. Slight variability in ADCP levels between 2G12-Hn 2 and In-house Trast was observed at each antibody concentration, however, overall AUC levels were similar (**Figure 4.21D**). 2G12 mediated a much higher level of ADCP in Kif-treated SKBR3 cells (**Figure 4.21D**) compared to untreated SKBR3s (**Figure 4.21C**). Despite this, the overall AUC for 2G12 was approximately half that of 2G12-Hn 2 (**Figure 4.21D**). Suggesting that targeting high-mannose epitopes alone is not as effective as dual targeting high-mannose and HER2. Interestingly, ADCP levels did not seem to saturate at 10 µg/mL for 2G12 (**Figure 4.21D**). Indeed, the difference in ADCP levels between 2G12-Hn 2 and 2G12 decreased as concentration increased; 2G12-Hn 2 ADCP levels were 2-fold, 1.6-fold, and 1.26-fold greater than 2G12 at 0.1, 1, and 10 µg/mL, respectively (**Figure 4.21D**).

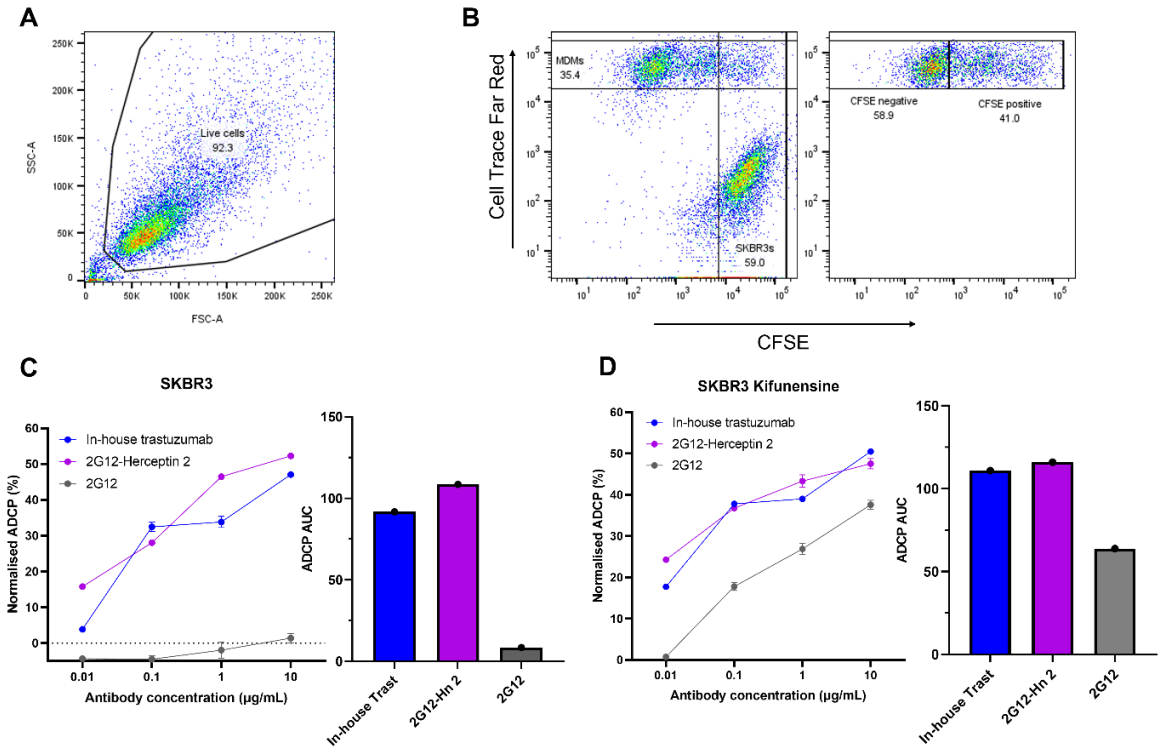

Figure 4.21: ADCP activity of 2G12-Hn 2 in HER2-high SKBR3 +/- Kifunensine. Cells were cultured with 10 µM Kifunensine for 48 hours prior to assay. (A) Representative dot-plot of live cell gating strategy, in which SKBR3 cells are depicted. (B) Representative dot-plots of CellTrace Far Red stained MDMs (y-axis) and CFSE stained SKBR3 cells (x-axis) in the presence of 1 µg/mL In-house Trastuzumab. (C) ADCP activity in SKBR3 cells. (D) ADCP activity in SKBR3.Kif cells. CFSE positive MDMs were plotted against mAb concentration and used to calculate area under the concentration-response curve (AUC). To normalise, the percentage of background CFSE high macrophages (taken from control wells with no mAb treatment) was subtracted from test wells. Bar charts represent summed area under the curve data from all antibody concentrations. Data are from one experiment with mean + SEM from triplicate wells shown. Analysis was performed using FlowJo software. n = 1.

2G12-Hn 2 mediated the highest levels of ADCP activity across all concentrations in MCF7 cells (**Figure 4.22C**). The total AUC value was 1.4-fold greater than In-house Trast and 2.6-fold greater than 2G12. ADCP levels of MCF7 cells titred with all constructs up to 1 µg/mL. At 10 µg/mL 2G12-

Hn 2 and In-house Trast ADCP levels plateaued and dropped, whereas ADCP-induced by 2G12 continued to increase (**Figure 4.22C**). At 0.01, and 0.1 μg/mL ADCP levels of 2G12-Hn 2 and In-house Trast were similar. However, at 1 μg/mL ADCP induced by In-house Trast started to plateau and decrease. At 1 μg/mL ADCP induced by 2G12-Hn 2 was 1.5-fold greater than In-house Trast. At 10 μg/mL ADCP induced by 2G12-Hn 2 was 1.7-fold greater than In-house Trast. 2G12 did not induce ADCP levels greater than the isotype control until 1 μg/mL. At 1 μg/mL 2G12-induced ADCP was 6.7-fold and 4.2-fold lower than 2G12-Hn 2 and In-house Trast, respectively. At 10 μg/mL, 2G12-induced ADCP activity increased by >8-fold, relative to 1 μg/mL (**Figure 4.22C**). Additionally, this activity was 1.5-fold greater than In-house Trast, and modestly lower than 2G12-Hn 2.

2G12-Hn 2 induced the highest levels of ADCP in MCF7.Kif cells (**Figure 4.22D**). AUC values were 1.6-fold greater than In-house Trast, and modestly greater than 2G12. ADCP levels titrated with 2G12-Hn 2 and In-house Trast concentrations across 0.01 and 0.1 μg/mL. At 1 μg/mL ADCP levels dropped and plateaued for both antibodies. Despite this, ADCP values at each concentration were greater for 2G12-Hn 2 than In-house Trast. At 1 μg/mL ADCP values were 1.75-fold greater for 2G12-Hn 2 than In-house Trast. 2G12 titrated linearly across concentrations. Similar to that observed with MCF7 cells, no ADCP was induced by 2G12 below 1 μg/mL (**Figure 4.22C**). However, at 1 μg/mL ADCP levels induced by 2G12 were 1.5-fold and 2.5-fold greater than 2G12-Hn 2 and In-house Trast, respectively. At 10 μg/mL, this rose to 2.4-fold and 6.9-fold greater than 2G12-Hn 2 and In-house Trast, respectively.

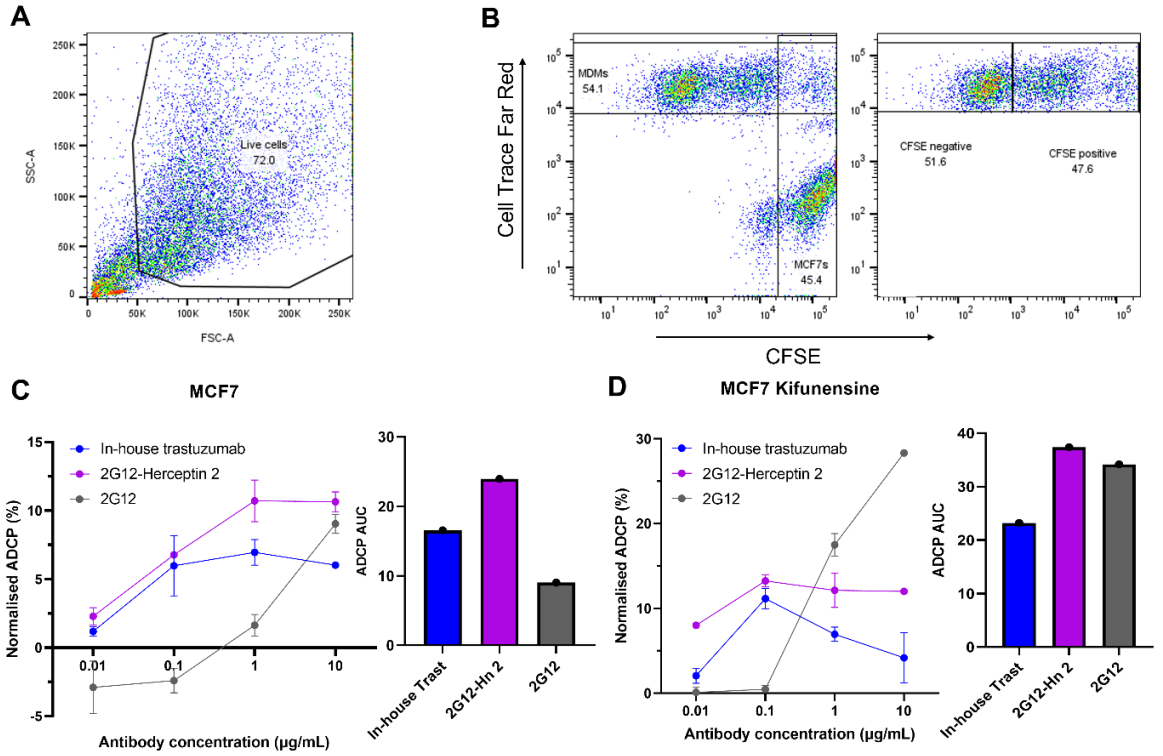

Figure 4.22: ADCP activity of 2G12-Hn 2 in HER2-low MCF7 +/- Kifunensine. Cells were cultured with 10 µM Kifunensine for 48 hours prior to assay. (A) Representative dot-plot of live cell gating strategy, in which MCF7 cells are depicted. (B) Representative dot-plots of CellTrace Far Red stained MDMs (y-axis) and CFSE stained MCF7 cells (x-axis) in the presence of 1 µg/mL In-house Trastuzumab. (C) ADCP activity in MCF7 cells. (D) ADCP activity in MCF7.Kif cells. CFSE positive MDMs were plotted against mAb concentration and used to calculate area under the concentration-response curve (AUC). To normalise, the percentage of background CFSE high macrophages (taken from control wells with no mAb treatment) was subtracted from test wells. Bar charts represent summed area under the curve data from all antibody concentrations. Data are from one experiment with mean + SEM from triplicate wells shown. Analysis was performed using FlowJo software. n = 1.

The titration results confirmed that a concentration of 1 µg/mL was suitable for the next steps. We conducted more ADCP assays at this concentration using multiple donors. Moreover, we explored the mechanism behind ADCP-mediated cell death by examining both phagocytosis and trogocytosis. Our lab has previously demonstrated that MDMs form three distinct populations when cocultured with CFSE labelled, antibody opsonised-BC cells (Smith 2022 *unpublished*). These

are CFSE negative (CFSE-), CFSE low, and CFSE high. CFSE- contain no trace of tumour cell in the MDMs. CFSE low MDMs contain tumour particulate within the cytoplasm, indicative of trogocytosis. CFSE high MDMs contain fully engulfed tumour cells, indicating phagocytosis. Therefore, cell trace far red (CTFR) stained MDMs were gated as CFSE-, CFSE low, or CFSE high (**Figure 4.23B; Figure 4.24B; Figure 4.25B; Figure 4.26B**).

SKBR3 Phagocytosis (CFSE high), trogocytosis (CFSE low), and total ADCP (pooled CFSE high and low) are plotted as a percentage of total macrophages (**Figure 4.23C; Figure 4.24C; Figure 4.25C; Figure 4.26C**). As before, target cells, either $HER2^{+}$-high (SKBR3) +/- Kif or $HER2^{+}$-low (MCF7) +/- Kif, were opsonised with 1 μg/mL primary antibody and cocultured with MDMs. ADCP activity was examined by flow cytometry.

ADCP activity in the HER2-high SKBR3 cells was first investigated (**Figure 4.23**). Representative dot-plots of live cell gating and population gating strategies are shown in **Figure 4.23A** and **Figure 4.23B**, respectively. Overall, all HER2-targeting antibodies induced significantly higher levels of ADCP towards SKBR3 cells than Rituximab, and this was statistically significant (**Figure 4.23C**). 2G12-Hn 2, Herceptin, and In-house Trast induced the highest, and similar levels of phagocytosis and trogocytosis. 2G12 did not induce ADCP activity above that of the isotype control. 2G12-Hn 1 and 2G12-Hn 3 induced similar levels of total ADCP. Both constructs induced less phagocytic activity than 2G12-Hn 2, Herceptin, and In-house Trast. However, 2G12-Hn 1 and 2G12-Hn 3 induced the highest levels of trogocytosis, suggesting an alternative primary mechanism of ADCP-directed cell death compared to Herceptin, In-house Trast and 2G12-Hn 2.

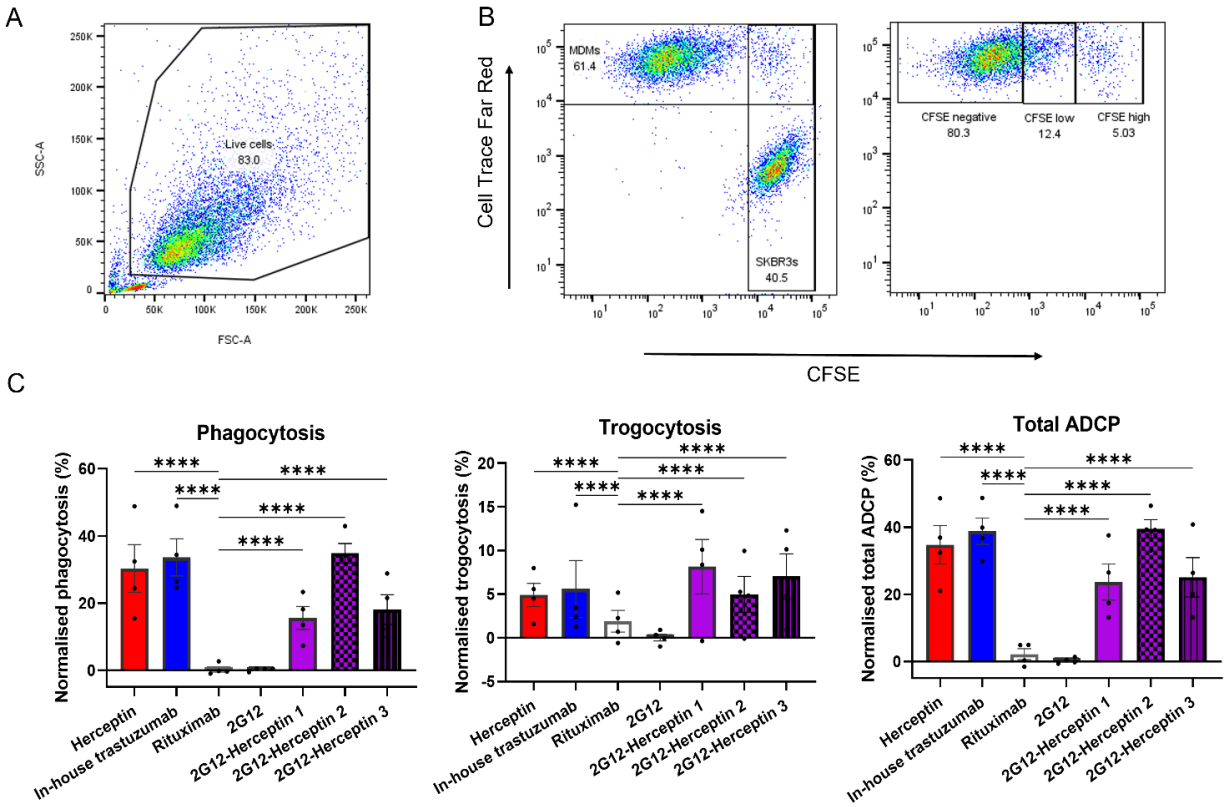

Figure 4.23: ADCP activity of 2G12-Hn constructs against HER2-high SKBR3 tumour cells. (A) Representative dot-plot of live cell gating strategy. (B) Representative dot-plots of CellTrace Far Red stained MDMs (y-axis) and CFSE stained SKBR3 cells (x-axis). MDMs were further gated into CFSE negative MDMs, CFSE low MDMs, and CFSE high MDMs. (C) The normalised percentage of CFSE high (Phagocytosis), CFSE low (Trogocytosis), and pooled CFSE high and low (Total ADCP) MDMs was calculated by subtracting background activity (control wells absent of mAb). Data are from three independent experiments with mean + SEM from triplicate wells shown. Analysis was performed using FlowJo software. Statistical analysis comparing treatment groups was performed using 2-way ANOVA on GraphPad Prism. ****p<0.0001.

ADCP levels in SKBR3.Kif cells were next determined (**Figure 4.24**). Representative dot-plots of live cell gating and population gating strategies are shown in **Figure 4.24A** and **Figure 4.24B**, respectively. Overall, all HER2-targeting constructs induced higher ADCP levels than Rituximab in the HER2-high, SKBR3.Kif cells (**Figure 4.23C**). 2G12-Hn 2, Herceptin, and In-house Trast induced the highest, and similar levels of phagocytosis and trogocytosis. 2G12 did induce higher ADCP activity than the isotype control, but total ADCP activity was less than all other antibodies. 2G12-

Hn 1 and 2G12-Hn 3 induced similar levels of ADCP to each other. Both antibodies induced less phagocytic activity than 2G12-Hn 2, Herceptin, and In-house Trast. However, as before, these antibodies, along with 2G12, induced comparable levels of trogocytosis. Suggesting an alternative primary mechanism of ADCP-directed cell death when targeting mannose glycans.

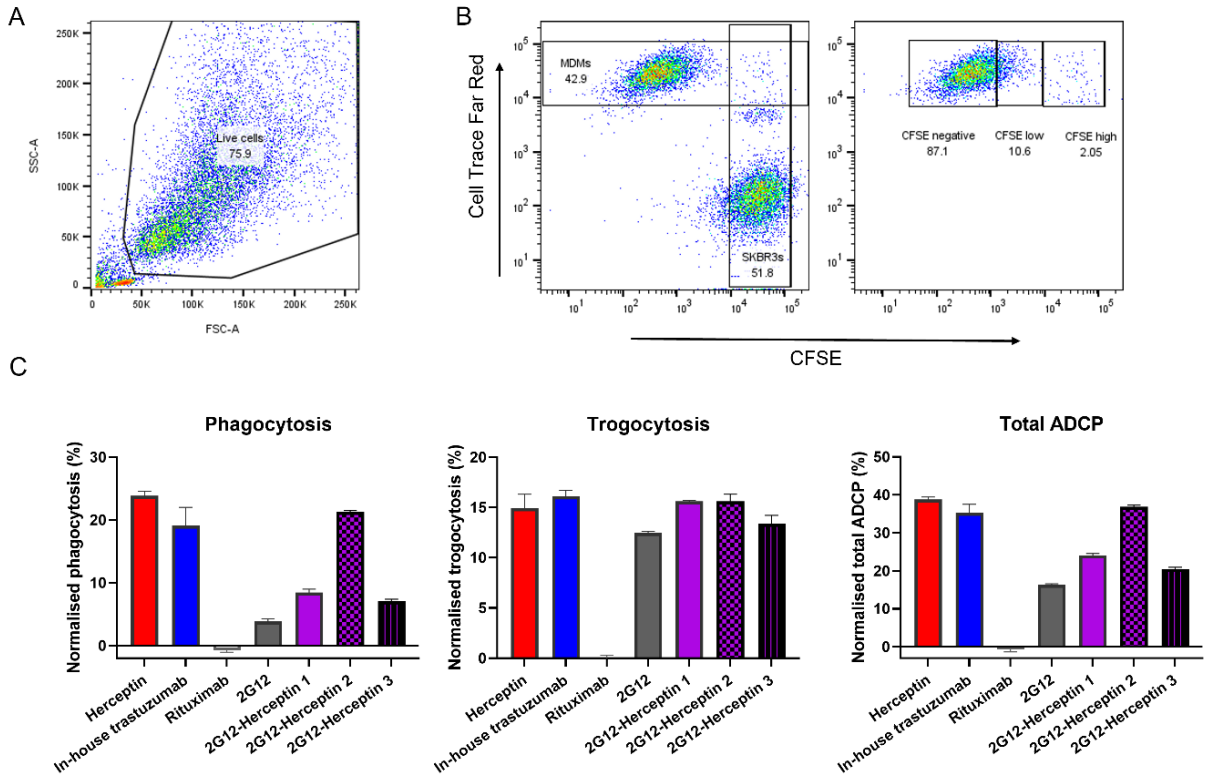

Figure 4.24: ADCP activity of 2G12-Hn constructs against HER2-high mannose-high SKBR3.Kif tumour cells. Cells were cultured with 10 µM Kifunensine for 48 hours prior to assay. (A) Representative dot-plot of live cell gating strategy. (B) Representative dot-plots of CellTrace Far Red stained MDMs (y-axis) and CFSE stained SKBR3.Kif cells (x-axis). MDMs were further gated into CFSE negative MDMs, CFSE low MDMs, and CFSE high MDMs. The normalised percentage of CFSE high (Phagocytosis), CFSE low (Trogocytosis), and pooled CFSE high and low (Total ADCP) MDMs was calculated by subtracting background activity (control wells absent of mAb). Analysis was performed using FlowJo software. Data are from one experiment with mean + SEM from triplicate wells shown.

ADCP activity in HER2-low, MCF7 cells was next investigated (**Figure 4.25**). Representative dot-plots of live cell gating and population gating strategies are shown **Figure 4.25A** and **Figure 4.25B**, respectively. In the low-HER2 expressing MCF7 cells, only 2G12-Hn 2 induced significantly higher

total ADCP levels than Rituximab (**Figure 4.25C**). 2G12-Hn 2, 2G12-Hn 1, 2G12-Hn 3, and In-house Trast induced significantly more phagocytic activity, compared to the isotype control. Within this, 2G12-Hn 2 induced the highest levels of phagocytosis, followed by In-house Trast. Induced phagocytic activity by Herceptin did not reach statistical significance due to donor variability. Only 2G12-Hn 2 induced significantly more trogocytosis, compared to isotype control. 2G12-Hn 1, 2G12-Hn 3, Herceptin, and In-house Trast induced similar levels of trogocytosis and total ADCP to Rituximab. 2G12 did not induce ADCP activity above that of the isotype control. This suggests that 2G12-Hn 2 may offer an advantage over other HER2-targeting constructs by increasing trogocytosis.

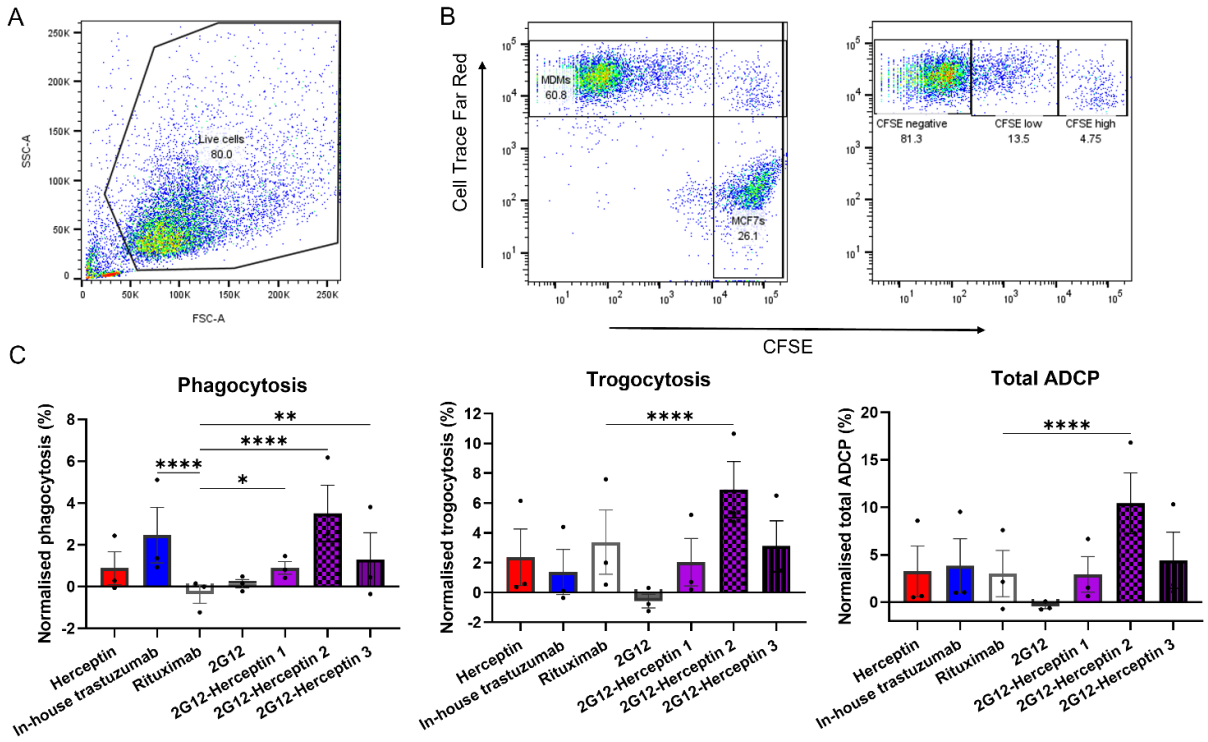

Figure 4.25: ADCP activity of 2G12-Hn constructs against HER2-low MCF7 tumour cells. (A) Representative dot-plot of live cell gating strategy. (B) Representative dot-plots of CellTrace Far Red stained MDMs (y-axis) and CFSE stained MCF7 cells (x-axis). MDMs were further gated into CFSE negative MDMs, CFSE low MDMs, and CFSE high MDMs. The normalised percentage of CFSE high (Phagocytosis), CFSE low (Trogocytosis), and pooled CFSE high and low (Total ADCP) MDMs was calculated by subtracting background activity (control wells absent of mAb). Data are from three independent experiments with mean + SEM from triplicate wells shown. Analysis was performed using FlowJo software. Statistical analysis comparing treatment groups was performed using 2-way ANOVA on GraphPad Prism. *P<0.05, **p<0.01, ****p<0.0001.

ADCP levels in MCF7.Kif cells were next determined (**Figure 4.26**). Representative dot-plots of live cell gating and population gating strategies are shown in **Figure 4.26A** and **Figure 4.26B**, respectively. Overall, all antibodies induced higher levels of total ADCP against MCF7.Kif cells than Rituximab (**Figure 4.26C**). Within this, the mannose-targeting constructs induced the greatest levels of ADCP. 2G12-Hn 1 and 2G12, induced the highest, and similar levels of phagocytosis and trogocytosis; total ADCP was 4-fold greater than Herceptin and In-house Trast (**Figure 4.26C**). Additionally, 2G12-Hn 2 and 2G12-Hn 3 induced similar levels of phagocytosis and trogocytosis; total ADCP was 3-fold greater than Herceptin and In-house Trast (**Figure 4.26C**). Mannose-targeting constructs induced similar levels of phagocytosis, which were 5- to 6-fold greater than Herceptin and In-house Trast. 2G12-Hn 1 and 2G12 induced 2-fold more trogocytosis than all other constructs. This further suggests an alternative primary mechanism of ADCP-directed cell death when targeting mannose glycans.

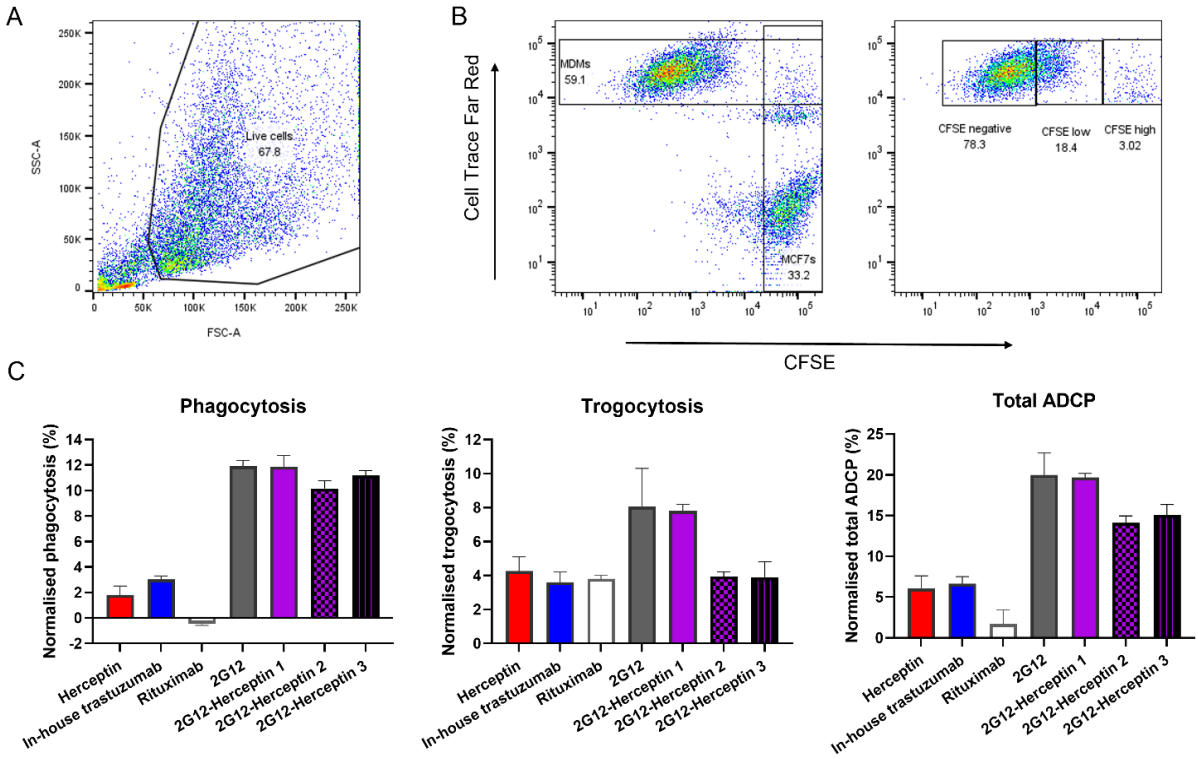

Figure 4.26: ADCP activity of 2G12-Hn constructs against HER2-low mannose-high MCF7.Kif tumour cells. Cells were cultured with 10 µM Kifunensine for 48 hours prior to assay. (A) Representative dot-plot of live cell gating strategy. (B) Representative dot-plots of CellTrace Far Red stained MDMs (y-axis) and CFSE stained MCF7.Kif cells (x-axis). MDMs were further gated into CFSE negative MDMs, CFSE low MDMs, and CFSE high MDMs. The normalised percentage of CFSE high (Phagocytosis), CFSE low (Trogocytosis), and pooled CFSE high and low (Total ADCP) MDMs was calculated by subtracting background activity (control wells absent of mAb). Analysis was performed using FlowJo software. Data are from one experiment with mean + SEM from triplicate wells shown. n = 1.

4.3 Discussion

Growing evidence suggests that high-mannose glycans are prevalent in BC progression (see Chapter 3), making glycan-targeting an attractive therapeutic strategy for BC patients. Indeed, some glycan-targeting antibodies have demonstrated their efficacy and been approved by the FDA for treatment (Spring and Therapeutics, 2015; European Medicines Agency, 2017) while several others are currently in clinical trials (Tarhini *et al.*, 2017; O'Reilly *et al.*, 2018; Smaletz *et al.*, 2021; Chu *et al.*, 2022; Tsimberidou *et al.*, 2023). However, glycans are extremely heterogenous. It is suspected that the relative proportion of high-mannose glycans expressed on the tumour cell is variable throughout different stages of BC oncogenesis, which may impede targeting efficacy. Current therapeutics for $HER2^+$ BC include anti-HER2 targeting mAbs such as Trastuzumab. However, the increased risk of cardiotoxicity (Slamon *et al.*, 2001b; Seidman *et al.*, 2002), small scope of patient suitability, and high occurrence of therapeutic resistance (Valabrega *et al.*, 2005; Gallardo *et al.*, 2012), require the development of novel anti-HER2 antibodies. To address the potential limitations of targeting high-mannose glycans alone and the current challenges faced by Trastuzumab, we created novel antibody constructs which target both high-mannose glycans and HER2, with the aim to enhance anti-HER2 therapy.

HER2 expression across different BC subtypes in clinical samples was first assessed. Gene expression levels of HER2 in the TCGA Breast Cancer cohort were determined using the open-source Xena Browser platform (**Figure 4.1**). This demonstrated that HER2 was expressed within subtypes which are not classed as $HER2^+$, indicating that targeting HER2 may be clinically efficacious across several subtypes, and not purely limited to $HER2^+$ BC. *In vitro*, we determined HER2 was expressed on the cell surface of human $HER2^+$ BC and TNBC cell lines (**Figure 4.2**). In the previous chapter, we demonstrated that high-mannose glycans were present on the cell surface of BC cells (**Figure 3.9**). Additionally, we observed that TNBC cells had more high-mannose glycans than $HER2^+$ BC cells. Collectively, this data built the rationale for investigating dual targeting of HER2 and high-mannose as a therapeutic strategy to increase on target anti-HER2 specificity across several BC subtypes.

The mannose-binding 2G12 Fab cDNA sequence was ligated with human IgG1 Fc and hinge region as the cDNA backbone for these constructs. 2G12 is a broadly neutralising antibody originally isolated from human HIV patients (Kunert, Rüker and Katinger, 1998). 2G12 has been highly studied and its crystal structure has been resolved (Calarese *et al.*, 2003; Stanfield *et al.*, 2015). To bind mannose, 2G12 requires the domain exchange of variable heavy (VH) chains, resulting in a linear IgG molecule with two tethered Fab regions (Calarese *et al.*, 2003). This results in a high-avidity multivalent molecule with four binding sites capable of interacting with large high-mannose glycans ($Man_9GlcNAc_2$) and smaller mannose disaccharides (Calarese *et al.*, 2003; Stanfield *et al.*, 2015). Indeed, due to the close spacing of the Fab domains, 2G12 can bind bivalently with low entropy. The additional interface of the two VH domains provides two additional binding sites, further increasing the valency of this interaction (Calarese *et al.*, 2003). Residues within the domain exchange interface stabilise this interaction, and mutations of these residues result in loss of 2G12 binding (Calarese *et al.*, 2003). Additionally, to allow this domain exchange, initial weakening of VH and VL chains must occur.

In the hope of avoiding interference with this process, 2G12-Hn 1 was designed where Herceptin scFvs were arranged off the constant light (CL) domain (**Figure 4.3**). 2G12-Hn 1 was initially designed and investigated, before further iterations, namely 2G12-Hn 2 and 2G12-Hn 3, were produced. Herceptin scFvs were arranged off the variable light (VL) domain for 2G12-Hn 2, and off both the CL and VL domains for 2G12-Hn 3 (**Figure 4.10**).

It has been previously demonstrated that the type of linker between a multi-domain antibody can interfere with its flexibility, stability, and immunogenicity (Chen, Zaro and Shen, 2013). Flexibility between domains has been demonstrated to be critical for the physical properties and antigen binding of the molecule (DiGiammarino *et al.*, 2011). Within this work, we decided to employ the traditional flexible amino acid linker of three repeating polyglycine and serine $(Glyc_4Ser_1)_3$ units. This linker is comprised of small and polar amino acids and is commonly employed for its flexibility and resistance to proteases (Wen *et al.*, 2013). The use of the linker $(Glyc_4Ser_1)_3$ has been previously

demonstrated to increase ScFv stability and flexibility (Ridgway, Presta and Carter, 1996). Therefore, three repeating units were chosen to achieve appropriate separation between the variable fragments of each Herceptin scFv. The same linker was used to connect each scFv with the constant light domain of 2G12.

Once these constructs were generated, the physiochemical and immunochemical properties were characterised, and biological function was assessed. All constructs expressed and assembled at the expected sizes (**Figure 4.11**). The initial expression of In-house Trast and 2G12-Hn 1 in HEK293F cells produced low yields, therefore further expressions of all constructs were performed in the high-throughput MEXi293E cell line (Durocher, Perret and Kamen, 2002). 2G12-Hn constructs can be expressed within mainstream mammalian cell lines providing logistical advantages over other, high-mannose targeting lectin-based constructs which require plant-viral-based systems for expression (Hamorsky *et al.*, 2019).

Purity was assessed by HPLC after protein A purification. All constructs had some aggregation. In ascending order, aggregation percentages were 3%, 3.3%, 10%, and 11.4%, for 2G12-Hn 3, In-house Trast, 2G12-Hn 2, and 2G12-Hn 1, respectively (**Appendix 8**). Of note, 2G12-Hn 3 had the lowest aggregation as measured by HPLC, however, 2G12-Hn 3 partially precipitated out of solution during purification, resulting in reduced yield (**Appendix 8**). Since larger, multitargeting constructs such as bispecific antibodies are known to experience significantly higher levels of aggregation during the manufacturing process than parental mAbs, resulting in low product yields (Andrade et al., 2019), this was unsurprising. After SEC purification, all antibodies showed one species and 0% aggregation (**Appendix 9**). Glycopeptide analysis by mass spectrometry showed 100% peptide coverage, confirming the quality and deducing the amino acid sequences of antibody samples.

The Fc glycosylation pattern of the antibodies were next characterised. The glycosylation pattern of antibodies affects its stability and function. IgG1 antibodies have a single N-linked glycan at position N297 in each of the heavy chains. Glycan composition has been demonstrated to modulate interactions between the Fc to FcγRs, and in turn, impact their ability to initiate antibody effector

functions. For example, deglycosylation of IgG1 abolishes its capacity to bind FcγRs and consequently results in loss of effector functions (Tao and Morrison, 1989; Krapp *et al.*, 2003). High-mannose glycans increase binding to FcγRIIIA, enhancing ADCC activity but reducing C1q binding (Zhou *et al.*, 2008; Yu *et al.*, 2012). Afucosylated glycoforms have increased binding to FcγRIIIA and enhanced ADCC potency (Royston Jefferis, 2009). Increased Fc sialylation results in decreased FcγRIIIA engagement and decreased ADCC potency (Raju and Lang, 2014). Terminal galactosylation has been demonstrated to enhance C1q binding, ADCC and ADCP *in vitro* (Tsuchiya *et al.*, 1989; Chung *et al.*, 2014; Peschke *et al.*, 2017), and its presence *in vivo* has been suggested to mediate anti-inflammatory activity through FcγRIIB binding (Karsten *et al.*, 2012).

Additionally, the glycoforms can have implications on antibody confirmation, stability, and half-life. For example, deglycosylated antibodies have higher aggregation rates, are less thermally stable, and have increased susceptibility to proteolytic cleavage (Zheng, Bantog and Bayer, 2011). High-mannose glycans have been demonstrated to increase the rate of antibody serum clearance compared to hybrid- or complex-type glycans (Goetze *et al.*, 2011). Increased terminal sialylation improves serum half-life. However, it is suspected that sialylation alters the overall charge of the molecule, impacting cellular antigen binding and increasing susceptibility to proteases (Raju and Lang, 2014).

Initial glycan analysis of 2G12-Hn 1 produced in HEK293F showed it to have slightly elevated high-mannose glycans and decreased fucosylated glycans relative to In-house Trast (**Figure 4.5**). It was initially suspected that increased high-mannose glycans could be due to increased steric hindrance by the positioning of the scFvs obstructing mannosidase enzymes. However, since 2G12-Hn 3 does not have high-mannose glycans elevated at the same proportion this is likely not the case (**Figure 4.13**). 2G12-Hn 1 had less galactosylated glycoforms than In-house Trast, but no difference in terminal sialic acid composition (**Figure 4.5**). This suggests that 2G12-Hn 1 may have decreased potential for effector function activity relative to In-house Trast. To address this, we utilised an ADCP assay as this is a very robust assay, and ADCP is a key mechanism mediating the clinical action

of Trastuzumab. However, in the future, ADCC and CDC should also be investigated. Further, the serum half-life of these constructs and clearance rates *in vivo* should be determined, due to the increased high-mannose glycans.

As the antibody yield with HEK293F cells was low, we transferred the production of all antibodies into the MEXi293E cell line. This gave increased yields allowing us to further investigate the biophysical and biological function of these new antibodies. Many factors can influence the composition and heterogeneity of attached glycans, including host cell line production (Goh and Ng, 2017). Therefore, it was important to determine any potential differences in glycosylation patterns of In-house Trast expressed in HEK293F and MEXi293E cell lines (**Figure 4.12**). This analysis demonstrated a slight increase in high-mannose and a decrease in fucosylated glycans in MEXi293E expressed In-house Trast. No difference was observed for sialylated glycans. The most notable difference was the elevated levels of galactosylated glycoforms in MEXi293E expressed In-house Trast.

Further glycan analysis with MEXi293E-expressed antibodies confirmed that 2G12-Hn 1 had increased high-mannose and decreased galactosylated and fucosylated glycoforms relative to In-house Trast (**Figure 4.13**). While galactosylation is known to be highly variable in therapeutic antibody production and is not associated with any adverse events or safety issues (Shantha Raju and Jordan, 2012), reduced galactosylation may influence biological function *in vitro* or *in vivo*.

2G12-Hn 3 was found to have similar levels of high-mannose glycans and slightly less fucosylated glycoforms, than In-house Trast (**Figure 4.13**). 2G12-Hn 3 had negligeable amounts of sialic acid. As with 2G12-Hn 1, these differences in glycosylation may have the potential to decrease ADCP, ADCC and CDC activity. 2G12-Hn 3 glycans may not influence *in vivo* clearance as with 2G12-Hn 1.

Relative levels of galactosylated glycoforms were most similar between 2G12-Hn 2 and In-house Trast (**Figure 4.13**). 2G12-Hn 2 had decreased levels of high-mannose glycans and increased levels of fucose, relative to In-house Trast. This suggests that 2G12-Hn 2 may have a comparable ability to initiate antibody effector functions. Modestly elevated levels of sialic acid were observed.

Although increased sialic acid has the potential to influence cellular antigen binding, it did not impact binding to SKBR3, MCF7, or MDA-MB-231 cells (**Figure 4.15**). *In vivo* serum clearance rates may be more favourable and should be investigated further.

It is important to note, that generally the differences in glycoforms observed were very modest. Since all antibodies were able to be expressed within the same recombinant expression system, typical Fc glycosylation patterns were maintained. Maintaining typical mammalian-type glycosylation patterns may prove challenging for other high-mannose targeting lectin-based constructs expressed within plant-viral systems, to achieve (Hamorsky *et al.*, 2019). Overall, it is unlikely that large differences in functionality between these constructs could be attributed only to glycosylation patterns.

Immunological properties of the antibodies were next characterised. This included assessing cellular binding assays and determining epitope binding kinetics and affinity.

Binding kinetics to molecular targets is informative of pharmacological activity and essential to investigate for drug development (Copeland, Pompliano and Meek, 2006). Surface plasmon resonance (SRP) can provide quantitative measurements of affinity and reaction kinetics of biomolecular interactions (Fägerstam *et al.*, 1992). Binding kinetics can be indicative of the antibody's mode of action (Teeling *et al.*, 2004; Meyer *et al.*, 2018). Pharmacokinetics can also be extrapolated. For example, a faster on rate can elicit a more efficacious drug, reducing dosing requirements (Copeland, Pompliano and Meek, 2006), and a slower dissociation rate can lead to a longer duration of effect and be indicative of *in vivo* efficacy (Copeland, Pompliano and Meek, 2006). SPR was employed to assess antigen binding to HER2. Initial screening of 2G12-Hn 1 demonstrated it had a smaller K_a revealing it bound at a slower rate than Herceptin and In-house Trast (**Figure 4.6**). In addition, 2G12-Hn 1 showed reduced binding capability at lower concentrations (**Figure 4.6**).

These results were generally corroborated when constructs were re-expressed in MEXi293E cells. However, the RMax of MEXi293E expressed 2G12-Hn 1 was lower than that observed for HEK293F

expressed 2G12-Hn 1, and lower than all other constructs tested (**Figure 4.14**). These results should be validated by repeated experiments, however, Herceptin and In-house Trast presented similar relative binding affinities to each other between the two experiments (**Figure 4.6; Figure 4.14**), suggesting experimental consistency. 2G12-Hn 2 and 2G12-Hn 3 both have slower association rates, than Herceptin and In-house Trast (**Table 4.2**). Calculated affinity constants and observed sensorgrams were similar to each other. Both constructs showed reduced binding capability at lower concentrations (**Figure 4.14**). 2G12-Hn 2 and 2G12-Hn 3 had higher association rates than 2G12-Hn 1. Although calculated affinity constants were similar between 2G12-Hn 1 and 2G12-Hn 2 and 2H12-Hn 3, the observed sensorgrams suggest increased binding of 2G12-Hn 2 and 2G12-Hn 3 to HER2. The observed RMax of 2G12-Hn 2 and 2G12-Hn 3 at 100 nM and 20 nM were similar to Herceptin and In-house Trast.

These data suggest that 2G12-Hn 1 does not bind HER2 as efficiently as Herceptin or In-house Trast. 2G12-Hn 2 and 2G12-Hn 3 can only bind HER2 comparably to Herceptin or In-house Trast at higher concentrations, suggesting they would require higher dosing requirements to be clinically efficacious.

Additionally, none of the antibodies dissociated after binding HER2 in the parameters set in our experiments. It has been proposed that the duration of the receptor-ligand complex, measured by K_d, can indicate drug efficacy *in vivo* (Copeland, Pompliano and Meek, 2006). K_d was demonstrated to correlate with a capacity to induce *in vitro* cellular activity (Berezov *et al.*, 2001). Further, the off rate, along with structural features, can be indicative of an antibody's ability to elicit complement-dependent cytotoxicity (CDC) (Teeling *et al.*, 2004; Meyer *et al.*, 2018). In some instances, the measured dissociative half-life was 300 minutes (Wood *et al.*, 2004). Therefore, experiments with longer off rates should be designed in future to explore this.

While the use of SPR was employed for testing binding kinetics to HER2, investigating binding kinetics to mannose should also be performed. Although SPR is traditionally employed to measure protein-protein biomolecular interactions, it has been previously demonstrated that protein-

nucleic acid interactions can be analysed by immobilising biotinylated oligonucleotides onto a streptavidin-coated sensor chip (Webster *et al.*, 2000). Due to the strong interaction between biotin and streptavidin, this immobilisation is extremely stable and constructs are almost irreversibly bound (Hutsell *et al.*, 2010). Biotinylated N-glycan scaffold mimics are commercially available for purchase. Therefore, biotinylated high-mannose glycans could be immobilised onto a streptavidin-coated sensor chip and exposed to the 2G12-Hn constructs. Future experiments should characterise the binding kinetics and affinity of the multivalent constructs to the mannose epitope.

Cell binding assays were next employed to investigate antigen binding of HER2 and mannose under more physiological conditions. Initial data suggested 2G12-Hn 1 does not bind $HER2^{+}$-high SKBR3 cells as strongly as Herceptin or In-house Trast, where MFI values for 2G12-Hn 1 were 14-fold lower (**Figure 4.7**). When treated with Kif to artificially elevate high-mannose glycans, 2G12-Hn 1 cell binding increased by 14-fold to a level comparable to Herceptin and In-house Trast (**Figure 4.7**). Across all cell lines, Kif-treatment led to increased MFI levels of Herceptin binding HER2 (**Figure 4.8**), which was unsurprising since Kif interferes with ERAD degradation and thus a slight elevation in protein levels is expected (Wang *et al.*, 2011). While important to consider, the elevated binding of 2G12-Hn 1 observed in Kif-treated cells was mainly attributed to increased mannose expression and binding.

The reduced ability of 2G12-Hn 1 to bind HER2 could be due to the placement of scFvs, which may be constrained by proximal distance, or the length of flexible linkers may not be long enough, thus sterically hindering its interaction with HER2. This was investigated through the generation of two further antibody constructs, 2G12-Hn 2 and 2G12-Hn 3. Cell binding assays were repeated with these new antibody formats using $HER2^{+}$-high SKBR3, $HER2^{+}$-low MCF7, and TNBC MDA-MB-231 cell lines +/- Kif (**Figure 4.15**). At 1 µg/mL, 2G12-Hn 2 showed similar levels of binding to SKBR3, MCF7, and MDA-MB-231 cells, compared to In-house Trast and Herceptin (**Figure 4.15**). This suggests that the new positioning of the anti-HER2 scFv in 2G12-Hn 2 improved HER2 targeting ability over the original 2G12-Hn 1.

Kif-treatment enhanced the binding of 2G12-Hn 2 to all BC subtypes to a greater level than In-house Trast or Herceptin, suggesting that the mannose-binding portion is increasing overall avidity due to its multivalency (**Figure 4.16**). However, binding of 2G12, 2G12-Hn 1 and 2G12-Hn 3 to both MCF7.Kif and MDA-MB-231.Kif cells were considerably higher than 2G12-Hn 2 (**Figure 4.16**). This may suggest a restricted function of the mannose-binding portion of 2G12-Hn 2 relative to the other 2G12 constructs. Potentially the placement of anti-HER2 scFv domains on 2G12-Hn 2 could be obstructing the 2G12 HC domain which facilitates mannose binding.

Antibody titrations revealed that In-house Trast cell binding dropped off at 10 µg/mL across all cell lines and conditions (**Figure 4.17; Figure 4.18; Figure 4.19; Figure 4.20**). It has been described that the proportion of antibody stabilised by bivalency can decrease when free antibody is present in solution (Bondza *et al.*, 2020). As the concentration increases, slower binding caused by a reduced number of free epitopes within the vicinity of occupied epitopes impacts bivalent stabilisation. Within this cell binding assay, multiple wash steps occur after cells are opsonised with the primary antibody and secondary anti-Fc antibody, respectively. Therefore, at 10 µg/mL epitopes are suspected to be saturated by monovalent binding, limiting bivalent stabilisation, and enabling constructs to come off with excessive washes. This drop-off was not observed in the ADCP titration assay to the same extent (**Figure 4.21; Figure 4.22**). This may be explained by the fact that in the ADCP assay, the antibody is always maintained within the system thus allowing it to re-bind the epitope if it does drop off due to increased monovalent binding and reduced bivalent stabilisation. Directly labelling primary antibody constructs and repeating the cell binding assay with limited washes could confirm this theory.

2G12-Hn 2 bound most strongly to $HER2^{+}$-high SKBR3 +/- Kif compared to all 2G12-Hn antibodies (**Figure 4.17; Figure 4.18**). This supports SPR data suggesting 2G12-Hn 2 has an increased ability to bind HER2 compared to 2G12-Hn 1 (**Figure 4.14**). A possible explanation could be due to the differential placement of anti-HER2 scFv arms compared to 2G12-Hn 1. Interestingly, despite having similar binding kinetics profiles (**Figure 4.14**), and the same scFv placement, 2G12-Hn 3 did not bind

SKBR3 cells as well as 2G12-Hn 2 (**Figure 4.17; Figure 4.18**). 2G12-Hn 3 binding to untreated SKBR3 cells was greater than 2G12-Hn 1 (**Figure 4.17**), however was less strong when cells were treated with Kif (**Figure 4.18**).

Generally, 2G12-Hn construct interactions were more stable at higher concentrations (**Figure 4.17; Figure 4.18; Figure 4.20**). This could be due to a predominantly bivalent binding characteristic. The initial monovalent binding to HER2 of these constructs allows time for these interactions to be stabilised by 2G12 binding. This corroborates data suggesting a slower on rate from SPR (**Figure 4.14**). Untreated MCF7 cells were the only condition where 2G12-Hn 2 binding dropped off at 10 µg/mL, similar to In-house Trast (**Figure 4.19**). However, the magnitude of this was less than In-house Trast, suggesting 2G12-mannose binding helped stabilise this interaction. Kif-treatment stabilised 2G12-Hn 2 binding to MCF7 cells at higher concentrations (**Figure 4.20**), further confirming this hypothesis.

2G12-Hn 1 bound untreated MCF7 cells comparably to the isotype control, with only a modest increase in binding with dosing (**Figure 4.19**). At lower concentrations, 2G12-Hn 3 bound modestly better than 2G12-Hn 1. However, at 10 µg/mL 2G12-Hn 3 binding increased to a similar level as 2G12-Hn 2. This suggests dosing could overcome initial difficulties binding of 2G12-Hn 3 to a $HER2^{+}$-low target, and supports the observations with SPR, where 2G12-Hn 3 performed comparably at higher doses (**Figure 4.14**). Indeed, a slow on rate can be overcome by increasing the dose (Copeland, Pompliano and Meek, 2006).

2G12 and 2G12-Hn 1 bound the strongest to MCF7.Kif, and this binding titrated with concentration (**Figure 4.20**). This binding was greater than 2G12-Hn 2 and 2G12-Hn 3, respectively. This further suggests a restricted function of the mannose-binding portion of 2G12-Hn 2 and 2G12-Hn 3, relative to the other 2G12 constructs.

Interestingly, 2G12 did not bind SKBR3 or MCF7 cells any better than the isotype control (**Figure 4.7**). This is of interest since both cells harbour high-mannose glycans on their cell surface (**Figure 3.9**). Low 2G12 binding was not overcome by increasing concentration. Additionally, MFI levels of

2G12 binding between MCF7 and SKBR3 were of similar values across all concentrations, ranging from 500-700 MFI. This is despite MCF7 harbouring 3-fold less cell surface mannose than SKBR3 (**Figure 3.9**). Indeed, 2G12 binding did not become meaningful until cells were treated with Kif (**Figure 4.7**). This describes a threshold required for 2G12 binding. Since 2G12 is a broadly neutralising antibody initially isolated from HIV patients (Kunert, Rüker and Katinger, 1998), and the HIV viral spike is heavily glycosylated with dense patches of high-mannose glycans (Stanfield *et al.*, 2015), 2G12 may require a high threshold of high-mannose glycans epitopes to initiate binding. Previous findings support this notion, in which the high-mannose binding lectibody, AvFc, required a threshold for binding clusters of high-mannose glycans (Oh *et al.*, 2022). AvFc was demonstrated to bind high-mannose epitopes with similar affinity as 2G12 (Hamorsky *et al.*, 2019). This describes the limitations of targeting high-mannose epitopes alone and supports the notion of dual targeting of HER2 and high-mannose glycans to enhance HER2-targeting therapies.

Overall binding data suggests the positioning of anti-HER2 scFvs accounts for differences in binding dynamics. In decreasing order, antibody affinity for high-mannose was as follows: 2G12-Hn 1 > 2G12-Hn 3 > 2G12-Hn 2. Similarly, in decreasing order, antibody affinity for HER2 was as follows: 2G12-Hn 2 > 2G12-Hn 3 > 2G12-Hn 1. Despite this, 2G12-Hn 2 still retained its ability to bind mannose epitopes to some degree. Binding of 2G12-Hn 2 to $HER2^{+}$-high SKBR3 cells was comparable to Herceptin or In-house Trast. Mannose targeting stabilised binding of 2G12-Hn 2 at higher dosing regardless of HER2 expression status, providing advantages over Herceptin and In-house Trast. Additionally, binding strength increased with increased high-mannose epitopes once a threshold was reached.

Another important factor to consider is how each epitope individually contributes to antibody binding. Within this work, different cell lines harbouring different levels of cell surface HER2 and mannose were employed, and Kif was used to artificially increase cell surface mannose. However, to ascertain the mode of action for the increased stabilisation, future experiments to block each epitope are required. For example, HER2 could be blocked by first opsonising cells with Herceptin

F(ab')2. For the mannose epitope, one option is to treat the cells with Endo H to cleave high-mannose N-glycans from the cell surface. This may not be the best solution, since complete demannosylation is often not possible due to steric constraints, and the proportion of demannosylation by Endo H would be difficult to quantify. Alternatively, introducing free mannose sugars, such as alpha-methylmannoside, into solution could occupy and saturate the mannose-binding site within the 2G12 domain, constraining the mannose-binding of the 2G12-Hn constructs. Additionally, cell surface high-mannose glycans on target cells could be occupied by first blocking with the lectin, NPA before 2G12-Hn antibody binding.

Further, antibodies were titrated based on μg/mL and not molarity. Since 2G12-Hn constructs are larger, fewer molecules are present, and the impact of epitopes becoming saturated by monovalent binding may be less pronounced than with In-house Trast. Titrations based on molarity should therefore be employed to investigate this.

An important mechanism in the therapeutic action of Trastuzumab is through ADCP, thus ADCP assays were utilised to assess the biological function of these antibodies. An antibody titration was first performed to explore the dosing range and activity (**Figure 4.21; Figure 4.22**). Levels of ADCP induced by In-house Trast and 2G12-Hn 2 towards SKBR3 were comparable, regardless of Kif treatment (**Figure 4.21C-D**). This supports SPR and cell binding data that 2G12-Hn 2 can bind HER2 comparably to In-house Trast, and suggests that 2G12-Hn 2 could be as efficacious as an anti-HER2 therapeutic in $HER2^{+}$-high BC. Additionally, this confirms that the marginal differences observed in Fc glycosylation patterns did not impede Fc:FcγR interactions initiating ADCP. 2G12-Hn 2 may induce slightly more ADCP in untreated SKBR3 cells at higher concentrations (**Figure 4.23C**), however further biological repeats should confirm this.

The comparable binding data suggests that in a $HER2^{+}$-high BC setting, the mannose targeting domain of 2G12-Hn 2 may not offer a biological advantage, possibly due to the saturation of cellular epitopes. However, more potent ADCP responses to MCF7 cells were observed with 2G12-Hn 2 compared to In-house Trast (**Figure 4.22C-D**).

ADCP mediated by In-house Trast dropped off with increasing concentration in MCF7 cells (**Figure 4.22C-D**), but not SKBR3 cells (**Figure 4.21C-D**). Since free antibody is maintained within the system in the ADCP assay, it can re-bind if it drops off. Due to reduced HER2 epitopes on MCF7 cells, once In-house Trast has saturated HER2 there is a higher level of free unbound antibody in solution. Unbound In-house Trast may be binding Fc on macrophages, dampening activity at higher antibody concentrations (**Figure 4.22C-D**). Conversely, ADCP potency was maintained by 2G12-Hn 2 across all doses (**Figure 4.22**). The additional mannose targeting by 2G12 appears to stabilise interactions at higher antibody concentrations (**Figure 4.19**). Presumably, this reduces the amount of unbound antibody in solution to block Fc receptors on macrophages, thus preventing a drop off in ADCP activity at higher doses (**Figure 4.22C**). Further, increasing the mannose by Kif-treatment increased 2G12-Hn 2 cell avidity (**Figure 4.20**), thus enabling 2G12-Hn 2 to maintain ADCP activity at higher doses (**Figure 4.22D**). Kif-treatment was previously demonstrated to not affect cell proliferation or viability (**Figure 3.13; Figure 3.16**), suggesting that activity is likely ADCP rather than efferocytosis.

2G12 induced some ADCP activity in untreated MCF7 cells at higher doses (**Figure 4.22C**) despite the lack of activity in SKBR3 cells (**Figure 4.21C**). This is possibly due to the reduced density of cell surface HER2 on MCF7 cells, and therefore increased access to mannose epitopes. Indeed, 2G12 induced some ADCP activity in SKBR3.Kif cells, however, overall levels were less potent than In-house Trast or Herceptin (**Figure 4.21**). Thus, suggesting that therapies targeting high-mannose glycans alone would be efficacious only when a threshold of high-mannose glycans is reached.

Biological function was further investigated with all 2G12-Hn constructs at 1 µg/mL and increased amounts of donors, which is important due to the inherent inter-donor variability (**Figure 4.23; Figure 4.24; Figure 4.25; Figure 4.26**). In addition, the mechanism of ADCP-induced activity was assessed further. Phagocytosis is the primary mechanism of macrophages eliminating tumour cells (Clynes *et al.*, 2000; Gül and Van Egmond, 2015; Vermi *et al.*, 2018). However, trogocytosis has also been demonstrated to be an important mechanism of macrophage-mediated tumour cell death (Velmurugan *et al.*, 2016). It is important to distinguish between mechanisms of action since

trogocytosis can result in antigen depletion and exhaustion of effector pathways (Beum *et al.*, 2011), and thus is not always a desired outcome (Taylor and Lindorfer, 2015).

As seen before, comparable and high levels of ADCP potency towards SKBR3 +/- Kif were observed between 2G12-Hn 2, In-house Trast, and Herceptin (**Figure 4.23C; Figure 4.24C**). All constructs induced similar levels of phagocytosis, trogocytosis, and total ADCP, suggesting 2G12-Hn 2 employs the same mechanism of action.

2G12-Hn 1 and 2G12-Hn 3 were less potent inducers of ADCP activity than 2G12-Hn 2 (**Figure 4.23C; Figure 4.24C; Figure 4.25C**). However, 2G12-Hn 1, 2H12-Hn 3, and 2G12 constructs showed enhanced levels of trogocytosis (**Figure 4.23C**). It has been previously demonstrated that the proximal position of the epitope to the cell membrane can influence the antibody effector function engaged (Cleary *et al.*, 2017). Indeed, 2G12, 2G12-Hn 1 and 2G12-Hn 3 showed an increased ability to bind high-mannose epitopes (**Figure 4.20**). Therefore, trogocytosis may be the prominent mechanism by which the 2G12 mannose-targeting portion induces ADCP. Studying the proximity of bound 2G12-Hn constructs to each other and cell clustering are therefore of interest and should investigated.

Further, 2G12-Hn 1 and 2G12-Hn 3 both harbour less galactosylated glycoforms than In-house Trast or 2G12-Hn 2 (**Figure 4.13**). Terminal galactose has been previously correlated with ADCP activity (Chung *et al.*, 2014). Thus, differences in glycosylation may be influencing Fc:FcγR interactions. However, since the reduced potential to induce ADCP also reflects reduced cell epitope binding seen previously (**Figure 4.17; Figure 4.18**), this reduced ability to bind the HER2 epitope is likely responsible.

BC patients expressing lower levels of HER2 have a reduced response to targeted therapeutics than patients with increased HER2 expression (Vogel *et al.*, 2001). It has been shown that lower antigen expression led to reduced antibody effector function *in vitro* (Tang *et al.*, 2007; Cleary *et al.*, 2017). In the $HER2^{+}$-low MCF7 cells, 2G12-Hn 2 showed an enhanced ability to induce ADCP compared to all other constructs (**Figure 4.25C**). In-house Trast induced modest and comparable phagocytic

activity in MCF7 cells. However, 2G12-Hn 2 was able to also induce high levels of trogocytosis, presumably through the mannose-targeting portion of 2G12. Therefore, the combined targeting of these two epitopes provides an advantage over In-house Trast for eliciting ADCP activity in HER2^{+}-low BC cells.

Future experiments to investigate how these constructs initiate ADCC and CDC activity would be important to assess.

2G12-Hn 2 offers additional advantages over the recently produced high-mannose targeting lectibody, AvFc (Oh *et al.*, 2022). 2G12-Hn 2 can be expressed in mammalian expression systems, producing similar patterns of glycosylation. 2G12-Hn 2 has demonstrated advantages over In-house Trast, whereas AvFc has not shown enhanced functional anti-tumour activity over a current clinically approved therapy. Further, AvFc elicited immune reactions in immunocompetent mice (Hamorsky *et al.*, 2019), presumably due to the lectin-binding domain and non-mammalian Fc glycosylation patterns. Since the 2G12 backbone of 2G12-Hn 2 is a human-derived IgG1 antibody, it should elicit minimal immunogenicity. However, future *in vivo* experiments are required to establish this.

To conclude, these findings provide proof of concept that dual targeting aberrant high-mannose glycans may enhance HER2-targeting therapies for BC. 2G12-Hn 2 was demonstrated to bind HER2^{+}-high, HER2^{+}-low and TNBC cells as well as Herceptin or In-house Trast. The multivalent action of 2G12-Hn 2 further stabilises antibody binding at higher doses. 2G12-Hn 2 binding kinetics to HER2 exhibit similar observed off-rates to Herceptin and In-house Trast, which translates most to clinical efficacy. 2G12-Hn 2 was a potent inducer of ADCP in HER2^{+}-high BC cells and was able to restore ADCP potential in HER2^{+}-low BC cells through what is suspected to be trogocytosis. Future experiments to validate binding kinetics, *in vitro* ADCC and CDC, and interrogate anti-tumour responses and half-life *in vivo* are essential. Ultimately, dual targeting aberrant high-mannose glycans may enhance the efficacy of anti-HER2 therapies by addressing antigen heterogeneity and providing additional stabilisation, thus improving patient outcomes.

Chapter 5 Replicon delivery of Breast Cancer therapeutics

5.1 Introduction

The use of monoclonal antibodies (mAb) in cancer has revolutionised therapeutic treatment options and patient outcomes. However, generating high quantities of clinical-grade mAbs is logistically and economically demanding (Birch and Racher, 2006). Indeed, mAbs are large molecules with a single N-linked glycan at position N297 in each of the heavy chains, and thus have requirements of mammalian glycosylation and folding (see Chapter 1.13). Therefore, chemical synthesis methods or lower organism expression systems are unsuitable, and mammalian expression systems are required. Recombinant protein production in mammalian cell lines is expensive due to slow cell growth and low yields. Additionally, integral glycosylation patterns are affected by the cell line used, nutrient and supplement availability, pH and growth phase (Zhou *et al.*, 2008; Slade *et al.*, 2016; Zhang *et al.*, 2019). Differences in glycosylation can have major implications for antibody function (Roy Jefferis, 2009), immunogenicity (Prabakaran *et al.*, 2012; Zavala-Cerna *et al.*, 2014), and stability (Zheng, Bantog and Bayer, 2011), and therefore factors influencing this need to be carefully monitored. Additionally, purification and rigorous batch testing are laborious, time-consuming and costly (L and K, 2019; Erasmus *et al.*, 2020). The removal of any biological contaminants introduced by manufacturing expression and purification processes can result in protein aggregation and yield loss (Arosio *et al.*, 2011).

This costly process makes mAb therapeutic production complicated, expensive, and often inaccessible to patients accessing public healthcare bodies which cannot afford to provide it. In addition to this, most mAbs are administered intravenously in hospitals and require multiple administrations to maintain efficiency. Although progress has been made for subcutaneous administration (Hegg *et al.*, 2012), not all mAbs can be delivered subcutaneously due to the constructs intrinsic stability and self-association, solubility, viscosity, and aggregation profiles

(Sifniotis *et al.*, 2019). Collectively, all these factors add to the limitations of mAb delivery to patients, and drug accessibility.

mAbs in a clinical setting require high-antigen binding, high stability, and low immunogenicity. Antibody immunogenicity refers to how a host immune system recognises and reacts to therapeutic agents. Therapeutic antibodies can be neutralised by anti-drug antibodies (ADA), impacting their safety and efficacy in a clinical setting (Hansel *et al.*, 2010; Harding *et al.*, 2010). Several factors are known to influence immunogenicity profiles in patients including species origin, structural features such as sequence variation and glycosylation, impurities, aggregation, dosage, and administration route (Kuriakose, Chirmule and Nair, 2016; Waldmann, 2019). For example, despite the same species origin, amino acid sequence, and route of administration, Herceptin was found to elicit differential amounts of ADA in two previous separate clinical trials. ADAs were observed in 0.5% of patients treated with Herceptin with metastatic breast cancer (Cobleigh *et al.*, 1999), while in a more recent clinical trial, ADAs were reported in 7.1% of patients who received Herceptin via the same route (Hegg *et al.*, 2012). Differences in patient genetic background and race can contribute to this (Hegg *et al.*, 2012; Vaisman-Mentesh *et al.*, 2020), however, other explanations involving drug manufacture and administration may also be of importance. As an example, protein aggregation can reduce mAb efficacy and increase immunogenicity (Biro and García, 1965; Filipe *et al.*, 2012). Protein aggregation can occur at many stages from drug manufacture, storage, shipping, and drug infusion (Wang, 2000; Chi *et al.*, 2003; Demeule *et al.*, 2009), to differences in administration by healthcare professionals, such as excessive shaking (Carpenter *et al.*, 1999; Filipe *et al.*, 2012). Other factors involved in mAb administration can also influence immunogenicity. For example, increased dose and increased frequency of dosing have been documented to decrease immunogenicity, by mechanisms of immune tolerance (Rutgeerts *et al.*, 2004; Cheifetz and Mayer, 2005; Van Schouwenburg, Rispens and Wolbink, 2013). Therefore, the delivery of mAbs can play a huge role in the efficacy and safety of treatment, even with the same drug. These factors place a further burden on the healthcare system to increase drug efficacy and reduce adverse events.

Another limitation of mAb therapy is the emergence of therapeutic resistance (Gallardo et al., 2012; Schick, Ritchie and Restini, 2021), thus innovative approaches utilising ever more complex antibody formats are being employed to overcome this. One such format is that of multitargeting constructs, such as bispecific antibodies (Staerz, Kanagawa and Bevan, 1985; Kufer, Lutterbüse and Baeuerle, 2004). These constructs have the advantage of targeting multiple epitopes due to the dual binding affinities while retaining the efficacy of parental mAbs (Baeuerle and Reinhardt, 2009; Correia et al., 2013; Labrijn et al., 2019). However, these constructs experience significantly higher levels of aggregation during the manufacturing process than parental mAbs, resulting in low product yields (Andrade et al., 2019). Additionally, since aggregates have similar biochemical properties to monomers, typical aggregate removal steps are inadequate for aggregate clearance. Thus more robust purification steps are required but these generally result in even lower yields (Andrade et al., 2019; Sifniotis et al., 2019). While efforts to reduce aggregation during the manufacturing process are underway (Ho et al., 2012; Andrade et al., 2019), more solutions are required to combat this.

Self-replicating RNA (Replicon) delivery has the potential to be an eloquent solution to this problem. Replicons deliver self-amplifying recombinant RNA molecules encoding proteins of interest directly into the cytosol of cells for protein expression (Strauss and Strauss, 1994; Erasmus *et al.*, 2020). Replicons are being considered for ease of production, cost and protein stability (Ljungberg and Liljeström, 2015). Indeed, the use of Replicons for the delivery of vaccine antigens and therapeutic proteins has recently gained traction (L and K, 2019; T *et al.*, 2019; Komdeur *et al.*, 2021; Lundstrom, 2021; Comes, Pijlman and Hick, 2023). Nucleic acid delivery to host cells enables the production of therapeutic proteins that retain their native conformations and post-translational modifications, such as glycosylation, which can be challenging to achieve with recombinant proteins. Importantly, Replicons have several advantages over DNA-based therapies such as they don't require delivery by retroviruses, there is no requirement for nuclear delivery, and there is no risk of chromosome integration.

Replicon delivery systems are typically based on positive-strand RNA viruses, such as alphaviruses. Within this, the Venezuelan encephalitis virus (VEEV) genomic backbone has been most widely studied (Hikke and Pijlman, 2017; Lundstrom, 2020; Comes, Pijlman and Hick, 2023). The VEEV genome encodes non-structural proteins (replicase) and structural proteins (replaced by genes of interest (GOI)) (**Figure 5.1**A). There are four non-structural proteins (nsPs1-4) which are responsible for genome replication, and transcription of the structural proteins (GOI) under the subgenomic promoter. Additionally, non-structural proteins can be mutated to mediate Replicon RNA persistence and subgenomic gene expression strength within the cells (Li *et al.*, 2019).

Once delivered to the target cell, Replicon mRNA is translated to produce the replicase complex (comprised of nsPs1-4) (**Figure 5.3**). The replicase can efficiently self-amplify the original RNA (AB *et al.*, 2018) at an expression level of more than 10^5 copies of subgenomic RNA in the cytosol of each target cell (Frolov *et al.*, 1996), and produce 15-20% of the total cell protein (Pushko *et al.*, 1997; Comes, Pijlman and Hick, 2023). The clear advantage is that Replicons can be administered at lower doses than conventional nucleic acid delivery methods (mRNA and DNA plasmids) (AB *et al.*, 2018). In addition, Replicon expression has been reported to last ~5-10 days compared to standard mRNA expression lasting ~3 days (AB *et al.*, 2018).

To date, most Replicon research has focused on therapeutic vaccines delivering monocistronic antigens. Replicon delivery could also be applied to mAbs, however, mAbs are more complex due to the need for proper HC and LC assembly. Thus, research into Replicon mAb production is currently limited. One of the only published examples demonstrated successful Replicon delivery of anti-Zika virus antibodies by expressing both HC and LC within the same RNA Replicon plasmid, separated by an internal ribosomal entry site (IRES) (Erasmus *et al.*, 2020). This success suggests the potential for Replicons for delivering anti-cancer mAbs. Compared to traditional mAb production, Replicon-based delivery offers ease of manufacturing, reduced dosing, fewer clinic visits, and an improved patient experience. Additionally, Replicons may address increased

production challenges faced by more complex mAb formats, such as reduced yield and increased aggregation.

Thus, we aimed to investigate the use of Replicon systems for generating and delivering anti-cancer mAbs. In the previous chapter, we generated an anti-HER2 bispecific antibody that co-targets mannose on BC cells. However, as this is a proof of concept, we initially wanted to deliver an established and well-characterised mAb, anti-HER2 Trastuzumab. Therefore, our objectives were to assess whether the Replicon system could express Trastuzumab with retained function compared to conventional recombinant expression. To do this Replicon Trastuzumab was synthesised *in vitro* and HEK293F cells were transfected by lipofectamine. Antibodies were purified by affinity and size exclusion chromatography. Antibody expression and assembly were assessed, and glycopeptide analysis was performed. Binding kinetics for HER2 was analysed by surface plasmon resonance, and biological activity was explored by antibody-dependent cellular phagocytosis assays.

5.2 Results

5.2.1 Construct design and production of Replicon Trastuzumab

The construct for Replicon delivery of Trastuzumab (Replicon Trast) was first designed. The alphavirus genome-based, Venezuelan encephalitis virus (VEEV) viral vector was employed encoding Trastuzumab heavy chain (HC) and light chain (LC) genes separated by an internal ribosomal entry site (IRES) sequence, and non-structural proteins (nsPs1-4) which form mature replication complexes (**Figure 5.1**A).

To produce the Replicon Trast construct, gene synthesis and molecular cloning into the VEEV vector was performed by NBS Biologicals. Once we received this construct, we validated it by sequencing. Once validated with the correct sequence, competent *E. coli* were transformed with Replicon Trast DNA, and bacterial cultures were grown at 37˚C overnight, with shaking. At this point, glycerol stocks were made for long-term storage, and plasmid DNA was purified.

DNA was checked for the correct size using restriction enzymes. DNA was digested with Mlu1 to linearise it for downstream RNA production and digested with Kpn1 as a quality control step to ensure the correct product was synthesised (**Figure 5.1**). Predicted molecular weights of 6084bp, 4787bp, and 1404bp should be produced after Kpn1 digest. Three fragments at the correct predicted molecular weights were produced (**Figure 5.1**B).

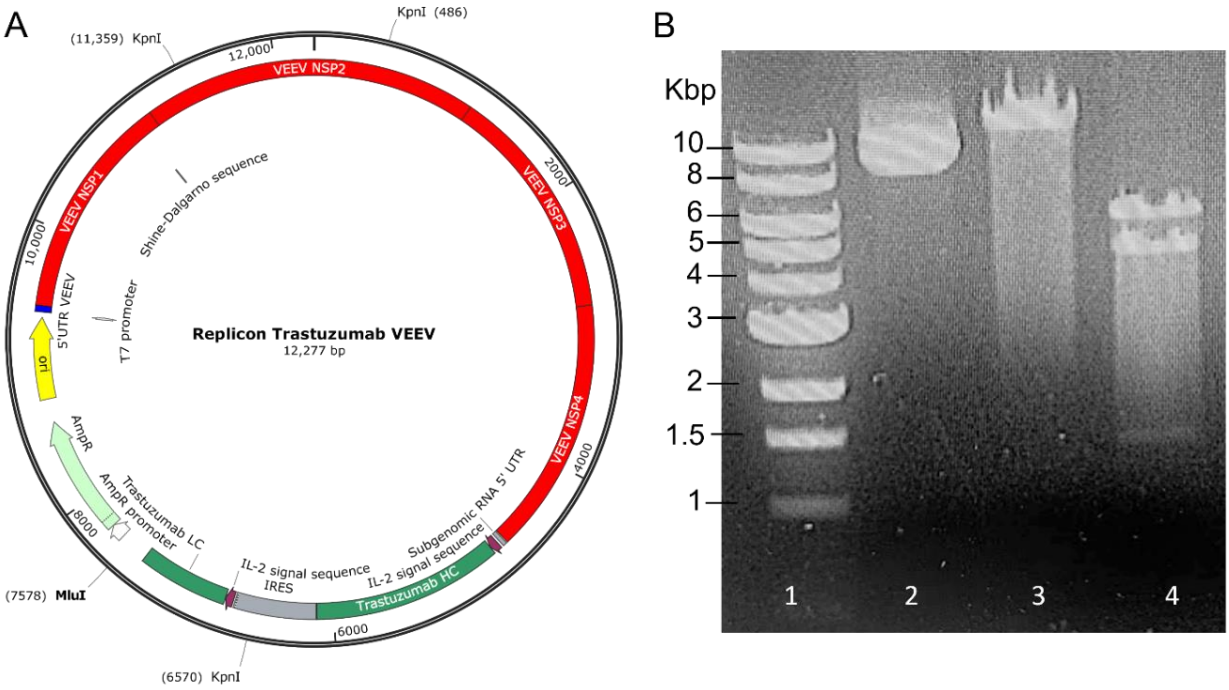

Figure 5.1: Design and validation of Replicon Trastuzumab. (A) Vector map of Replicon Trastuzumab VEEV vector encoding Trastuzumab heavy chain (HC) and light chain (LC), and non-structural proteins (nsPs1-4). Trastuzumab HC and LC are separated by an internal ribosomal entry site (IRES) sequence. (B) DNA gel electrophoresis of Replicon Trastuzumab VEEV vector. Vector was linearised with a single digestion by Mlu1. Kpn1 digest was performed to ensure the synthesis of correct product. Digestion with Kpn1 produced 3 fragments of 6Kbp, 5Kbp and 1.5Kbp. Lane 1; 1kbp NEB ladder. Lane 2; Uncut Replicon Trastuzumab VEEV. Lane 3; Linearised Replicon Trastuzumab VEEV with MuI1. Lane 4; Digest of Replicon Trastuzumab VEEV with Kpn1.

DNA was linearised with Mlu1 for use as template for *in vitro* RNA transcription (**Figure 5.2**). Briefly, RNA transcription was performed using the mMESSAGE mMACHINE T7 transcription kit, in which synthesised RNA was capped with Eukaryotic mRNA cap analogue [m^7G(5')ppp(5')G] to prevent degradation. Residual DNA was degraded by DNase treatment, and Replicon RNA was purified. Replicon RNA was aliquoted and stored at -80˚C ready for transfection. **Figure 5.3** shows a simplified schematic of this process.

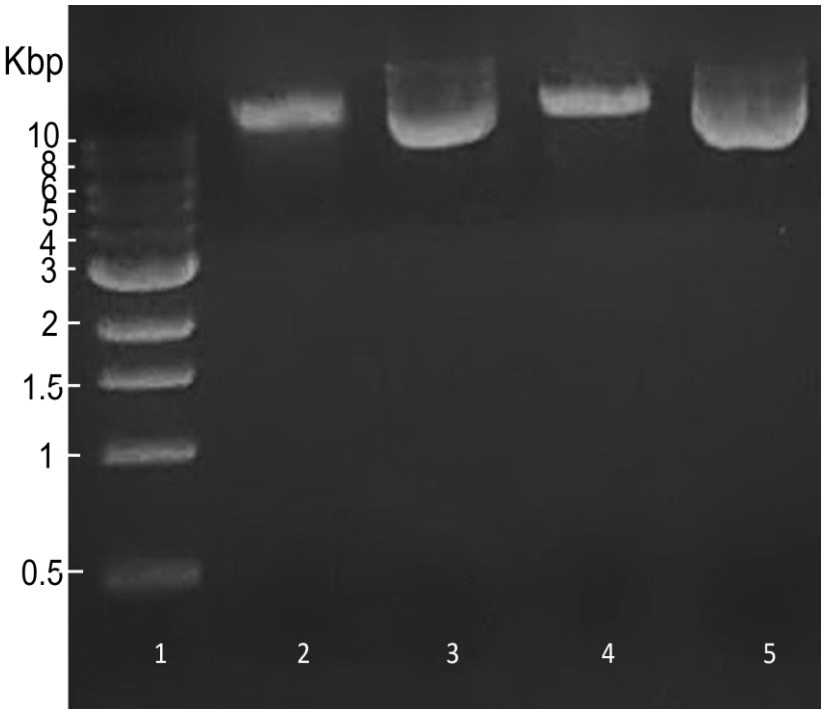

Figure 5.2: Linearisation of Replicon Trastuzumab VEEV with Mlu1 for RNA transcription. DNA gel electrophoresis of Replicon Trastuzumab VEEV vector. Vector was linearised with a single digestion of MuI1 as template for in vitro RNA transcription. Lane 1; 1Kbp NEB ladder. Lane 2; Linearised Replicon Trastuzumab VEEV with MuI1. Lane 3; Uncut Replicon Trastuzumab VEEV. Lane 4; Linearised Fluc1 control VEEV vector with MuI1. Lane 3; Uncut Fluc1 control VEEV vector

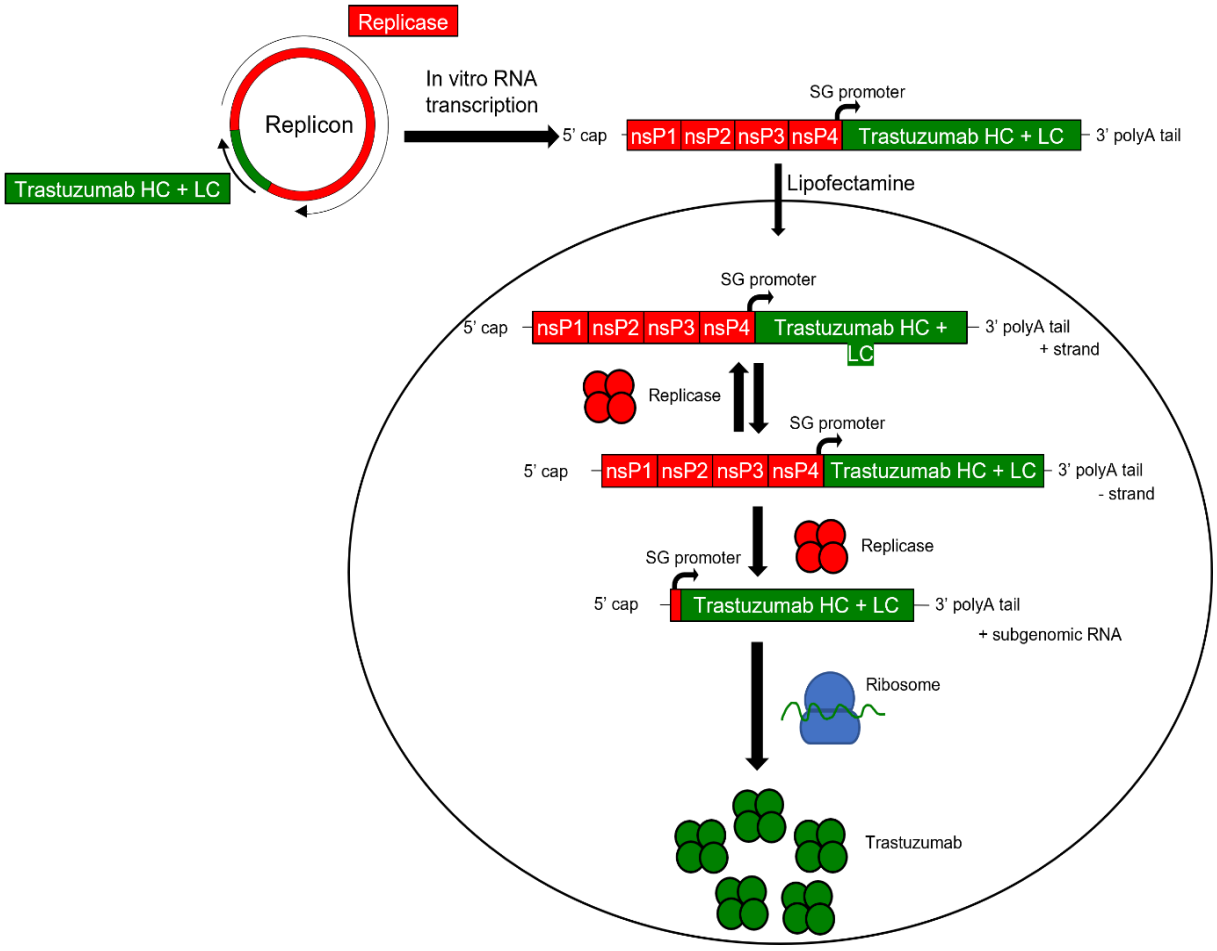

Figure 5.3: Schematic of Replicon Trastuzumab production and delivery. Replicon Trastuzumab was synthesised in vitro and capped, before being transfected by lipofectamine into HEK293F cells. Replicon RNA is translated, and non-structural proteins form mature replication complexes. Replicase action further amplifies Trastazumab genes through the action of SG promotor, while ribosomes and cellular machinery translate and process mature Trastuzumab proteins for secretion.

5.2.2 Expression and assembly of Replicon Trastuzumab

HEK293F cells were transfected with Replicon Trast using the lipofectamine transfection reagent. In-house Trastuzumab (Recombinant Trast) transfections were performed alongside, to provide an appropriate control. Protein was purified from the supernatant by affinity (protein A) and size exclusion chromatography after 7 days. Protein size was visualised by non-reducing SDS-PAGE (**Figure 5.4**). Replicon Trast did express antibody as can be seen by the band at the predicted size of ~150 kDa, running at the same size as Recombinant Trast. Recombinant Trast and Replicon Trast expressed within the HEK293F system provided similar relative protein yields, however, as seen

within the previous chapter yields obtained were low within this system. A more suitable expression, such as the MEXi293E system, should be employed in future to investigate relative mAb expression yields.

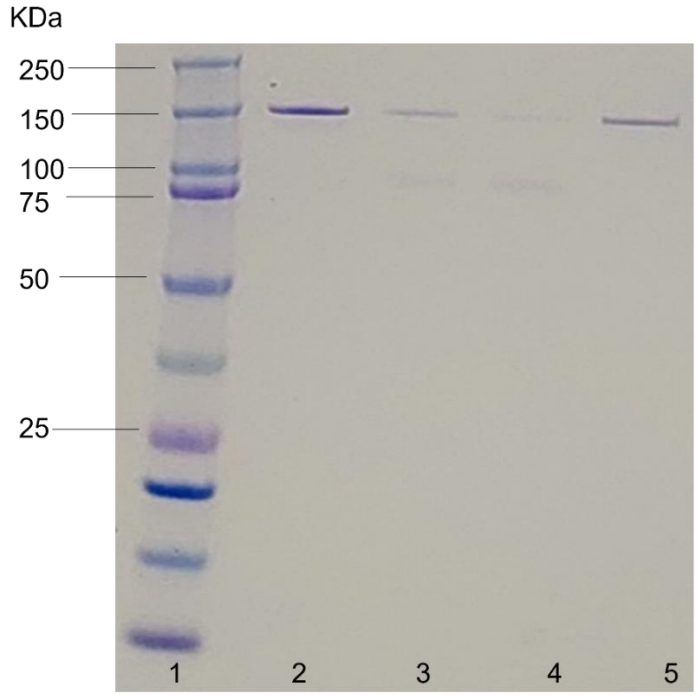

Figure 5.4: SDS-PAGE analysis of SEC purified Replicon Trastuzumab. NuPAGE 4-12% Bis-Tris gradient gel ran in MES buffer. 10 µg sample was mixed with 4X loading buffer and electrophoresed at 160 volts for 40 minutes. Lane 1; Kaleidoscope protein ladder was loaded alongside to establish molecular weights. Lane 2; Replicon Trastuzumab, SEC fraction 12. Lane 3; Replicon Trastuzumab, SEC fraction 13. Lane 4; Replicon Trastuzumab, SEC fraction 14. Lane 5; In-house recombinant Trastuzumab.

5.2.3 Glycopeptide analysis of Replicon Trastuzumab

As previously discussed, antibody glycosylation can influence binding capabilities and biological function, therefore patterns in Fc glycosylation of Replicon Trast and Recombinant Trast were compared. SDS-PAGE gel bands from **Figure 5.4** were excised and an in-gel reduction, alkylation, and digestion with trypsin was performed. Peptides were extracted and analysed by liquid chromatography-mass spectrometry (LC-MS).

Overall, the presence of 20 unique glycoforms was determined for each construct, of which the most prominent glycoform is G0F, **Figure 5.5A**. Overall glycosylation patterns were similar, suggesting similar biological function between the two delivery systems. Minor differences observed between Replicon and Recombinant Trast include a slight increase in G1F and G2F glycoforms and a slight decrease in high-mannose type glycans in Replicon Trast (**Figure 5.5A-C**).

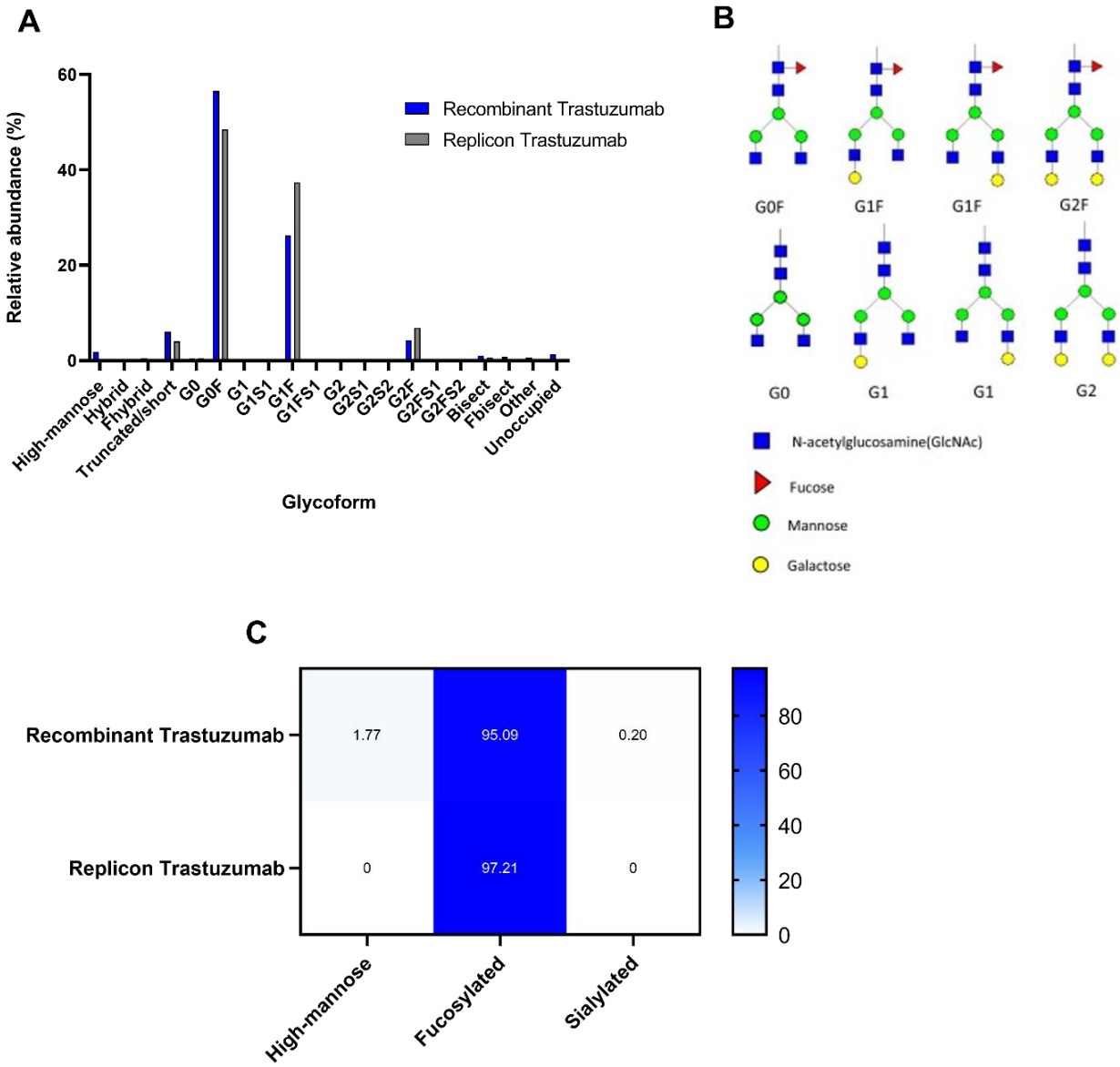

Figure 5.5: Analysis of Fc glycosylation of Replicon Trastuzumab. (A) Categorisation of the relative abundance of glycoforms detected by LC-MS. (B) Schematic of glycan nomenclature. (C) Table of the relative abundance of high-mannose-type, fucosylated, and sialylated glycans for each construct. n = 1.

5.2.4 Replicon Trastuzumab retains HER2 binding

To determine Replicon Trast HER2 ligand binding capability and affinity, surface plasmon resonance (SPR) was utilised. His-tagged HER2 was captured on a CM5 sensor chip immobilised with anti-His antibody to 1000 RU. The captured HER2 was exposed to 5-fold dilutions of Herceptin, Recombinant Trast, or of Replicon Trast. Sensorgrams of HER2 binding were fitted to the 1:1 binding model using the Biacore Bioevalutation software and plotted in GraphPad prism 9 (**Figure 5.6**).

Analysis of the sensorgrams revealed that the 1:1 binding model provided an appropriate fit for the construct binding. The dip in the middle of the sensorgrams shows a bulk shift, which is suggestive of slight differences in analyte running buffer and sample buffer. Indeed, fresh sample buffer was made for samples which was prepared separately from the stock running buffer.

Sensorgrams show a similar curvature for all constructs (**Figure 5.6**). The maximal response signal (Rmax) at 100 nM of all constructs was approximately 50 RU, suggesting similar binding properties. Additionally, all constructs reached saturation at all concentrations tested, suggesting high binding affinity.

Analysis of the association, dissociation, and equilibrium constants are shown in **Table 5.1**. The association constant (k_a) represents the initial binding affinity to HER2. Herceptin has the highest K_a value. This is reflected in the sensorgrams, where Herceptin reached a higher RU than the other constructs, at lower concentrations (**Figure 5.6**). The K_d value is the dissociation constant, representing how quickly the interaction between HER2 and the antibody constructs decays. The smaller this value, the slower the dissociation. The calculated K_d values show that Replicon Trast had the highest K_d so it dissociated the fastest (**Table 5.1**). However, when looking at the sensorgrams, none of the constructs dissociated once bound.

KD is the equilibrium constant between the construct and HER2. KD is inversely proportional to affinity, therefore the lower the KD the higher the construct affinity for HER2. Herceptin had the lowest KD value overall, followed by Recombinant Trast, and Replicon Trast (**Table 5.1**).

Overall, the sensorgrams and binding kinetics of all constructs are similar (**Figure 5.6**; **Table 5.1**). All three constructs reached saturation across all antibody concentrations, indicating strong and similar binding affinity. Therefore, Replicon Trast did not appear to show any differences in binding affinity or kinetics.

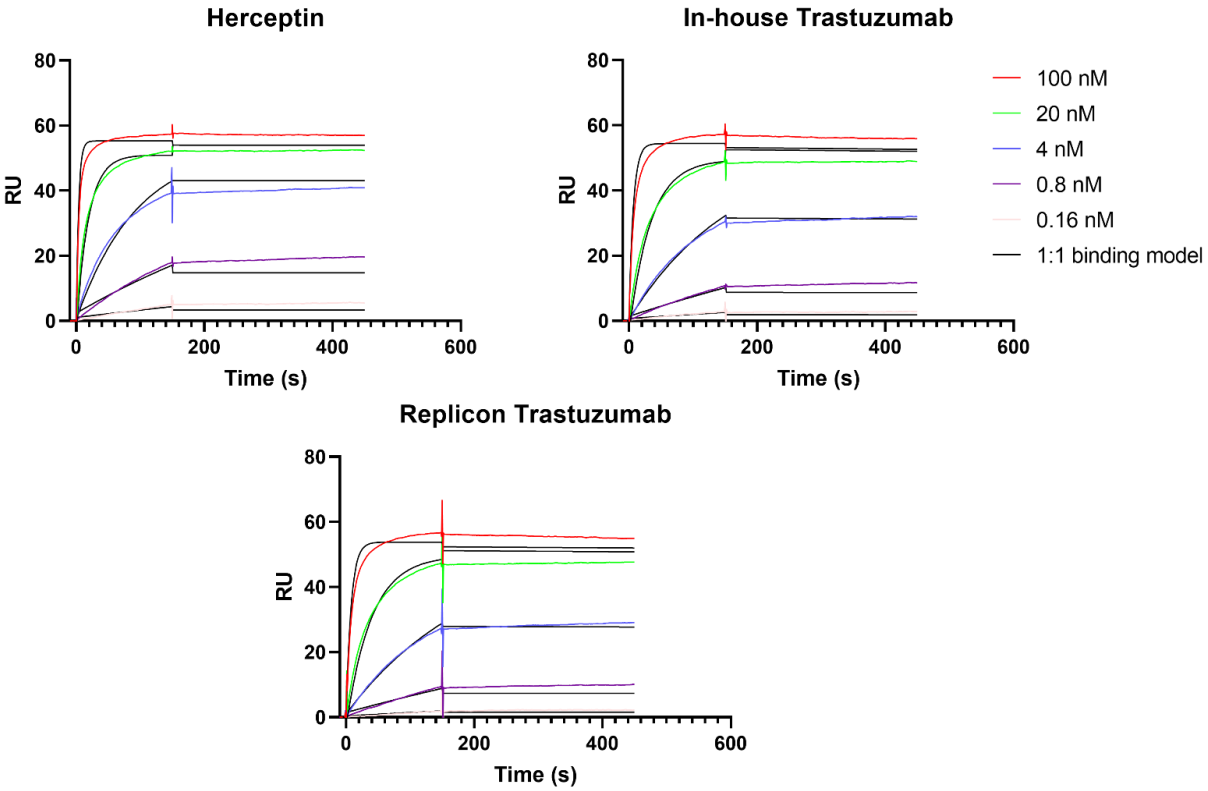

Figure 5.6: SPR analysis of Replicon Trastuzumab mAb. Sensorgrams of Herceptin, In-house Trastuzumab (Recombinant Trastuzumab), and Replicon Trastuzumab for the HER2 ligand. HER2 was immobilised on a chip (5 µg/mL) and antibody constructs were flowed over in 150 second associations and 300 second dissociations on a Cytiva Biacore T200. 5-fold dilution series were performed. The dissociation model was fitted at 150-300 seconds in GraphPad Prism. n=1.

Table 5.1: SPR analysis of Replicon expressed Trastuzumab. Avidity of mAbs to HER2 ligand (0.5 µg/mL) was assessed by SPR. Antibodies were run on the Cytiva Biacore T200.

Construct	k_a (1/Ms)	k_d (1/s)	KD (M)
Herceptin	2.66E+06	1.10E-06	4.13E-13
In-house Trastuzumab	1.50E+06	3.28E-05	2.18E-11
Replicon Trastuzumab	1.27E+06	2.32E-05	1.83E-11

5.2.5 Replicon Trastuzumab retains biological function

Next, the biological activity of Replicon Trast was assessed using the *in vitro* antibody-dependent cellular phagocytosis (ADCP) assay. Briefly, peripheral blood mononuclear cells (PBMCs) were isolated from the blood of healthy human donors and differentiated into M0 macrophages (MDMs). The $HER2^+$ high-expressing BC cell line, SKBR3, was opsonised with 1 µg/mL of antibody and cocultured with MDMs. ADCP activity was examined by flow cytometry (**Figure 5.7**).

It was previously demonstrated that MDMs form three distinct populations when cocultured with CFSE labelled, antibody opsonised-BC cells (Smith et al., 2022 *unpublished*). These are CFSE negative (CFSE-), CFSE low, and CFSE high. CFSE- contain no trace of tumour cell in the population. CFSE low contain tumour particulate within the cytoplasm, indicative of trogocytosis. CFSE high contain fully engulfed tumour cells, indicating phagocytosis. Therefore, cell trace far red (CTFR) stained MDMs were gated as CFSE-, CFSE low, or CFSE high (**Figure 5.7B**).

Phagocytosis (CFSE high), trogocytosis (CFSE low), and total ADCP (pooled CFSE high and low) are plotted as a percentage of total macrophages (**Figure 5.7C**). Overall, there was little difference between Replicon Trast, Recombinant Trast, and Herceptin. Phagocytosis levels were around 35% and comparable across all three constructs. As expected, the irrelevant isotype control, Rituximab showed little effect. Trogocytosis levels were similar for all three constructs. In addition, levels were similar to Rituximab, suggesting that phagocytosis is the likely mechanism of MDM-induced cell death for SKBR3 cells opsonised with these constructs. When accounting for phagocytosis and

trogocytosis activity, total ADCP was ~40% for Herceptin, Recombinant Trast and Replicon Trast (**Figure 5.7**). Overall, there is no statistical significance in ADCP activity between mAbs, and thus Replicon delivery did not impact the biological activity of Trastuzumab.

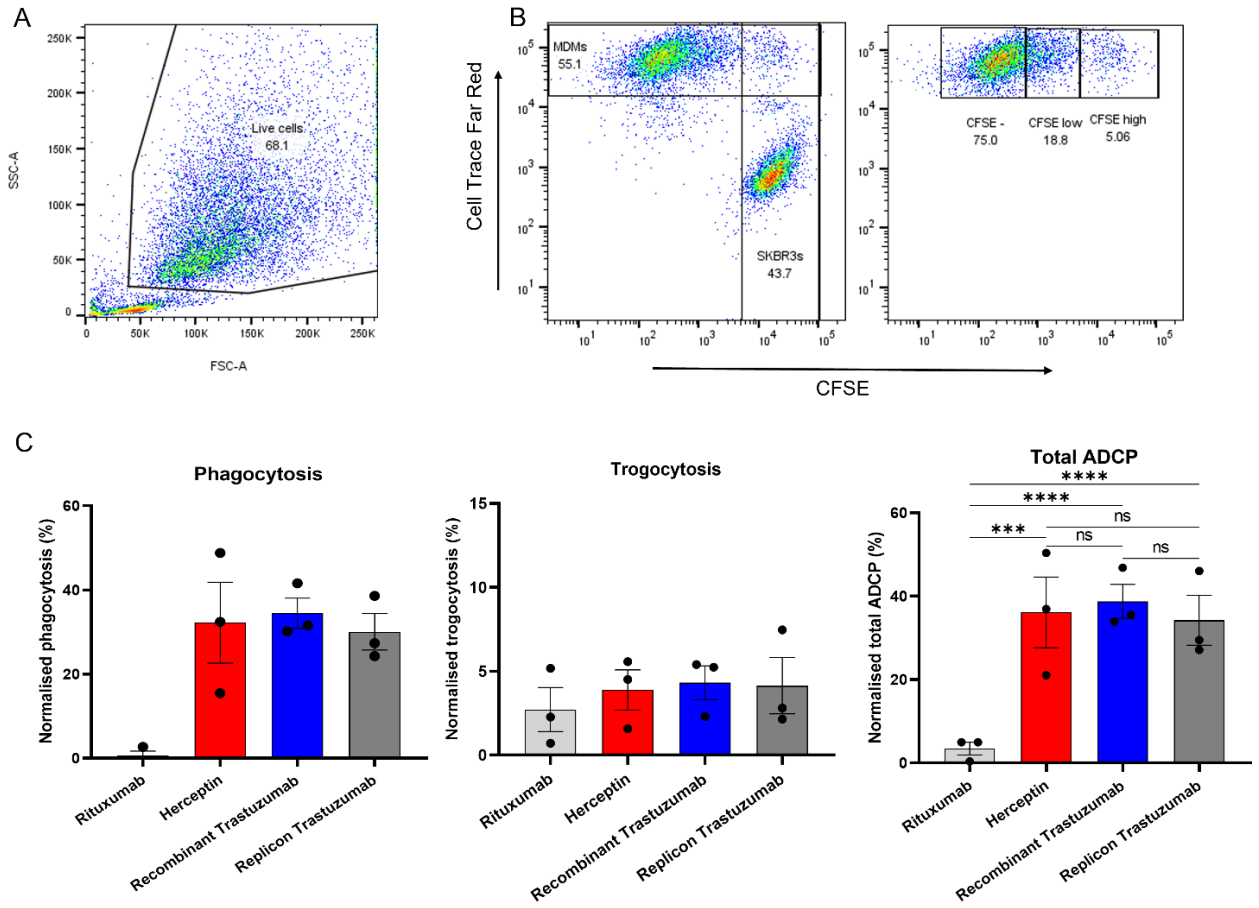

Figure 5.7: Antibody-dependent phagocytosis of Replicon Trastuzumab against SKBR3 cells. (A) Representative flow cytometry dot-plot of live cell gating strategy employed. Rituximab control wells were used to determine population gating. (B) Representative dot-plot of CellTrace Far Red stained MDMs (y-axis) and CFSE stained SKBR3 cells (x-axis). MDMs were further gated into CFSE-, CFSE low, and CFSE high MDMs. (C) The normalised percentage of CFSE high (Phagocytosis), CFSE low (Trogocytosis), and pooled CFSE high and low (Total ADCP) MDMs was calculated by subtracting background activity (control wells absent of mAb). Analysis was performed using FlowJo software. Data are from three independent experiments with mean + SEM from triplicate wells shown. Statistical analysis was performed using 2-way ANOVA on GraphPad Prism. ***$p < 0.001$, ****$p < 0.0001$.

5.3 Discussion

Although monoclonal antibody (mAb) therapy in cancer has revolutionised patient outcomes, it is currently inaccessible to many patients. Generating high quantities of clinical-grade mAbs is logistically and economically demanding (Birch and Racher, 2006), and intravenous delivery of mAb therapy in hospitals further burdens the healthcare system. In addition to this, differences in drug manufacture, storage, and administration can affect mAb aggregation, a major factor in patient immunogenicity (Biro and García, 1965; Filipe *et al.*, 2012). Indeed, immunogenicity impacts mAb efficacy and patient safety. Further, to combat challenges of therapeutic resistance in anti-cancer mAb treatment (Gallardo *et al.*, 2012; Schick, Ritchie and Restini, 2021), novel mAb constructs are produced which are often increasing in complexity. However, with the production of larger, more complex constructs, the challenges in production increase since they are more prone to reduced yield, aggregation and require more robust purification methods (Andrade et al., 2019; Sifniotis et al., 2019). Therefore, as the field of mAb therapeutics expands, more solutions to optimise mAb manufacturing and delivery are required to increase drug accessibility for patients.

Replicon delivery may provide a simple solution to this dilemma. Currently, a large proportion of Replicon research has been conducted for vaccine delivery of single antigens (Lundstrom, 2021; Comes, Pijlman and Hick, 2023). Therefore, further investigations are required to determine the efficacy of Replicon delivered anti-cancer mAb therapeutics. To address this, we designed a Replicon construct to express the anti-HER2 mAb Trastuzumab and compared the expression and function *in vitro* to traditionally made Recombinant Trastuzumab.

For Replicon construction, we utilised the alphavirus genome-based Venezuelan encephalitis virus (VEEV) viral vector as this has been widely studied for Replicons (Hikke and Pijlman, 2017; Lundstrom, 2020; Comes, Pijlman and Hick, 2023). Several approaches can be used to deliver two separate genes within the same vector, however, it was previously demonstrated that the use of an internal ribosomal entry site (IRES) sequence was the most optimal for mAb expression (Erasmus

et al., 2020). Thus, Trastuzumab heavy chain (HC) and light chain (LC) genes were packaged within the same vector, separated by an IRES sequence.

In vitro transcription of DNA to Replicon RNA was performed and HEK293F cells were transfected. Once the Replicon Trast mAb was expressed, the physiochemical and immunochemical properties were characterised, and biological function was assessed. Replicon Trast expressed and assembled at the expected size (**Figure 5.4**) and showed a comparable size profile to Recombinant Trast. Glycopeptide analysis by mass spectrometry showed 100% peptide coverage, confirming the quality and the amino acid sequence of antibody samples.

Immunological properties, namely epitope binding kinetics and affinity, of Replicon Trast were characterised. Binding kinetics to molecular targets is informative of pharmacological activity and essential to investigate for drug development (Copeland, Pompliano and Meek, 2006). Surface plasmon resonance (SRP) can provide quantitative measurements of affinity and reaction kinetics of biomolecular interactions (Fägerstam *et al.*, 1992). Binding kinetics can be indicative of the antibody's mode of action (Teeling *et al.*, 2004; Meyer *et al.*, 2018). Overall, Replicon Trast and Recombinant Trast had similar relative binding affinities for HER2 (**Figure 5.6**). Calculated affinity constants and observed sensorgrams were similar, and binding for both antibodies titrated with lower concentrations (**Figure 5.6**; **Table 5.1**). Pharmacokinetics can also be extrapolated from SPR data. For example, a faster on rate can elicit a more efficacious drug, reducing dosing requirements (Copeland, Pompliano and Meek, 2006), and a slower dissociation rate can lead to a longer duration of effect and be indicative of *in vivo* efficacy (Copeland, Pompliano and Meek, 2006). Binding kinetics data suggests that Replicon and Recombinant Trast both had similar K_a revealing they bound at a similar rate. Since none of the antibodies dissociated after binding HER2 in the parameters set in our experiments, the K_d value cannot be accurately interpreted. Indeed, in previous instances, the measured dissociative half-life was up to 300 minutes (Wood *et al.*, 2004). K_d can indicate drug efficacy *in vivo* (Copeland, Pompliano and Meek, 2006). Further, K_d was demonstrated to correlate with a capacity to induce *in vitro* cellular activity (Berezov *et al.*, 2001),

and to be indicative of an antibody's ability to elicit complement-dependent cytotoxicity (CDC) (Teeling *et al.*, 2004; Meyer *et al.*, 2018). Therefore, experiments with longer off rates should be designed in future to investigate this.

Differences in antibody glycosylation can have major implications on stability and function (Roy Jefferis, 2009; Zheng, Bantog and Bayer, 2011). Glycan analysis of Replicon Trast demonstrated it has a very similar profile of glycoforms to Recombinant Trast (**Figure 5.5**). A slight decrease in high-mannose glycans may be beneficial for serum half-life and reduce clearance *in vivo* (Goetze *et al.*, 2011). Increased fucosylation has been demonstrated to impede FcγRIIIA binding (Royston Jefferis, 2009), whereas decreased sialylation has been demonstrated to enhance FcγRIIIA binding (Raju and Lang, 2014). Despite this, the differences in Replicon Trast glycoforms observed here are minor and unlikely impact on biological function.

To confirm this, we utilised an ADCP assay since ADCP is a key mechanism mediating the clinical action of Trastuzumab. Multiple donors were used due to the inherent inter-donor variability (**Figure 5.7**). The mechanism of ADCP-induced activity was assessed further by gating trogocytosis, phagocytosis, and total ADCP separately (**Figure 5.7B**). Phagocytosis is the primary mechanism of macrophages eliminating tumour cells (Clynes *et al.*, 2000; Gül and Van Egmond, 2015; Vermi *et al.*, 2018). However, trogocytosis has also been demonstrated to be an important mechanism of macrophage-mediated tumour cell death (Velmurugan *et al.*, 2016). It is important to distinguish between mechanisms of action since trogocytosis can result in antigen depletion and exhaustion of effector pathways (Beum *et al.*, 2011) and thus is not always a desired outcome (Taylor and Lindorfer, 2015). Overall, levels of total ADCP, phagocytosis, and trogocytosis induced by Replicon Trast and Recombinant Trast were comparable (**Figure 5.7C**). This suggests a similar mechanism of ADCP-induced activity between Trastuzumab generated by the two delivery systems. Further experiments to investigate other effector functions such as ADCC and CDC activity are important to establish the functional capability of Replicon Trast.

Within this report, we have demonstrated the use of Replicons to deliver a well-characterised mAb of standard format, anti-HER2 Trastuzumab. Advantages over the traditional production of therapeutic mAbs currently in the clinic include easier manufacture, reduced visits to the clinic, and improved patient experience, as discussed earlier. Additionally, Replicons may address increased production challenges faced by more complex mAb formats such as reduced yield and increased aggregation. To investigate this, future work should next establish the use of Replicons to deliver more complex formats, such as 2G12-Hn 2 generated in Chapter 4.

Further, within the project Replicon Trast and Recombinant Trast were expressed in HEK293F cells. However, previous studies have proposed that the clinical administration of Replicon therapeutics would be via intramuscular (IM) injection (Erasmus *et al.*, 2020). Therefore, the suspected cells which would be producing the Replicon construct would be dendritic and muscle cells (Englezou *et al.*, 2018; Li *et al.*, 2019; Erasmus *et al.*, 2020). Since expression profiles, glycosylation patterns, and biological function are impacted by the host cell lines used for expression (Zhou *et al.*, 2008; Slade *et al.*, 2016; Zhang *et al.*, 2019), future experiments to investigate these for Replicon Trast expressed within other cell lines should be performed.

Moreover, before Replicon delivery can be considered for clinical use, several challenges need to be overcome. One of the major current challenges of Replicon delivery concerns trying to achieve a systemic effect. Studies have demonstrated that the delivery method influences the locality of protein expression, for example, IV delivery of mRNA led to expression within the liver or spleen (Thran *et al.*, 2017; Sabnis *et al.*, 2018), and intratracheal aerosol administration led to expression within the lung (Tiwari *et al.*, 2018). IM administration of Replicon mRNA *in vivo* has demonstrated an adequate expression of antibody serum levels in mice (Erasmus *et al.*, 2020). However, difficulties may be faced when translating this into larger animals and humans. Since an effective dose is a function of animal size, it must be demonstrated that meaningful expression can be obtained with a feasible mRNA dose, and is of particular importance for systemically acting proteins (Thess *et al.*, 2015).

Additionally, since Replicon research has predominantly resided within the context of viral therapeutics, it still needs to be established whether the delivery of immunotherapies in the presence of intact type I IFN signalling can produce high enough antibody levels (Erasmus *et al.*, 2020). Type I INF signaling is the primary antiviral innate immune response to RNA infections in mammals. Viruses such as Zika virus employ mechanisms to evade human INF signaling to mediate infection, however, they are unable to attenuate mouse INF response (Sheehan *et al.*, 2006). Therefore, blockade of type I INF signaling is employed in immunocompetent viral mouse models to increase the translatability of results (Gorman *et al.*, 2018). Indeed, blockade of type I INF signaling facilitated protection in mice, and as the effects of temporary INF blockade waned, reduced antibody concentrations and lack of viral protection were observed (Erasmus *et al.*, 2020). Therefore, strategies to attenuate this response may be required to facilitate protein secretion.

To overcome the need to reach systemic therapeutically relevant doses, a possible solution for BC treatment could be the delivery of Replicon-mAb via intra-tumoural injections. This would exhibit a local effect and would bypass the need to reach systemic levels. Further, local administration may provide additional benefits of reducing off-target toxicities, such as cardiotoxicity associated with systemic anti-HER2 BC therapies such as Trastuzumab (Slamon *et al.*, 2001b; Seidman *et al.*, 2002).

To conclude, these findings provide initial proof of concept that Trastuzumab can be effectively expressed utilising the Replicon system. Replicon Trast had similar glycosylation patterns and binding kinetics to HER2, compared to Recombinant Trast. Replicon Trast retained its biological activity and acted by similar ADCP-induced mechanisms of action, to Recombinant Trast. Future experiments to ascertain the expression and function of Replicon Trast in more appropriate host cell lines are essential. Additional experiments including *in vitro* ADCC and CDC and *in vivo* anti-tumour responses and half-life are required to establish Replicons as an efficacious system for Trastuzumab delivery to BC patients. The use of Replicons to deliver mAbs for BC treatment, particularly complex mAbs such as 2G12-Hn 2, shows potential, and the major challenges hindering translation to the clinical which need to be overcome are discussed.

Chapter 6 Discussion

Breast cancer (BC) is the most commonly diagnosed cancer among women and accounted for ~685,000 global deaths in 2020 (Bray *et al.*, 2018; WHO, 2023). The global incidence of BC has risen annually (Bray *et al.*, 2015; Giaquinto *et al.*, 2022), and this trend is predicted to continue. Advancements in targeted therapies mean the five-year relative survival for non-metastatic disease is approximately 80% (NIH, 2020b). Despite these advancements, therapies are not always appropriate for all individuals, can be accompanied by drug toxicity, and therapeutic resistance occurs in almost all patients (Valabrega et al., 2005; Gallardo et al., 2012). In addition to this, therapeutic options for patients with the most aggressive forms of BC, namely TNBC and metastatic disease, are limited with the fewest number and most toxic targeted therapies available. Thus, there is a clear unmet clinical need for new treatment options.

The aim of this thesis was to investigate the potential significance of high-mannose glycans in BC progression and determine whether therapeutically targeting high-mannose antigens could enhance current BC therapeutics.

Aberrant glycosylation is considered one of the established hallmarks of cancer. Previous studies have identified mechanisms which contribute to cancer cell pathology. Well-studied examples include increased β1,6-*N*-linked branched glycans, sialylation and fucosylation, and their roles in epithelial-mesenchymal transition (EMT), invasion, metastasis, and immunosuppression (Cohen *et al.*, 2010; Chen *et al.*, 2013; Taniguchi and Kizuka, 2015; Perdicchio *et al.*, 2016; Tu *et al.*, 2017; Stanczak *et al.*, 2018; Gray *et al.*, 2020). In particular, a growing body of evidence is emerging associating high-mannose glycans with many types of cancer, including BC.

In Chapter 3 we identified the presence of high-mannose glycans on the cell surface of BC cell lines and within clinical tissues. Although it was difficult to establish the proximal location of positive mannose staining within the TME by IHC (**Figure 3.3**), previous findings in gastric tissue have reported similar staining patterns and revealed mannose staining was localised to the cell

membrane and cytoplasm (Liu *et al.*, 2020). Additionally, our findings identifying high-mannose glycans on the cell surface of BC cell lines, support previous findings within the literature (Liu *et al.*, 2013; Ščupáková *et al.*, 2021). Of note, cell surface levels of mannose on BC cells were very variable, despite efforts to control external variables. For example, experiments were consistently performed at set times post-cell passaging to obtain the same log phase. Glycosylation can be variable even within controlled systems (Zhou *et al.*, 2008; Slade *et al.*, 2016; Zhang *et al.*, 2019), demonstrating the challenges associated with studying cancer-associated glycosylation changes within biological systems. However, trends were observed where levels of high-mannose glycans were elevated across the non-metastatic BC cell lines relative to the metastatic BC cell lines (**Figure 3.9**). This may be in part, due to an elevation of complex-type glycans, such as β1,6-*N*-linked branched glycans, in the metastatic lines known to substantiate invasion (Varki, 1993; Demetriou *et al.*, 1995; Meany and Chan, 2011; Pinho and Reis, 2015). Indeed, we observed increased expression of glycosyltransferases responsible for the initiation and production of hybrid- and complex-type glycans within the murine TNBC metastatic cell line EO771.LG relative to EO771 (**Figure 3.6**). Additionally, previous studies have pointed to a shift from increased relative levels of high-mannose glycans in early oncogenesis to complex-type glycans elevated in advanced disease (Boyaval *et al.*, 2022). However, the levels of cell surface complex-type glycans were not determined within this study, and thus this was not confirmed.

Moreover, we observed that mannose processing enzymes were aberrantly regulated in BC clinical datasets, but what was most striking was the heterogeneity of expression across samples (**Figure 3.1**). Our results showed samples were not stratified by clinical features such as BC subtype or stage. These data collectively give insight into the potential significance and extreme heterogeneity of high-mannose glycans in BC and implicate aberrant glycosyltransferase expression levels as a potential mechanism for their presence, which requires further investigation. Another potential mechanism for the increased abundance of under-processed high-mannose glycoforms in cancer is whereby the increased rates of protein synthesis and cell growth lead to the saturation of the glycosylation pathway (Johns *et al.*, 2005; Chatterjee, Kawahara, *et al.*, 2021). Previous studies

focusing on characterising the presence of high-mannose glycans within different BC entities have provided conflicting results as to the presence of high-mannose glycans in BC. Along with our data, this demonstrates a vast heterogeneity of BC glycosylation which is dictated by a multitude of factors including BC stage, subtype, biological sample assessed and treatment regimens (Abd Hamid *et al.*, 2008; Leoz *et al.*, 2011; Saldova *et al.*, 2017; Vreeker *et al.*, 2021). Indeed, this is likely one of the reasons why appropriate high-mannose targeting therapeutics have so far not undergone clinical assessment.

To understand the functional impact of high-mannose glycans, we performed a series of experiments that showed the induction of high-mannose glycans reduced BC cell migration and invasion (**Figure 3.19; Figure 3.20; Figure 3.23; Figure 3.32; Figure 3.33; Figure 3.34**). Aberrant glycosylation of cell surface integrins, cadherins, selectins, and immunoglobulin-like cell adhesion molecules, can mediate cell adhesion, motility, migration, and invasion (Kölbl, Andergassen and Jeschke, 2015). For example, aberrant β1,6 branched glycans in cancer can impede α5β1 integrin clustering (Guo *et al.*, 2002) perturbing EMT processes such as reduced cell adhesion and increased migration and invasion abilities (Dennis, Demetrio and Dennis, 1991; Demetriou *et al.*, 1995; Taniguchi and Kizuka, 2015). Our results confirmed a previous finding that induced high-mannose glycans on BC cells reduced sheet migration (Legler, Rosprim, Karius, Eylmann, Rossberg, Ralph M Wirtz, *et al.*, 2018). Additionally, previous work demonstrated that induced high-mannose glycans increased BC cell adhesive capabilities (Legler, Rosprim, Karius, Eylmann, Rossberg, Ralph M Wirtz, *et al.*, 2018). We observed that EO771-mannose-high cells appeared flatter with fewer budding cells and were more elongated and spindle-shaped than control cells (**Figure 3.28**), which may suggest increased focal contact with the culture plate, and potentially an alteration to cellular adhesive properties. During EMT, mechanisms which control cell adhesion, such as integrin- and E-cadherin-mediated interactions are lost (Hirohashi and Kanai, 2003), allowing cells to become more migrative and invasive through cadherin switching and changes to integrins (Wheelock *et al.*, 2008). Therefore, the induction of high-mannose glycans may attenuate EMT processes such as migration

and invasion and enhance cellular adhesion by modulating glycosylation patterns of cell adhesion molecules and preventing the formation of β1,6 branched glycans.

We next wanted to determine whether these functional changes induced by high-mannose impacted tumour growth *in vivo*. We observed that transient high-mannose glycans induced by Kif treatment disrupted the engraftment and initial growth phase of EO771 tumours (**Figure 3.24**). In EO771 cells showing stable high-mannose phenotype through MGAT1 disruption, the effects on disruption of engraftment and slowed tumour growth were more pronounced (**Figure 3.36**). One explanation for this could be due to the aberrant function of cell adhesion proteins impacting the initial attachment of cells to the surrounding stroma. Previous studies have demonstrated that the number of cells which manage to initially engraft is critical for tumour growth (Hoffmann *et al.*, 2020). An additional explanation could be due to increased immune control resulting from the presence of non-self-glycans. C-type lectins which bind high-mannose and branched-fucosylated antigens are expressed on macrophages and dendritic cells (DC) to distinguish between self- and invading organisms (Geurtsen, Driessen and Appelmelk, 2010). Tumour associated macrophages (TAMS) represent the most prominent myeloid population infiltrating BCs (Williams, Yeh and Soloff, 2016), and they have been demonstrated to bind aberrantly fucosylated glycans through DC-SIGN, inducing a proangiogenic profile and promoting tumour progression (Merlotti *et al.*, 2019; Hu *et al.*, 2020). The induction of high-mannose glycans disrupts the formation of complex-fucosylated glycans, thus preventing the formation of this protumour environment. Moreover, DCs recognise many pathogens as foreign through DC-SIGN binding high-mannose glycans, initiating DC maturation and migration to secondary lymphoid organs (Geurtsen, Driessen and Appelmelk, 2010). Therefore, the disrupted tumour growth of high-mannose BC cells may be due to an adaptive immune response initiated through DC-SIGN binding.

The interplay between high-mannose glycans and the immune system is of interest, and future IHC analysis of the immune infiltrate within the BC tumours from our *in vivo* experiments may be able to shed light on this. Collectively, these findings suggest that high-mannose glycans may play a

critical role in modulating cellular behaviours associated with BC progression. We suspect there is a dynamic interplay between high-mannose glycoforms and highly branched glycoforms, and this may potentially be contributing to the complex nature of BC development and metastasis.

Taken together our data may suggest a potential mechanism for the progression from a non-metastatic to metastatic phenotype. Increased high-mannose glycans in early disease may reduce cell migration and invasion, acting to constrain the tumour to the primary site. A shift from high-mannose to complex-type glycans may then assist with the establishment of a protumour environment through DC-SIGN binding of highly branched fucosylated glycans, and in EMT processes such as tumour escape and migration to a secondary site due to the increased presence of β1-6 branched glycans. Therefore, the possibility of inducing high-mannose glycans in patients may be of therapeutic benefit to prevent disease progression.

While inducing high-mannose glycans on BC cells may be challenging to do in a targeted way, several therapeutic approaches can induce aberrant high-mannose glycoforms on targets important for cancer therapy. For example, PD-L1 natively harbours predominantly complex-type glycoforms (Li et al., 2016) which is important for its function and stability. D-mannose administration was demonstrated to activate PD-L1 phosphorylation by AMP-activated protein kinase (AMPK) promoting its degradation, while also limiting PD-L1 glycosylation and thus suppressing PD-L1 membrane expression (Zhang *et al.*, 2022). This mechanism led to enhanced immunotherapy and radiotherapy outcomes in an *in vivo* TNBC model (Zhang et al., 2022). It was demonstrated in a separate study that D-mannose supplementation increased high-mannose glycoforms on IgG and reduced mannosidase expression (Kildegaard et al., 2016; Slade et al., 2016), suggesting a negative regulation of nucleotide-sugar donor availability and glycosidase expression. Therefore, methods to induce high-mannose glycans could be a potential therapeutic strategy to drive PD-L1 instability. Interestingly, metformin has been demonstrated to elicit anti-tumour effects by a similar mechanism of action. Metformin increases AMPK-mediated phosphorylation of PD-L1 (Zhou *et al.*, 2001), which induces aberrant high-mannose glycoforms (Cha *et al.*, 2018). High-

mannose glycoforms resulted in increased ER-associated degradation, and decreased stability and translocation of PD-L1 to the cell surface, inducing anti-tumour effects and increasing cytotoxic T-lymphocyte activity (Cha *et al.*, 2018).

The therapeutic induction of high-mannose glycans may be challenging due to difficulties in tumour targeting, and thus one might envisage off-target effects. Nonetheless, strategies to deliver indiscriminate glycan-targeting molecules by conjugating them to tumour-specific mAb have previously been demonstrated (Gray *et al.*, 2020; Che *et al.*, 2022). The delivery of D-mannose supplements may induce high-mannose glycoforms to assist current therapies by the mechanisms described above.

Alternatively, directly targeting high-mannose glycoforms is also of therapeutic interest. The recent production of a novel high-mannose targeting lectibody identified EGRF and IGF1R as two of its predominant targets harbouring high-mannose glycans (Oh *et al.*, 2022). It was demonstrated that EGRF overexpression increased the proportion of high-mannose glycoforms, due to saturation of the glycosylation pathway (Johns *et al.*, 2005). Interestingly, one of the proposed mechanisms of Trastuzumab resistance is EGFR and IGF1R overexpression (Gallardo *et al.*, 2012). Therefore, paired HER2- and high-mannose glycan-targeting may be a novel approach to combat mechanisms of Trastuzumab resistance, while broadening target specificity for lower antigen-expressing BC subsets.

Thus, in Chapter 4, we designed novel antibody constructs utilising the mannose-targeting IgG1 antibody, 2G12, in combination with anti-HER2 scFVs. These antibody constructs can be expressed within commercial mammalian expression systems that allow Fc glycosylation and retention of Fc-mediated effector functions. We generated three constructs and demonstrated that one construct, 2G12-Hn 2, retained HER2 and mannose-binding abilities. Specifically, it showed increased binding stabilisation at higher antibody doses (**Figure 4.17; Figure 4.18; Figure 4.19; Figure 4.20**), potent ADCP in $HER2^{+}$-high BC cells (**Figure 4.23; Figure 4.24**) and the ability to restore ADCP in $HER2^{+}$-low BC cells (**Figure 4.25**) and those with high-mannose expression (**Figure 4.26**), through what is

suspected to be trogocytosis. Previous studies have indicated the importance of trogocytosis as a mechanism of ADCP tumour depletion by macrophages (Velmurugan *et al.*, 2016). The potential safety and efficacy of 2G12-Hn 2 is yet to be determined; therefore *in vivo* testing of 2G12-Hn 2 is required in murine models to establish these outcomes in a more physiological condition.

This could have potential implications for patients who do not overexpress HER2. Anti-HER2 therapeutics are associated with cardiotoxicity due to HER2 expression on cardiac cells (Slamon *et al.*, 2001b; Seidman *et al.*, 2002). Therefore, standard practices to define BC as $HER2^+$ are stringent (Ahn *et al.*, 2020), and patients who do not meet this high $HER2^+$ expression threshold are not considered suitable for therapy. We have demonstrated that HER2 was expressed within clinical samples not classed as $HER2^+$, indicating that HER2 targeting may be clinically efficacious across several subtypes (**Figure 4.1**). Dual anti-mannose and anti-HER2 targeting may alleviate some of the off-target effects of standard anti-HER2 therapy since high-mannose glycans are not commonly expressed within mammalian tissues but have been demonstrated to be elevated in BC (**Figure 3.9**). However, the presence of high-mannose glycans on cardiac cells was not investigated within the scope of this thesis and must first be determined.

Our 2G12-Hn 2 antibody may also offer advantages that could overcome some of the clinical and manufacturing challenges of current mannose-targeting lectin-based therapeutics. Lectin-based drugs show increased aggregation and immunogenicity (Matoba *et al.*, 2010). Plant-viral-vector-based systems for the expression of lectin-based therapeutics would produce non-mammalian glycosylation patterns, having functional implications for antibody function (Roy Jefferis, 2009), immunogenicity (Prabakaran *et al.*, 2012; Zavala-Cerna *et al.*, 2014), and stability (Zheng, Bantog and Bayer, 2011). Additionally, we and others have demonstrated that mannose targeting therapeutics require a threshold of epitope expression to facilitate binding (Oh *et al.*, 2022) (**Figure 4.19**; **Figure 4.20**). This threshold may not always be met due to the heterogeneity of glycan expression in BC, thus impacting the efficacy of high-mannose targeting alone. Thus, dual targeting HER2 may help overcome this threshold and stabilise binding.

Although 2G12-Hn 2 shows promise, the production of larger multitargeting constructs commonly results in reduced yield, and aggregation and require more robust purification methods (Andrade et al., 2019; Sifniotis et al., 2019). Indeed, we observed increased aggregation of our constructs relative to expressed Trastuzumab control (**Appendix 8**). Clinically, mAb aggregation is a major factor leading to loss of mAb efficacy and reduced patient safety. In terms of manufacture, mAb aggregation leads to reduced yield. This is of note, since generating high quantities of clinical-grade mAbs is logistically and economically demanding (Birch and Racher, 2006), and can often make mAb therapeutics inaccessible to patients accessing public healthcare systems which cannot afford it. Therefore, the reduced production yield and increased aggregation of multitargeting therapeutics, such as 2G12-Hn 2, would increase the economic and logistical burden of clinical mAb production, and potentially decrease drug accessibility for patients.

One such solution to overcome this could be the use of Replicons for antibody delivery. Replicon delivery has the potential to bypass issues with manufacturing large molecules, such as increased aggregation, harsh methods of purification, protein instability and loss in yield, resulting in increased efficacy and lower immunogenicity in mAb treatment. In addition, Replicon delivery could result in reduced visits to the clinic and improved patient experience, as discussed previously.

Extensive research on Replicons has focused on vaccine delivery, which are mainly monocistronic antigens (Lundstrom, 2021; Comes, Pijlman and Hick, 2023). To the best of our knowledge, at the time of writing only one published example has utilised the replicon system for antibody production, in which they produced an anti-Zika virus antibody (Erasmus *et al.*, 2020). Therefore, we wanted to determine whether we could utilise replicons for the delivery of anti-cancer antibodies. In Chapter 5, we investigated the use of replicons for the delivery of antibodies. As a starting point, we used a standard, well-characterised BC antibody, anti-HER2 Trastuzumab. We established that Replicon-produced Trastuzumab retained similar target binding to HER2 and mediated comparable effector functions as traditional recombinant-made Trastuzumab (**Figure 5.6**; **Figure 5.7**). Now that we have demonstrated that the Replicon system can produce a functioning

antibody, the next step would be to investigate whether it could be used for producing/delivering more complex formats such as bispecifics, including our construct 2G12-Hn 2.

Before antibody delivery by Replicons could be considered for clinical use, several challenges still need to be overcome, predominantly the ability of Replicons to produce therapeutically relevant doses of anti-cancer mAbs. Although proof of concept of IM administration of Replicon mRNA has demonstrated an adequate expression of antibody serum levels in mice *in vivo* (Erasmus et al., 2020), this needs to be translated to larger animals and humans. Since an effective dose is a function of animal size, it must be demonstrated that meaningful expression can be obtained with a feasible mRNA dose, and is of particular importance for systemically acting proteins (Thess *et al.*, 2015). Additionally, more research is needed to establish whether Replicon delivery of anti-cancer immunotherapies in the presence of intact type I IFN signalling can produce a therapeutically relevant effect. Blockade of type I INF signaling is employed in immunocompetent viral mouse models to increase the translatability of results to mimic human infections (Gorman *et al.*, 2018). However, it was demonstrated that as the effects of temporary INF blockade waned, reduced antibody concentrations and lack of viral protection were observed (Erasmus *et al.*, 2020). Therefore, strategies to attenuate this response may be required to facilitate protein secretion.

To overcome the need to reach systemic therapeutically relevant doses, a possible solution for BC treatment could be the delivery of Replicon-mAbs via intra-tumoural injections. This would exhibit a local effect within the tumour and would bypass the need to reach systemic levels. Further, an additional benefit of this approach may be to reduce off-target toxicities such as cardiac toxicity, which is associated with systemic anti-HER2 therapies.

6.1 Conclusions and future perspectives

High-mannose glycans are emerging as a cancer-associated phenotype in breast cancer (BC). We have demonstrated differences in the regulation of mannose-processing enzymes between healthy tissues and BC tissues. We have identified the presence of high-mannose glycans on the cell surface

of multiple BC subtypes, and within the tissues of clinically relevant BC samples. Despite being prevalent in the BC setting, artificially increasing their presence both transiently and stably reduced cancer-associated phenotypes *in vitro*. Additionally, increased high-mannose glycans reduced tumour growth and metastatic burden *in vivo*. The role of high-mannose glycans is dynamic and is suspected to be favourable at the early stages of BC development. Therefore, targeting high-mannose glycans is of interest. By developing a multivalent anti-HER2 and anti-high-mannose mAb, 2G12-Hn 2, we demonstrated an increased benefit in binding stability, and ability to induce ADCP activity in low antigen expressing BCs, over anti-HER2 therapy. This may provide an advantage to anti-HER2 therapy, however, difficulties in the production and administration of multi-domain and complex mAbs may make them inaccessible to many patients. Therefore, we investigated the use of Replicon delivery for mAb Trastuzumab and provided the initial proof of concept of its production *in vitro*. Indeed, differences in Replicon and Recombinant Trastuzumab expression, glycosylation patterns, binding kinetics, and biological activity were minor. The use of Replicons to deliver mAb for BC treatment, particularly complex mAbs such as 2G12-Hn 2, shows potential, and the major challenges hindering translation to the clinical which need to be overcome are discussed.

Future work is required to underpin variables which influence the expression of mannosidase processing enzymes, and levels of high-mannose glycans in BC. Further stratification of samples based on clinical data may shed light on the stage of BC progression which high-mannose glycans may facilitate. The relationship between high-mannose glycans and complex-type glycans should be directly studied, and the relative proportions of these two glycan phenotypes should be quantified at different stages of BC oncogenesis to establish their role in pathology. The effect of inducing high-mannose glycans on the function of cell adhesion proteins should be ascertained to establish their significance in attenuating EMT processes such as cell migration and invasion. Additionally, the mechanism of how high-mannose glycans impact tumour growth needs to be established, in which changes in immune infiltration and the relationship between high-mannose BC cells and mannose-binding lectins, such as DC-SIGN, *in vivo* should be investigated. Further, the levels of high-mannose glycans on cardiac tissue need to be assessed to determine the impact of

dual targeting high-mannose and HER2 by 2G12-Hn 2. The safety and efficacy profile of 2G12-Hn 2 in more physiological conditions needs to be established, starting with *in vivo* models. At the same time, the ability of Replicons to deliver more complex formats such as 2G12-Hn 2, should be determined.

Chapter 7 Appendices

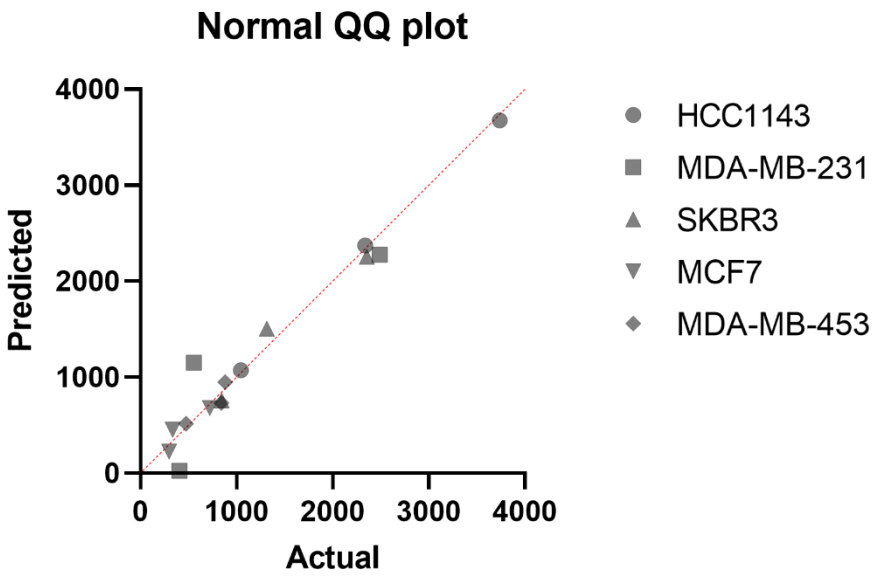

Appendix 1: Shapiro-Wilk test was performed on cell surface mannose flow cytometry data for human breast cancer cell lines to ensure data fit a normal Gaussian distribution prior to statistical analyses.

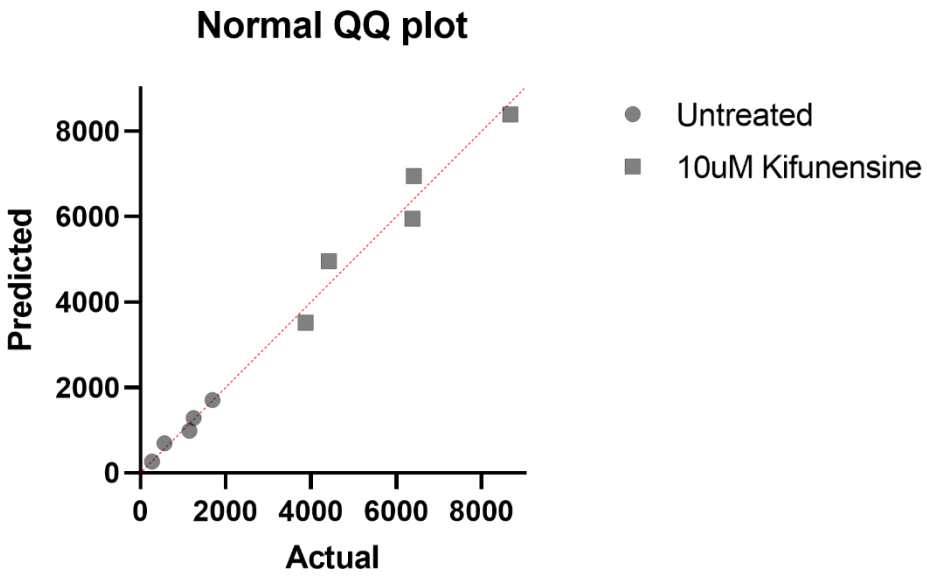

Appendix 2: Shapiro-Wilk test was performed on Untreated vs Kifunensine treated cell human breast cancer cell lines to ensure data fit a normal Gaussian distribution prior to statistical analyses.

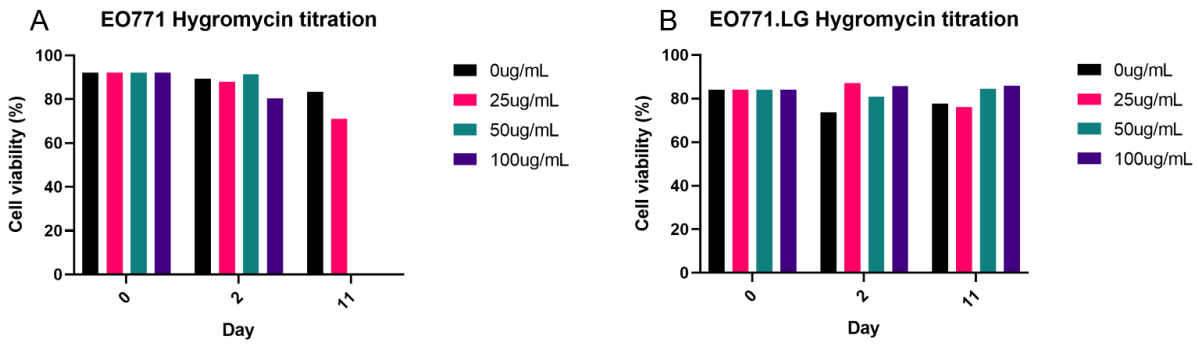

Appendix 3: Hygromycin titration to ascertain the concentration required to select for EO771.LG cells. A EO771 and B EO771.LG cells were grown in 0, 25, 50, or 100 ug/mL hygromycin-rich media, respectively. Cells were harvested and viability was measured by AO/PI stain at 0, 2, and 11 days respectively. Hygromycin-rich media was replenished every 2-3 days.

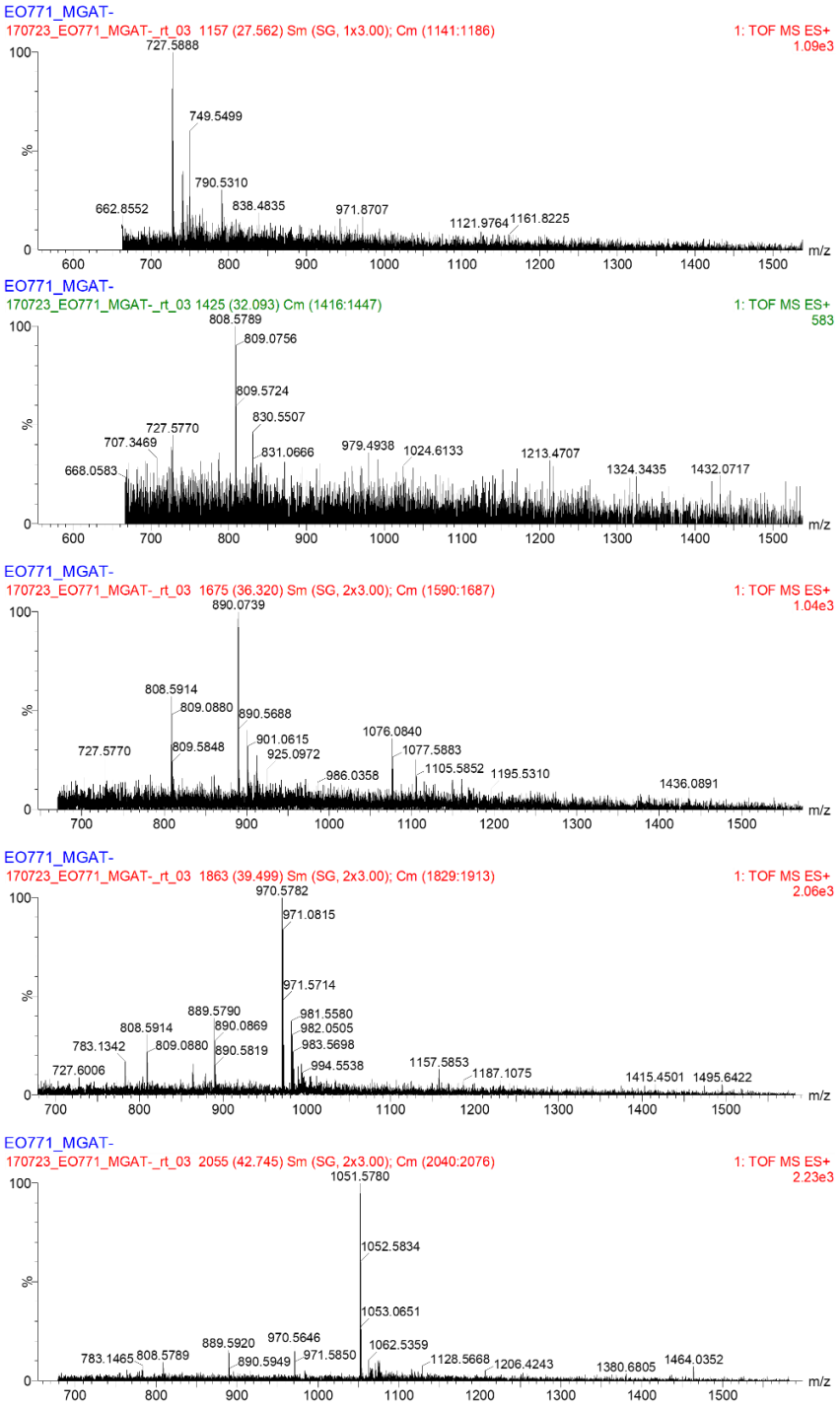

Appendix 4: MS2 data of mannose series species identified from released procainamide labelled glycans from EO771 MGAT1 KO cell line. Cell lysate was extracted and trypsinised. N-glycans were released in solution from glycopeptides using PNGase F, procainamide-labelled, desalted and purified by carbon column and porous graphite column chromatography. LC-MS [direct infusion into Synapt G2Si (Waters)] was performed in tandem. High-mannose structures were deduced from their doubly charged negative ion monoisotopic masses.

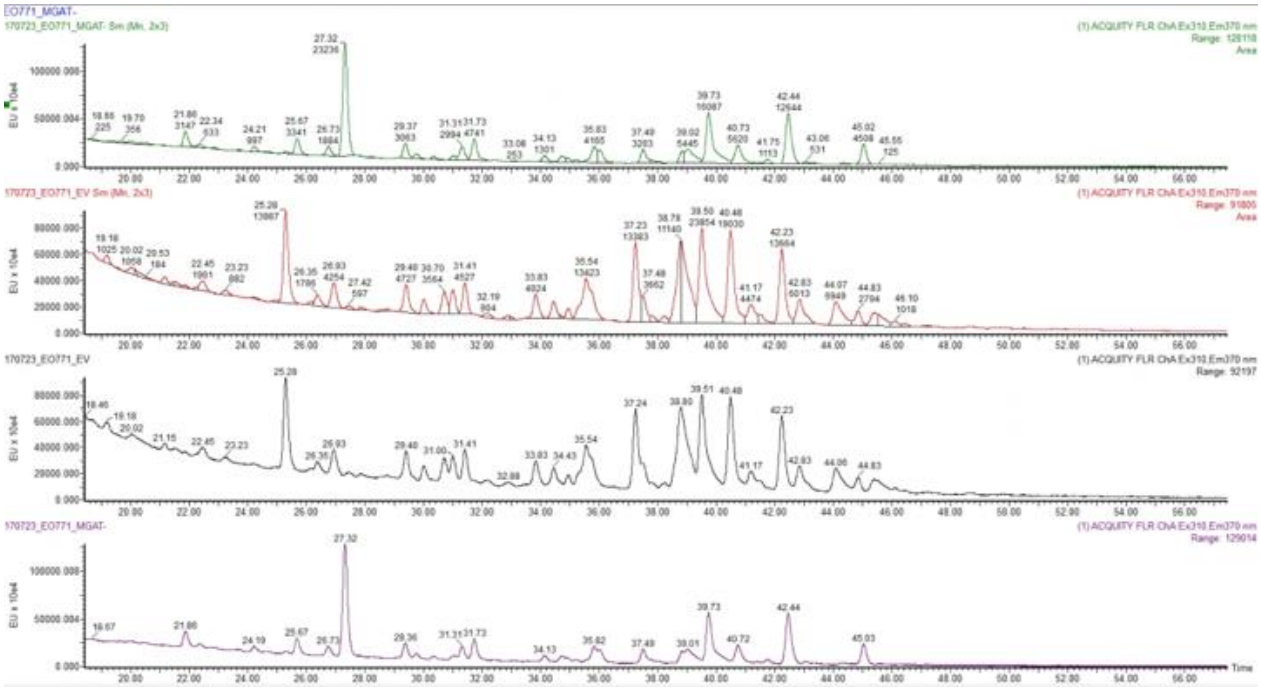

Appendix 5: Chromatogram of released labelled MGAT1 KO and Empty Vector N-glycans. The area of each peak integrated and the relative percentage of peaks identified as a mannose series from appendix 4 was quantified. Cell lysate was extracted and trypsinised. N-glycans were released in solution from glycopeptides using PNGase F, procainamide-labelled, desalted and purified by carbon column and porous graphite column chromatography. LC-MS [direct infusion into Synapt G2Si (Waters)] was performed in tandem.

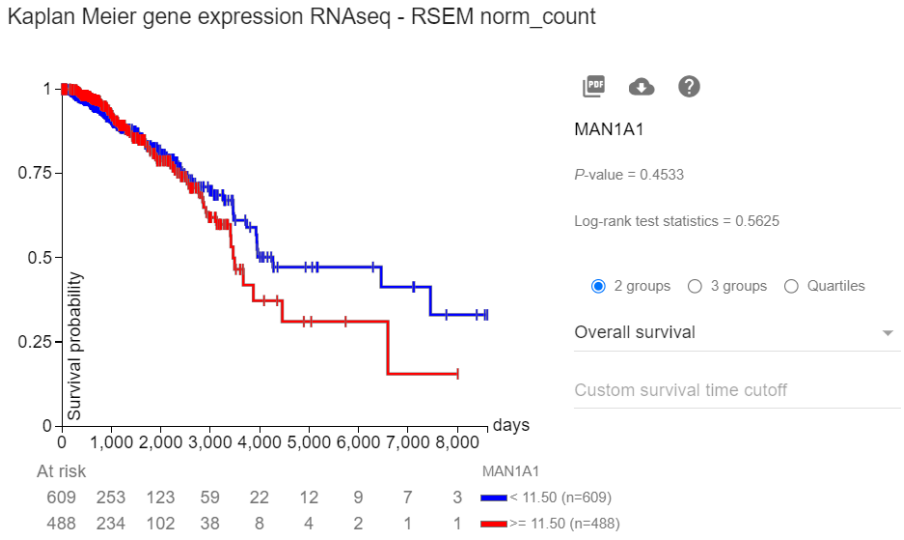

Appendix 6: Kaplan Meier plot of MAN1A1 expression on overall survival from Xena platform. TCGA, TARGET and GTEx sample dataset was re-analyzed (re-aligned to hg38 genome and expressions are called using RSEM and Kallisto methods) by the same RNA-seq pipeline. Default Kaplan Meier function on Xena platform using default cut-offs.

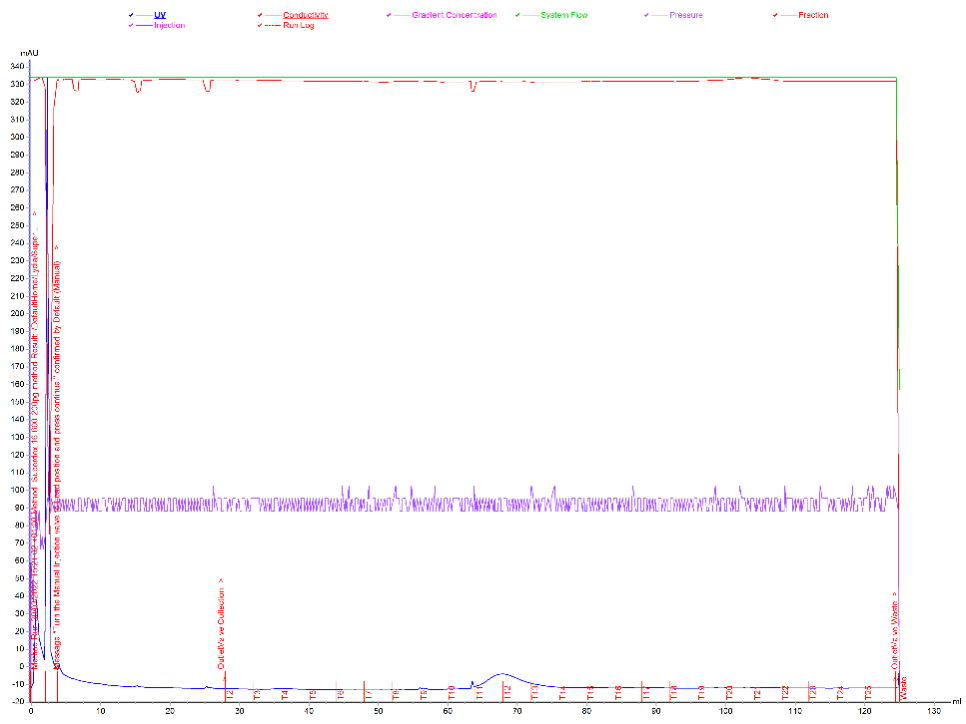

Appendix 7: SEC of 2G12-Hn 1 construct expressed in HEK293F cells.

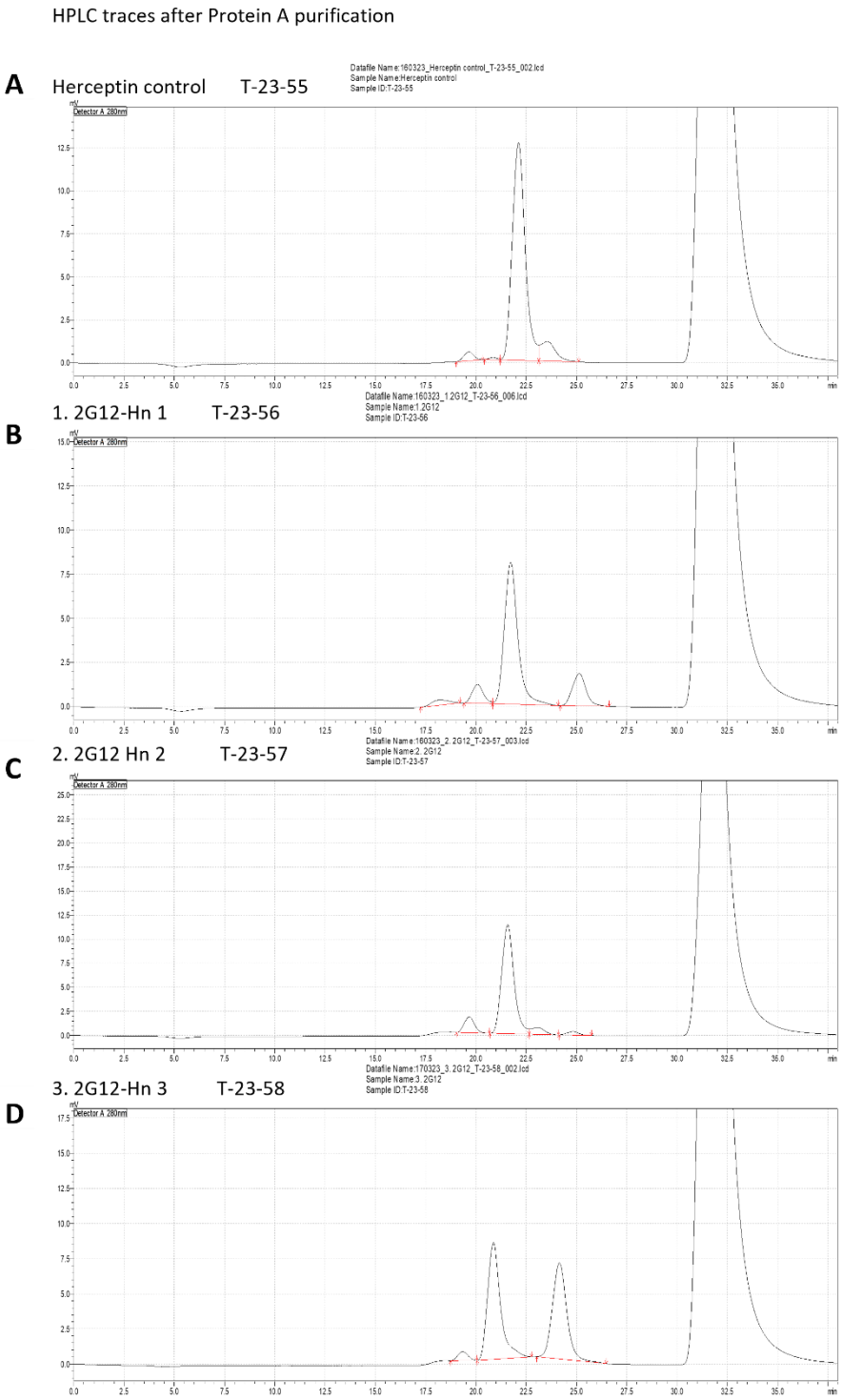

Appendix 8: Purity and aggregation of Mexi293e expressed 2G12-Hn constructs before SEC. High performance liquid-chromatography (HPLC) analysis of (A) In-house Trast, (B) 2G12-Hn 1, (C) 2G12-Hn 2, (D) 2G12-Hn 3 after protein A affinity chromatography. All constructs contained some aggregation and required further purification by SEC. Aggregation % were (A) 3.3%, (B) 11.4%, (C) 10%, (D) 3%.

Lydia 28/03/23
The HPLC traces after SEC

A Herceptin control T-23-55

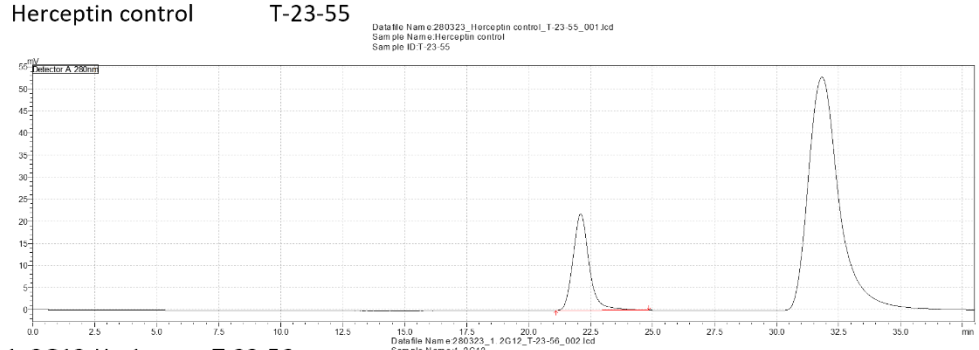

B 1. 2G12-Hn 1 T-23-56

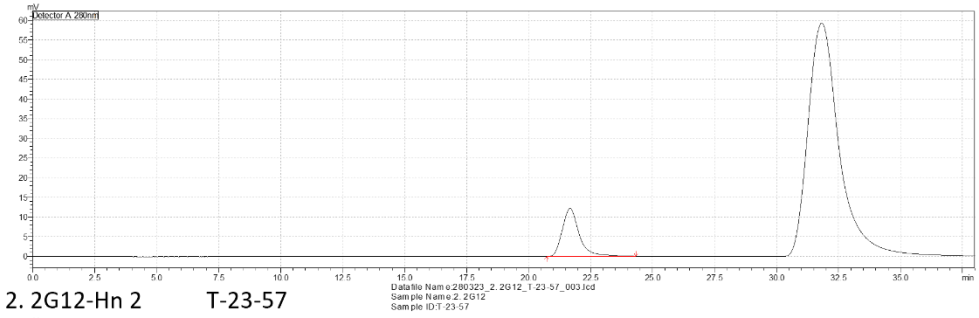

C 2. 2G12-Hn 2 T-23-57

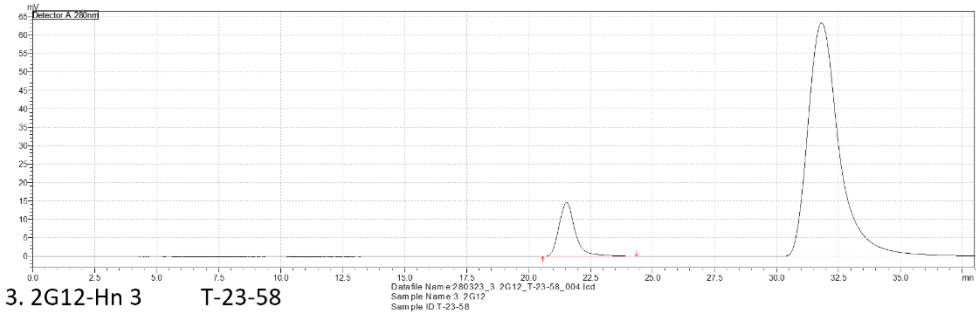

D 3. 2G12-Hn 3 T-23-58

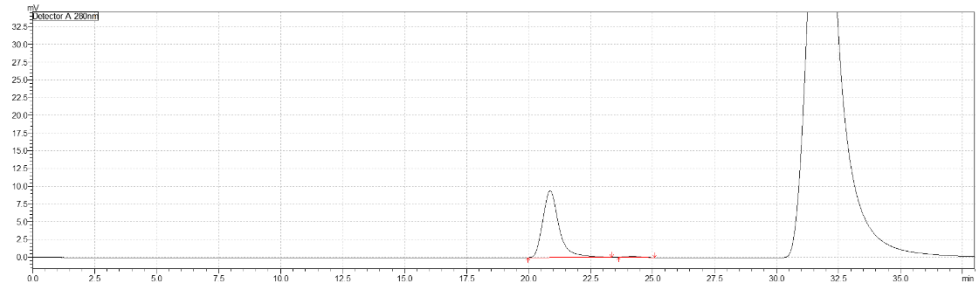

Appendix 9: Purity and aggregation of Mexi293e expressed 2G12-Hn constructs after SEC. High performance liquid-chromatography (HPLC) analysis of (A) In-house Trast, (B) 2G12-Hn 1, (C) 2G12-Hn 2, (D) 2G12-Hn 3 after protein A affinity and size exclusion chromatography.

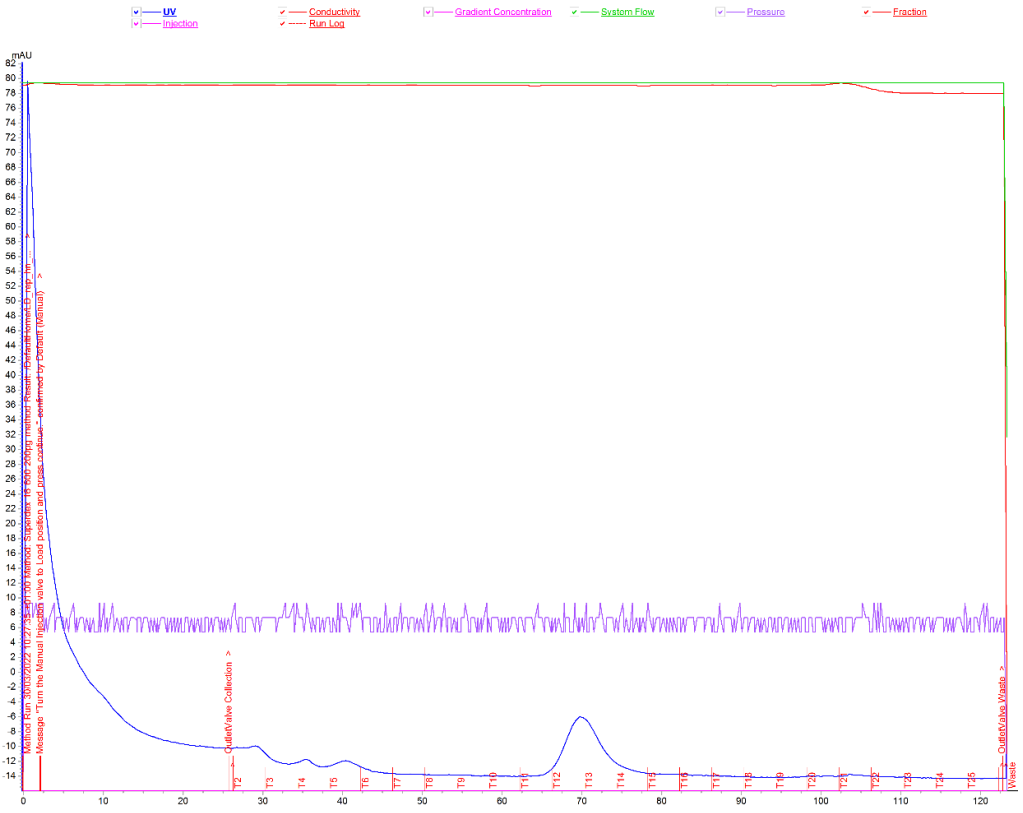

Appendix 10: SEC of Replicon Trastuzumab expressed in HEK293F cells.

Day	Mannose-high											Empty Vector										
6	15.05	17.85	1	*0**	21	9.25	14.4	13.94	1	11.2	15.96	0	1	1	19.72	9.62	0	20.58	22.8	*0**	0	15.91
7	22.8	19.14	0	*0**	19.89	9.62	19	15.4	0	19.8	14.62	0	9	6	25.9	19.8	0	30.55	42.66	*0**	0	18.86
8	27.88	16.8	6	*0**	12	10.36	11.9	12.6	0	17.2	9	0	9.24	17.2	30.66	16.45	0	-	35.04	*0**	0	23
10	-	18.3	14.4	*0**	0	17.2	31.85	0	0	30.24	14	0	9.9	13.65	30.1	19.14	27	-	37.05	*0**	0	30.72
13	-	14.7	11.22	*0**	0	24.05	45	9.75	9	28.67	6	72.8	40.92	59.16	72.45	38.76	-	-	85.32	*0**	40.81	64.08
14	-	16.17	14.4	*0**	0	34.56	57.42	13.65	22	51.03	9	69.3	48.18	63	82.49	-	-	-	86.58	*0**	65.7	-
15	-	21.45	20.52	*0**	0	44.72	63.24	13.94	27	50.7		-	54.67	64.68	81	-	-	-	100.3	*0**	-	-
17	-	29.58	27.36	*0**	0	66	117	15.48	64.68	73.72	11.2	-	66.42	107.1	112.5	-	-	-	-	*0**	-	-
20	-	-	-	*0**	0	-	-	14	-	109.9	9	-	-	-	-	-	-	-	-	-	-	-
22	-	-	-	*0**	0	-	-	0	-	-	1	-	-	-	-	-	-	-	-	-	-	-

Appendix 11: Raw measurement data for tumours derived from Mannose-high and Empty vector cells within each mouse. 3.5X10^5 cells in PBS were subcutaneously injected into the mammary fad pad of EO771 mice. Tumours were measured every 2-3 days.

- FASTA nucleotide sequence of VEEV Replicon vector with Trastuzumab insert

GTGAACGTCCTACTGACCCGCACGGAGGACCGCATCGTGTGGAAAACACTAGCCGGCGACCCAT
GGATAAAAACACTGACTGCCAAGTACCCTGGGAATTTCACTGCCACGATAGAGGAGTGGCAAGC
AGAGCATGATGCCATCATGAGGCACATCTTGGAGAGACCGGACCCTACCGACGTCTTCCAGAATA
AGGCAAACGTGTGTTGGGCCAAGGCTTTAGTGCCGGTGCTGAAGACCGCTGGCATAGACATGAC
CACTGAACAATGGAACACTGTGGATTATTTTGAAACGGACAAAGCTCACTCAGCAGAGATAGTAT
TGAACCAACTATGCGTGAGGTTCTTTGGACTCGATCTGGACTCCGGTCTATTTTCTGCACCCACTG
TTCCGTTATCCATTAGGAATAATCACTGGGATAACTCCCCGTCGCCTAACATGTACGGGCTGAATA
AAGAAGTGGTCCGTCAGCTCTCTCGCAGGTACCCACAACTGCCTCGGGCAGTTGCCACTGGAAGA
GTCTATGACATGAACACTGGTACACTGCGCAATTATGATCCGCGCATAAACCTAGTACCTGTAAAC
AGAAGACTGCCTCATGCTTTAGTCCTCCACCATAATGAACACCCACAGAGTGACTTTTCTTCATTCG
TCAGCAAATTGAAGGGCAGAACTGTCCTGGTGGTCGGGGAAAAGTTGTCCGTCCCAGGCAAAAT
GGTTGACTGGTTGTCAGACCGGCCTGAGGCTACCTTCAGAGCTCGGCTGGATTTAGGCATCCCAG
GTGATGTGCCCAAATATGACATAATATTTGTTAATGTGAGGACCCCATATAAATACCATCACTATC
AGCAGTGTGAAGACCATGCCATTAAGCTTAGCATGTTGACCAAGAAAGCTTGTCTGCATCTGAAT
CCCGGCGGAACCTGTGTCAGCATAGGTTATGGTTACGCTGACAGGGCCAGCGAAAGCATCATTG
GTGCTATAGCGCGGCAGTTCAAGTTTTCCCGGGTATGCAAACCGAAATCCTCACTTGAAGAGACG
GAAGTTCTGTTTGTATTCATTGGGTACGATCGCAAGGCCCGTACGCACAATTCTTACAAGCTTTCA
TCAACCTTGACCAACATTTATACAGGTTCCAGACTCCACGAAGCCGGATGTGCACCCTCATATCAT
GTGGTGCGAGGGGATATTGCCACGGCCACCGAAGGAGTGATTATAAATGCTGCTAACAGCAAAG
GACAACCTGGCGGAGGGGTGTGCGGAGCGCTGTATAAGAAATTCCCGGAAAGCTTCGATTTACA
GCCGATCGAAGTAGGAAAAGCGCGACTGGTCAAAGGTGCAGCTAAACATATCATTCATGCCGTA
GGACCAAACTTCAACAAAGTTTCGGAGGTTGAAGGTGACAAACAGTTGGCAGAGGCTTATGAGT
CCATCGCTAAGATTGTCAACGATAACAATTACAAGTCAGTAGCGATTCCACTGTTGTCCACCGGCA

TCTTTTCCGGGAACAAAGATCGACTAACCCAATCATTGAACCATTTGCTGACAGCTTTAGACACCA
CTGATGCAGATGTAGCCATATACTGCAGGGACAAGAAATGGGAAATGACTCTCAAGGAAGCAGT
GGCTAGGAGAGAAGCAGTGGAGGAGATATGCATATCCGACGACTCTTCAGTGACAGAACCTGAT
GCAGAGCTGGTGAGGGTGCATCCGAAGAGTTCTTTGGCTGGAAGGAAGGGCTACAGCACAAGC
GATGGCAAAACTTTCTCATATTTGGAAGGGACCAAGTTTCACCAGGCGGCCAAGGATATAGCAGA
AATTAATGCCATGTGGCCCGTTGCAACGGAGGCCAATGAGCAGGTATGCATGTATATCCTCGGAG
AAAGCATGAGCAGTATTAGGTCGAAATGCCCCGTCGAAGAGTCGGAAGCCTCCACACCACCTAGC
ACGCTGCCTTGCTTGTGCATCCATGCCATGACTCCAGAAAGAGTACAGCGCCTAAAAGCCTCACG
TCCAGAACAAATTACTGTGTGCTCATCCTTTCCATTGCCGAAGTATAGAATCACTGGTGTGCAGAA
GATCCAATGCTCCCAGCCTATATTGTTCTCACCGAAAGTGCCTGCGTATATTCATCCAAGGAAGTA
TCTCGTGGAAACACCACCGGTAGACGAGACTCCGGAGCCATCGGCAGAGAACCAATCCACAGAG
GGGACACCTGAACAACCACCACTTATAACCGAGGATGAGACCAGGACTAGAACGCCTGAGCCGA
TCATCATCGAAGAGGAAGAAGAGGATAGCATAAGTTTGCTGTCAGATGGCCCGACCCACCAGGT
GCTGCAAGTCGAGGCAGACATTCACGGGCCGCCCTCTGTATCTAGCTCATCCTGGTCCATTCCTCA
TGCATCCGACTTTGATGTGGACAGTTTATCCATACTTGACACCCTGGAGGGAGCTAGCGTGACCA
GCGGGGCAACGTCAGCCGAGACTAACTCTTACTTCGCAAAGAGTATGGAGTTTCTGGCGCGACC
GGTGCCTGCGCCTCGAACAGTATTCAGGAACCCTCCACATCCCGCTCCGCGCACAAGAACACCGT
CACTTGCACCCAGCAGGGCCTGCTCGAGAACCAGCCTAGTTTCCACCCCGCCAGGCGTGAATAGG
GTGATCACTAGAGAGGAGCTCGAGGCGCTTACCCCGTCACGCACTCCTAGCAGGTCGGTCTCGAG
AACCAGCCTGGTCTCCAACCCGCCAGGCGTAAATAGGGTGATTACAAGAGAGGAGTTTGAGGCG
TTCGTAGCACAACAACAATGACGGTTTGATGCGGGTGCATACATCTTTTCCTCCGACACCGGTCAA
GGGCATTTACAACAAAAATCAGTAAGGCAAACGGTGCTATCCGAAGTGGTGTTGGAGAGGACCG
AATTGGAGATTTCGTATGCCCCGCGCCTCGACCAAGAAAAAGAAGAATTACTACGCAAGAAATTA
CAGTTAAATCCCACACCTGCTAACAGAAGCAGATACCAGTCCAGGAAGGTGGAGAACATGAAAG
CCATAACAGCTAGACGTATTCTGCAAGGCCTAGGGCATTATTTGAAGGCAGAAGGAAAAGTGGA
GTGCTACCGAACCCTGCATCCTGTTCCTTTGTATTCATCTAGTGTGAACCGTGCCTTTTCAAGCCCC
AAGGTCGCAGTGGAAGCCTGTAACGCCATGTTGAAAGAGAACTTTCCGACTGTGGCTTCTTACTG
TATTATTCCAGAGTACGATGCCTATTTGGACATGGTTGACGGAGCTTCATGCTGCTTAGACACTGC
CAGTTTTTGCCCTGCAAAGCTGCGCAGCTTTCCAAAGAAACACTCCTATTTGGAACCCACAATACG
ATCGGCAGTGCCTTCAGCGATCCAGAACACGCTCCAGAACGTCCTGGCAGCTGCCACAAAAAGAA
ATTGCAATGTCACGCAAATGAGAGAATTGCCCGTATTGGATTCGGCGGCCTTTAATGTGGAATGC
TTCAAGAAATATGCGTGTAATAATGAATATTGGGAAACGTTTAAAGAAAACCCCATCAGGCTTAC
TGAAGAAAACGTGGTAAATTACATTACCAAATTAAAAGGACCAAAAGCTGCTGCTCTTTTTGCGA
AGACACATAATTTGAATATGTTGCAGGACATACCAATGGACAGGTTTGTAATGGACTTAAAGAGA
GACGTGAAAGTGACTCCAGGAACAAAACATACTGAAGAACGGCCCAAGGTACAGGTGATCCAGG
CTGCCGATCCGCTAGCAACAGCGTATCTGTGCGGAATCCACCGAGAGCTGGTTAGGAGATTAAAT

GCGGTCCTGCTTCCGAACATTCATACACTGTTTGATATGTCGGCTGAAGACTTTGACGCTATTATA

GCCGAGCACTTCCAGCCTGGGGATTGTGTTCTGGAAACTGACATCGCGTCGTTTGATAAAAGTGA

GGACGACGCCATGGCTCTGACCGCGTTAATGATTCTGGAAGACTTAGGTGTGGACGCAGAGCTG

TTGACGCTGATTGAGGCGGCTTTCGGCGAAATTTCATCAATACATTTGCCCACTAAAACTAAATTT

AAATTCGGAGCCATGATGAAATCTGGAATGTTCCTCACACTGTTTGTGAACACAGTCATTAACATT

GTAATCGCAAGCAGAGTGTTGAGAGAACGGCTAACCGGATCACCATGTGCAGCATTCATTGGAG

ATGACAATATCGTGAAAGGAGTCAAATCGGACAAATTAATGGCAGACAGGTGCGCCACCTGGTT

GAATATGGAAGTCAAGATTATAGATGCTGTGGTGGGCGAGAAAGCGCCTTATTTCTGTGGAGGG

TTTATTTTGTGTGACTCCGTGACCGGCACAGCGTGCCGTGTGGCAGACCCCCTAAAAAGGCTGTTT

AAGCTTGGCAAACCTCTGGCAGCAGACGATGAACATGATGATGACAGGAGAAGGGCATTGCATG

AAGAGTCAACACGCTGGAACCGAGTGGGTATTCTTTCAGAGCTGTGCAAGGCAGTAGAATCAAG

GTATGAAACCGTAGGAACTTCCATCATAGTTATGGCCATGACTACTCTAGCTAGCAGTGTTAAATC

ATTCAGCTACCTGAGAGGGGCCCCTATAACTCTCTACGGCTAACCTGAATGGACTACGACATAGT

CTAGTCCGCCAAGTCTAGCATATG

GCCACCATGTACAGGATGCAACTCCTGTCTTGCATTGCACTAAGTCTTGCACTTGTCACGAATTCG

GAGGTGCAGCTGGTAGAGTCCGGAGGCGGCCTCGTGCAGCCCGGTGGCAGCCTTAGGCTGAGCT

GTGCCGCGAGTGGCTTCAACATCAAAGACACCTACATCCACTGGGTCCGACAAGCCCCTGGGAAG

GGCCTGGAGTGGGTCGCCCGAATCTACCCCACCAACGGCTACACAAGGTACGCTGATAGCGTGA

AGGGGAGGTTTACCATTAGCGCAGACACCAGCAAAAACACCGCATACCTCCAAATGAACAGCTTG

CGAGCGGAGGACACCGCCGTGTACTACTGCAGCCGATGGGGCGGAGACGGCTTCTATGCCATGG

ACTACTGGGGCCAAGGCACACTTGTTACCGTGTCCAGCGCTAGCACCAAGGGCCCATCGGTCTTC

CCCCTGGCACCCTCCTCCAAGAGCACCTCTGGGGGCACAGCGGCCCTGGGCTGCCTGGTCAAGGA

CTACTTCCCCGAACCGGTGACGGTGTCGTGGAACTCAGGCGCCCTGACCAGCGGCGTGCACACCT

TCCCGGCTGTCCTACAGTCCTCAGGACTCTACTCCCTCAGCAGCGTGGTGACCGTGCCCTCCAGCA

GCTTGGGCACCCAGACCTACATCTGCAACGTGAATCACAAGCCCAGCAACACCAAGGTGGACAA

GAAAGTTGAGCCCAAATCTTGTGACAAAACTCACACATGCCCACCGTGCCCAGCACCTGAACTCCT

GGGGGGACCGTCAGTCTTCCTCTTCCCCCCAAAACCCAAGGACACCCTCATGATCTCCCGGACCCC

TGAGGTCACATGCGTGGTGGTGGACGTGAGCCACGAAGACCCTGAGGTCAAGTTCAACTGGTAC

GTGGACGGCGTGGAGGTGCATAATGCCAAGACAAAGCCGCGGGAGGAGCAGTACAACAGCACG

TACCGTGTGGTCAGCGTCCTCACCGTCCTGCACCAGGACTGGCTGAATGGCAAGGAGTACAAGTG

CAAGGTCTCCAACAAAGCCCTCCCAGCCCCCATCGAGAAAACCATCTCCAAAGCCAAAGGGCAGC

CCCGAGAACCACAGGTGTACACCCTGCCCCCATCCCGGGAGGAGATGACCAAGAACCAGGTCAG

CCTGACCTGCCTGGTCAAAGGCTTCTATCCCAGCGACATCGCCGTGGAGTGGGAGAGCAATGGG

CAGCCGGAGAACAACTACAAGACCACGCCTCCCGTGCTGGACTCCGACGGCTCCTTCTTCCTCTAC

AGCAAGCTCACCGTGGACAAGAGCAGGTGGCAGCAGGGGAACGTCTTCTCATGCTCCGTGATGC

ATGAGGCTCTGCACAACCACTACACGCAGAAGAGCCTCTCCCTGTCTCCGGGTAAATGAtctagacc

cctctccctccccccccctaacgttactggccgaagccgcttggaataaggccggtgtgcgtttgtctatatgttattttccaccat
attgccgtcttttggcaatgtgagggcccggaaacctggccctgtcttcttgacgagcattcctaggggtctttcccctctcgccaa
aggaatgcaaggtctgttgaatgtcgtgaaggaagcagttcctctggaagcttcttgaagacaaacaacgtctgtagcgacccctt
tgcaggcagcggaacccccacctggcgacaggtgcctctgcggccaaaagccacgtgtataagatacacctgcaaaggcggc
acaaccccagtgccacgttgtgagttggatagttgtggaaagagtcaaatggctctcctcaagcgtattcaacaaggggctgaa
ggatgcccagaaggtaccccattgtatgggatctgatctggggcctcggtgcacatgctttacatgtgtttagtcgaggttaaaaa
acgtctaggccccccgaaccacggggacgtggttttcctttgaaaaacacgatgataatatggccacaacccaattgGCCACC
ATGTACAGGATGCAACTCCTGTCTTGCATTGCACTAAGTCTTGCACTTGTCACGAATTCGGACATC
CAGATGACCCAGAGTCCCTCTTCCCTGAGCGCCAGCGTGGGGGACAGGGTGACCATAACTTGCA
GGGCGTCTCAAGACGTGAACACCGCCGTGGCCTGGTATCAACAGAAGCCGGGCAAAGCCCCCAA
ACTGCTGATCTATAGCGCCTCCTTCCTCTACAGCGGCGTGCCCTCTAGGTTCAGTGGTAGCCGCAG
CGGCACCGACTTTACCCTTACTATCAGCTCCCTCCAGCCCGAAGACTTCGCCACCTACTACTGCCAA
CAGCACTACACCACCCCCCCTACCTTTGGCCAGGGCACCAAAGTGGAGATCAAGCGTACGGTGGC
TGCACCATCTGTCTTCATCTTCCCGCCATCTGATGAGCAGTTGAAATCTGGAACTGCCTCTGTTGTG
TGCCTGCTGAATAACTTCTATCCCAGAGAGGCCAAAGTACAGTGGAAGGTGGATAACGCCCTCCA
ATCGGGTAACTCCCAGGAGAGTGTCACAGAGCAGGACAGCAAGGACAGCACCTACAGCCTCAGC
AGCACCCTGACGCTGAGCAAAGCAGACTACGAGAAACACAAAGTCTACGCCTGCGAAGTCACCC
ATCAGGGCCTGAGCTCGCCCGTCACAAAGAGCTTCAACAGGGGAGAGTGTTAG
GCGGCCGCGAATTGGCAAGCTGCTTACATAGAACTCGCGGCGATTGGCATGCCGCCTTAAAATTT
TTATTTTATTTTTCTTTTCTTTTCCGAATCGGATTTTGTTTTTAATATTTCAAAAAAAAAAAAAAAAA
AAAAAAAAAAAAAAAAAACGCGTCGAGGGGAATTAATTCTTGAAGACGAAAGGGCCAGGTGGC
ACTTTTCGGGGAAATGTGCGCGGAACCCCTATTTGTTTATTTTTCTAAATACATTCAAATATGTATC
CGCTCATGAGACAATAACCCTGATAAATGCTTCAATAATATTGAAAAAGGAAGAGTATGAGTATT
CAACATTTCCGTGTCGCCCTTATTCCCTTTTTTGCGGCATTTTGCCTTCCTGTTTTTGCTCACCCAGA
AACGCTGGTGAAAGTAAAAGATGCTGAAGATCAGTTGGGTGCACGAGTGGGTTACATCGAACTG
GATCTCAACAGCGGTAAGATCCTTGAGAGTTTTCGCCCCGAAGAACGTTTTCCAATGATGAGCAC
TTTTAAAGTTCTGCTATGTGGCGCGGTATTATCCCGTGTTGACGCCGGGCAAGAGCAACTCGGTC
GCCGCATACACTATTCTCAGAATGACTTGGTTGAGTACTCACCAGTCACAGAAAAGCATCTTACGG
ATGGCATGACAGTAAGAGAATTATGCAGTGCTGCCATAACCATGAGTGATAACACTGCGGCCAAC
TTACTTCTGACAACGATCGGAGGACCGAAGGAGCTAACCGCTTTTTTGCACAACATGGGGGATCA
TGTAACTCGCCTTGATCGTTGGGAACCGGAGCTGAATGAAGCCATACCAAACGACGAGCGTGAC
ACCACGATGCCTGTAGCAATGGCAACAACGTTGCGCAAACTATTAACTGGCGAACTACTTACTCTA
GCTTCCCGGCAACAATTAATAGACTGGATGGAGGCGGATAAAGTTGCAGGACCACTTCTGCGCTC
GGCCCTTCCGGCTGGCTGGTTTATTGCTGATAAATCTGGAGCCGGTGAGCGTGGGTCTCGCGGTA
TCATTGCAGCACTGGGGCCAGATGGTAAGCCCTCCCGTATCGTAGTTATCTACACGACGGGGAGT
CAGGCAACTATGGATGAACGAAATAGACAGATCGCTGAGATAGGTGCCTCACTGATTAAGCATT

GGTAACTGTCAGACCAAGTTTACTCATATATACTTTAGATTGATTTAAAACTTCATTTTTAATTTAA

AAGGATCTAGGTGAAGATCCTTTTTGATAATCTCATGACCAAAATCCCTTAACGTGAGTTTTCGTT

CCACTGAGCGTCAGACCCCGTAGAAAAGATCAAAGGATCTTCTTGAGATCCTTTTTTTCTGCGCGT

AATCTGCTGCTTGCAAACAAAAAAACCACCGCTACCAGCGGTGGTTTGTTTGCCGGATCAAGAGC

TACCAACTCTTTTTCCGAAGGTAACTGGCTTCAGCAGAGCGCAGATACCAAATACTGTCCTTCTAG

TGTAGCCGTAGTTAGGCCACCACTTCAAGAACTCTGTAGCACCGCCTACATACCTCGCTCTGCTAA

TCCTGTTACCAGTGGCTGCTGCCAGTGGCGATAAGTCGTGTCTTACCGGGTTGGACTCAAGACGA

TAGTTACCGGATAAGGCGCAGCGGTCGGGCTGAACGGGGGGTTCGTGCACACAGCCCAGCTTGG

AGCGAACGACCTACACCGAACTGAGATACCTACAGCGTGAGCATTGAGAAAGCGCCACGCTTCCC

GAAGGGAGAAAGGCGGACAGGTATCCGGTAAGCGGCAGGGTCGGAACAGGAGAGCGCACGAG

GGAGCTTCCAGGGGGAAACGCCTGGTATCTTTATAGTCCTGTCGGGTTTCGCCACCTCTGACTTG

AGCGTCGATTTTTGTGATGCTCGTCAGGGGGGCGGAGCCTATGGAAAAACGCCAGCAACGCGAG

CTCTAATACGACTCACTATAGATGGGCGGCGCATGAGAGAAGCCCAGACCAATTACCTACCCAAA

ATGGAGAAAGTTCACGTTGACATCGAGGAAGACAGCCCATTCCTCAGAGCTTTGCAGCGGAGCTT

CCCGCAGTTTGAGGTAGAAGCCAAGCAGGTCACTGATAATGACCATGCTAATGCCAGAGCGTTTT

CGCATCTGGCTTCAAAACTGATCGAAACGGAGGTGGACCCATCCGACACGATCCTTGACATTGGA

AGTGCGCCCGCCCGCAGAATGTATTCTAAGCACAAGTATCATTGTATCTGTCCGATGAGATGTGC

GGAAGATCCGGACAGATTGTATAAGTATGCAACTAAGCTGAAGAAAAACTGTAAGGAAATAACT

GATAAGGAATTGGACAAGAAAATGAAGGAGCTGGCCGCCGTCATGAGCGACCCTGACCTGGAAA

CTGAGACTATGTGCCTCCACGACGACGAGTCGTGTCGCTACGAAGGGCAAGTCGCTGTTTACCAG

GATGTATACGCGGTTGACGGACCGACAAGTCTCTATCACCAAGCCAATAAGGGAGTTAGAGTCG

CCTACTGGATAGGCTTTGACACCACCCCTTTTATGTTTAAGAACTTGGCTGGAGCATATCCATCAT

ACTCTACCAACTGGGCCGACGAAACCGTGTTAACGGCTCGTAACATAGGCCTATGCAGCTCTGAC

GTTATGGAGCGGTCACGTAGAGGGATGTCCATTCTTAGAAAGAAGTATTTGAAACCATCCAACAA

TGTTCTATTCTCTGTTGGCTCGACCATCTACCACGAGAAGAGGGACTTACTGAGGAGCTGGCACCT

GCCGTCTGTATTTCACTTACGTGGCAAGCAAAATTACACATGTCGGTGTGAGACTATAGTTAGTTG

CGACGGGTACGTCGTTAAAAGAATAGCTATCAGTCCAGGCCTGTATGGGAAGCCTTCAGGCTATG

CTGCTACGATGCACCGCGAGGGATTCTTGTGCTGCAAAGTGACAGACACATTGAACGGGGAGAG

GGTCTCTTTTCCCGTGTGCACGTATGTGCCAGCTACATTGTGTGACCAAATGACTGGCATACTGGC

AACAGATGTCAGTGCGGACGACGCGCAAAAACTGCTGGTTGGGCTCAACCAGCGTATAGTCGTC

AACGGTCGCACCCAGAGAAACACCAATACCATGAAAAATTACCTTTTGCCCGTAGTGGCCCAGGC

ATTTGCTAGGTGGGCAAAGGAATATAAGGAAGATCAAGAAGATGAAAGGCCACTAGGACTACGA

GATAGACAGTTAGTCATGGGGTGTTGTTGGGCTTTTAGAAGGCACAAGATAACATCTATTTATAA

GCGCCCGGATACCCAAACCATCATCAAAGTGAACAGCGATTTCCACTCATTCGTGCTGCCCAGGA

TAGGCAGTAACACATTGGAGATCGGGCTGAGAACAAGAATCAGGAAAATGTTAGAGGAGCACA

AGGAGCCGTCACCTCTCATTACCGCCGAGGACGTACAAGAAGCTAAGTGCGCAGCCGATGAGGC

TAAGGAGGTGCGTGAAGCCGAGGAGTTGCGCGCAGCTCTACCACCTTTGGCAGCTGATGTTGAG
GAGCCCACTCTGGAAGCCGATGTCGACTTGATGTTACAAGAGGCTGGGGCCGGCTCAGTGGAGA
CACCTCGTGGCTTGATAAAGGTTACCAGCTACGATGGCGAGGACAAGATCGGCTCTTACGCTGTG
CTTTCTCCGCAGGCTGTACTCAAGAGTGAAAAATTATCTTGCATCCACCCTCTCGCTGAACAAGTC
ATAGTGATAACACACTCTGGCCGAAAAGGGCGTTATGCCGTGGAACCATACCATGGTAAAGTAGT
GGTGCCAGAGGGACATGCAATACCCGTCCAGGACTTTCAAGCTCTGAGTGAAAGTGCCACCATTG
TGTACAACGAACGTGAGTTCGTAAACAGGTACCTGCACCATATTGCCACACATGGAGGAGCGCTG
AACACTGATGAAGAATATTACAAAACTGTCAAGCCCAGCGAGCACGACGGCGAATACCTGTACG
ACATCGACAGGAAACAGTGCGTCAAGAAAGAACTAGTCACTGGGCTAGGGCTCACAGGCGAGCT
GGTGGATCCTCCCTTCCATGAATTCGCCTACGAGAGTCTGAGAACACGACCAGCCGCTCCTTACCA
AGTACCAACCATAGGGGTGTATGGCGTGCCAGGATCAGGCAAGTCTGGCATCATTAAAAGCGCA
GTCACCAAAAAAGATCTAGTGGTGAGCGCCAAGAAAGAAAACTGTGCAGAAATTATAAGGGACG
TCAAGAAAATGAAAGGGCTGGACGTCAATGCCAGAACTGTGGACTCAGTGCTCTTGAATGGATG
CAAACACCCCGTAGAGACCCTGTATATTGACGAAGCTTTTGCTTGTCATGCAGGTACTCTCAGAGC
GCTCATAGCCATTATAAGACCTAAAAAGGCAGTGCTCTGCGGGGATCCCAAACAGTGCGGTTTTT
TTAACATGATGTGCCTGAAAGTGCATTTTAACCACGAGATTTGCACACAAGTCTTCCACAAAAGCA
TCTCTCGCCGTTGCACTAAATCTGTGACTTCGGTCGTCTCAACCTTGTTTTACGACAAAAAAATGA
GAACGACGAATCCGAAAGAGACTAAGATTGTGATTGACACTACCGGCAGTACCAAACCTAAGCA
GGACGATCTCATTCTCACTTGTTTCAGAGGGTGGGTGAAGCAGTTGCAAATAGATTACAAAGGCA
ACGAAATAATGACGGCAGCTGCCTCTCAAGGGCTGACCCGTAAAGGTGTGTATGCCGTTCGGTAC
AAGGTGAATGAAAATCCTCTGTACGCACCCACCTCAGAACAT

Appendix 12: Nucleotide FASTA sequence of Replicon VEEV vector with Trastuzumab insert. MluI restriction sites for insertion of Trastuzumab sequence in red. Trastuzumab insert comprised of heavy chain and light chain domains, separated by IRES sequence.

- FASTA sequence of Trastuzumab heavy chain in pFuse2SS vector for 2G12-Hn constructs

GGATCTGCGATCGCTCCGGTGCCCGTCAGTGGGCAGAGCGCACATCGCCCACAGTCCCCGAGAAGTTGGG
GGGAGGGGTCGGCAATTGAACGGGTGCCTAGAGAAGGTGGCGCGGGGTAAACTGGGAAAGTGATGTCG
TGTACTGGCTCCGCCTTTTTCCCGAGGGTGGGGGAGAACCGTATATAAGTGCAGTAGTCGCCGTGAACGTT
CTTTTTCGCAACGGGTTTGCCGCCAGAACACAGCTGAAGCTTCGAGGGGCTCGCATCTCTCCTTCACGCGCC
CGCCGCCCTACCTGAGGCCGCCATCCACGCCGGTTGAGTCGCGTTCTGCCGCCTCCCGCCTGTGGTGCCTCC
TGAACTGCGTCCGCCGTCTAGGTAAGTTTAAAGCTCAGGTCGAGACCGGGCCTTTGTCCGGCGCTCCCTTG
GAGCCTACCTAGACTCAGCCGGCTCTCCACGCTTTGCCTGACCCTGCTTGCTCAACTCTACGTCTTTGTTTCG
TTTTCTGTTCTGCGCCGTTACAGATCCAAGCTGTGACCGGCGCCTACCTGAGATCAccggcGAAGGAGGGCC

ACCATGTACAGGATGCAACTCCTGTCTTGCATTGCACTAAGTCTTGCACTTGTCACGAATTCGGAGGTGCAG
CTGGTAGAGTCCGGAGGCGGCCTCGTGCAGCCCGGTGGCAGCCTTAGGCTGAGCTGTGCCGCGAGTGGCT
TCAACATCAAAGACACCTACATCCACTGGGTCCGACAAGCCCCTGGGAAGGGCCTGGAGTGGGTCGCCCG
AATCTACCCCACCAACGGCTACACAAGGTACGCTGATAGCGTGAAGGGGAGGTTTACCATTAGCGCAGAC
ACCAGCAAAAACACCGCATACCTCCAAATGAACAGCTTGCGAGCGGAGGACACCGCCGTGTACTACTGCA
GCCGATGGGGCGGAGACGGCTTCTATGCCATGGACTACTGGGGCCAAGGCACACTTGTTACCGTGTCCAG
CGCTAGCACCAAGGGCCCATCGGTCTTCCCCCTGGCACCCTCCTCCAAGAGCACCTCTGGGGGCACAGCGG
CCCTGGGCTGCCTGGTCAAGGACTACTTCCCCGAACCGGTGACGGTGTCGTGGAACTCAGGCGCCCTGACC
AGCGGCGTGCACACCTTCCCGGCTGTCCTACAGTCCTCAGGACTCTACTCCCTCAGCAGCGTGGTGACCGT
GCCCTCCAGCAGCTTGGGCACCCAGACCTACATCTGCAACGTGAATCACAAGCCCAGCAACACCAAGGTGG
ACAAGAAAGTTGAGCCCAAATCTTGTGACAAAACTCACACATGCCCACCGTGCCCAGCACCTGAACTCCTG
GGGGGACCGTCAGTCTTCCTCTTCCCCCCAAAACCCAAGGACACCCTCATGATCTCCCGGACCCCTGAGGTC
ACATGCGTGGTGGTGGACGTGAGCCACGAAGACCCTGAGGTCAAGTTCAACTGGTACGTGGACGGCGTG
GAGGTGCATAATGCCAAGACAAAGCCGCGGGAGGAGCAGTACAACAGCACGTACCGTGTGGTCAGCGTC
CTCACCGTCCTGCACCAGGACTGGCTGAATGGCAAGGAGTACAAGTGCAAGGTCTCCAACAAAGCCCTCCC
AGCCCCCATCGAGAAAACCATCTCCAAAGCCAAAGGGCAGCCCCGAGAACCACAGGTGTACACCCTGCCC
CCATCCCGGGAGGAGATGACCAAGAACCAGGTCAGCCTGACCTGCCTGGTCAAAGGCTTCTATCCCAGCG
ACATCGCCGTGGAGTGGGAGAGCAATGGGCAGCCGGAGAACAACTACAAGACCACGCCTCCCGTGCTGG
ACTCCGACGGCTCCTTCTTCCTCTACAGCAAGCTCACCGTGGACAAGAGCAGGTGGCAGCAGGGGAACGT
CTTCTCATGCTCCGTGATGCATGAGGCTCTGCACAACCACTACACGCAGAAGAGCCTCTCCCTGTCTCCGGG
TAAATGAGTCCTAGCTGGCCAGACATGATAAGATACATTGATGAGTTTGGACAAACCACAACTAGAATGCA
GTGAAAAAAATGCTTTATTTGTGAAATTTGTGATGCTATTGCTTTATTTGTAACCATTATAAGCTGCAATAAA
CAAGTTAACAACAACAATTGCATTCATTTTATGTTTCAGGTTCAGGGGGAGGTGTGGGAGGTTTTTTAAAG
CAAGTAAAACCTCTACAAATGTGGTATGGAATTAATTCTAAAATACAGCATAGCAAAACTTTAACCTCCAAA
TCAAGCCTCTACTTGAATCCTTTTCTGAGGGATGAATAAGGCATAGGCATCAGGGGCTGTTGCCAATGTGC
ATTAGCTGTTTGCAGCCTCACCTTCTTTCATGGAGTTTAAGATATAGTGTATTTTCCCAAGGTTTGAACTAGC
TCTTCATTTCTTTATGTTTTAAATGCACTGACCTCCCACATTCCCTTTTTAGTAAAATATTCAGAAATAATTTA
AATACATCATTGCAATGAAAATAAATGTTTTTTATTAGGCAGAATCCAGATGCTCAAGGCCCTTCATAATAT
CCCCCAGTTTAGTAGTTGGACTTAGGGAACAAAGGAACCTTTAATAGAAATTGGACAGCAAGAAAGCGAG
CTTCTAGCTTATCCTCAGTCCTGCTCCTCTGCCACAAAGTGCACGCAGTTGCCGGCCGGGTCGCGCAGGGC
GAACTCCCGCCCCCACGGCTGCTCGCCGATCTCGGTCATGGCCGGCCCGGAGGCGTCCCGGAAGTTCGTG
GACACGACCTCCGACCACTCGGCGTACAGCTCGTCCAGGCCGCGCACCCACACCCAGGCCAGGGTGTTGTC
CGGCACCACCTGGTCCTGGACCGCGCTGATGAACAGGGTCACGTCGTCCCGGACCACACCGGCGAAGTCG
TCCTCCACGAAGTCCCGGGAGAACCCGAGCCGGTCGGTCCAGAACTCGACCGCTCCGGCGACGTCGCGCG
CGGTGAGCACCGGAACGGCACTGGTCAACTTGGCCATGATGGCTCCTCctgtcaggagaggaaagagaagaaggtt
agtacaattgCTATAGTGAGTTGTATTATACTATGCAGATATACTATGCCAATGATTAATTGTCAAACTAGGGC

TGCAgggttcatagtgccacttttcctgcactgccccatctcctgcccacccctttcccaggcatagacagtcagtgacttacCAAACTCAC
AGGAGGGAGAAGGCAGAAGCTTGAGACAGACCCGCGGGACCGCCGAACTGCGAGGGGACGTGGCTAGG
GCGGCTTCTTTTATGGTGCGCCGGCCCTCGGAGGCAGGGCGCTCGGGGAGGCCTAGCGGCCAATCTGCGG
TGGCAGGAGGCGGGGCCGAAGGCCGTGCCTGACCAATCCGGAGCACATAGGAGTCTCAGCCCCCCGCCCC
AAAGCAAGGGGAAGTCACGCGCCTGTAGCGCCAGCGTGTTGTGAAATGGGGGCTTGGGGGGGTTGGGG
CCCTGACTAGTCAAAACAAACTCCCATTGACGTCAATGGGGTGGAGACTTGGAAATCCCCGTGAGTCAAAC
CGCTATCCACGCCCATTGATGTACTGCCAAAACCGCATCATCATGGTAATAGCGATGACTAATACGTAGAT
GTACTGCCAAGTAGGAAAGTCCCATAAGGTCATGTACTGGGCATAATGCCAGGCGGGCCATTTACCGTCAT
TGACGTCAATAGGGGGCGTACTTGGCATATGATACACTTGATGTACTGCCAAGTGGGCAGTTTACCGTAAA
TACTCCACCCATTGACGTCAATGGAAAGTCCCTATTGGCGTTACTATGGGAACATACGTCATTATTGACGTC
AATGGGCGGGGGTCGTTGGGCGGTCAGCCAGGCGGGCCATTTACCGTAAGTTATGTAACGCCTGCAGGTT
AATTAAGAACATGTGAGCAAAAGGCCAGCAAAAGGCCAGGAACCGTAAAAAGGCCGCGTTGCTGGCGTTT
TTCCATAGGCTCCGCCCCCCTGACGAGCATCACAAAAATCGACGCTCAAGTCAGAGGTGGCGAAACCCGAC
AGGACTATAAAGATACCAGGCGTTTCCCCCTGGAAGCTCCCTCGTGCGCTCTCCTGTTCCGACCCTGCCGCT
TACCGGATACCTGTCCGCCTTTCTCCCTTCGGGAAGCGTGGCGCTTTCTCATAGCTCACGCTGTAGGTATCT
CAGTTCGGTGTAGGTCGTTCGCTCCAAGCTGGGCTGTGTGCACGAACCCCCCGTTCAGCCCGACCGCTGCG
CCTTATCCGGTAACTATCGTCTTGAGTCCAACCCGGTAAGACACGACTTATCGCCACTGGCAGCAGCCACTG
GTAACAGGATTAGCAGAGCGAGGTATGTAGGCGGTGCTACAGAGTTCTTGAAGTGGTGGCCTAACTACGG
CTACACTAGAAGAACAGTATTTGGTATCTGCGCTCTGCTGAAGCCAGTTACCTTCGGAAAAAGAGTTGGTA
GCTCTTGATCCGGCAAACAAACCACCGCTGGTAGCGGTGGTTTTTTTGTTTGCAAGCAGCAGATTACGCGC
AGAAAAAAAGGATCTCAAGAAGATCCTTTGATCTTTTCTACGGGGTCTGACGCTCAGTGGAACGAAAACTC
ACGTTAAGGGATTTTGGTCATGGCTAGTTAATTAACATTTAAATCAGCGGCCGCAATAAAATATCTTTATTT
TCATTACATCTGTGTGTTGGTTTTTTGTGTGAATCGTAACTAACATACGCTCTCCATCAAAACAAAACGAAAC
AAAACAAACTAGCAAAATAGGCTGTCCCCAGTGCAAGTGCAGGTGCCAGAACATTTCTCTATCGAA

Appendix 13: Nucleotide FASTA sequence of pFuse2SS vector with Trastuzumab heavy chain insert (blue). EcoRI and AgeI restriction sites for insertion of Trastuzumab heavy chain sequence in red.

- FASTA sequence of 2G12-Hn 1 light chain in pFuse2SS vector for 2G12-Hn 1 construct

ggatctgcgatcgctccggtgcccgtcagtgggcagagcgcacatcgcccacagtccccgagaagttgggggggaggggtcggcaatt
gaacgggtgcctagagaaggtggcgcggggtaaactgggaaagtgatgtcgtgtactggctccgccttttttcccgagggtgggggag
aaccgtatataagtgcagtagtcgccgtgaacgttctttttcgcaacgggtttgccgccagaacacagctgaagcttcgaggggctcgc
atctctccttcacgcgcccgccgccctacctgaggccgccatccacgccggttgagtcgcgttctgccgcctcccgcctgtggtgcctcct
gaactgcgtccgccgtctaggtaagtttaaagctcaggtcgagaccgggcctttgtccggcgctcccttggagcctacctagactcagc

cggctctccacgctttgcctgaccctgcttgctcaactctacgtctttgtttcgttttctgttctgcgccgttacagatccaagctgtgaccg

gcgcctacctgagatcaacatgtacaggatgcaactcctgtcttgcattgcactaagtcttgcacttgtcacgaattcGGATGTGGT

GATGACCCAGTCTCCATCCACCCTGAGCGCCAGCGTGGGCGATACAATCACAATTACCTGTAG

AGCCTCACAGAGCATCGAGACATGGCTGGCCTGGTACCAGCAGAAGCCCGGCAAGGCACCAAA

GCTGCTGATCTACAAGGCTTCTACCCTGAAAACCGGCGTGCCTAGCCGGTTCAGCGGTTCTGG

CAGCGGCACAGAGTTCACCCTGACAATCAGCGGTCTTCAATTTGACGACTTCGCCACATACCA

CTGTCAGCATTACGCCGGATATAGCGCCACCTTCGGCCAAGGCACCCGGGTGGAAATCAAGCG

GACCGTGGCCGCTCCTTCCGTTTTCATCTTCCCTCCTTCCGACGAGCAGCTCAAGTCTGGCAC

CGCCTCAGTGGTGTGCCTGCTGAACAACTTCTACCCCAGAGAGGCCAAGGTCCAGTGGAAGGT

GGACAACGCCCTGCAGAGCGGCAATTCCCAGGAGAGCGTGACTGAACAGGACAGCAAGGACAG

CACATACTCCCTGAGCAGCACCCTGACCCTGTCCAAGGCCGACTACGAGAAGCACAAGGTGTA

CGCTTGTGAAGTGACCCACCAGGGCCTGAGCAGCCCTGTGACAAAGAGCTTCAATAGAGGCGA

GTGCGGCGGCGGCGGCTCTGGCGGCGGCGGCAGCGGCGGCGGCGGCAGTGAAGTGCAGCTGGT

GGAAAGCGGCGGCGGCCTGGTGCAGCCTGGAGGCTCCCTGAGACTGAGCTGCGCCGCTTCCGG

GTTTAACATCAAAGACACCTACATTCACTGGGTCAGACAGGCCCCTGGCAAAGGCCTGGAATG

GGTTGCTAGAATCTATCCTACCAACGGCTACACCAGATACGCCGACTCTGTGAAGGGCAGATT

TACCATCTCTGCTGATACCAGCAAAAACACCGCCTACCTGCAGATGAACAGCCTGCGGGCCGA

GGATACCGCTGTGTACTACTGCAGCAGATGGGGAGGCGACGGCTTCTACGCCATGGACTACTG

GGGCCAGGGCACCCTCGTGACAGTGTCCTCCGGAGGCGGCGGAAGCGGAGGAGGAGGAAGCGG

CGGCGGAGGTAGCGATATCCAGATGACACAGAGCCCCAGCAGCCTGTCTGCCAGCGTGGGCGA

CAGAGTGACCATCACCTGCAGGGCCAGCCAAGACGTGAACACCGCCGTCGCCTGGTATCAGCA

GAAACCTGGCAAGGCCCCTAAGCTGCTGATCTACTCCGCCAGCTTCCTGTACAGCGGAGTGCC

CTCTCGGTTCAGCGGCTCCCGCAGCGGCACTGATTTTACCCTGACAATCAGCGCCTGCAGCCC

GAGGACTTCGCCACCTACTACTGCCAGCAACACTACACAACACCTCCAACATTCGGCCAGGGA

ACCAAGGTAGAGATCAAGTAGAGGGAgctagctggccagacatgataagatacattgatgagtttggacaaaccacaa

ctagaatgcagtgaaaaaaatgctttatttgtgaaatttgtgatgctattgctttatttgtaaccattataagctgcaataaacaagttaa

caacaacaattgcattcattttatgtttcaggttcaggggggaggtgtgggaggttttttaaagcaagtaaaacctctacaaatgtggtat

ggaattaattctaaaatacagcatagcaaaactttaacctccaaatcaagcctctacttgaatccttttctgagggatgaataaggcat

aggcatcaggggctgttgccaatgtgcattagctgtttgcagcctcaccttctttcatggagtttaagatatagtgtattttcccaaggttt

gaactagctcttcatttctttatgttttaaatgcactgacctcccacattccctttttagtaaaatattcagaaataatttaaatacatcatt

gcaatgaaaataaatgtttttttattaggcagaatccagatgctcaaggcccttcataatatcccccagtttagtagttggacttagggaa

caaaggaacctttaatagaaattggacagcaagaaagcgagcttctagctttagttcctggtgtacttgaggggatgagttcctcaat

ggtggttttgaccagcttgccattcatctcaatgagcacaaagcagtcaggagcatagtcagagatgagctctctgcacatgccacag

gggctgaccaccctgatggatctgtccacctcatcagagtaggggtgcctgacagccacaatggtgtcaaagtccttctgcccgttgct

cacagcagacccaatggcaatggcttcagcacagacagtgaccctgccaatgtaggcctcaatgtggacagcagagatgatctcccc

agtcttggtcctgatggccgccccgacatggtgcttgttgtcctcatagagcatggtgatcttctcagtggcgacctccaccagctccag

atcctgctgagagatgttgaaggtcttcatgatggctcctcctgtcaggagaggaaagagaagaaggttagtacaattgctatagtga

gttgtattatactatgcttatgattaattgtcaaactagggctgcagggttcatagtgccacttttcctgcactgccccatctcctgcccac
cctttcccaggcatagacagtcagtgacttaccaaactcacaggagggagaaggcagaagcttgagacagacccgcgggaccgccg
aactgcgaggggacgtggctagggcggcttcttttatggtgcgccggccctcggaggcagggcgctcggggaggcctagcggccaat
ctgcggtggcaggaggcggggccgaaggccgtgcctgaccaatccggagcacataggagtctcagccccccgccccaaagcaaggg
gaagtcacgcgcctgtagcgccagcgtgttgtgaaatgggggcttgggggggttggggccctgactagtcaaaacaaactcccattga
cgtcaatggggtggagacttggaaatccccgtgagtcaaaccgctatccacgcccattgatgtactgccaaaaccgcatcatcatggt
aatagcgatgactaatacgtagatgtactgccaagtaggaaagtcccataaggtcatgtactgggcataatgccaggcgggccattta
ccgtcattgacgtcaataggggggcgtacttggcatatgatacacttgatgtactgccaagtgggcagtttaccgtaaatactccacccat
tgacgtcaatggaaagtccctattggcgttactatgggaacatacgtcattattgacgtcaatgggcgggggtcgttgggcggtcagcc
aggcgggccatttaccgtaagttatgtaacgcctgcaggttaattaagaacatgtgagcaaaaggccagcaaaaggccaggaaccgt
aaaaaggccgcgttgctggcgtttttccataggctccgccccccctgacgagcatcacaaaaatcgacgctcaagtcagaggtggcgaa
acccgacaggactataaagataccaggcgtttccccctggaagctccctcgtgcgctctcctgttccgaccctgccgcttaccggatacc
tgtccgcctttctcccttcgggaagcgtggcgctttctcatagctcacgctgtaggtatctcagttcggtgtaggtcgttcgctccaagctg
ggctgtgtgcacgaaccccccgttcagcccgaccgctgcgccttatccggtaactatcgtcttgagtccaacccggtaagacacgactt
atcgccactggcagcagccactggtaacaggattagcagagcgaggtatgtaggcggtgctacagagttcttgaagtggtggcctaac
tacggctacactagaagaacagtatttggtatctgcgctctgctgaagccagttaccttcggaaaaagagttggtagctcttgatccgg
caaacaaaccaccgctggtagcggtggtttttttgtttgcaagcagcagattacgcgcagaaaaaaggatctcaagaagatcctttg
atcttttctacggggtctgacgctcagtggaacgaaaactcacgttaagggattttggtcatggctagttaattaacatttaaatcagcg
gccgcaataaaatatctttatttttcattacatctgtgtgttggttttttgtgtgaatcgtaactaacatacgctctccatcaaaacaaaacg
aaacaaaacaaactagcaaaataggctgtccccagtgcaagtgcaggtgccagaacatttctctatcgaa

Appendix 14: Nucleotide FASTA sequence of pFuse2SS vector with 2G12-Hn 1 light chain insert. EcoRI and NheI restriction sites for insertion in red. 2G12 light chain in blue. Flexible linker in green. Trastuzumab variable heavy and light chain domains in pink and purple, respectively.

- FASTA sequence of 2G12-Hn 2 light chain in pFuse2SS vector for 2G12-Hn 2 construct

GGATCTGCGATCGCTCCGGTGCCCGTCAGTGGGCAGAGCGCACATCGCCCACAGTCCCCGAGAAGTTGGG
GGGAGGGGTCGGCAATTGAACGGGTGCCTAGAGAAGGTGGCGCGGGGTAAACTGGGAAAGTGATGTCG
TGTACTGGCTCCGCCTTTTTCCCGAGGGTGGGGGAGAACCGTATATAAGTGCAGTAGTCGCCGTGAACGTT
CTTTTTCGCAACGGGTTTGCCGCCAGAACACAGCTGAAGCTTCGAGGGGCTCGCATCTCTCCTTCACGCGCC
CGCCGCCCTACCTGAGGCCGCCATCCACGCCGGTTGAGTCGCGTTCTGCCGCCTCCCGCCTGTGGTGCCTCC
TGAACTGCGTCCGCCGTCTAGGTAAGTTTAAAGCTCAGGTCGAGACCGGGCCTTTGTCCGGCGCTCCCTTG
GAGCCTACCTAGACTCAGCCGGCTCTCCACGCTTTGCCTGACCCTGCTTGCTCAACTCTACGTCTTTGTTTCG
TTTTCTGTTCTGCGCCGTTACAGATCCAAGCTGTGACCGGCGCCTACCTGAGATCAccggcGAAGGAGGGCC

ACCATGTACAGGATGCAACTCCTGTCTTGCATTGCACTAAGTCTTGCACTTGTCACgaattcGGATATCCAGAT
GACACAGAGCCCCAGCAGCCTGTCTGCCAGCGTGGGCGACAGAGTGACCATCACCTGCAGGGCCAGCCAA
GACGTGAACACCGCCGTCGCCTGGTATCAGCAGAAACCTGGCAAGGCCCCTAAGCTGCTGATCTACTCCGC
CAGCTTCCTGTACAGCGGAGTGCCCTCTCGGTTCAGCGGCTCCCGCAGCGGCACTGATTTTACCCTGACAAT
CAGCAGCCTGCAGCCCGAGGACTTCGCCACCTACTACTGCCAGCAACACTACACAACACCTCCAACATTCG
GCCAGGGAACCAAGGTAGAGATCAAGGGCGGCGGCGGCTCTGGCGGCGGCGGCAGCGGCGGCGGCGGC
AGTGAAGTGCAGCTGGTGGAAAGCGGCGGCGGCCTGGTGCAGCCTGGAGGCTCCCTGAGACTGAGCTGC
GCCGCTTCCGGGTTTAACATCAAAGACACCTACATTCACTGGGTCAGACAGGCCCCTGGCAAAGGCCTGGA
ATGGGTTGCTAGAATCTATCCTACCAACGGCTACACCAGATACGCCGACTCTGTGAAGGGCAGATTTACCA
TCTCTGCTGATACCAGCAAAAACACCGCCTACCTGCAGATGAACAGCCTGCGGGCCGAGGATACCGCTGTG
TACTACTGCAGCAGATGGGGAGGCGACGGCTTCTACGCCATGGACTACTGGGGCCAGGGCACCCTCGTGA
CAGTGTCCTCCGGCGGCGGCGGCTCTGGCGGCGGCGGCAGCGGCGGCGGCGGCAGTGATGTGGTGATGA
CCCAGTCTCCATCCACCCTGAGCGCCAGCGTGGGCGATACAATCACAATTACCTGTAGAGCCTCACAGAGC
ATCGAGACATGGCTGGCCTGGTACCAGCAGAAGCCCGGCAAGGCACCAAAGCTGCTGATCTACAAGGCTT
CTACCCTGAAAACCGGCGTGCCTAGCCGGTTCAGCGGTTCTGGCAGCGGCACAGAGTTCACCCTGACAATC
AGCGGTCTTCAATTTGACGACTTCGCCACATACCACTGTCAGCATTACGCCGGATATAGCGCCACCTTCGGC
CAAGGCACCCGGGTGGAAATCAAGCGGACCGTGGCCGCTCCTTCCGTTTTCATCTTCCCTCCTTCCGACGA
GCAGCTCAAGTCTGGCACCGCCTCAGTGGTGTGCCTGCTGAACAACTTCTACCCCAGAGAGGCCAAGGTCC
AGTGGAAGGTGGACAACGCCCTGCAGAGCGGCAATTCCCAGGAGAGCGTGACTGAACAGGACAGCAAGG
ACAGCACATACTCCCTGAGCAGCACCCTGACCCTGTCCAAGGCCGACTACGAGAAGCACAAGGTGTACGCT
TGTGAAGTGACCCACCAGGGCCTGAGCAGCCCTGTGACAAAGAGCTTCAATAGAGGCGAGTGCtagAGGG
AgctagcTGGCCAGACATGATAAGATACATTGATGAGTTTGGACAAACCACAACTAGAATGCAGTGAAAAAA
ATGCTTTATTTGTGAAATTTGTGATGCTATTGCTTTATTTGTAACCATTATAAGCTGCAATAAACAAGTTAAC
AACAACAATTGCATTCATTTTATGTTTCAGGTTCAGGGGGAGGTGTGGGAGGTTTTTTAAAGCAAGTAAAA
CCTCTACAAATGTGGTATGGAATTAATTCTAAAATACAGCATAGCAAAACTTTAACCTCCAAATCAAGCCTC
TACTTGAATCCTTTTCTGAGGGATGAATAAGGCATAGGCATCAGGGGCTGTTGCCAATGTGCATTAGCTGT
TTGCAGCCTCACCTTCTTTCATGGAGTTTAAGATATAGTGTATTTTCCCAAGGTTTGAACTAGCTCTTCATTT
CTTTATGTTTTAAATGCACTGACCTCCCACATTCCCTTTTTAGTAAAATATTCAGAAATAATTTAAATACATCA
TTGCAATGAAAATAAATGTTTTTTATTAGGCAGAATCCAGATGCTCAAGGCCCTTCATAATATCCCCCAGTTT
AGTAGTTGGACTTAGGGAACAAAGGAACCTTTAATAGAAATTGGACAGCAAGAAAGCGAGCTTCTAGCTT
ATCCTCAGTCCTGCTCCTCTGCCACAAAGTGCACGCAGTTGCCGGCCGGGTCGCGCAGGGCGAACTCCCGC
CCCCACGGCTGCTCGCCGATCTCGGTCATGGCCGGCCCGGAGGCGTCCCGGAAGTTCGTGGACACGACCT
CCGACCACTCGGCGTACAGCTCGTCCAGGCCGCGCACCCACACCCAGGCCAGGGTGTTGTCCGGCACCACC
TGGTCCTGGACCGCGCTGATGAACAGGGTCACGTCGTCCCGGACCACACCGGCGAAGTCGTCCTCCACGA
AGTCCCGGGAGAACCCGAGCCGGTCGGTCCAGAACTCGACCGCTCCGGCGACGTCGCGCGCGGTGAGCA
CCGGAACGGCACTGGTCAACTTGGCCATGATGGCTCCTCctgtcaggagaggaaagagaagaaggttagtacaattgCT

ATAGTGAGTTGTATTATACTATGCAGATATACTATGCCAATGATTAATTGTCAAACTAGGGCTGCAgggttcat
agtgccacttttcctgcactgccccatctcctgcccacccctttcccaggcatagacagtcagtgacttacCAAACTCACAGGAGGGAG
AAGGCAGAAGCTTGAGACAGACCCGCGGGACCGCCGAACTGCGAGGGGACGTGGCTAGGGCGGCTTCTT
TTATGGTGCGCCGGCCCTCGGAGGCAGGGCGCTCGGGGAGGCCTAGCGGCCAATCTGCGGTGGCAGGAG
GCGGGGCCGAAGGCCGTGCCTGACCAATCCGGAGCACATAGGAGTCTCAGCCCCCCGCCCCAAAGCAAGG
GGAAGTCACGCGCCTGTAGCGCCAGCGTGTTGTGAAATGGGGGCTTGGGGGGGTTGGGGCCCTGACTAG
TCAAAACAAACTCCCATTGACGTCAATGGGGTGGAGACTTGGAAATCCCCGTGAGTCAAACCGCTATCCAC
GCCCATTGATGTACTGCCAAAACCGCATCATCATGGTAATAGCGATGACTAATACGTAGATGTACTGCCAA
GTAGGAAAGTCCCATAAGGTCATGTACTGGGCATAATGCCAGGCGGGCCATTTACCGTCATTGACGTCAAT
AGGGGGCGTACTTGGCATATGATACACTTGATGTACTGCCAAGTGGGCAGTTTACCGTAAATACTCCACCC
ATTGACGTCAATGGAAAGTCCCTATTGGCGTTACTATGGGAACATACGTCATTATTGACGTCAATGGGCGG
GGGTCGTTGGGCGGTCAGCCAGGCGGGCCATTTACCGTAAGTTATGTAACGCCTGCAGGTTAATTAAGAA
CATGTGAGCAAAAGGCCAGCAAAAGGCCAGGAACCGTAAAAAGGCCGCGTTGCTGGCGTTTTTCCATAGG
CTCCGCCCCCCTGACGAGCATCACAAAAATCGACGCTCAAGTCAGAGGTGGCGAAACCCGACAGGACTAT
AAAGATACCAGGCGTTTCCCCCTGGAAGCTCCCTCGTGCGCTCTCCTGTTCCGACCCTGCCGCTTACCGGAT
ACCTGTCCGCCTTTCTCCCTTCGGGAAGCGTGGCGCTTTCTCATAGCTCACGCTGTAGGTATCTCAGTTCGG
TGTAGGTCGTTCGCTCCAAGCTGGGCTGTGTGCACGAACCCCCCGTTCAGCCCGACCGCTGCGCCTTATCC
GGTAACTATCGTCTTGAGTCCAACCCGGTAAGACACGACTTATCGCCACTGGCAGCAGCCACTGGTAACAG
GATTAGCAGAGCGAGGTATGTAGGCGGTGCTACAGAGTTCTTGAAGTGGTGGCCTAACTACGGCTACACT
AGAAGAACAGTATTTGGTATCTGCGCTCTGCTGAAGCCAGTTACCTTCGGAAAAAGAGTTGGTAGCTCTTG
ATCCGGCAAACAAACCACCGCTGGTAGCGGTGGTTTTTTTGTTTGCAAGCAGCAGATTACGCGCAGAAAAA
AAGGATCTCAAGAAGATCCTTTGATCTTTTCTACGGGGTCTGACGCTCAGTGGAACGAAAACTCACGTTAA
GGGATTTTGGTCATGGCTAGTTAATTAACATTTAAATCAGCGGCCGCAATAAAATATCTTTATTTTCATTACA
TCTGTGTGTTGGTTTTTTGTGTGAATCGTAACTAACATACGCTCTCCATCAAAACAAAACGAAACAAAACAA
ACTAGCAAAATAGGCTGTCCCCAGTGCAAGTGCAGGTGCCAGAACATTTCTCTATCGAA

Appendix 15: Nucleotide FASTA sequence of pFuse2SS vector with 2G12-Hn 2 light chain insert. EcoRI and NheI restriction sites for insertion in red. 2G12 light chain in blue. Flexible linker in green. Trastuzumab variable heavy and light chain domains in pink and purple, respectively.

- FASTA sequence of 2G12-Hn 3 light chain in pFuse2SS vector for 2G12-Hn 3 construct

GGATCTGCGATCGCTCCGGTGCCCGTCAGTGGGCAGAGCGCACATCGCCCACAGTCCCCGAGAAGTTGGG
GGGAGGGGTCGGCAATTGAACGGGTGCCTAGAGAAGGTGGCGCGGGGTAAACTGGGAAAGTGATGTCG
TGTACTGGCTCCGCCTTTTTCCCGAGGGTGGGGGAGAACCGTATATAAGTGCAGTAGTCGCCGTGAACGTT

CTTTTTCGCAACGGGTTTGCCGCCAGAACACAGCTGAAGCTTCGAGGGGCTCGCATCTCTCCTTCACGCGCC
CGCCGCCCTACCTGAGGCCGCCATCCACGCCGGTTGAGTCGCGTTCTGCCGCCTCCCGCCTGTGGTGCCTCC
TGAACTGCGTCCGCCGTCTAGGTAAGTTTAAAGCTCAGGTCGAGACCGGGCCTTTGTCCGGCGCTCCCTTG
GAGCCTACCTAGACTCAGCCGGCTCTCCACGCTTTGCCTGACCCTGCTTGCTCAACTCTACGTCTTTGTTTCG
TTTTCTGTTCTGCGCCGTTACAGATCCAAGCTGTGACCGGCGCCTACCTGAGATCAccggcGAAGGAGGGCC
ACCATGTACAGGATGCAACTCCTGTCTTGCATTGCACTAAGTCTTGCACTTGTCACgaattcGGATATCCAGAT
GACACAGAGCCCCAGCAGCCTGTCTGCCAGCGTGGGCGACAGAGTGACCATCACCTGCAGGGCCAGCCAA
GACGTGAACACCGCCGTCGCCTGGTATCAGCAGAAACCTGGCAAGGCCCCTAAGCTGCTGATCTACTCCGC
CAGCTTCCTGTACAGCGGAGTGCCCTCTCGGTTCAGCGGCTCCCGCAGCGGCACTGATTTTACCCTGACAAT
CAGCAGCCTGCAGCCCGAGGACTTCGCCACCTACTACTGCCAGCAACACTACACAACACCTCCAACATTCG
GCCAGGGAACCAAGGTAGAGATCAAGGGCGGCGGCGGCTCTGGCGGCGGCGGCAGCGGCGGCGGCGGC
AGTGAAGTGCAGCTGGTGGAAAGCGGCGGCGGCCTGGTGCAGCCTGGAGGCTCCCTGAGACTGAGCTGC
GCCGCTTCCGGGTTTAACATCAAAGACACCTACATTCACTGGGTCAGACAGGCCCCTGGCAAAGGCCTGGA
ATGGGTTGCTAGAATCTATCCTACCAACGGCTACACCAGATACGCCGACTCTGTGAAGGGCAGATTTACCA
TCTCTGCTGATACCAGCAAAAACACCGCCTACCTGCAGATGAACAGCCTGCGGGCCGAGGATACCGCTGTG
TACTACTGCAGCAGATGGGGAGGCGACGGCTTCTACGCCATGGACTACTGGGGCCAGGGCACCCTCGTGA
CAGTGTCCTCCGGCGGCGGCGGCTCTGGCGGCGGCGGCAGCGGCGGCGGCGGCAGTGATGTGGTGATGA
CCCAGTCTCCATCCACCCTGAGCGCCAGCGTGGGCGATACAATCACAATTACCTGTAGAGCCTCACAGAGC
ATCGAGACATGGCTGGCCTGGTACCAGCAGAAGCCCGGCAAGGCACCAAAGCTGCTGATCTACAAGGCTT
CTACCCTGAAAACCGGCGTGCCTAGCCGGTTCAGCGGTTCTGGCAGCGGCACAGAGTTCACCCTGACAATC
AGCGGTCTTCAATTTGACGACTTCGCCACATACCACTGTCAGCATTACGCCGGATATAGCGCCACCTTCGGC
CAAGGCACCCGGGTGGAAATCAAGCGGACCGTGGCCGCTCCTTCCGTTTTCATCTTCCCTCCTTCCGACGA
GCAGCTCAAGTCTGGCACCGCCTCAGTGGTGTGCCTGCTGAACAACTTCTACCCCAGAGAGGCCAAGGTCC
AGTGGAAGGTGGACAACGCCCTGCAGAGCGGCAATTCCCAGGAGAGCGTGACTGAACAGGACAGCAAGG
ACAGCACATACTCCCTGAGCAGCACCCTGACCCTGTCCAAGGCCGACTACGAGAAGCACAAGGTGTACGCT
TGTGAAGTGACCCACCAGGGCCTGAGCAGCCCTGTGACAAAGAGCTTCAATAGAGGCGAGTGCGGCGGC
GGCGGCTCTGGCGGCGGCGGCAGCGGCGGCGGCGGCAGTGAAGTGCAGCTGGTGGAAAGCGGCGGCG
GCCTGGTGCAGCCTGGAGGCTCCCTGAGACTGAGCTGCGCCGCTTCCGGGTTTAACATCAAAGACACCTAC
ATTCACTGGGTCAGACAGGCCCCTGGCAAAGGCCTGGAATGGGTTGCTAGAATCTATCCTACCAACGGCTA
CACCAGATACGCCGACTCTGTGAAGGGCAGATTTACCATCTCTGCTGATACCAGCAAAAACACCGCCTACC
TGCAGATGAACAGCCTGCGGGCCGAGGATACCGCTGTGTACTACTGCAGCAGATGGGGAGGCGACGGCT
TCTACGCCATGGACTACTGGGGCCAGGGCACCCTCGTGACAGTGTCCTCCGGAGGCGGCGGAAGCGGAG
GAGGAGGAAGCGGCGGCGGAGGTAGCGATATCCAGATGACACAGAGCCCCAGCAGCCTGTCTGCCAGCG
TGGGCGACAGAGTGACCATCACCTGCAGGGCCAGCCAAGACGTGAACACCGCCGTCGCCTGGTATCAGCA
GAAACCTGGCAAGGCCCCTAAGCTGCTGATCTACTCCGCCAGCTTCCTGTACAGCGGAGTGCCCTCTCGGT
TCAGCGGCTCCCGCAGCGGCACTGATTTTACCCTGACAATCAGCAGCCTGCAGCCCGAGGACTTCGCCACC

TACTACTGCCAGCAACACTACACAACACCTCCAACATTCGGCCAGGGAACCAAGGTAGAGATCAAGTAGA
GGGAgctagcTGGCCAGACATGATAAGATACATTGATGAGTTTGGACAAACCACAACTAGAATGCAGTGAA
AAAAATGCTTTATTTGTGAAATTTGTGATGCTATTGCTTTATTTGTAACCATTATAAGCTGCAATAAACAAGT
TAACAACAACAATTGCATTCATTTTATGTTTCAGGTTCAGGGGGAGGTGTGGGAGGTTTTTTAAAGCAAGT
AAAACCTCTACAAATGTGGTATGGAATTAATTCTAAAATACAGCATAGCAAAACTTTAACCTCCAAATCAAG
CCTCTACTTGAATCCTTTTCTGAGGGATGAATAAGGCATAGGCATCAGGGGCTGTTGCCAATGTGCATTAG
CTGTTTGCAGCCTCACCTTCTTTCATGGAGTTTAAGATATAGTGTATTTTCCCAAGGTTTGAACTAGCTCTTC
ATTTCTTTATGTTTTAAATGCACTGACCTCCCACATTCCCTTTTTAGTAAAATATTCAGAAATAATTTAAATAC
ATCATTGCAATGAAAATAAATGTTTTTTATTAGGCAGAATCCAGATGCTCAAGGCCCTTCATAATATCCCCC
AGTTTAGTAGTTGGACTTAGGGAACAAAGGAACCTTTAATAGAAATTGGACAGCAAGAAAGCGAGCTTCT
AGCTTATCCTCAGTCCTGCTCCTCTGCCACAAAGTGCACGCAGTTGCCGGCCGGGTCGCGCAGGGCGAACT
CCCGCCCCCACGGCTGCTCGCCGATCTCGGTCATGGCCGGCCCGGAGGCGTCCCGGAAGTTCGTGGACAC
GACCTCCGACCACTCGGCGTACAGCTCGTCCAGGCCGCGCACCCACACCCAGGCCAGGGTGTTGTCCGGCA
CCACCTGGTCCTGGACCGCGCTGATGAACAGGGTCACGTCGTCCCGGACCACACCGGCGAAGTCGTCCTCC
ACGAAGTCCCGGGAGAACCCGAGCCGGTCGGTCCAGAACTCGACCGCTCCGGCGACGTCGCGCGCGGTG
AGCACCGGAACGGCACTGGTCAACTTGGCCATGATGGCTCCTCctgtcaggagaggaaagagaagaaggttagtacaa
ttgCTATAGTGAGTTGTATTATACTATGCAGATATACTATGCCAATGATTAATTGTCAAACTAGGGCTGCAgg
gttcatagtgccacttttcctgcactgccccatctcctgcccacccttтcccaggcatagacagtcagtgacttacCAAACTCACAGGAG
GGAGAAGGCAGAAGCTTGAGACAGACCCGCGGGACCGCCGAACTGCGAGGGGACGTGGCTAGGGCGGC
TTCTTTTATGGTGCGCCGGCCCTCGGAGGCAGGGCGCTCGGGGAGGCCTAGCGGCCAATCTGCGGTGGCA
GGAGGCGGGGCCGAAGGCCGTGCCTGACCAATCCGGAGCACATAGGAGTCTCAGCCCCCCGCCCCAAAG
CAAGGGGAAGTCACGCGCCTGTAGCGCCAGCGTGTTGTGAAATGGGGGCTTGGGGGGGTTGGGGCCCTG
ACTAGTCAAAACAAACTCCCATTGACGTCAATGGGGTGGAGACTTGGAAATCCCCGTGAGTCAAACCGCTA
TCCACGCCCATTGATGTACTGCCAAAACCGCATCATCATGGTAATAGCGATGACTAATACGTAGATGTACTG
CCAAGTAGGAAAGTCCCATAAGGTCATGTACTGGGCATAATGCCAGGCGGGCCATTTACCGTCATTGACGT
CAATAGGGGGCGTACTTGGCATATGATACACTTGATGTACTGCCAAGTGGGCAGTTTACCGTAAATACTCC
ACCCATTGACGTCAATGGAAAGTCCCTATTGGCGTTACTATGGGAACATACGTCATTATTGACGTCAATGG
GCGGGGGTCGTTGGGCGGTCAGCCAGGCGGGCCATTTACCGTAAGTTATGTAACGCCTGCAGGTTAATTA
AGAACATGTGAGCAAAAGGCCAGCAAAAGGCCAGGAACCGTAAAAAGGCCGCGTTGCTGGCGTTTTTCCA
TAGGCTCCGCCCCCCTGACGAGCATCACAAAAATCGACGCTCAAGTCAGAGGTGGCGAAACCCGACAGGA
CTATAAAGATACCAGGCGTTTCCCCCTGGAAGCTCCCTCGTGCGCTCTCCTGTTCCGACCCTGCCGCTTACC
GGATACCTGTCCGCCTTTCTCCCTTCGGGAAGCGTGGCGCTTTCTCATAGCTCACGCTGTAGGTATCTCAGT
TCGGTGTAGGTCGTTCGCTCCAAGCTGGGCTGTGTGCACGAACCCCCCGTTCAGCCCGACCGCTGCGCCTT
ATCCGGTAACTATCGTCTTGAGTCCAACCCGGTAAGACACGACTTATCGCCACTGGCAGCAGCCACTGGTA
ACAGGATTAGCAGAGCGAGGTATGTAGGCGGTGCTACAGAGTTCTTGAAGTGGTGGCCTAACTACGGCTA
CACTAGAAGAACAGTATTTGGTATCTGCGCTCTGCTGAAGCCAGTTACCTTCGGAAAAAGAGTTGGTAGCT

CTTGATCCGGCAAACAAACCACCGCTGGTAGCGGTGGTTTTTTTGTTTGCAAGCAGCAGATTACGCGCAGA
AAAAAAGGATCTCAAGAAGATCCTTTGATCTTTTCTACGGGGTCTGACGCTCAGTGGAACGAAAACTCACG
TTAAGGGATTTTGGTCATGGCTAGTTAATTAACATTTAAATCAGCGGCCGCAATAAAATATCTTTATTTTCAT
TACATCTGTGTGTTGGTTTTTTGTGTGAATCGTAACTAACATACGCTCTCCATCAAAACAAAACGAAACAAA
ACAAACTAGCAAAATAGGCTGTCCCCAGTGCAAGTGCAGGTGCCAGAACATTTCTCTATCGAA

Appendix 16: Nucleotide FASTA sequence of pFuse2SS vector with 2G12-Hn 3 light chain insert. EcoRI and NheI restriction sites for insertion in red. 2G12 light chain in blue. Flexible linker in green. Trastuzumab variable heavy and light chain domains in pink and purple, respectively.

Chapter 8 List of References

AB, V. *et al.* (2018) 'Self-Amplifying RNA Vaccines Give Equivalent Protection against Influenza to mRNA Vaccines but at Much Lower Doses', *Molecular therapy : the journal of the American Society of Gene Therapy*. Mol Ther, 26(2), pp. 446–455. doi: 10.1016/J.YMTHE.2017.11.017.

Abd Hamid, U. M. *et al.* (2008) 'A strategy to reveal potential glycan markers from serum glycoproteins associated with breast cancer progression', *Glycobiology*. Oxford Academic, 18(12), pp. 1105–1118. doi: 10.1093/GLYCOB/CWN095.

Adams, S. *et al.* (2014) 'Prognostic value of tumor-infiltrating lymphocytes in triple-negative breast cancers from two phase III randomized adjuvant breast cancer trials: ECOG 2197 and ECOG 1199', *Journal of Clinical Oncology*. American Society of Clinical Oncology, 32(27), pp. 2959–2966. doi: 10.1200/JCO.2013.55.0491.

Agarwal, G. *et al.* (2007) 'Spectrum of breast cancer in Asian women', *World Journal of Surgery*. Springer, 31(5), pp. 1031–1040. doi: 10.1007/s00268-005-0585-9.

Ahn, S. *et al.* (2020) 'HER2 status in breast cancer: changes in guidelines and complicating factors for interpretation', *Journal of Pathology and Translational Medicine*. Korean Society of Pathologists and Korean Society for Cytopathology, 54(1), p. 34. doi: 10.4132/JPTM.2019.11.03.

Alas, S. and Bonavida, B. (2001) 'Rituximab Inactivates Signal Transducer and Activation of Transcription 3 (STAT3) Activity in B-Non-Hodgkin's Lymphoma through Inhibition of the Interleukin 10 Autocrine/Paracrine Loop and Results in Down-Regulation of Bcl-2 and Sensitization to Cytotoxic Drugs 1', *CANCER RESEARCH*, 61, pp. 5137–5144. Available at: http://aacrjournals.org/cancerres/article-pdf/61/13/5137/2487114/5137.pdf (Accessed: 20 September 2023).

Albrechtsen, R. *et al.* (1981) 'Basement Membrane Changes in Breast Cancer Detected by Immunohistochemical Staining for Laminin', *Cancer Research*, 41(12 Part 1).

Ålgars, A. *et al.* (2012) 'Type and location of tumor-infiltrating macrophages and lymphatic vessels predict survival of colorectal cancer patients', *International Journal of Cancer*. John Wiley & Sons, Ltd, 131(4), pp. 864–873. doi: 10.1002/IJC.26457.

Alimandi, M. *et al.* (1995) 'Cooperative signaling of ErbB3 and ErbB2 in neoplastic transformation and human mammary carcinomas', *Oncogene*. Nature Publishing Group, 10(9), pp. 1813–1821.

Allemani, C. *et al.* (2015) 'Global surveillance of cancer survival 1995-2009: Analysis of individual data for 25 676 887 patients from 279 population-based registries in 67 countries (CONCORD-2)', *The Lancet*. Lancet Publishing Group, 385(9972), pp. 977–1010. doi: 10.1016/S0140-6736(14)62038-9.

Alon, Y. *et al.* (1986) 'Immunofluorescent characterization of fibronectin, laminin, and keratin in normal and neoplastic human mammary epithelial cells in culture and in breast tissue sections', *International Journal of Tissue Reactions*, 8(5), pp. 401–410. Available at: https://europepmc.org/article/med/2430910 (Accessed: 22 September 2020).

Alonso-Garcia, V. *et al.* (2020) 'High mannose N-glycans promote migration of Bone-Marrow-Derived mesenchymal stromal cells', *International Journal of Molecular Sciences*, 21(19), pp. 1–21. doi: 10.3390/ijms21197194.

Althuis, M. D. *et al.* (2005) 'Global trends in breast cancer incidence and mortality 1973-1997', *International Journal of Epidemiology*. Int J Epidemiol, 34(2), pp. 405–412. doi:

10.1093/ije/dyh414.

Anderluh, M. *et al.* (2022) 'Recent advances on smart glycoconjugate vaccines in infections and cancer', *The Febs Journal*. Wiley-Blackwell, 289(14), p. 4251. doi: 10.1111/FEBS.15909.

Andrade, C. *et al.* (2019) 'An Integrated Approach to Aggregate Control for Therapeutic Bispecific Antibodies Using an Improved Three Column Mab Platform-Like Purification Process', *Biotechnology Progress*. American Chemical Society (ACS), 35(1), p. e2720. doi: 10.1002/BTPR.2720.

Apostolopoulos, V. and Mckenzie, I. (2005) 'Role of the Mannose Receptor in the Immune Response', *Current Molecular Medicine*. Bentham Science Publishers Ltd., 1(4), pp. 469–474. doi: 10.2174/1566524013363645.

Appelmelk, B. J. *et al.* (2003) 'Cutting edge: carbohydrate profiling identifies new pathogens that interact with dendritic cell-specific ICAM-3-grabbing nonintegrin on dendritic cells', *Journal of immunology (Baltimore, Md. : 1950)*. J Immunol, 170(4), pp. 1635–1639. doi: 10.4049/JIMMUNOL.170.4.1635.

Arosio, P. *et al.* (2011) 'Aggregation stability of a monoclonal antibody during downstream processing', *Pharmaceutical research*. Pharm Res, 28(8), pp. 1884–1894. doi: 10.1007/S11095-011-0416-7.

Aryal, R. P., Ju, T. and Cummings, R. D. (2010) 'The Endoplasmic Reticulum Chaperone Cosmc Directly Promotes in Vitro Folding of T-synthase', *The Journal of Biological Chemistry*. American Society for Biochemistry and Molecular Biology, 285(4), p. 2456. doi: 10.1074/JBC.M109.065169.

Bacac, M. and Stamenkovic, I. (2008) 'Metastatic cancer cell', *Annual Review of Pathology: Mechanisms of Disease*. Annu Rev Pathol, pp. 221–247. doi: 10.1146/annurev.pathmechdis.3.121806.151523.

Baeuerle, P. A. and Reinhardt, C. (2009) 'Bispecific T-cell engaging antibodies for cancer therapy', *Cancer Research*. American Association for Cancer Research, 69(12), pp. 4941–4944. doi: 10.1158/0008-5472.CAN-09-0547/655159/P/BISPECIFIC-T-CELL-ENGAGING-ANTIBODIES-FOR-CANCER.

Balasubramanian, M. and Johnson, D. S. (2019) 'MAN1B-CDG: Novel variants with a distinct phenotype and review of literature', *European journal of medical genetics*. Eur J Med Genet, 62(2), pp. 109–114. doi: 10.1016/J.EJMG.2018.06.011.

Bardia, A. *et al.* (2019) 'Sacituzumab Govitecan-hziy in Refractory Metastatic Triple-Negative Breast Cancer', *New England Journal of Medicine*. Massachusetts Medical Society, 380(8), pp. 741–751. doi: 10.1056/NEJMOA1814213/SUPPL_FILE/NEJMOA1814213_DATA-SHARING.PDF.

Barondes, S. H. *et al.* (1994) 'Galectins: a family of animal beta-galactoside-binding lectins', *Cell*. Cell, 76(4), pp. 597–598. doi: 10.1016/0092-8674(94)90498-7.

Barsky, S. H. *et al.* (1982) 'Increased content of type V collagen in desmoplasia of human breast carcinoma', *American Journal of Pathology*, 108(3), pp. 276–283.

Beatson, R. *et al.* (2015) 'The Breast Cancer-Associated Glycoforms of MUC1, MUC1-Tn and sialyl-Tn, Are Expressed in COSMC Wild-Type Cells and Bind the C-Type Lectin MGL', *PLOS ONE*. Edited by L.-G. Yu. Public Library of Science, 10(5), p. e0125994. doi: 10.1371/journal.pone.0125994.

Bennett, E. P. *et al.* (2012) 'Control of mucin-type O-glycosylation: A classification of the polypeptide GalNAc-transferase gene family', *Glycobiology*. Glycobiology, pp. 736–756. doi: 10.1093/glycob/cwr182.

Berezov, A. *et al.* (2001) 'Disabling erbB receptors with rationally designed exocyclic mimetics of antibodies: structure-function analysis', *Journal of medicinal chemistry*. J Med Chem, 44(16), pp. 2565–2574. doi: 10.1021/JM000527M.

Bessler, H. *et al.* (1995) 'Interferon alpha-2b modulates beta-galactoside alpha-2,6-sialyltransferase gene expression in rat testes', *Biology of reproduction*. Biol Reprod, 53(6), pp. 1474–1477. doi: 10.1095/BIOLREPROD53.6.1474.

Beum, P. V. *et al.* (2011) 'Loss of CD20 and bound CD20 antibody from opsonized B cells occurs more rapidly because of trogocytosis mediated by Fc receptor-expressing effector cells than direct internalization by the B cells', *Journal of immunology (Baltimore, Md. : 1950)*. J Immunol, 187(6), pp. 3438–3447. doi: 10.4049/JIMMUNOL.1101189.

Birch, J. M. *et al.* (2001) 'Relative frequency and morphology of cancers in carriers of germline TP53 mutations', *Oncogene*. Nature Publishing Group, 20(34), pp. 4621–4628. doi: 10.1038/sj.onc.1204621.

Birch, J. R. and Racher, A. J. (2006) 'Antibody production', *Advanced drug delivery reviews*. Adv Drug Deliv Rev, 58(5–6), pp. 671–685. doi: 10.1016/J.ADDR.2005.12.006.

Biro, C. E. and García, G. (1965) 'The antigenicity of aggregated and aggregate-free human gamma-globulin for rabbits', *Immunology*. Wiley-Blackwell, 8(4), p. 411. Available at: /pmc/articles/PMC1423503/?report=abstract (Accessed: 19 September 2023).

Biswas, S., Medina, S. H. and Barchi, J. J. (2015) 'Synthesis and cell-selective antitumor properties of amino acid conjugated tumor-associated carbohydrate antigen-coated gold nanoparticles', *Carbohydrate research*. Carbohydr Res, 405, pp. 93–101. doi: 10.1016/J.CARRES.2014.11.002.

Blixt, O. *et al.* (2004) 'Printed covalent glycan array for ligand profiling of diverse glycan binding proteins', *Proceedings of the National Academy of Sciences of the United States of America*. Proc Natl Acad Sci U S A, 101(49), pp. 17033–17038. doi: 10.1073/PNAS.0407902101.

Bondza, S. *et al.* (2020) 'Bivalent binding on cells varies between anti-CD20 antibodies and is dose-dependent', *mAbs*. Taylor & Francis, 12(1). doi: 10.1080/19420862.2020.1792673.

Boscher, C., Dennis, J. W. and Nabi, I. R. (2011) 'Glycosylation, galectins and cellular signaling', *Current Opinion in Cell Biology*. Curr Opin Cell Biol, pp. 383–392. doi: 10.1016/j.ceb.2011.05.001.

Boyaval, F. *et al.* (2022) 'High-Mannose N-Glycans as Malignant Progression Markers in Early-Stage Colorectal Cancer', *Cancers*, 14(6), pp. 1–14. doi: 10.3390/cancers14061552.

Brandsma, A. M. *et al.* (2015) 'Fc receptor inside-out signaling and possible impact on antibody therapy', *Immunological Reviews*. John Wiley & Sons, Ltd, 268(1), pp. 74–87. doi: 10.1111/IMR.12332.

Bray, F. *et al.* (2015) 'Cancer Incidence in Five Continents: Inclusion criteria, highlights from Volume X and the global status of cancer registration', *International Journal of Cancer*. Wiley-Liss Inc., 137(9), pp. 2060–2071. doi: 10.1002/ijc.29670.

Bray, F. *et al.* (2018) 'Global cancer statistics 2018: GLOBOCAN estimates of incidence and mortality worldwide for 36 cancers in 185 countries', *CA: A Cancer Journal for Clinicians*. Wiley, 68(6), pp. 394–424. doi: 10.3322/caac.21492.

Brockhausen, I., Narasimhan, S. and Schachter, H. (1988) 'The biosynthesis of highly branched N-glycans: studies on the sequential pathway and functional role of N-actylglucosaminyltransferases I, II, III, IV, V and VI', *Biochimie*. Elsevier, 70(11), pp. 1521–1533. doi: 10.1016/0300-9084(88)90289-1.

Brown, G. D., Willment, J. A. and Whitehead, L. (2018) 'C-type lectins in immunity and homeostasis', *Nature Reviews Immunology 2018 18:6*. Nature Publishing Group, 18(6), pp. 374–389. doi: 10.1038/s41577-018-0004-8.

Buckhaults, P. *et al.* (1997) 'Transcriptional Regulation of N-Acetylglucosaminyltransferase V by the src Oncogene*'. Available at: http://www.jbc.org/ (Accessed: 11 September 2023).

Burchell, J. *et al.* (1999) *An α α α α2,3 sialyltransferase (ST3Gal I) is elevated in primary breast carcinomas*, *Glycobiology*. Available at: https://academic.oup.com/glycob/article-abstract/9/12/1307/612214 (Accessed: 19 June 2020).

Buskas, T., Li, Y. and Boons, G. J. (2004) 'The immunogenicity of the tumor-associated antigen Lewis(y) may be suppressed by a bifunctional cross-linker required for coupling to a carrier protein', *Chemistry (Weinheim an der Bergstrasse, Germany)*. Chemistry, 10(14), pp. 3517–3524. doi: 10.1002/CHEM.200400074.

BV, A., S, A. and R, O. (2016) 'Coming-of-Age of Antibodies in Cancer Therapeutics', *Trends in pharmacological sciences*. Trends Pharmacol Sci, 37(12), pp. 1009–1028. doi: 10.1016/J.TIPS.2016.09.005.

Byrne, B., Donohoe, G. G. and O'Kennedy, R. (2007) 'Sialic acids: carbohydrate moieties that influence the biological and physical properties of biopharmaceutical proteins and living cells', *Drug Discovery Today*. Drug Discov Today, pp. 319–326. doi: 10.1016/j.drudis.2007.02.010.

Cai, H. *et al.* (2014) 'Synthetic multivalent glycopeptide-lipopeptide antitumor vaccines: impact of the cluster effect on the killing of tumor cells', *Angewandte Chemie (International ed. in English)*. Angew Chem Int Ed Engl, 53(6), pp. 1699–1703. doi: 10.1002/ANIE.201308875.

Calarese, D. A. *et al.* (2003) 'Antibody domain exchange is an immunological solution to carbohydrate cluster recognition', *Science*, 300(5628), pp. 2065–2071. doi: 10.1126/SCIENCE.1083182.

Caldwell, S. A. *et al.* (2010) 'Nutrient sensor O-GlcNAc transferase regulates breast cancer tumorigenesis through targeting of the oncogenic transcription factor FoxM1', *Oncogene*. Oncogene, 29(19), pp. 2831–2842. doi: 10.1038/onc.2010.41.

Cao, L. *et al.* (2022) 'Abstract LB203: Assessment of the safety, pharmacokinetics, and pharmacodynamics of a first-in-class cancer drug candidate E-602, a sialoglycan degrader, in non-human primates', *Cancer Research*. American Association for Cancer Research, 82(12_Supplement), pp. LB203–LB203. doi: 10.1158/1538-7445.AM2022-LB203.

Cardoso, F. *et al.* (2018) 'Global analysis of advanced/metastatic breast cancer: Decade report (2005–2015)', *Breast*. Churchill Livingstone, 39, pp. 131–138. doi: 10.1016/j.breast.2018.03.002.

Carpenter, J. F. *et al.* (1999) '[16] Inhibition of stress-induced aggregation of protein therapeutics', *Methods in Enzymology*. Academic Press, 309, pp. 236–255. doi: 10.1016/S0076-6879(99)09018-7.

Cascio, S. *et al.* (2013) 'Altered glycosylation of MUC1 influences its association with CIN85: The role of this novel complex in cancer cell invasion and migration', *Oncotarget*. Impact Journals LLC, 4(10), pp. 1700–1711. doi: 10.18632/oncotarget.1265.

Casey, A. E., Laster, W. R. and Ross, G. L. (1951) 'Sustained Enhanced Growth of Carcinoma EO771 in C57 Black Mice', *Experimental Biology and Medicine*. SAGE PublicationsSage UK: London, England, 77(2), pp. 358–362. doi: 10.3181/00379727-77-18779.

Cerliani, J. P. *et al.* (2017) 'Translating the "Sugar Code" into Immune and Vascular Signaling

Programs', *Trends in Biochemical Sciences*. Elsevier, 42(4), pp. 255–273. doi: 10.1016/J.TIBS.2016.11.003.

Cha, J. H. *et al.* (2018) 'Metformin Promotes Antitumor Immunity via Endoplasmic-Reticulum-Associated Degradation of PD-L1', *Molecular cell*. Mol Cell, 71(4), pp. 606-620.e7. doi: 10.1016/J.MOLCEL.2018.07.030.

Chatterjee, S., Kawahara, R., *et al.* (2021) 'Oligomannosylation and MAN1A1 expression associate strongly with a subset of human cancer types', *bioRxiv*. Cold Spring Harbor Laboratory, p. 2021.05.08.443254. doi: 10.1101/2021.05.08.443254.

Chatterjee, S., Ugonotti, J., *et al.* (2021) 'Trends in oligomannosylation and α1,2-mannosidase expression in human cancers', *Oncotarget*. Impact Journals LLC, pp. 2188–2205. doi: 10.18632/ONCOTARGET.28064.

Chauhan, A. K. (2016) 'Human CD4+ T-cells: A role for low-affinity Fc receptors', *Frontiers in Immunology*. Frontiers Research Foundation, 7(JUN), p. 184179. doi: 10.3389/FIMMU.2016.00215/BIBTEX.

Che, J. *et al.* (2022) 'Abstract LB221: Development of PD-L1-targeted sialidase as a novel cancer immunotherapeutic approach', *Cancer Research*. American Association for Cancer Research, 82(12_Supplement), pp. LB221–LB221. doi: 10.1158/1538-7445.AM2022-LB221.

Cheifetz, A. and Mayer, L. (2005) 'Monoclonal antibodies, immunogenicity, and associated infusion reactions.', *The Mount Sinai Journal of Medicine, New York*, 72(4), pp. 250–256. Available at: https://europepmc.org/article/med/16021319 (Accessed: 6 September 2023).

Chen, C. Y. *et al.* (2013) 'Fucosyltransferase 8 as a functional regulator of nonsmall cell lung cancer', *Proceedings of the National Academy of Sciences of the United States of America*. National Academy of Sciences, 110(2), pp. 630–635. doi: 10.1073/pnas.1220425110.

Chen, W. Y. *et al.* (2011) 'Moderate alcohol consumption during adult life, drinking patterns, and breast cancer risk', *JAMA - Journal of the American Medical Association*. JAMA, 306(17), pp. 1884–1890. doi: 10.1001/jama.2011.1590.

Chen, X., Zaro, J. L. and Shen, W. C. (2013) 'Fusion protein linkers: Property, design and functionality', *Advanced Drug Delivery Reviews*. Elsevier, 65(10), pp. 1357–1369. doi: 10.1016/J.ADDR.2012.09.039.

Chi, E. Y. *et al.* (2003) 'Physical stability of proteins in aqueous solution: Mechanism and driving forces in nonnative protein aggregation', *Pharmaceutical Research*. Springer, 20(9), pp. 1325–1336. doi: 10.1023/A:1025771421906/METRICS.

Chiang, A. C. and Massagué, J. (2008) 'Molecular basis of metastasis', *New England Journal of Medicine*. Massachussetts Medical Society, p. 2814. doi: 10.1056/NEJMra0805239.

Chieppa, M. *et al.* (2003) 'Cross-linking of the mannose receptor on monocyte-derived dendritic cells activates an anti-inflammatory immunosuppressive program', *Journal of immunology (Baltimore, Md. : 1950)*. J Immunol, 171(9), pp. 4552–4560. doi: 10.4049/JIMMUNOL.171.9.4552.

Cho, H. S. *et al.* (2003) 'Structure of the extracellular region of HER2 alone and in complex with the Herceptin Fab', *Nature*. Nature Publishing Group, 421(6924), pp. 756–760. doi: 10.1038/nature01392.

Chu, Q. *et al.* (2022) 'BMS-986012, an Anti–Fucosyl-GM1 Monoclonal Antibody as Monotherapy or in Combination With Nivolumab in Relapsed/Refractory SCLC: Results From a First-in-Human Phase 1/2 Study', *JTO Clinical and Research Reports*. Elsevier, 3(11), p. 100400. doi:

10.1016/J.JTOCRR.2022.100400.

Chung, A. W. *et al.* (2014) 'Identification of antibody glycosylation structures that predict monoclonal antibody Fc-effector function', *AIDS (London, England)*. NIH Public Access, 28(17), p. 2523. doi: 10.1097/QAD.0000000000000444.

Ciborowski, P. and Finn, O. J. (2002) *Non-glycosylated tandem repeats of MUC1 facilitate attachment of breast tumor cells to normal human lung tissue and immobilized extracellular matrix proteins (ECM) in vitro: Potential role in metastasis*, *Clinical & Experimental Metastasis*.

Cleary, K. L. S. *et al.* (2017) 'Antibody Distance from the Cell Membrane Regulates Antibody Effector Mechanisms', *Journal of immunology (Baltimore, Md. : 1950)*. J Immunol, 198(10), pp. 3999–4011. doi: 10.4049/JIMMUNOL.1601473.

Clynes, R. A. *et al.* (2000) 'Inhibitory Fc receptors modulate in vivo cytotoxicity against tumor targets', *Nature medicine*. Nat Med, 6(4), pp. 443–446. doi: 10.1038/74704.

Cobleigh, M. A. *et al.* (1999) 'Multinational study of the efficacy and safety of humanized anti-HER2 monoclonal antibody in women who have HER2-overexpressing metastatic breast cancer that has progressed after chemotherapy for metastatic disease', *Journal of Clinical Oncology*. J Clin Oncol, 17(9), pp. 2639–2648. doi: 10.1200/jco.1999.17.9.2639.

Cohen, M. *et al.* (2010) 'Sialylation of 3-Methylcholanthrene–Induced Fibrosarcoma Determines Antitumor Immune Responses during Immunoediting', *The Journal of Immunology*. The American Association of Immunologists, 185(10), pp. 5869–5878. doi: 10.4049/jimmunol.1001635.

Cohenuram, M. and Saif, M. W. (2007) 'Panitumumab the first fully human monoclonal antibody: From the bench to the clinic', *Anti-Cancer Drugs*, 18(1), pp. 7–15. doi: 10.1097/CAD.0B013E32800FEECB.

Comes, J. D. G., Pijlman, G. P. and Hick, T. A. H. (2023) 'Rise of the RNA machines – self-amplification in mRNA vaccine design', *Trends in Biotechnology*. Elsevier Current Trends. doi: 10.1016/J.TIBTECH.2023.05.007.

Copeland, R. A., Pompliano, D. L. and Meek, T. D. (2006) 'Drug-target residence time and its implications for lead optimization', *Nature reviews. Drug discovery*. Nat Rev Drug Discov, 5(9), pp. 730–739. doi: 10.1038/NRD2082.

Correia, I. *et al.* (2013) 'The structure of dual-variable-domain immunoglobulin molecules alone and bound to antigen', *mAbs*. Landes Bioscience, 5(3), pp. 364–372. doi: 10.4161/MABS.24258/SUPPL_FILE/KMAB_A_10924258_SM0001.ZIP.

Cortes, J. *et al.* (2020) 'Pembrolizumab plus chemotherapy versus placebo plus chemotherapy for previously untreated locally recurrent inoperable or metastatic triple-negative breast cancer (KEYNOTE-355): a randomised, placebo-controlled, double-blind, phase 3 clinical trial', *The Lancet*. Lancet Publishing Group, 396(10265), pp. 1817–1828. doi: 10.1016/S0140-6736(20)32531-9.

Crocker, P. R., Paulson, J. C. and Varki, A. (2007) 'Siglecs and their roles in the immune system', *Nature Reviews Immunology 2007 7:4*. Nature Publishing Group, 7(4), pp. 255–266. doi: 10.1038/nri2056.

Daëron, M. (1997) 'Fc receptor biology', *Annual review of immunology*. Annu Rev Immunol, 15, pp. 203–234. doi: 10.1146/ANNUREV.IMMUNOL.15.1.203.

Dall'Olio, F. and Trinchera, M. (2017) 'Epigenetic bases of aberrant glycosylation in cancer', *International Journal of Molecular Sciences*. MDPI AG. doi: 10.3390/ijms18050998.

Daniel, A. R., Hagan, C. R. and Lange, C. A. (2011) 'Progesterone receptor action: Defining a role in breast cancer', *Expert Review of Endocrinology and Metabolism*. NIH Public Access, pp. 359–369. doi: 10.1586/eem.11.25.

Demetriou, M. *et al.* (1995) 'Reduced contact-inhibition and substratum adhesion in epithelial cells expressing GlcNAc-transferase V', *Journal of Cell Biology*. The Rockefeller University Press, 130(2), pp. 383–392. doi: 10.1083/jcb.130.2.383.

Demeule, B. *et al.* (2009) 'New methods allowing the detection of protein aggregates', *https://doi.org/10.4161/mabs.1.2.7632*. Taylor & Francis, 1(2), pp. 142–150. doi: 10.4161/MABS.1.2.7632.

Demotte, N. *et al.* (2010) 'A galectin-3 ligand corrects the impaired function of human CD4 and CD8 tumor-infiltrating lymphocytes and favors tumor rejection in mice', *Cancer Research*. Cancer Res, 70(19), pp. 7476–7488. doi: 10.1158/0008-5472.CAN-10-0761.

Dennis, J. W. *et al.* (1987) 'β1-6 branching of Asn-linked oligosaccharides is directly associated with metastasis', *Science*, 236(4801), pp. 582–585. doi: 10.1126/science.2953071.

Dennis, J. W., Demetrio, M. and Dennis, J. W. (1991) 'β1-6 Branched Oligosaccharides as a Marker of Tumor Progression in Human Breast and Colon Neoplasia', *Cancer Research*, 51(2), pp. 718–723.

DeSantis, C. E. *et al.* (2016) 'Breast cancer statistics, 2015: Convergence of incidence rates between black and white women', *CA: A Cancer Journal for Clinicians*. American Cancer Society, 66(1), pp. 31–42. doi: 10.3322/caac.21320.

DiGiammarino, E. L. *et al.* (2011) 'Ligand association rates to the inner-variable-domain of a dual-variable-domain immunoglobulin are significantly impacted by linker design', *mAbs*. Taylor & Francis, 3(5), pp. 487–494. doi: 10.4161/MABS.3.5.16326/SUPPL_FILE/KMAB_A_10916326_SM0001.ZIP.

Dorsett, K. A. *et al.* (2019) 'Sox2 promotes expression of the ST6Gal-I glycosyltransferase in ovarian cancer cells', *Journal of Ovarian Research*. BioMed Central Ltd., 12(1). doi: 10.1186/s13048-019-0574-5.

Dorsett, K. A. *et al.* (2021) 'Regulation of ST6GAL1 sialyltransferase expression in cancer cells', *Glycobiology*. Oxford Academic, 31(5), pp. 530–539. doi: 10.1093/GLYCOB/CWAA110.

Durocher, Y., Perret, S. and Kamen, A. (2002) 'High-level and high-throughput recombinant protein production by transient transfection of suspension-growing human 293-EBNA1 cells', *Nucleic acids research*. Nucleic Acids Res, 30(2). doi: 10.1093/NAR/30.2.E9.

DW, S. *et al.* (2012) 'Role of endothelial N-glycan mannose residues in monocyte recruitment during atherogenesis', *Arteriosclerosis, thrombosis, and vascular biology*. Arterioscler Thromb Vasc Biol, 32(8). doi: 10.1161/ATVBAHA.112.253203.

E, Bause *et al.* (1993) 'Molecular cloning and primary structure of Man9-mannosidase from human kidney', *European journal of biochemistry*. Eur J Biochem, 217(2), pp. 535–540. doi: 10.1111/J.1432-1033.1993.TB18274.X.

Elbein, A. D. *et al.* (1991) 'Kifunensine inhibits glycoprotein processing and the function of the modified LDL receptor in endothelial cells', *Archives of Biochemistry and Biophysics*, 288(1), pp. 177–184. doi: 10.1016/0003-9861(91)90181-H.

Van Den Elsen, J. M. H., Kuntz, D. A. and Rose, D. R. (2001) 'Structure of Golgi α-mannosidase II: A target for inhibition of growth and metastasis of cancer cells', *EMBO Journal*. European Molecular

Biology Organization, 20(12), pp. 3008–3017. doi: 10.1093/emboj/20.12.3008.

Elward, K. and Gasque, P. (2003) '"Eat me" and "don't eat me" signals govern the innate immune response and tissue repair in the CNS: Emphasis on the critical role of the complement system', in *Molecular Immunology*. Elsevier Ltd, pp. 85–94. doi: 10.1016/S0161-5890(03)00109-3.

Englezou, P. C. *et al.* (2018) 'Self-Amplifying Replicon RNA Delivery to Dendritic Cells by Cationic Lipids', *Molecular Therapy. Nucleic Acids*. American Society of Gene & Cell Therapy, 12, p. 118. doi: 10.1016/J.OMTN.2018.04.019.

English, N. M., Lesley, J. F. and Hyman, R. (1998) 'Site-specific de-N-glycosylation of CD44 can activate hyaluronan binding, and CD44 activation states show distinct threshold densities for hyaluronan binding.', *Cancer research*. American Association for Cancer Research, 58(16), pp. 3736–42. Available at: http://www.ncbi.nlm.nih.gov/pubmed/9721887 (Accessed: 19 June 2020).

Ennis S Lamon, D. J. *et al.* (2001) 'Use of Chemotherapy plus a Monoclonal Antibody against HER2 for Metastatic Breast Cancer That Overexpresses HER2', *https://doi.org/10.1056/NEJM200103153441101*. Massachusetts Medical Society , 344(11), pp. 783–792. doi: 10.1056/NEJM200103153441101.

Erasmus, J. H. *et al.* (2020) 'Intramuscular Delivery of Replicon RNA Encoding ZIKV-117 Human Monoclonal Antibody Protects against Zika Virus Infection', *Molecular Therapy - Methods & Clinical Development*. Elsevier, 18, pp. 402–414. doi: 10.1016/J.OMTM.2020.06.011.

European Medicines Agency (2017) 'Assessment report - Dinutuximab beta Apeiron', *Science Medicines Health*, 44(March), pp. 1–129.

Everest-Dass, A. V. *et al.* (2016) 'N-glycan MALDI Imaging Mass Spectrometry on Formalin-Fixed Paraffin-Embedded Tissue Enables the Delineation of Ovarian Cancer Tissues', *Molecular & Cellular Proteomics*. Elsevier, 15(9), pp. 3003–3016. doi: 10.1074/MCP.M116.059816.

F, Y. *et al.* (2017) 'Breast cancer stem cell: the roles and therapeutic implications', *Cellular and molecular life sciences : CMLS*. Cell Mol Life Sci, 74(6), pp. 951–966. doi: 10.1007/S00018-016-2334-7.

Fägerstam, L. G. *et al.* (1992) 'Biospecific interaction analysis using surface plasmon resonance detection applied to kinetic, binding site and concentration analysis', *Journal of chromatography*. J Chromatogr, 597(1–2), pp. 397–410. doi: 10.1016/0021-9673(92)80137-J.

Faivre, E. J. *et al.* (2008) 'Progesterone receptor rapid signaling mediates serine 345 phosphorylation and tethering to specificity protein 1 transcription factors', *Molecular Endocrinology*. Mol Endocrinol, 22(4), pp. 823–837. doi: 10.1210/me.2007-0437.

Faivre, E. J. and Lange, C. A. (2007) 'Progesterone Receptors Upregulate Wnt-1 To Induce Epidermal Growth Factor Receptor Transactivation and c-Src-Dependent Sustained Activation of Erk1/2 Mitogen-Activated Protein Kinase in Breast Cancer Cells', *Molecular and Cellular Biology*. American Society for Microbiology, 27(2), pp. 466–480. doi: 10.1128/mcb.01539-06.

Fan, P. *et al.* (2009) 'Mechanisms of resistance to structurally diverse antiestrogens differ under premenopausal and postmenopausal conditions: Evidence from in Vitro breast cancer cell models', *Endocrinology*. Endocrinology, 150(5), pp. 2036–2045. doi: 10.1210/en.2008-1195.

Feng, D., Shaikh, A. S. and Wang, F. (2016) 'Recent Advance in Tumor-associated Carbohydrate Antigens (TACAs)-based Antitumor Vaccines', *ACS chemical biology*. ACS Chem Biol, 11(4), pp. 850–863. doi: 10.1021/ACSCHEMBIO.6B00084.

Filipe, V. *et al.* (2012) 'Immunogenicity of different stressed IgG monoclonal antibody

formulations in immune tolerant transgenic mice', *mAbs*. Taylor & Francis, 4(6), pp. 740–752. doi: 10.4161/MABS.22066.

FitzGerald, M. G. *et al.* (1998) 'Germline mutations in PTEN are an infrequent cause of genetic predisposition to breast cancer', *Oncogene*. Nature Publishing Group, 17(6), pp. 727–731. doi: 10.1038/sj.onc.1201984.

Fox, A. H. *et al.* (2018) 'Paraspeckles: Where Long Noncoding RNA Meets Phase Separation', *Trends in biochemical sciences*. Trends Biochem Sci, 43(2), pp. 124–135. doi: 10.1016/J.TIBS.2017.12.001.

Fragomeni, S. M., Sciallis, A. and Jeruss, J. S. (2018) 'Molecular Subtypes and Local-Regional Control of Breast Cancer', *Surgical Oncology Clinics of North America*. W.B. Saunders, pp. 95–120. doi: 10.1016/j.soc.2017.08.005.

Franklin, M. C. *et al.* (2004) 'Insights into ErbB signaling from the structure of the ErbB2-pertuzumab complex', *Cancer Cell*. Cancer Cell, 5(4), pp. 317–328. doi: 10.1016/S1535-6108(04)00083-2.

Frolov, I. *et al.* (1996) 'Alphavirus-based expression vectors: Strategies and applications', *Proceedings of the National Academy of Sciences of the United States of America*. National Academy of Sciences, 93(21), pp. 11371–11377. doi: 10.1073/PNAS.93.21.11371.

Fu, Y. and Li, H. (2016) 'Assessing Clinical Significance of Serum CA15-3 and Carcinoembryonic Antigen (CEA) Levels in Breast Cancer Patients: A Meta-Analysis', *Medical Science Monitor : International Medical Journal of Experimental and Clinical Research*. International Scientific Information, Inc., 22, p. 3154. doi: 10.12659/MSM.896563.

Fuster, M. M. and Esko, J. D. (2005) 'The sweet and sour of cancer: Glycans as novel therapeutic targets', *Nature Reviews Cancer*. Nat Rev Cancer, pp. 526–542. doi: 10.1038/nrc1649.

G, P. *et al.* (2011) 'Impact of body mass index on the efficacy of endocrine therapy in premenopausal patients with breast cancer: an analysis of the prospective ABCSG-12 trial', *Journal of clinical oncology : official journal of the American Society of Clinical Oncology*. J Clin Oncol, 29(19), pp. 2653–2659. doi: 10.1200/JCO.2010.33.2585.

Gabrilovich, D. I. and Nagaraj, S. (2009) 'Myeloid-derived suppressor cells as regulators of the immune system', *Nature Reviews Immunology*. Nat Rev Immunol, pp. 162–174. doi: 10.1038/nri2506.

Gadjeva, M., Takahashi, K. and Thiel, S. (2004) 'Mannan-binding lectin - A soluble pattern recognition molecule', in *Molecular Immunology*. Mol Immunol, pp. 113–121. doi: 10.1016/j.molimm.2004.03.015.

Gaidzik, N., Westerlind, U. and Kunz, H. (2013) 'The development of synthetic antitumour vaccines from mucin glycopeptide antigens', *Chemical Society reviews*. Chem Soc Rev, 42(10), pp. 4421–4442. doi: 10.1039/C3CS35470A.

Gallardo, A. *et al.* (2012) 'Increased signalling of EGFR and IGF1R, and deregulation of PTEN/PI3K/Akt pathway are related with trastuzumab resistance in HER2 breast carcinomas', *British journal of cancer*. Br J Cancer, 106(8), pp. 1367–1373. doi: 10.1038/BJC.2012.85.

Geijtenbeek, T. B. H. *et al.* (2000) 'Identification of DC-SIGN, a novel dendritic cell-specific ICAM-3 receptor that supports primary immune responses', *Cell*. Cell, 100(5), pp. 575–585. doi: 10.1016/S0092-8674(00)80693-5.

Geurtsen, J., Driessen, N. N. and Appelmelk, B. J. (2010) 'Mannose–fucose recognition by DC-

SIGN', *Microbial Glycobiology*. Elsevier, p. 673. doi: 10.1016/B978-0-12-374546-0.00034-1.

Giaquinto, A. N. *et al.* (2022) 'Breast Cancer Statistics, 2022', *CA: A Cancer Journal for Clinicians*. American Cancer Society, 72(6), pp. 524–541. doi: 10.3322/CAAC.21754.

Gilkes, D. M. *et al.* (2013) 'Collagen prolyl hydroxylases are essential for breast cancer metastasis', *Cancer Research*. Cancer Res, 73(11), pp. 3285–3296. doi: 10.1158/0008-5472.CAN-12-3963.

Gill, D. J. *et al.* (2010) 'Regulation of O-glycosylation through Golgi-to-ER relocation of initiation enzymes', *The Journal of cell biology*. J Cell Biol, 189(5), pp. 843–858. doi: 10.1083/JCB.201003055.

Ginsburg, O. *et al.* (2017) 'The global burden of women's cancers: a grand challenge in global health', *The Lancet*. Lancet Publishing Group, pp. 847–860. doi: 10.1016/S0140-6736(16)31392-7.

Goetze, A. M. *et al.* (2011) 'High-mannose glycans on the Fc region of therapeutic IgG antibodies increase serum clearance in humans', *Glycobiology*. Glycobiology, 21(7), pp. 949–959. doi: 10.1093/GLYCOB/CWR027.

Gogesch, P. *et al.* (2021) 'The Role of Fc Receptors on the Effectiveness of Therapeutic Monoclonal Antibodies', *International Journal of Molecular Sciences 2021, Vol. 22, Page 8947*. Multidisciplinary Digital Publishing Institute, 22(16), p. 8947. doi: 10.3390/IJMS22168947.

Goh, J. B. and Ng, S. K. (2017) 'Impact of host cell line choice on glycan profile', *https://doi.org/10.1080/07388551.2017.1416577*. Taylor & Francis, 38(6), pp. 851–867. doi: 10.1080/07388551.2017.1416577.

Goldenberg, D. M. *et al.* (2015) 'Trop-2 is a novel target for solid cancer therapy with sacituzumab govitecan (IMMU-132), an antibody-drug conjugate (ADC)', *Oncotarget*. Impact Journals, LLC, 6(26), p. 22496. doi: 10.18632/ONCOTARGET.4318.

Goldenberg, D. M., Stein, R. and Sharkey, R. M. (2018) 'The emergence of trophoblast cell-surface antigen 2 (TROP-2) as a novel cancer target', *Oncotarget*. Impact Journals, LLC, 9(48), p. 28989. doi: 10.18632/ONCOTARGET.25615.

Gonzalez, D. S. *et al.* (1999) 'Identification, expression, and characterization of a cDNA encoding human endoplasmic reticulum mannosidase I, the enzyme that catalyzes the first mannose trimming step in mammalian Asn-linked oligosaccharide biosynthesis', *The Journal of biological chemistry*. J Biol Chem, 274(30), pp. 21375–21386. doi: 10.1074/JBC.274.30.21375.

Gordon-Alonso, M. *et al.* (2017a) 'Galectin-3 captures interferon-gamma in the tumor matrix reducing chemokine gradient production and T-cell tumor infiltration', *Nature Communications*. Nature Publishing Group, 8(1), pp. 1–15. doi: 10.1038/s41467-017-00925-6.

Gordon-Alonso, M. *et al.* (2017b) 'Galectin-3 captures interferon-gamma in the tumor matrix reducing chemokine gradient production and T-cell tumor infiltration', *Nature Communications*. Nature Publishing Group, 8(1), pp. 1–15. doi: 10.1038/s41467-017-00925-6.

Gordon-Alonso, M., Demotte, N. and van der Bruggen, P. (2014) 'Sugars boost exhausted tumorinfiltrating lymphocytes by counteracting immunosuppressive activities of galectins', *OncoImmunology*. Landes Bioscience, 3(4). doi: 10.4161/onci.28783.

Gorman, M. J. *et al.* (2018) 'An immunocompetent mouse model of Zika virus infection', *Cell host & microbe*. NIH Public Access, 23(5), p. 672. doi: 10.1016/J.CHOM.2018.04.003.

Graus-Porta, D. *et al.* (1997) *ErbB-2, the preferred heterodimerization partner of all ErbB receptors, is a mediator of lateral signaling for interaction with polypeptide ligands. A direct con-of*

receptor dimers and stimulation of the intrinsic kinase, *The EMBO Journal*.

Gray, M. A. *et al.* (2020) 'Targeted glycan degradation potentiates the anticancer immune response in vivo', *Nature Chemical Biology*. Nature Publishing Group, pp. 1–9. doi: 10.1038/s41589-020-0622-x.

Greenwood, K. and Foster, J. (2017) 'Dinutuximab for the treatment of pediatric patients with neuroblastoma', *Drugs of today (Barcelona, Spain : 1998)*. Drugs Today (Barc), 53(9), pp. 469–476. doi: 10.1358/DOT.2017.53.9.2693023.

Groux-Degroote, S. *et al.* (2018) 'Gangliosides in Cancer Cell Signaling', in *Progress in Molecular Biology and Translational Science*. Elsevier B.V., pp. 197–227. doi: 10.1016/bs.pmbts.2017.10.003.

Gül, N. and Van Egmond, M. (2015) 'Antibody-Dependent Phagocytosis of Tumor Cells by Macrophages: A Potent Effector Mechanism of Monoclonal Antibody Therapy of Cancer', *Cancer research*. Cancer Res, 75(23), pp. 5008–5013. doi: 10.1158/0008-5472.CAN-15-1330.

Von Gunten, S. and Bochner, B. S. (2008) 'Basic and Clinical Immunology of Siglecs', *Annals of the New York Academy of Sciences*. NIH Public Access, 1143, p. 61. doi: 10.1196/ANNALS.1443.011.

Guo, H.-B. *et al.* (2002) 'Aberrant N-glycosylation of beta1 integrin causes reduced alpha5beta1 integrin clustering and stimulates cell migration - PubMed', *Cancer Research*, 62(23), pp. 6837–45. Available at: https://pubmed.ncbi.nlm.nih.gov/12460896/.

Guo, H. B. *et al.* (2009) 'Regulation of homotypic cell-cell adhesion by branched N-glycosylation of N-cadherin extracellular EC2 and EC3 domains', *Journal of Biological Chemistry*. JBC Papers in Press, 284(50), pp. 34986–34997. doi: 10.1074/jbc.M109.060806.

Guo, H. B. *et al.* (2010) 'Specific posttranslational modification regulates early events in mammary carcinoma formation', *Proceedings of the National Academy of Sciences of the United States of America*. National Academy of Sciences, 107(49), pp. 21116–21121. doi: 10.1073/PNAS.1013405107/SUPPL_FILE/PNAS.201013405SI.PDF.

Hall, J. M. *et al.* (1990) 'Linkage of early-onset familial breast cancer to chromosome 17q21', *Science*. American Association for the Advancement of Science, 250(4988), pp. 1684–1689. doi: 10.1126/science.2270482.

Hallouin, F. *et al.* (1999) 'Increased tumorigenicity of rat colon carcinoma cells after alpha1,2-fucosyltransferase FTA anti-sense cDNA transfection.', *International journal of cancer*, 80(4), pp. 606–11. doi: 10.1002/(sici)1097-0215(19990209)80:4<606::aid-ijc20>3.0.co;2-m.

Haltiwanger, R. S. and Lowe, J. B. (2004) 'Role of glycosylation in development', *Annual Review of Biochemistry*. Annu Rev Biochem, pp. 491–537. doi: 10.1146/annurev.biochem.73.011303.074043.

Hamilton, S. R. *et al.* (2005) 'Intact α-1,2-endomannosidase is a typical type II membrane protein', *Glycobiology*. Oxford Academic, 15(6), pp. 615–624. doi: 10.1093/GLYCOB/CWI045.

Hamorsky, K. T. *et al.* (2019) 'Engineering of a Lectibody Targeting High-Mannose-Type Glycans of the HIV Envelope', *Molecular Therapy*. Cell Press, 27(11), pp. 2038–2052. doi: 10.1016/J.YMTHE.2019.07.021.

Hanahan, D. and Robert A, W. (2017) 'Biological Hallmarks of cancer', *Holland-Frei cancer Medicine*. American Cancer Society, 01(April), pp. 1–10. doi: 10.1002/9781119000822.hfcm002.

Hanahan, D. and Weinberg, R. A. (2000) 'The hallmarks of cancer', *Cell*. Elsevier, pp. 57–70. doi: 10.1016/S0092-8674(00)81683-9.

Hanahan, D. and Weinberg, R. A. (2011) 'Hallmarks of cancer: The next generation', *Cell*. Elsevier, pp. 646–674. doi: 10.1016/j.cell.2011.02.013.

Handerson, T. *et al.* (2005) 'β1,6-Branched Oligosaccharides Are Increased in Lymph Node Metastases and Predict Poor Outcome in Breast Carcinoma', *Clinical Cancer Research*. American Association for Cancer Research, 11(8), pp. 2969–2973. doi: 10.1158/1078-0432.CCR-04-2211.

Hansel, T. T. *et al.* (2010) 'The safety and side effects of monoclonal antibodies', *Nature Reviews Drug Discovery 2010 9:4*. Nature Publishing Group, 9(4), pp. 325–338. doi: 10.1038/nrd3003.

Hara, R. I., Yoshioka, K. and Yokota, T. (2020) 'DNA-RNA Heteroduplex Oligonucleotide for Highly Efficient Gene Silencing', *Methods in molecular biology (Clifton, N.J.)*. Methods Mol Biol, 2176, pp. 113–119. doi: 10.1007/978-1-0716-0771-8_8.

Harbeck, N. *et al.* (2019) 'Breast cancer', *Nature Reviews Disease Primers*. Nature Publishing Group, 5(1). doi: 10.1038/s41572-019-0111-2.

Harding, F. A. *et al.* (2010) 'The immunogenicity of humanized and fully human antibodies: residual immunogenicity resides in the CDR regions', *mAbs*. MAbs, 2(3), pp. 256–265. doi: 10.4161/MABS.2.3.11641.

Harlin, H. *et al.* (2009) 'Chemokine expression in melanoma metastases associated with CD8 + T-CeII recruitment', *Cancer Research*. Cancer Res, 69(7), pp. 3077–3085. doi: 10.1158/0008-5472.CAN-08-2281.

Harpaz, N. and Schachter, H. (1980) *Control of Glycoprotein Synthesis PROCESSING OF ASPARAGINE-LINKED OLIGOSACCHARIDES BY ONE OR MORE RAT LIVER GOLGI α-D-MANNOSIDASES DEPENDENT ON THE PRIOR ACTION OF UDP-N-ACETYLGLUCOSAMINE:CI-D-MANNOSIDE P2-N-ACETYLGLUCOSAMINYLTRANSFERASE I* Rat liver Golgi membranes cannot remove any man-nosy1 residues from These results indicate that the physiological substrate for GlcNAc-transferase I is Mancvl + 3(Rlal"-* 6)ManPl*, *rHE JOURNAL OF BIOLOGICAL CHEMISTRY*.

Hassinen, A. *et al.* (2010) 'Golgi N-glycosyltransferases form both homo- and heterodimeric enzyme complexes in live cells', *Journal of Biological Chemistry*, 285(23), pp. 17771–17777. doi: 10.1074/jbc.M110.103184.

Hatano, K. *et al.* (2011) 'Expression of gangliosides, GD1a, and sialyl paragloboside is regulated by NF-κB-dependent transcriptional control of α2,3-sialyltransferase I, II, and VI in human castration-resistant prostate cancer cells', *International journal of cancer*. Int J Cancer, 129(8), pp. 1838–1847. doi: 10.1002/IJC.25860.

Häuselmann, I. and Borsig, L. (2014) 'Altered tumor-cell glycosylation promotes metastasis', *Frontiers in Oncology*. Frontiers Research Foundation. doi: 10.3389/fonc.2014.00028.

HB, M. *et al.* (2009) 'Adjuvant chemotherapy in older women with early-stage breast cancer', *The New England journal of medicine*. N Engl J Med, 360(20), pp. 2055–2065. doi: 10.1056/NEJMOA0810266.

Hegg, R. *et al.* (2012) 'Immunogenicity of Trastuzumab Intravenous and Subcutaneous Formulations in the Phase III Hannah Study', *Annals of Oncology*. Elsevier, 23, p. ix103. doi: 10.1016/S0923-7534(20)32835-0.

Heilbron, K. *et al.* (2021) 'Advancing drug discovery using the power of the human genome', *The Journal of Pathology*. John Wiley & Sons, Ltd, 254(4), pp. 418–429. doi: 10.1002/PATH.5664.

Heldin, P. *et al.* (2014) 'HAS2 and CD44 in breast tumorigenesis', in *Advances in Cancer Research*. Academic Press Inc., pp. 211–229. doi: 10.1016/B978-0-12-800092-2.00008-3.

Helm, J. *et al.* (2022) 'The Mouse N-Glycome Atlas – High-resolution N-glycan analysis of 23 mouse tissues', *bioRxiv*. Cold Spring Harbor Laboratory, p. 2022.09.19.508483. doi: 10.1101/2022.09.19.508483.

Henke, E., Nandigama, R. and Ergün, S. (2020) 'Extracellular Matrix in the Tumor Microenvironment and Its Impact on Cancer Therapy', *Frontiers in Molecular Biosciences*. Frontiers Media S.A., p. 160. doi: 10.3389/fmolb.2019.00160.

Hikke, M. C. and Pijlman, G. P. (2017) 'Veterinary Replicon Vaccines', *https://doi.org/10.1146/annurev-animal-031716-032328*. Annual Reviews , 5, pp. 89–109. doi: 10.1146/ANNUREV-ANIMAL-031716-032328.

Hills, D., Rowlinson-Busza, G. and Gullick, W. J. (1995) 'Specific targeting of a mutant, activated FGF receptor found in glioblastoma using a monoclonal antibody', *International journal of cancer*. Int J Cancer, 63(4), pp. 537–543. doi: 10.1002/IJC.2910630414.

Hirohashi, S. and Kanai, Y. (2003) 'Cell adhesion system and human cancer morphogenesis', *Cancer science*. Cancer Sci, 94(7), pp. 575–581. doi: 10.1111/J.1349-7006.2003.TB01485.X.

Ho, S. C. L. *et al.* (2012) 'IRES-mediated Tricistronic vectors for enhancing generation of high monoclonal antibody expressing CHO cell lines', *Journal of Biotechnology*. Elsevier, 157(1), pp. 130–139. doi: 10.1016/J.JBIOTEC.2011.09.023.

Hoadley, K. A. *et al.* (2014) *Breast cancer intrinsic subtypes*. Available at: https://www.nature.com/documents/nrclinonc_posters_breastcancer.pdf (Accessed: 22 September 2020).

Hoffmann, B. *et al.* (2020) 'The initial engraftment of tumor cells is critical for the future growth pattern: A mathematical study based on simulations and animal experiments', *BMC Cancer*. BioMed Central Ltd., 20(1), pp. 1–14. doi: 10.1186/S12885-020-07015-9/FIGURES/6.

Hofmeister, V., Schrama, D. and Becker, J. C. (2008) 'Anti-cancer therapies targeting the tumor stroma', *Cancer Immunology, Immunotherapy*. Springer, 57(1), pp. 1–17. doi: 10.1007/S00262-007-0365-5/FIGURES/3.

Holbro, T. *et al.* (2003) 'The ErbB2/ErbB3 heterodimer functions as an oncogenic unit: ErbB2 requires ErbB3 to drive breast tumor cell proliferation', *Proceedings of the National Academy of Sciences of the United States of America*. Proc Natl Acad Sci U S A, 100(15), pp. 8933–8938. doi: 10.1073/pnas.1537685100.

Holdbrooks, A. T., Britain, C. M. and Bellis, S. L. (2018) 'ST6Gal-I sialyltransferase promotes tumor necrosis factor (TNF)-mediated cancer cell survival via sialylation of the TNF receptor 1 (TNFR1) death receptor', *Journal of Biological Chemistry*. American Society for Biochemistry and Molecular Biology Inc., 293(5), pp. 1610–1622. doi: 10.1074/jbc.m117.801480.

Holmberg, L. A. and Sandmaier, B. M. (2004) 'Vaccination with Theratope (STn-KLH) as treatment for breast cancer', *Expert review of vaccines*. Expert Rev Vaccines, 3(6), pp. 655–663. doi: 10.1586/14760584.3.6.655.

Hossain, M. S., Ferdous, S. and Karim-Kos, H. E. (2014) 'Breast cancer in South Asia: A Bangladeshi perspective', *Cancer Epidemiology*. Elsevier Ltd, pp. 465–470. doi: 10.1016/j.canep.2014.08.004.

Hosseinahli, N. *et al.* (2018) 'Treating cancer with microRNA replacement therapy: A literature review', *Journal of Cellular Physiology*. John Wiley & Sons, Ltd, 233(8), pp. 5574–5588. doi: 10.1002/JCP.26514.

Hoy, S. M. (2018) 'Patisiran: First Global Approval', *Drugs*. Springer International Publishing,

78(15), pp. 1625–1631. doi: 10.1007/S40265-018-0983-6/METRICS.

Hu, B. *et al.* (2020) 'Blockade of DC-SIGN+ Tumor-associated macrophages reactivates antitumor immunity and improves immunotherapy in muscle-invasive bladder cancer', *Cancer Research*. American Association for Cancer Research Inc., 80(8), pp. 1707–1719. doi: 10.1158/0008-5472.CAN-19-2254/654225/AM/BLOCKADE-OF-DC-SIGN-TUMOR-ASSOCIATED-MACROPHAGES.

Huang, Y. L. *et al.* (2013) 'Carbohydrate-based vaccines with a glycolipid adjuvant for breast cancer', *Proceedings of the National Academy of Sciences of the United States of America*. Proc Natl Acad Sci U S A, 110(7), pp. 2517–2522. doi: 10.1073/PNAS.1222649110.

Hudis, C. A. (2007) 'Trastuzumab — Mechanism of Action and Use in Clinical Practice', *New England Journal of Medicine*. Massachussetts Medical Society, 357(1), pp. 39–51. doi: 10.1056/NEJMra043186.

Hudziak, R. M. *et al.* (1989) 'p185HER2 Monoclonal Antibody Has Antiproliferative Effects In Vitro and Sensitizes Human Breast Tumor Cells to Tumor Necrosis Factor', *Molecular and Cellular Biology*. Taylor & Francis, 9(3), pp. 1165–1172. doi: 10.1128/MCB.9.3.1165-1172.1989.

Hutsell, S. Q. *et al.* (2010) 'High affinity immobilization of proteins using biotin- and GST-based coupling strategies', *Methods in molecular biology (Clifton, N.J.)*. NIH Public Access, 627, p. 75. doi: 10.1007/978-1-60761-670-2_4.

Hwang, W. Y. K. and Foote, J. (2005) 'Immunogenicity of engineered antibodies', *Methods*. Academic Press, 36(1), pp. 3–10. doi: 10.1016/J.YMETH.2005.01.001.

Ishida, Y. (2020) 'PD-1: Its Discovery, Involvement in Cancer Immunotherapy, and Beyond', *Cells 2020, Vol. 9, Page 1376*. Multidisciplinary Digital Publishing Institute, 9(6), p. 1376. doi: 10.3390/CELLS9061376.

Itkonen, H. M. *et al.* (2013) 'O-GlcNAc transferase integrates metabolic pathways to regulate the stability of c-MYC in human prostate cancer cells', *Cancer Research*. American Association for Cancer Research, 73(16), pp. 5277–5287. doi: 10.1158/0008-5472.CAN-13-0549.

JA, G. *et al.* (2009) 'Glycomic profiling of invasive and non-invasive breast cancer cells', *Glycoconjugate journal*. Glycoconj J, 26(2), pp. 117–131. doi: 10.1007/S10719-008-9170-4.

Jefferis, Roy (2009) 'Glycosylation as a strategy to improve antibody-based therapeutics', *Nature Reviews Drug Discovery*, pp. 226–234. doi: 10.1038/nrd2804.

Jefferis, Royston (2009) 'Recombinant antibody therapeutics: the impact of glycosylation on mechanisms of action', *Trends in Pharmacological Sciences*. Elsevier Current Trends, 30(7), pp. 356–362. doi: 10.1016/J.TIPS.2009.04.007.

Johns, T. G. *et al.* (2005) 'The antitumor monoclonal antibody 806 recognizes a high-mannose form of the EGF receptor that reaches the cell surface when cells over-express the receptor', *The FASEB Journal*. Wiley, 19(7), pp. 1–18. doi: 10.1096/FJ.04-1766FJE.

Johnstone, C. N. *et al.* (2015a) 'Functional and molecular characterisation of EO771.LMB tumours, a new C57BL/6-mouse-derived model of spontaneously metastatic mammary cancer', *DMM Disease Models and Mechanisms*. Company of Biologists Ltd, 8(3), pp. 237–251. doi: 10.1242/dmm.017830.

Johnstone, C. N. *et al.* (2015b) 'Functional and molecular characterisation of EO771.LMB tumours, a new C57BL/6-mouse-derived model of spontaneously metastatic mammary cancer', *DMM Disease Models and Mechanisms*. Company of Biologists Ltd, 8(3), pp. 237–251. doi: 10.1242/dmm.017830.

Jones, P. T. *et al.* (1986) 'Replacing the complementarity-determining regions in a human antibody with those from a mouse', *Nature 1986 321:6069*. Nature Publishing Group, 321(6069), pp. 522–525. doi: 10.1038/321522a0.

Ju, T. *et al.* (2008) 'Human tumor antigens Tn and sialyl Tn arise from mutations in Cosmc', *Cancer Research*. Cancer Res, 68(6), pp. 1636–1646. doi: 10.1158/0008-5472.CAN-07-2345.

Julien, S. *et al.* (2011) 'Selectin ligand sialyl-Lewis x antigen drives metastasis of hormone-dependent breast cancers', *Cancer research*. Cancer Res, 71(24), pp. 7683–7693. doi: 10.1158/0008-5472.CAN-11-1139.

Kagan, E. *et al.* (2005) 'Comparison of antigen constructs and carrier molecules for augmenting the immunogenicity of the monosaccharide epithelial cancer antigen Tn', *Cancer immunology, immunotherapy : CII*. Cancer Immunol Immunother, 54(5), pp. 424–430. doi: 10.1007/S00262-004-0584-Y.

Kaku, H. *et al.* (1990) 'Carbohydrate-binding specificity of the daffodil (Narcissus pseudonarcissus) and amaryllis (Hippeastrum hybr.) bulb lectins', *Archives of biochemistry and biophysics*. Arch Biochem Biophys, 279(2), pp. 298–304. doi: 10.1016/0003-9861(90)90495-K.

Kalluri, R. and Weinberg, R. A. (2009) 'The basics of epithelial-mesenchymal transition', *Journal of Clinical Investigation*. American Society for Clinical Investigation, pp. 1420–1428. doi: 10.1172/JCI39104.

Kannagi, R. *et al.* (2004) *Carbohydrate-mediated cell adhesion in cancer metastasis and angiogenesis*, *Cancer Sci*.

Kannagi, R. *et al.* (2008) 'Current relevance of incomplete synthesis and neo-synthesis for cancer-associated alteration of carbohydrate determinants--Hakomori's concepts revisited', *Biochimica et biophysica acta*. Biochim Biophys Acta, 1780(3), pp. 525–531. doi: 10.1016/J.BBAGEN.2007.10.007.

Karsten, C. M. *et al.* (2012) 'Anti-inflammatory activity of IgG1 mediated by Fc galactosylation and association of FcγRIIB and dectin-1', *Nature medicine*. Nat Med, 18(9), pp. 1401–1406. doi: 10.1038/NM.2862.

Kavunja, H. W. *et al.* (2017) 'Delivery of foreign cytotoxic T lymphocyte epitopes to tumor tissues for effective antitumor immunotherapy against pre-established solid tumors in mice', *Cancer immunology, immunotherapy : CII*. Cancer Immunol Immunother, 66(4), pp. 451–460. doi: 10.1007/S00262-016-1948-9.

Keam, S. J. (2018) 'Inotersen: First Global Approval', *Drugs*. Drugs, 78(13), pp. 1371–1376. doi: 10.1007/S40265-018-0968-5.

Kellokumpu, S., Sormunen, R. and Kellokumpu, I. (2002) 'Abnormal glycosylation and altered Golgi structure in colorectal cancer: Dependence on intra-Golgi pH', *FEBS Letters*. FEBS Lett, 516(1–3), pp. 217–224. doi: 10.1016/S0014-5793(02)02535-8.

Kildegaard, H. F. *et al.* (2016) 'Glycoprofiling effects of media additives on IgG produced by CHO cells in fed-batch bioreactors', *Biotechnology and Bioengineering*. John Wiley & Sons, Ltd, 113(2), pp. 359–366. doi: 10.1002/BIT.25715.

Kim, S. H., Turnbull, J. and Guimond, S. (2011) 'Extracellular matrix and cell signalling: The dynamic cooperation of integrin, proteoglycan and growth factor receptor', *Journal of Endocrinology*. J Endocrinol, pp. 139–151. doi: 10.1530/JOE-10-0377.

Kim, Y. J. and Varki, A. (1997) *Perspectives on the significance of altered glycosylation of*

glycoproteins in cancer, *Glycoconjugate Journal*.

King, C. R., Kraus, M. H. and Aaronson, S. A. (1985) 'Amplification of a novel v-erbB-related gene in a human mammary carcinoma', *Science*. American Association for the Advancement of Science, 229(4717), pp. 974–976. doi: 10.1126/science.2992089.

Koboldt, D. C. *et al.* (2012a) 'Comprehensive molecular portraits of human breast tumours', *Nature*. Nature Publishing Group, 490(7418), pp. 61–70. doi: 10.1038/nature11412.

Koboldt, D. C. *et al.* (2012b) 'Comprehensive molecular portraits of human breast tumours', *Nature*. Nature Publishing Group, 490(7418), pp. 61–70. doi: 10.1038/nature11412.

Kohler, B. A. *et al.* (2015) 'Annual report to the nation on the status of cancer, 1975-2011, featuring incidence of breast cancer subtypes by race/ethnicity, poverty, and state', *Journal of the National Cancer Institute*. Oxford University Press, 107(6). doi: 10.1093/jnci/djv048.

Köhler, G. and Milstein, C. (1975) 'Continuous cultures of fused cells secreting antibody of predefined specificity', *Nature 1975 256:5517*. Nature Publishing Group, 256(5517), pp. 495–497. doi: 10.1038/256495a0.

Kölbl, A. C., Andergassen, U. and Jeschke, U. (2015) 'The role of glycosylation in breast cancer metastasis and cancer control', *Frontiers in Oncology*. Frontiers Media S.A., p. 1. doi: 10.3389/fonc.2015.00219.

Kolch, W. *et al.* (1993) 'Protein kinase Cα activates RAF-1 by direct phosphorylation', *Nature*. Nature, 364(6434), pp. 249–252. doi: 10.1038/364249a0.

Komdeur, F. L. *et al.* (2021) 'First-in-Human Phase I Clinical Trial of an SFV-Based RNA Replicon Cancer Vaccine against HPV-Induced Cancers', *Molecular Therapy*. Cell Press, 29(2), pp. 611–625. doi: 10.1016/J.YMTHE.2020.11.002.

Krapp, S. *et al.* (2003) 'Structural Analysis of Human IgG-Fc Glycoforms Reveals a Correlation Between Glycosylation and Structural Integrity', *Journal of Molecular Biology*. Academic Press, 325(5), pp. 979–989. doi: 10.1016/S0022-2836(02)01250-0.

Kufer, P., Lutterbüse, R. and Baeuerle, P. A. (2004) 'A revival of bispecific antibodies', *Trends in Biotechnology*. Elsevier, 22(5), pp. 238–244. doi: 10.1016/j.tibtech.2004.03.006.

Kumamoto, K. *et al.* (2001) 'Increased Expression of UDP-Galactose Transporter Messenger RNA in Human Colon Cancer Tissues and Its Implication in Synthesis of Thomsen-Friedenreich Antigen and Sialyl Lewis A/X Determinants 1', *CANCER RESEARCH*, 61, pp. 4620–4627. Available at: http://aacrjournals.org/cancerres/article-pdf/61/11/4620/2486365/4620.pdf?casa_token=B43PG01cRTIAAAAA:X04IdiVJZ3BZsGXIHkwTMvkG7fvIDmnzrEBAD977_MGZXoBceo0aDNgjHt7jBfz1LnTw04F0 (Accessed: 11 September 2023).

Kumar, R. *et al.* (1990) 'Cloning and expression of N-acetylglucosaminyltransferase I, the medial Golgi transferase that initiates complex N-linked carbohydrate formation', *Proceedings of the National Academy of Sciences of the United States of America*. National Academy of Sciences, 87(24), pp. 9948–9952. doi: 10.1073/pnas.87.24.9948.

Kunert, R., Rüker, F. and Katinger, H. (1998) 'Molecular characterization of five neutralizing anti-HIV type 1 antibodies: Identification of nonconventional D segments in the human monoclonal antibodies 2G12 and 2F5', *AIDS Research and Human Retroviruses*, 14(13), pp. 1115–1128. doi: 10.1089/aid.1998.14.1115.

Kuriakose, A., Chirmule, N. and Nair, P. (2016) 'Immunogenicity of Biotherapeutics: Causes and Association with Posttranslational Modifications', *Journal of Immunology Research*. Hindawi

Limited, 2016. doi: 10.1155/2016/1298473.

L, V. *et al.* (2019) 'An Orally Active Galectin-3 Antagonist Inhibits Lung Adenocarcinoma Growth and Augments Response to PD-L1 Blockade', *Cancer research*. Cancer Res, 79(7), pp. 1480–1492. doi: 10.1158/0008-5472.CAN-18-2244.

L, V. H. and K, R. (2019) 'How mRNA therapeutics are entering the monoclonal antibody field', *Journal of translational medicine*. J Transl Med, 17(1). doi: 10.1186/S12967-019-1804-8.

Labrijn, A. F. *et al.* (2019) 'Bispecific antibodies: a mechanistic review of the pipeline', *Nature reviews. Drug discovery*. Nat Rev Drug Discov, 18(8), pp. 585–608. doi: 10.1038/S41573-019-0028-1.

Landskron, G. *et al.* (2014) 'Chronic inflammation and cytokines in the tumor microenvironment', *Journal of Immunology Research*. Hindawi Publishing Corporation. doi: 10.1155/2014/149185.

Lau, K. S. and Dennis, J. W. (2008) 'REVIEW N-Glycans in cancer progression', *Glycobiology*, 18(10), pp. 750–760. doi: 10.1093/glycob/cwn071.

Lee, T., Teng, T. Z. J. and Shelat, V. G. (2020) 'Carbohydrate antigen 19-9 - tumor marker: Past, present, and future', *World journal of gastrointestinal surgery*. World J Gastrointest Surg, 12(12), pp. 468–490. doi: 10.4240/WJGS.V12.I12.468.

Legler, K., Rosprim, R., Karius, T., Eylmann, K., Rossberg, M., Wirtz, Ralph M, *et al.* (2018) 'Reduced mannosidase MAN1A1 expression leads to aberrant N-glycosylation and impaired survival in breast cancer', *British Journal of Cancer 2018 118:6*. Nature Publishing Group, 118(6), pp. 847–856. doi: 10.1038/bjc.2017.472.

Legler, K., Rosprim, R., Karius, T., Eylmann, K., Rossberg, M., Wirtz, Ralph M., *et al.* (2018) 'Reduced mannosidase MAN1A1 expression leads to aberrant N-glycosylation and impaired survival in breast cancer', *British journal of cancer*. Br J Cancer, 118(6), pp. 847–856. doi: 10.1038/BJC.2017.472.

Lehmann, B. D. *et al.* (2011) 'Identification of human triple-negative breast cancer subtypes and preclinical models for selection of targeted therapies', *Journal of Clinical Investigation*. J Clin Invest, 121(7), pp. 2750–2767. doi: 10.1172/JCI45014.

Leoz, M. L. A. de *et al.* (2011) 'High-Mannose Glycans are Elevated during Breast Cancer Progression', *Molecular & Cellular Proteomics : MCP*. American Society for Biochemistry and Molecular Biology, 10(1), p. M110.002717. doi: 10.1074/MCP.M110.002717.

Levental, K. R. *et al.* (2009) 'Matrix Crosslinking Forces Tumor Progression by Enhancing Integrin Signaling', *Cell*. Cell, 139(5), pp. 891–906. doi: 10.1016/j.cell.2009.10.027.

Levin, E. R. and Pietras, R. J. (2008) 'Estrogen receptors outside the nucleus in breast cancer', *Breast Cancer Research and Treatment*. Breast Cancer Res Treat, pp. 351–361. doi: 10.1007/s10549-007-9618-4.

Li, C. W. *et al.* (2016) 'Glycosylation and stabilization of programmed death ligand-1 suppresses T-cell activity', *Nature Communications 2016 7:1*. Nature Publishing Group, 7(1), pp. 1–11. doi: 10.1038/ncomms12632.

Li, C. W. *et al.* (2018) 'Eradication of Triple-Negative Breast Cancer Cells by Targeting Glycosylated PD-L1', *Cancer Cell*. Cell Press, 33(2), pp. 187-201.e10. doi: 10.1016/j.ccell.2018.01.009.

Li, Y. *et al.* (2019) 'In vitro evolution of enhanced RNA replicons for immunotherapy', *Scientific Reports*. Nature Publishing Group, 9(1). doi: 10.1038/S41598-019-43422-0.

Liang, J. xiao, Gao, W. and Cai, L. (2017) 'Fucosyltransferase VII promotes proliferation via the EGFR/AKT/mTOR pathway in A549 cells', *OncoTargets and therapy*. Onco Targets Ther, 10, pp. 3971–3978. doi: 10.2147/OTT.S140940.

Lim, W. *et al.* (2004) 'Relative frequency and morphology of cancers in STK11 mutation carriers', *Gastroenterology*. W.B. Saunders, 126(7), pp. 1788–1794. doi: 10.1053/j.gastro.2004.03.014.

Liu, M. *et al.* (2021) 'FUT7 Promotes the Epithelial-Mesenchymal Transition and Immune Infiltration in Bladder Urothelial Carcinoma', *Journal of inflammation research*. J Inflamm Res, 14, pp. 1069–1084. doi: 10.2147/JIR.S296597.

Liu, S. S. *et al.* (2020) 'Expression of Narcissus pseudonarcissus lectin and mannose receptor positive macrophages predict progression and prognosis of patients with gastric cancer', *Translational Cancer Research*. AME Publications, 9(10), p. 5979. doi: 10.21037/TCR-20-1459.

Liu, X. *et al.* (2013) 'Cell surface-specific N-glycan profiling in breast cancer', *PloS one*. PLoS One, 8(8). doi: 10.1371/JOURNAL.PONE.0072704.

Ljungberg, K. and Liljeström, P. (2015) 'Self-replicating alphavirus RNA vaccines', *http://dx.doi.org/10.1586/14760584.2015.965690*. Informa Healthcare, 14(2), pp. 177–194. doi: 10.1586/14760584.2015.965690.

Lloyd, K. O. *et al.* (1996) 'Comparison of O-linked carbohydrate chains in MUC-1 mucin from normal breast epithelial cell lines and breast carcinoma cell lines: Demonstration of simpler and fewer glycan chains in tumor cells', *Journal of Biological Chemistry*. J Biol Chem, 271(52), pp. 33325–33334. doi: 10.1074/jbc.271.52.33325.

Loi, S. *et al.* (2014) 'Tumor infiltrating lymphocytes are prognostic in triple negative breast cancer and predictive for trastuzumab benefit in early breast cancer: Results from the FinHER trial', *Annals of Oncology*. Oxford University Press, 25(8), pp. 1544–1550. doi: 10.1093/annonc/mdu112.

Loke, I. *et al.* (2016) 'Emerging roles of protein mannosylation in inflammation and infection', *Molecular Aspects of Medicine*. Pergamon, 51, pp. 31–55. doi: 10.1016/J.MAM.2016.04.004.

Lubas, W. A. and Spiro, R. G. (1988) 'Evaluation of the role of rat liver Golgi endo-alpha-D-mannosidase in processing N-linked oligosaccharides.', *Journal of Biological Chemistry*. Elsevier, 263(8), pp. 3990–3998. doi: 10.1016/S0021-9258(18)69024-6.

Lübbers, J., Rodríguez, E. and van Kooyk, Y. (2018) 'Modulation of Immune Tolerance via Siglec-Sialic Acid Interactions', *Frontiers in immunology*. NLM (Medline), p. 2807. doi: 10.3389/fimmu.2018.02807.

Lundstrom, K. (2020) 'Self-Amplifying RNA Viruses as RNA Vaccines', *International Journal of Molecular Sciences 2020, Vol. 21, Page 5130*. Multidisciplinary Digital Publishing Institute, 21(14), p. 5130. doi: 10.3390/IJMS21145130.

Lundstrom, K. (2021) 'Self-Replicating RNA Viruses for Vaccine Development against Infectious Diseases and Cancer', *Vaccines 2021, Vol. 9, Page 1187*. Multidisciplinary Digital Publishing Institute, 9(10), p. 1187. doi: 10.3390/VACCINES9101187.

Mahmoud, S. M. A. *et al.* (2012) 'The prognostic significance of B lymphocytes in invasive carcinoma of the breast', *Breast Cancer Research and Treatment*. Breast Cancer Res Treat, 132(2), pp. 545–553. doi: 10.1007/s10549-011-1620-1.

Mammoto, T. *et al.* (2013) 'Role of collagen matrix in tumor angiogenesis and glioblastoma multiforme progression', *American Journal of Pathology*. Am J Pathol, 183(4), pp. 1293–1305. doi: 10.1016/j.ajpath.2013.06.026.

MARIAMPILLAI, A. I. *et al.* (2017) 'Cancer Antigen 72-4 for the Monitoring of Advanced Tumors of the Gastrointestinal Tract, Lung, Breast and Ovaries', *Anticancer Research*, 37(7).

Mariño, K. V. *et al.* (2023) 'Targeting galectin-driven regulatory circuits in cancer and fibrosis', *Nature Reviews Drug Discovery 2023 22:4*. Nature Publishing Group, 22(4), pp. 295–316. doi: 10.1038/s41573-023-00636-2.

Markowska, A. I., Jefferies, K. C. and Panjwani, N. (2011) 'Galectin-3 protein modulates cell surface expression and activation of vascular endothelial Growth factor receptor 2 in human endothelial cells', *Journal of Biological Chemistry*. J Biol Chem, 286(34), pp. 29913–29921. doi: 10.1074/jbc.M111.226423.

Martins, F. *et al.* (2019) 'Adverse effects of immune-checkpoint inhibitors: epidemiology, management and surveillance', *Nature Reviews Clinical Oncology 2019 16:9*. Nature Publishing Group, 16(9), pp. 563–580. doi: 10.1038/s41571-019-0218-0.

Marty, M. *et al.* (2005) 'Randomized phase II trial of the efficacy and safety of trastuzumab combined with docetaxel in patients with human epidermal growth factor receptor 2-positive metastatic breast cancer administered as first-line treatment: The M77001 study group', *Journal of Clinical Oncology*. American Society of Clinical Oncology, 23(19), pp. 4265–4274. doi: 10.1200/JCO.2005.04.173.

Matikas, A. *et al.* (2019) 'Prognostic implications of PD-L1 expression in breast cancer: Systematic review and meta-analysis of immunohistochemistry and pooled analysis of transcriptomic data', *Clinical Cancer Research*. American Association for Cancer Research Inc., 25(18), pp. 5717–5726. doi: 10.1158/1078-0432.CCR-19-1131/75408/AM/PROGNOSTIC-IMPLICATIONS-OF-PD-L1-EXPRESSION-IN.

Matoba, N. *et al.* (2010) 'HIV-1 Neutralization Profile and Plant-Based Recombinant Expression of Actinohivin, an Env Glycan-Specific Lectin Devoid of T-Cell Mitogenic Activity', *PLoS ONE*. PLOS, 5(6), p. 11143. doi: 10.1371/JOURNAL.PONE.0011143.

Matsushita, Y. *et al.* (1990) 'Sialyl-dimeric Lewis-X antigen expressed on mucin-like glycoproteins in colorectal cancer metastases.', *Laboratory investigation; a journal of technical methods and pathology*, 63(6), pp. 780–91. Available at: http://www.ncbi.nlm.nih.gov/pubmed/1979361 (Accessed: 30 March 2020).

Meany, D. L. and Chan, D. W. (2011) 'Aberrant glycosylation associated with enzymes as cancer biomarkers', *Clinical proteomics*. Clin Proteomics, 8(1). doi: 10.1186/1559-0275-8-7.

Medicines Agency, E. (2008) 'Committee for medicinal products for human use (CHMP) Guideline on development, production, characterisation and specification for monoclonal antibodies and related products Guideline on development, production, characterisation and specification for monoclonal antibodies and related products'. Available at: www.ema.europa.eu/contact (Accessed: 4 September 2023).

Meezan, E. *et al.* (1969) 'Comparative Studies on the Carbohydrate-Containing Membrane Components of Normal and Virus-Transformed Mouse Fibroblasts. II. Separation of Glycoproteins and Glycopeptides by Sephadex Chromatography', *Biochemistry*, 8(6), pp. 2518–2524. doi: 10.1021/bi00834a039.

Mendoza, L. *et al.* (1998) 'Mannose receptor-mediated endothelial cell activation contributes to B16 melanoma cell adhesion and metastasis in liver', *Journal of Cellular Physiology*, 174(3), pp. 322–330. doi: 10.1002/(SICI)1097-4652(199803)174:3<322::AID-JCP6>3.0.CO;2-Q.

Merlotti, A. *et al.* (2019) 'Aberrant fucosylation enables breast cancer clusterin to interact with dendritic cell-specific ICAM-grabbing non-integrin (DC-SIGN)',

https://doi.org/10.1080/2162402X.2019.1629257. Taylor & Francis, 8(9). doi: 10.1080/2162402X.2019.1629257.

Mettu, R., Chen, C. Y. and Wu, C. Y. (2020) 'Synthetic carbohydrate-based vaccines: challenges and opportunities', *Journal of Biomedical Science 2020 27:1*. BioMed Central, 27(1), pp. 1–22. doi: 10.1186/S12929-019-0591-0.

Meyer, S. *et al.* (2018) 'New insights in Type I and II CD20 antibody mechanisms-of-action with a panel of novel CD20 antibodies', *British Journal of Haematology*. John Wiley & Sons, Ltd, 180(6), pp. 808–820. doi: 10.1111/BJH.15132.

Milde-Langosch, K. *et al.* (2014) 'Prognostic relevance of glycosylation-associated genes in breast cancer', *Breast Cancer Research and Treatment*. Springer New York LLC, 145(2), pp. 295–305. doi: 10.1007/S10549-014-2949-Z/FIGURES/2.

Miles, D. W. *et al.* (1995) 'Expression of sialyl-Tn in gastric cancer: Correlation with known prognostic factors', *British Journal of Cancer*. Br J Cancer, 71(5), pp. 1074–1076. doi: 10.1038/bjc.1995.207.

Misago, M. *et al.* (1995) 'Molecular cloning and expression of cDNAs encoding human α-mannosidase II and a previously unrecognized α-mannosidase IIX isozyme', *Proceedings of the National Academy of Sciences of the United States of America*. National Academy of Sciences, 92(25), pp. 11766–11770. doi: 10.1073/pnas.92.25.11766.

Mittal, D. *et al.* (2014) 'New insights into cancer immunoediting and its three component phases-elimination, equilibrium and escape', *Current Opinion in Immunology*. NIH Public Access, pp. 16–25. doi: 10.1016/j.coi.2014.01.004.

Miyazaki, K. *et al.* (2004) 'Loss of disialyl Lewisa, the ligand for lymphocyte inhibitory receptor sialic acid-binding immunoglobulin-like lectin-7 (Siglec-7) associated with increased sialyl Lewisa expression on human colon cancers', *Cancer Research*. American Association for Cancer Research, 64(13), pp. 4498–4505. doi: 10.1158/0008-5472.CAN-03-3614.

Montero, A. J. *et al.* (2012) 'Bevacizumab in the Treatment of Metastatic Breast Cancer: Friend or Foe?', *Current Oncology Reports*. NIH Public Access, 14(1), p. 1. doi: 10.1007/S11912-011-0202-Z.

Moo, T.-A. *et al.* (2018) 'Overview of Breast Cancer Therapy', *PET clinics*. NIH Public Access, 13(3), p. 339. doi: 10.1016/J.CPET.2018.02.006.

Mora, J. (2018) *Anti-GD2 mAbs for the treatment of high-risk neuroblastoma - Hospital Healthcare EuropeHospital Healthcare Europe*. Available at: https://hospitalhealthcare.com/latest-issue-2018/anti-gd2-mabs-for-the-treatment-of-high-risk-neuroblastoma/ (Accessed: 15 September 2021).

Mørch, L. S. *et al.* (2017) 'Contemporary Hormonal Contraception and the Risk of Breast Cancer', *New England Journal of Medicine*. Massachussetts Medical Society, 377(23), pp. 2228–2239. doi: 10.1056/NEJMoa1700732.

Moremen, K. W. and Nairn, A. V. (2014) 'Mannosidase, alpha, class 1 (MAN1A1 (Golgi alpha-mannnosidase IA), Man1A2 (Golgi alpha-mannosidase IB), MAN1B1(ER alpha-mannosidase I), MAN1C1 (Golgi alpha-mannosidase IC))', *Handbook of Glycosyltransferases and Related Genes, Second Edition*. Springer Japan, 2(1), pp. 1297–1312. doi: 10.1007/978-4-431-54240-7_84/FIGURES/2.

Morrison, S. L. *et al.* (1984) 'Chimeric human antibody molecules: mouse antigen-binding domains with human constant region domains.', *Proceedings of the National Academy of Sciences*. Proceedings of the National Academy of Sciences, 81(21), pp. 6851–6855. doi:

10.1073/PNAS.81.21.6851.

Movahedi, K. *et al.* (2010) 'Different tumor microenvironments contain functionally distinct subsets of macrophages derived from Ly6C(high) monocytes', *Cancer Research*. American Association for Cancer Research, 70(14), pp. 5728–5739. doi: 10.1158/0008-5472.CAN-09-4672/656065/P/DIFFERENT-TUMOR-MICROENVIRONMENTS-CONTAIN.

Muhammed, Y. (2020) 'The Best IgG Subclass for the Development of Therapeutic Monoclonal Antibody Drugs and their Commercial Production: A Review', *Immunome Research*. Longdom Publishing S.L, 16(1), pp. 1–12. doi: 10.35248/1745-7580.20.16.173.

Munkley, J. and Elliott, D. J. (2016) 'Hallmarks of glycosylation in cancer', *Oncotarget*. Impact Journals LLC, 7(23), pp. 35478–35489. doi: 10.18632/oncotarget.8155.

Murray, T. V. *et al.* (2021) 'An efficient system for bioconjugation based on a widely applicable engineered O-glycosylation tag: Short title: Controlled bioconjugation via O-glycan engineering', *mAbs*. Taylor & Francis, 13(1). doi: 10.1080/19420862.2021.1992068.

N, D. *et al.* (2014) 'A short treatment with galactomannan GM-CT-01 corrects the functions of freshly isolated human tumor-infiltrating lymphocytes', *Clinical cancer research : an official journal of the American Association for Cancer Research*. Clin Cancer Res, 20(7), pp. 1823–1833. doi: 10.1158/1078-0432.CCR-13-2459.

Nabi, I. R., Shankar, J. and Dennis, J. W. (2015) 'The galectin lattice at a glance', *Journal of Cell Science*. Company of Biologists Ltd, 128(13), pp. 2213–2219. doi: 10.1242/JCS.151159/259231/AM/THE-GALECTIN-LATTICE-AT-A-GLANCE.

Nagarajan, D. and McArdle, S. E. B. (2018) 'Immune landscape of breast cancers', *Biomedicines*. MDPI AG. doi: 10.3390/biomedicines6010020.

Nahta, R. and Esteva, F. J. (2006) 'Herceptin: mechanisms of action and resistance', *Cancer Letters*. Elsevier, 232(2), pp. 123–138. doi: 10.1016/J.CANLET.2005.01.041.

NIH (2018) *A New Agent GM-CT-01 in Combination With 5-FU, Avastin and Leucovorin in Subjects With Colorectal Cancer - Full Text View - ClinicalTrials.gov*. Available at: https://clinicaltrials.gov/ct2/show/NCT00388700?term=DAVFU-006&draw=2&rank=1 (Accessed: 16 September 2021).

NIH (2020a) *Female Breast Cancer Subtypes — Cancer Stat Facts*. Available at: https://seer.cancer.gov/statfacts/html/breast-subtypes.html (Accessed: 23 September 2020).

NIH (2020b) *National Cancer Institute Female Breast Cancer — Cancer Stat Facts., 2020*, *2020*. Available at: https://seer.cancer.gov/statfacts/html/breast.html (Accessed: 24 August 2020).

Nik-Zainal, S. *et al.* (2016) 'Landscape of somatic mutations in 560 breast cancer whole-genome sequences', *Nature*. Nature Publishing Group, 534(7605), pp. 47–54. doi: 10.1038/nature17676.

Nimmerjahn, F. and Ravetch, J. V. (2006) 'Fcγ receptors: Old friends and new family members', *Immunity*. Elsevier, 24(1), pp. 19–28. doi: 10.1016/j.immuni.2005.11.010.

Ning, S. *et al.* (2018) 'Clinical significance and diagnostic capacity of serum TK1, CEA, CA 19-9 and CA 72-4 levels in gastric and colorectal cancer patients', *Journal of Cancer*. Ivyspring International Publisher, 9(3), pp. 494–501. doi: 10.7150/JCA.21562.

NUCK, R. *et al.* (1993) 'Comparative study of high-mannose-type oligosaccharides in membrane glycoproteins of rat hepatocytes and different rat hepatoma cell lines', *European journal of biochemistry*. Eur J Biochem, 216(1), pp. 215–221. doi: 10.1111/J.1432-1033.1993.TB18135.X.

O'Cearbhaill, R. E. *et al.* (2016) 'A Phase I Study of Unimolecular Pentavalent (Globo-H-GM2-sTn-TF-Tn) Immunization of Patients with Epithelial Ovarian, Fallopian Tube, or Peritoneal Cancer in First Remission', *Cancers 2016, Vol. 8, Page 46*. Multidisciplinary Digital Publishing Institute, 8(4), p. 46. doi: 10.3390/CANCERS8040046.

O'Hanlon, D. M. *et al.* (1995) 'An evaluation of preoperative CA 15-3 measurement in primary breast carcinoma', *British journal of cancer*. Br J Cancer, 71(6), pp. 1288–1291. doi: 10.1038/BJC.1995.249.

O'Reilly, E. M. *et al.* (2018) 'HuMab-5B1 (MVT-5873), a mAb targeting sLea, in combination with first-line gemcitabine plus nab-paclitaxel (gem/nab-P) for patients with pancreatic cancer (PDAC) and other CA19-9 positive malignancies.', *https://doi.org/10.1200/JCO.2018.36.15_suppl.e16235*. American Society of Clinical Oncology, 36(15_suppl), pp. e16235–e16235. doi: 10.1200/JCO.2018.36.15_SUPPL.E16235.

Ober, R. J. *et al.* (2001) 'Differences in promiscuity for antibody–FcRn interactions across species: implications for therapeutic antibodies', *International Immunology*. Oxford Academic, 13(12), pp. 1551–1559. doi: 10.1093/INTIMM/13.12.1551.

Oh, Y. J. *et al.* (2022) 'Antitumor activity of a lectibody targeting cancer-associated high-mannose glycans', *Molecular Therapy*. Cell Press, 30(4), pp. 1523–1535. doi: 10.1016/J.YMTHE.2022.01.030.

Olden, K. *et al.* (1991) 'The potential importance of swainsonine in therapy for cancers and immunology', *Pharmacology and Therapeutics*. Pergamon, pp. 285–290. doi: 10.1016/0163-7258(91)90046-O.

Oliveira-Ferrer, L., Legler, K. and Milde-Langosch, K. (2017) 'Role of protein glycosylation in cancer metastasis', *Seminars in Cancer Biology*, 44, pp. 141–152. doi: 10.1016/j.semcancer.2017.03.002.

Pally, D. *et al.* (2021) 'Heterogeneity in 2,6-Linked Sialic Acids PotentiatesInvasion of Breast Cancer Epithelia', *ACS Central Science*. American Chemical Society, 7(1), p. 110. doi: 10.1021/ACSCENTSCI.0C00601.

Pancino, G. *et al.* (1991) 'Purification and characterisation of a breast-cancer-associated glycoprotein not expressed in normal breast and identified by monoclonal antibody 83D4', *British Journal of Cancer*, 63(3), pp. 390–398. doi: 10.1038/bjc.1991.91.

Park, D. D. *et al.* (2020) 'Metastasis of cholangiocarcinoma is promoted by extended high-mannose glycans', *Proceedings of the National Academy of Sciences*. National Academy of Sciences, 117(14), pp. 7633–7644. doi: 10.1073/PNAS.1916498117.

Parker, J. S. *et al.* (2009) 'Supervised Risk Predictor of Breast Cancer Based on Intrinsic Subtypes', *J Clin Oncol*, 27, pp. 1160–1167. doi: 10.1200/JCO.2008.18.1370.

Partridge, E. A. *et al.* (2004) 'Regulation of cytokine receptors by golgi N-glycan processing and endocytosis', *Science*. American Association for the Advancement of Science, 306(5693), pp. 120–124. doi: 10.1126/science.1102109.

Paszek, M. J. *et al.* (2014) 'The cancer glycocalyx mechanically primes integrin-mediated growth and survival', *Nature*. Nature Publishing Group, 511(7509), pp. 319–325. doi: 10.1038/nature13535.

Patnaik, S. K. *et al.* (2006) 'Complex N-glycans are the major ligands for galectin-1, -3, and -8 on Chinese hamster ovary cells', *Glycobiology*. Oxford Academic, 16(4), pp. 305–317. doi: 10.1093/glycob/cwj063.

Pavone, G. *et al.* (2021) 'A New Kid on the Block: Sacituzumab Govitecan for the Treatment of

Breast Cancer and Other Solid Tumors', *Molecules 2021, Vol. 26, Page 7294*. Multidisciplinary Digital Publishing Institute, 26(23), p. 7294. doi: 10.3390/MOLECULES26237294.

Pearce, O. M. T. and Läubli, H. (2015) 'Sialic acids in cancer biology and immunity', *Glycobiology*. Oxford University Press, 26(2), pp. 111–128. doi: 10.1093/glycob/cwv097.

Pedram, K. *et al.* (2023) 'Design of a mucin-selective protease for targeted degradation of cancer-associated mucins', *Nature Biotechnology 2023*. Nature Publishing Group, pp. 1–11. doi: 10.1038/s41587-023-01840-6.

Peng, L. *et al.* (2021) '843 Development and engineering of human sialidase for degradation of immunosuppressive sialoglycans to treat cancer', *Journal for ImmunoTherapy of Cancer*. BMJ Specialist Journals, 9(Suppl 2), pp. A884–A884. doi: 10.1136/JITC-2021-SITC2021.843.

Perdicchio, M. *et al.* (2016) 'Tumor sialylation impedes T cell mediated anti-tumor responses while promoting tumor associated-regulatory T cells', *Oncotarget*. Impact Journals LLC, 7(8), pp. 8771–8782. doi: 10.18632/oncotarget.6822.

Perou, C. M. *et al.* (2000) 'Molecular portraits of human breast tumours', *Nature*. Nature, 406(6797), pp. 747–752. doi: 10.1038/35021093.

Peschke, B. *et al.* (2017) 'Fc-Galactosylation of Human Immunoglobulin Gamma Isotypes Improves C1q Binding and Enhances Complement-Dependent Cytotoxicity', *Frontiers in immunology*. Front Immunol, 8(JUN). doi: 10.3389/FIMMU.2017.00646.

Peyrol, S. *et al.* (1997) 'Lysyl oxidase gene expression in the stromal reaction to in situ and invasive ductal breast carcinoma', *American Journal of Pathology*. American Society for Investigative Pathology, 150(2), pp. 497–507. Available at: /pmc/articles/PMC1858268/?report=abstract (Accessed: 22 September 2020).

Pharoah, P. D. P., Guilford, P. and Caldas, C. (2001) 'Incidence of gastric cancer and breast cancer in CDH1 (E-cadherin) mutation carriers from hereditary diffuse gastric cancer families', *Gastroenterology*. W.B. Saunders, 121(6), pp. 1348–1353. doi: 10.1053/gast.2001.29611.

Picon-Ruiz, M. *et al.* (2017) 'Obesity and adverse breast cancer risk and outcome: Mechanistic insights and strategies for intervention', *CA: A Cancer Journal for Clinicians*. Wiley, 67(5), pp. 378–397. doi: 10.3322/caac.21405.

Pinho, S. S. and Reis, C. A. (2015) 'Glycosylation in cancer: mechanisms and clinical implications', *Nature Reviews Cancer 2015 15:9*. Nature Publishing Group, 15(9), pp. 540–555. doi: 10.1038/nrc3982.

Pinkas-Kramarski, R. *et al.* (1996) 'Diversification of Neu differentiation factor and epidermal growth factor signaling by combinatorial receptor interactions.', *The EMBO Journal*. Wiley, 15(10), pp. 2452–2467. doi: 10.1002/j.1460-2075.1996.tb00603.x.

Polyak, K. (2007) 'Breast cancer: origins and evolution', *The Journal of clinical investigation*. J Clin Invest, 117(11), pp. 3155–3163. doi: 10.1172/JCI33295.

Potapenko, I. O. *et al.* (2015) 'Glycan-related gene expression signatures in breast cancer subtypes; relation to survival', *Molecular Oncology*. Elsevier, 9(4), pp. 861–876. doi: 10.1016/j.molonc.2014.12.013.

Presta, L. G. (2006) 'Engineering of therapeutic antibodies to minimize immunogenicity and optimize function', *Advanced Drug Delivery Reviews*. Elsevier, 58(5–6), pp. 640–656. doi: 10.1016/J.ADDR.2006.01.026.

Prigent, S. A. and Gullick, W. J. (1994) 'Identification of c-erbB-3 binding sites for phosphatidylinositol 3'-kinase and SHC using an EGF receptor/c-erbB-3 chimera.', *The EMBO Journal*. Wiley, 13(12), pp. 2831–2841. doi: 10.1002/j.1460-2075.1994.tb06577.x.

Provenzano, P. P. *et al.* (2008) 'Collagen density promotes mammary tumor initiation and progression', *BMC Medicine*. BMC Med, 6. doi: 10.1186/1741-7015-6-11.

Pucci, M. *et al.* (2022) 'Glycosyltransferases in Cancer: Prognostic Biomarkers of Survival in Patient Cohorts and Impact on Malignancy in Experimental Models', *Cancers*. MDPI, 14(9). doi: 10.3390/CANCERS14092128/S1.

Del Pup, L., Codacci-Pisanelli, G. and Peccatori, F. (2019) 'Breast cancer risk of hormonal contraception: Counselling considering new evidence', *Critical Reviews in Oncology/Hematology*. Elsevier Ireland Ltd, pp. 123–130. doi: 10.1016/j.critrevonc.2019.03.001.

Pushko, P. *et al.* (1997) 'Replicon-Helper Systems from Attenuated Venezuelan Equine Encephalitis Virus: Expression of Heterologous Genesin Vitroand Immunization against Heterologous Pathogensin Vivo', *Virology*. Academic Press, 239(2), pp. 389–401. doi: 10.1006/VIRO.1997.8878.

Pyzik, M. *et al.* (2015) 'FcRn: The Architect Behind the Immune and Nonimmune Functions of IgG and Albumin', *The Journal of Immunology*. American Association of Immunologists, 194(10), pp. 4595–4603. doi: 10.4049/JIMMUNOL.1403014.

Qiu, X. *et al.* (2018) 'Laminin is over expressed in breast cancer and facilitate cancer cell metastasis', *Journal of Cancer Research and Therapeutics*. Wolters Kluwer Medknow Publications, 14(12), pp. S1170–S1172. doi: 10.4103/0973-1482.191035.

R, S. *et al.* (2014) 'Association of N-glycosylation with breast carcinoma and systemic features using high-resolution quantitative UPLC', *Journal of proteome research*. J Proteome Res, 13(5), pp. 2314–2327. doi: 10.1021/PR401092Y.

Rabinovich, G. A. and Croci, D. O. (2012) 'Review Regulatory Circuits Mediated by Lectin-Glycan Interactions in Autoimmunity and Cancer'. doi: 10.1016/j.immuni.2012.03.004.

Ragupathi, G. *et al.* (2006) 'Preparation and Evaluation of Unimolecular Pentavalent and Hexavalent Antigenic Constructs Targeting Prostate and Breast Cancer: A Synthetic Route to Anticancer Vaccine Candidates'. doi: 10.1021/JA057244.

Raju, T. S. and Lang, S. E. (2014) 'Diversity in structure and functions of antibody sialylation in the Fc', *Current Opinion in Biotechnology*. Elsevier Current Trends, 30, pp. 147–152. doi: 10.1016/J.COPBIO.2014.06.014.

Ransohoff, J. D., Wei, Y. and Khavari, P. A. (2017) 'The functions and unique features of long intergenic non-coding RNA', *Nature Reviews Molecular Cell Biology 2017 19:3*. Nature Publishing Group, 19(3), pp. 143–157. doi: 10.1038/nrm.2017.104.

Reily, C. *et al.* (2019) 'Glycosylation in health and disease', *Nature Reviews Nephrology*. Nature Publishing Group, pp. 346–366. doi: 10.1038/s41581-019-0129-4.

Ren, Z. *et al.* (2017) 'The biosynthesis pathway of swainsonine, a new anticancer drug from three endophytic fungi', *Journal of Microbiology and Biotechnology*. Korean Society for Microbiolog and Biotechnology, pp. 1897–1906. doi: 10.4014/jmb.1709.09003.

Richichi, B. *et al.* (2014) 'A cancer therapeutic vaccine based on clustered Tn-antigen mimetics induces strong antibody-mediated protective immunity', *Angewandte Chemie (International ed. in English)*. Angew Chem Int Ed Engl, 53(44), pp. 11917–11920. doi: 10.1002/ANIE.201406897.

Ridgway, J. B. B., Presta, L. G. and Carter, P. (1996) '"Knobs-into-holes" engineering of antibody C(H)3 domains for heavy chain heterodimerization', *Protein Engineering*, 9(7), pp. 617–621. doi: 10.1093/protein/9.7.617.

Ring, A. and Dowsett, M. (2004) 'Mechanisms of tamoxifen resistance', *Endocrine-Related Cancer*. Endocr Relat Cancer, pp. 643–658. doi: 10.1677/erc.1.00776.

Romagnani, P. *et al.* (2004) 'CXC chemokines: The regulatory link between inflammation and angiogenesis', *Trends in Immunology*. Trends Immunol, pp. 201–209. doi: 10.1016/j.it.2004.02.006.

Rosenbaum, E. *et al.* (2022) 'A randomised phase II trial of a trivalent ganglioside vaccine targeting GM2, GD2 and GD3 combined with immunological adjuvant OPT-821 versus OPT-821 alone in metastatic sarcoma patients rendered disease-free by surgery', *European Journal of Cancer*. Elsevier Ltd, 176, pp. 155–163. doi: 10.1016/j.ejca.2022.09.003.

Ross, Jeffrey S *et al.* (2003) 'The Her-2/neu gene and protein in breast cancer 2003: biomarker and target of therapy.', *The oncologist*. AlphaMed Press, 8(4), pp. 307–25. doi: 10.1634/theoncologist.8-4-307.

Ross, Jeffrey S. *et al.* (2003) 'The HER-2/ *neu* Gene and Protein in Breast Cancer 2003: Biomarker and Target of Therapy', *The Oncologist*. Alphamed Press, 8(4), pp. 307–325. doi: 10.1634/theoncologist.8-4-307.

Rossow, L. *et al.* (2018) 'LOX-catalyzed collagen stabilization is a proximal cause for intrinsic resistance to chemotherapy', *Oncogene*. Nature Publishing Group, 37(36), pp. 4921–4940. doi: 10.1038/s41388-018-0320-2.

Rubinstein, N. *et al.* (2016) 'Targeted inhibition of galectin-1 gene expression in tumor cells results in heightened T cell-mediated rejection: A potential mechanism of tumor-immune privilege'. Available at: http://www.cancercell.org/cgi/ (Accessed: 5 September 2023).

Rugo, H. S. *et al.* (2020) 'TROPiCS-02: A Phase III study investigating sacituzumab govitecan in the treatment of HR+/HER2-metastatic breast cancer', *Future Oncology*. Future Medicine Ltd., 16(12), pp. 705–712. doi: 10.2217/FON-2020-0163/ASSET/IMAGES/LARGE/FIGURE3.JPEG.

Rutgeerts, P. *et al.* (2004) 'Comparison of Scheduled and Episodic Treatment Strategies of Infliximab in Crohn's Disease', *Gastroenterology*. W.B. Saunders, 126(2), pp. 402–413. doi: 10.1053/j.gastro.2003.11.014.

Saal, L. H. *et al.* (2005) 'PIK3CA mutations correlate with hormone receptors, node metastasis, and ERBB2, and are mutually exclusive with PTEN loss in human breast carcinoma', *Cancer Research*. American Association for Cancer Research, 65(7), pp. 2554–2559. doi: 10.1158/0008-5472-CAN-04-3913.

Sabnis, S. *et al.* (2018) 'A Novel Amino Lipid Series for mRNA Delivery: Improved Endosomal Escape and Sustained Pharmacology and Safety in Non-human Primates', *Molecular therapy : the journal of the American Society of Gene Therapy*. Mol Ther, 26(6), pp. 1509–1519. doi: 10.1016/J.YMTHE.2018.03.010.

Sahin, U. *et al.* (2017) 'Personalized RNA mutanome vaccines mobilize poly-specific therapeutic immunity against cancer', *Nature*. Nature, 547(7662), pp. 222–226. doi: 10.1038/NATURE23003.

Sahin, U., Karikó, K. and Türeci, Ö. (2014) 'mRNA-based therapeutics--developing a new class of drugs', *Nature reviews. Drug discovery*. Nat Rev Drug Discov, 13(10), pp. 759–780. doi: 10.1038/NRD4278.

Saldova, R. *et al.* (2017) 'Serum N-glycome alterations in breast cancer during multimodal treatment and follow-up', *Molecular oncology*. Mol Oncol, 11(10), pp. 1361–1379. doi: 10.1002/1878-0261.12105.

Schick, J., Ritchie, R. P. and Restini, C. (2021) 'Breast Cancer Therapeutics and Biomarkers: Past, Present, and Future Approaches':, *https://doi.org/10.1177/1178223421995854*. SAGE PublicationsSage UK: London, England, 15. doi: 10.1177/1178223421995854.

Schietinger, A. *et al.* (2006) 'A mutant chaperone converts a wild-type protein into a tumor-specific antigen', *Science (New York, N.Y.)*. Science, 314(5797), pp. 304–308. doi: 10.1126/SCIENCE.1129200.

Schmid, P. *et al.* (2022) 'Event-free Survival with Pembrolizumab in Early Triple-Negative Breast Cancer', *New England Journal of Medicine*. Massachusetts Medical Society, 386(6), pp. 556–567. doi: 10.1056/NEJMOA2112651/SUPPL_FILE/NEJMOA2112651_DATA-SHARING.PDF.

Van Schouwenburg, P. A., Rispens, T. and Wolbink, G. J. (2013) 'Immunogenicity of anti-TNF biologic therapies for rheumatoid arthritis', *Nature reviews. Rheumatology*. Nat Rev Rheumatol, 9(3), pp. 164–172. doi: 10.1038/NRRHEUM.2013.4.

Ščupáková, K. *et al.* (2021) 'Clinical importance of high-mannose, fucosylated, and complex N-glycans in breast cancer metastasis', *JCI Insight*. American Society for Clinical Investigation, 6(24). doi: 10.1172/JCI.INSIGHT.146945.

Seberger, P. J. and Chaney, W. G. (1999) 'Control of metastasis by Asn-linked, beta1-6 branched oligosaccharides in mouse mammary cancer cells', *Glycobiology*. Glycobiology, 9(3), pp. 235–241. doi: 10.1093/GLYCOB/9.3.235.

Seidman, A. *et al.* (2002) 'Cardiac dysfunction in the trastuzumab clinical trials experience', *Journal of Clinical Oncology*. American Society of Clinical Oncology, 20(5), pp. 1215–1221. doi: 10.1200/JCO.20.5.1215.

Sewell, R. *et al.* (2006) 'The ST6GalNAc-I sialyltransferase localizes throughout the golgi and is responsible for the synthesis of the tumor-associated sialyl-Tn O-glycan in human breast cancer', *Journal of Biological Chemistry*. J Biol Chem, 281(6), pp. 3586–3594. doi: 10.1074/jbc.M511826200.

Seyfried, T. N. and Huysentruyt, L. C. (2013) 'On the origin of cancer metastasis', *Critical Reviews in Oncogenesis*. NIH Public Access, 18(1–2), pp. 43–73. doi: 10.1615/CritRevOncog.v18.i1-2.40.

Sgroi, D. C. (2010) 'Preinvasive breast cancer', *Annual review of pathology*. Annu Rev Pathol, 5, pp. 193–221. doi: 10.1146/ANNUREV.PATHOL.4.110807.092306.

Shantha Raju, T. and Jordan, R. E. (2012) 'Galactosylation variations in marketed therapeutic antibodies', *mAbs*. Taylor & Francis, 4(3), p. 385. doi: 10.4161/MABS.19868.

Sharma, M. *et al.* (2022) 'A PHASE 1/2 DOSE ESCALATION/EXPANSION STUDY EVALUATING THE SAFETY, PHARMACOKINETICS, PHARMACODYNAMICS, AND ANTITUMOR ACTIVITY OF E-602, A BI-SIALIDASE FUSION PROTEIN, IN ADVANCED CANCER (GLIMMER-01)', *Journal for ImmunoTherapy of Cancer*, 10. doi: 10.1136/jitc-2022-SITC2022.0772.

Sheehan, K. C. F. *et al.* (2006) 'Blocking Monoclonal Antibodies Specific for Mouse IFN-α/β Receptor Subunit 1 (IFNAR-1) from Mice Immunized by In Vivo Hydrodynamic Transfection', *https://home.liebertpub.com/jir*. Mary Ann Liebert, Inc. 2 Madison Avenue Larchmont, NY 10538 USA , 26(11), pp. 804–819. doi: 10.1089/JIR.2006.26.804.

Shenkman, M. and Lederkremer, G. Z. (2019) 'Compartmentalization and Selective Tagging for

Disposal of Misfolded Glycoproteins', *Trends in Biochemical Sciences*. Elsevier, 44(10), pp. 827–836. doi: 10.1016/J.TIBS.2019.04.012.

Shimada, H. *et al.* (2014) 'Clinical significance of serum tumor markers for gastric cancer: a systematic review of literature by the Task Force of the Japanese Gastric Cancer Association', *Gastric cancer : official journal of the International Gastric Cancer Association and the Japanese Gastric Cancer Association*. Gastric Cancer, 17(1), pp. 26–33. doi: 10.1007/S10120-013-0259-5.

Shiovitz, S. and Korde, L. A. (2015) 'Genetics of breast cancer: A topic in evolution', *Annals of Oncology*. Oxford University Press, 26(7), pp. 1291–1299. doi: 10.1093/annonc/mdv022.

Shiraishi, N. *et al.* (2000) 'Identification and Characterization of Three Novel 1,3-N-Acetylglucosaminyltransferases Structurally Related to the 1,3-Galactosyltransferase Family*'. JBC Papers in Press. doi: 10.1074/jbc.M004800200.

Shriver, Z., Raguram, S. and Sasisekharan, R. (2004) 'Glycomics: A pathway to a class of new and improved therapeutics', *Nature Reviews Drug Discovery*. Nature Publishing Group, pp. 863–873. doi: 10.1038/nrd1521.

Sifniotis, V. *et al.* (2019) 'Current Advancements in Addressing Key Challenges of Therapeutic Antibody Design, Manufacture, and Formulation', *Antibodies 2019, Vol. 8, Page 36*. Multidisciplinary Digital Publishing Institute, 8(2), p. 36. doi: 10.3390/ANTIB8020036.

Slade, P. G. *et al.* (2016) 'Mannose metabolism in recombinant CHO cells and its effect on IgG glycosylation', *Biotechnology and Bioengineering*. John Wiley & Sons, Ltd, 113(7), pp. 1468–1480. doi: 10.1002/BIT.25924.

Slamon, D. *et al.* (1987) 'Human breast cancer: correlation of relapse and survival with amplification of the HER-2/neu oncogene', *Science*. American Association for the Advancement of Science (AAAS), 235(4785), pp. 177–182. doi: 10.1126/science.3798106.

Slamon, D. J. *et al.* (2001a) 'Use of Chemotherapy plus a Monoclonal Antibody against HER2 for Metastatic Breast Cancer That Overexpresses HER2', *New England Journal of Medicine*. Massachusetts Medical Society , 344(11), pp. 783–792. doi: 10.1056/NEJM200103153441101.

Slamon, D. J. *et al.* (2001b) 'Use of Chemotherapy plus a Monoclonal Antibody against HER2 for Metastatic Breast Cancer That Overexpresses HER2', *New England Journal of Medicine*. Massachusetts Medical Society , 344(11), pp. 783–792. doi: 10.1056/NEJM200103153441101.

Smaletz, O. *et al.* (2021) 'Phase II consolidation trial with anti-Lewis-Y monoclonal antibody (hu3S193) in platinum-sensitive ovarian cancer after a second remission', *International journal of gynecological cancer : official journal of the International Gynecological Cancer Society*. Int J Gynecol Cancer, 31(4), pp. 562–568. doi: 10.1136/IJGC-2020-002239.

Sobala, Ł. F. *et al.* (2020) 'Structure of human endo-α-1,2-mannosidase (MANEA), an antiviral host-glycosylation target', *Proceedings of the National Academy of Sciences*, 117(47). doi: 10.1073/pnas.2013620117.

Solinas, C. *et al.* (2017) 'Tumor-infiltrating lymphocytes in breast cancer according to tumor subtype: Current state of the art', *Breast*. Churchill Livingstone, pp. 142–150. doi: 10.1016/j.breast.2017.07.005.

Soltoff, S. P. *et al.* (1994) 'ErbB3 is involved in activation of phosphatidylinositol 3-kinase by epidermal growth factor.', *Molecular and Cellular Biology*. American Society for Microbiology, 14(6), pp. 3550–3558. doi: 10.1128/mcb.14.6.3550.

Sørlie, T. *et al.* (2001) 'Gene expression patterns of breast carcinomas distinguish tumor

subclasses with clinical implications', *Proceedings of the National Academy of Sciences of the United States of America*. Proc Natl Acad Sci U S A, 98(19), pp. 10869–10874. doi: 10.1073/pnas.191367098.

Spring, S. and Therapeutics, P. U. (2015) 'FDA Approves Unituxin ™ (dinutuximab) for the Treatment of Pediatric High'.

Springer, G. F. (1984) 'T and Tn, general carcinoma autoantigens', *Science*. American Association for the Advancement of Science, pp. 1198–1206. doi: 10.1126/science.6729450.

Staerz, U. D., Kanagawa, O. and Bevan, M. J. (1985) 'Hybrid antibodies can target sites for attack by T cells', *Nature 1985 314:6012*. Nature Publishing Group, 314(6012), pp. 628–631. doi: 10.1038/314628a0.

Stanczak, M. A. *et al.* (2018) 'Self-associated molecular patterns mediate cancer immune evasion by engaging Siglecs on T cells', *Journal of Clinical Investigation*. American Society for Clinical Investigation, 128(11), pp. 4912–4923. doi: 10.1172/JCI120612.

Stanfield, R. L. *et al.* (2015) 'Crystal structure of the HIV neutralizing antibody 2G12 in complex with a bacterial oligosaccharide analog of mammalian oligomannose', *Glycobiology*. Oxford University Press, 25(4), p. 412. doi: 10.1093/GLYCOB/CWU123.

Stephens, L. R. *et al.* (1997) 'The Gβγ/sensitivity of a PI3K is dependent upon a tightly associated adaptor, p101', *Cell*. Cell Press, 89(1), pp. 105–114. doi: 10.1016/S0092-8674(00)80187-7.

Stowell, S. R., Ju, T. and Cummings, R. D. (2015) 'Protein Glycosylation in Cancer', *Annual Review of Pathology: Mechanisms of Disease*. Annual Reviews, 10(1), pp. 473–510. doi: 10.1146/annurev-pathol-012414-040438.

Strauss, J. H. and Strauss, E. G. (1994) 'The alphaviruses: gene expression, replication, and evolution', *Microbiological Reviews*. American Society for Microbiology, 58(3), pp. 491–562. doi: 10.1128/MR.58.3.491-562.1994.

Sun, S. *et al.* (2016) 'Synthesis and Evaluation of Glycoconjugates Comprising N-Acyl-Modified Thomsen-Friedenreich Antigens as Anticancer Vaccines', *ChemMedChem*. ChemMedChem, 11(10), pp. 1090–1096. doi: 10.1002/CMDC.201600094.

Sun, Y. *et al.* (2020) 'B3GNT3, a Direct Target of miR-149-5p, Promotes Lung Cancer Development and Indicates Poor Prognosis of Lung Cancer', *Cancer management and research*. Cancer Manag Res, 12, pp. 2381–2391. doi: 10.2147/CMAR.S236565.

Suzuki, Y. *et al.* (2017) 'BMI change and abdominal circumference are risk factors for breast cancer, even in Asian women', *Breast Cancer Research and Treatment*. Springer New York LLC, 166(3), pp. 919–925. doi: 10.1007/s10549-017-4481-4.

Švajger, U. *et al.* (2010) 'C-type lectin DC-SIGN: An adhesion, signalling and antigen-uptake molecule that guides dendritic cells in immunity', *Cellular Signalling*. Elsevier, 22(10), p. 1397. doi: 10.1016/J.CELLSIG.2010.03.018.

Swann, J. B. and Smyth, M. J. (2007) 'Immune surveillance of tumors', *Journal of Clinical Investigation*. American Society for Clinical Investigation, pp. 1137–1146. doi: 10.1172/JCI31405.

Swindall, A. F. and Bellis, S. L. (2011) 'Sialylation of the Fas death receptor by St6Gal-I provides protection against Fas-mediated apoptosis in colon carcinoma cells', *Journal of Biological Chemistry*. J Biol Chem, 286(26), pp. 22982–22990. doi: 10.1074/jbc.M110.211375.

Szabo, R. and Skropeta, D. (2017) 'Advancement of Sialyltransferase Inhibitors: Therapeutic

Challenges and Opportunities', *Medicinal Research Reviews*. John Wiley and Sons Inc., 37(2), pp. 219–270. doi: 10.1002/med.21407.

T, S. *et al.* (2019) 'mRNA: A Novel Avenue to Antibody Therapy?', *Molecular therapy : the journal of the American Society of Gene Therapy*. Mol Ther, 27(4), pp. 773–784. doi: 10.1016/J.YMTHE.2019.03.002.

Takamizawa, S. *et al.* (2022) 'Diagnostic value of tumor markers in identifying favorable or unfavorable subsets in patients with cancer of unknown primary: a retrospective study', *BMC Cancer*. BioMed Central Ltd, 22(1), pp. 1–8. doi: 10.1186/S12885-022-09514-3/TABLES/4.

Tan, J. *et al.* (2008) 'The human UDP-N-Acetylglucosamine:α-6-d-Mannoside-β-1,2-N-Acetylglucosaminyltransferase II Gene (MGAT2)', *European Journal of Biochemistry*. John Wiley & Sons, Ltd, 231(2), pp. 317–328. doi: 10.1111/j.1432-1033.1995.0317e.x.

Tan, M. H. *et al.* (2012) 'Lifetime cancer risks in individuals with germline PTEN mutations', *Clinical Cancer Research*. American Association for Cancer Research, 18(2), pp. 400–407. doi: 10.1158/1078-0432.CCR-11-2283.

Tang, Y. *et al.* (2007) 'Regulation of antibody-dependent cellular cytotoxicity by IgG intrinsic and apparent affinity for target antigen', *Journal of immunology (Baltimore, Md. : 1950)*. J Immunol, 179(5), pp. 2815–2823. doi: 10.4049/JIMMUNOL.179.5.2815.

Taniguchi, N. and Kizuka, Y. (2015) 'Glycans and cancer: Role of N-Glycans in cancer biomarker, progression and metastasis, and therapeutics', in *Advances in Cancer Research*. Academic Press Inc., pp. 11–51. doi: 10.1016/bs.acr.2014.11.001.

Tao, M. and Morrison, S. (1989) 'Studies of aglycosylated chimeric mouse-human IgG. Role of carbohydrate in the structure and effector functions mediated by the human IgG constant region - PubMed', *Journal of immunology (Baltimore, Md. : 1950)*, 143(8), pp. 2595–2601. Available at: https://pubmed.ncbi.nlm.nih.gov/2507634/ (Accessed: 31 August 2023).

Tarhini, A. A. *et al.* (2017) 'Safety and efficacy of the antiganglioside GD3 antibody ecromeximab (KW2871) combined with high-dose interferon-α2b in patients with metastatic melanoma', *Melanoma research*. Melanoma Res, 27(4), pp. 342–350. doi: 10.1097/CMR.0000000000000353.

Tarin, D. (2011) 'Cell and tissue interactions in carcinogenesis and metastasis and their clinical significance', *Seminars in Cancer Biology*. Semin Cancer Biol, pp. 72–82. doi: 10.1016/j.semcancer.2010.12.006.

Taylor-Papadimitriou, J. *et al.* (1999) 'MUC1 and cancer', *Biochimica et Biophysica Acta - Molecular Basis of Disease*. Biochim Biophys Acta, pp. 301–313. doi: 10.1016/S0925-4439(99)00055-1.

Taylor, R. P. and Lindorfer, M. A. (2015) 'Fcγ-receptor-mediated trogocytosis impacts mAb-based therapies: historical precedence and recent developments', *Blood*. Blood, 125(5), pp. 762–766. doi: 10.1182/BLOOD-2014-10-569244.

Teeling, J. L. *et al.* (2004) 'Characterization of new human CD20 monoclonal antibodies with potent cytolytic activity against non-Hodgkin lymphomas', *Blood*. Blood, 104(6), pp. 1793–1800. doi: 10.1182/BLOOD-2004-01-0039.

Teige, I., Mårtensson, L. and Frendéus, B. L. (2019) 'Targeting the antibody checkpoints to enhance cancer immunotherapy-focus on FcγRIIb', *Frontiers in Immunology*. Frontiers Media S.A., 10(MAR), p. 440068. doi: 10.3389/FIMMU.2019.00481/BIBTEX.

Thess, A. *et al.* (2015) 'Sequence-engineered mRNA Without Chemical Nucleoside Modifications

Enables an Effective Protein Therapy in Large Animals', *Molecular Therapy*. Nature Publishing Group, 23(9), pp. 1456–1464. doi: 10.1038/mt.2015.103.

Thompson, J. A., Grunert, F. and Zimmermann, W. (1991) 'Carcinoembryonic antigen gene family: molecular biology and clinical perspectives', *Journal of clinical laboratory analysis*. J Clin Lab Anal, 5(5), pp. 344–366. doi: 10.1002/JCLA.1860050510.

Thran, M. *et al.* (2017) 'mRNA mediates passive vaccination against infectious agents, toxins, and tumors', *EMBO molecular medicine*. EMBO Mol Med, 9(10), pp. 1434–1447. doi: 10.15252/EMMM.201707678.

Tiwari, P. M. *et al.* (2018) 'Engineered mRNA-expressed antibodies prevent respiratory syncytial virus infection', *Nature communications*. Nat Commun, 9(1). doi: 10.1038/S41467-018-06508-3.

Tremblay, L. O., Dyke, N. C. and Herscovics, A. (1998) 'Molecular cloning, chromosomal mapping and tissue-specific expression of a novel human α1,2-mannosidase gene involved in N-glycan maturation', *Glycobiology*. Oxford Academic, 8(6), pp. 585–595. doi: 10.1093/GLYCOB/8.6.585.

Tremblay, L. O. and Herscovics, A. (1999) 'Cloning and expression of a specific human alpha 1,2-mannosidase that trims Man9GlcNAc2 to Man8GlcNAc2 isomer B during N-glycan biosynthesis', *Glycobiology*. Glycobiology, 9(10), pp. 1073–1078. doi: 10.1093/GLYCOB/9.10.1073.

Tsimberidou, A. M. *et al.* (2023) 'First-in-Human Study of OBI-999, a Globo H-Targeting Antibody-Drug Conjugate, in Patients With Advanced Solid Tumors', *JCO precision oncology*. JCO Precis Oncol, 7(7). doi: 10.1200/PO.22.00496.

Tsuchida, A. *et al.* (2003) 'Synthesis of disialyl Lewis a (Lea) structure in colon cancer cell lines by a sialyltransferase, ST6GalNAc VI, responsible for the synthesis of α-series gangliosides', *Journal of Biological Chemistry*. J Biol Chem, 278(25), pp. 22787–22794. doi: 10.1074/jbc.M211034200.

Tsuchiya, N. *et al.* (1989) 'Effects of galactose depletion from oligosaccharide chains on immunological activities of human IgG - PubMed', *The journal of rheumatology*, 16(3), pp. 285–290. Available at: https://pubmed.ncbi.nlm.nih.gov/2498512/ (Accessed: 1 September 2023).

Tu, C. F. *et al.* (2017) 'FUT8 promotes breast cancer cell invasiveness by remodeling TGF-β receptor core fucosylation', *Breast Cancer Research*. BioMed Central Ltd., 19(1). doi: 10.1186/s13058-017-0904-8.

Uehara, M. *et al.* (2008) 'Long-term prognostic study of carcinoembryonic antigen (CEA) and carbohydrate antigen 15-3 (CA 15-3) in breast cancer', *International journal of clinical oncology*. Int J Clin Oncol, 13(5), pp. 447–451. doi: 10.1007/S10147-008-0773-3.

UK, B. and RS, C. (2011) 'Serum CA 19-9 as a Biomarker for Pancreatic Cancer-A Comprehensive Review', *Indian journal of surgical oncology*. Indian J Surg Oncol, 2(2), pp. 88–100. doi: 10.1007/S13193-011-0042-1.

Vaisman-Mentesh, A. *et al.* (2020) 'The Molecular Mechanisms That Underlie the Immune Biology of Anti-drug Antibody Formation Following Treatment With Monoclonal Antibodies', *Frontiers in immunology*. Front Immunol, 11. doi: 10.3389/FIMMU.2020.01951.

Valabrega, G. *et al.* (2005) 'TGFα expression impairs Trastuzumab-induced HER2 downregulation', *Oncogene 2005 24:18*. Nature Publishing Group, 24(18), pp. 3002–3010. doi: 10.1038/sj.onc.1208478.

Valkenburg, K. C., De Groot, A. E. and Pienta, K. J. (2018) 'Targeting the tumour stroma to improve cancer therapy', *Nature reviews. Clinical oncology*. NIH Public Access, 15(6), p. 366. doi: 10.1038/S41571-018-0007-1.

Varki, A. (1993) *Biological roles of oligosaccharides: all of the theories are correct*. Available at: https://academic.oup.com/glycob/article/3/2/97/822943.

Varki, A. C. R. D. . E. J. D. . F. H. H. . S. P. . B. C. R. . H. G. W. . E. M. and E. (2015) *Essentials of Glycobiology, 3rd edition*, *Cold Spring Harbor (NY)*. Edited by A. Varki et al. Cold Spring Harbor (NY): Cold Spring Harbor Laboratory Press. Available at: http://www.ncbi.nlm.nih.gov/pubmed/27010055%0Ahttps://www.ncbi.nlm.nih.gov/books/NBK310274/ (Accessed: 19 September 2020).

Vasudevan, D. and Haltiwanger, R. S. (2014) 'Novel roles for O-linked glycans in protein folding', *Glycoconjugate Journal*. Kluwer Academic Publishers, 31(6), pp. 417–426. doi: 10.1007/s10719-014-9556-4.

Vaughan, T. J. *et al.* (1996) 'Human Antibodies with Sub-nanomolar Affinities Isolated from a Large Non-immunized Phage Display Library', *Nature Biotechnology 1996 14:3*. Nature Publishing Group, 14(3), pp. 309–314. doi: 10.1038/nbt0396-309.

Velmurugan, R. *et al.* (2016) 'Macrophage-mediated trogocytosis leads to death of antibody-opsonized tumor cells', *Molecular Cancer Therapeutics*. American Association for Cancer Research Inc., 15(8), pp. 1879–1889. doi: 10.1158/1535-7163.MCT-15-0335/85491/AM/MACROPHAGE-MEDIATED-TROGOCYTOSIS-LEADS-TO-DEATH-OF.

Vermi, W. *et al.* (2018) 'Tumor Biology and Immunology slan þ Monocytes and Macrophages Mediate CD20-Dependent B-cell Lymphoma Elimination via ADCC and ADCP = RTX + RTX + RTX CD16A CD16A CD20 CD20 CD32 CD64 ADCC ADCP slan + monocyte Lymphoma cell Lymphoma cell slan + macrophage slan + monocytes perform RTX-mediated antibody-dependent cell-mediated cytotoxicity (ADCC) via CD16A, while slan + macrophages exert RTX-mediated antibody-dependent cellular phagocytosis (ADCP) via CD16A, CD32 and CD64', *Cancer Research Cancer Res*, 78(13). doi: 10.1158/0008-5472.CAN-17-2344.

Vogel, C. L. *et al.* (2001) 'First-line Herceptin monotherapy in metastatic breast cancer', *Oncology*. Oncology, 61 Suppl 2(SUPPL. 2), pp. 37–42. doi: 10.1159/000055400.

Vreeker, G. C. M. *et al.* (2021) 'Serum N-glycan profiles differ for various breast cancer subtypes', *Glycoconjugate Journal*. Springer, 38(3), pp. 387–395. doi: 10.1007/s10719-021-10001-3.

Waldmann, H. (2019) 'Human monoclonal antibodies: The benefits of humanization', *Methods in Molecular Biology*. Humana Press Inc., 1904, pp. 1–10. doi: 10.1007/978-1-4939-8958-4_1/FIGURES/4.

Wang, F. *et al.* (2011) 'Inhibition of endoplasmic reticulum-associated degradation rescues native folding in loss of function protein misfolding diseases', *The Journal of biological chemistry*. J Biol Chem, 286(50), pp. 43454–43464. doi: 10.1074/JBC.M111.274332.

Wang, W. (2000) 'Lyophilization and development of solid protein pharmaceuticals', *International Journal of Pharmaceutics*, 203, pp. 1–60. Available at: www.elsevier.com/locate/ijpharm (Accessed: 6 September 2023).

Wang, X. *et al.* (1993) 'Chromosome mapping and organization of the human β-galactoside α2,6-sialyltransferase gene. Differential and cell-type specific usage of upstream exon sequences in B-lymphoblastoid cells', *Journal of Biological Chemistry*, 268(6), pp. 4355–4361.

Webster, C. I. *et al.* (2000) 'Kinetic analysis of high-mobility-group proteins HMG-1 and HMG-I/Y binding to cholesterol-tagged DNA on a supported lipid monolayer', *Nucleic acids research*. Nucleic Acids Res, 28(7), pp. 1618–1624. doi: 10.1093/NAR/28.7.1618.

Wei, M. M., Wang, Y. S. and Ye, X. S. (2018) 'Carbohydrate-based vaccines for oncotherapy',

Medicinal Research Reviews. John Wiley & Sons, Ltd, 38(3), pp. 1003–1026. doi: 10.1002/MED.21493.

Wen, D. *et al.* (2013) 'Discovery and investigation of O-xylosylation in engineered proteins containing a (GGGGS)n linker', *Analytical Chemistry*. American Chemical Society, 85(9), pp. 4805–4812. doi: 10.1021/AC400596G/ASSET/IMAGES/LARGE/AC-2013-00596G_0007.JPEG.

Wheelock, M. J. *et al.* (2008) 'Cadherin switching', *Journal of cell science*. J Cell Sci, 121(Pt 6), pp. 727–735. doi: 10.1242/JCS.000455.

Whiteside, T. L. (2008) 'The tumor microenvironment and its role in promoting tumor growth', *Oncogene*. NIH Public Access, pp. 5904–5912. doi: 10.1038/onc.2008.271.

WHO (2023) *Breast cancer*. Available at: https://www.who.int/news-room/fact-sheets/detail/breast-cancer (Accessed: 13 September 2023).

Williams, A. F. *et al.* (1993) 'Comparative analysis of the N-glycans of rat, mouse and human Thy-1. Site-specific oligosaccharide patterns of neural Thy-1, a member of the immunoglobulin superfamily', *Glycobiology*. Glycobiology, 3(4), pp. 339–348. doi: 10.1093/GLYCOB/3.4.339.

Williams, C. B., Yeh, E. S. and Soloff, A. C. (2016) 'Tumor-associated macrophages: unwitting accomplices in breast cancer malignancy', *npj Breast Cancer 2016 2:1*. Nature Publishing Group, 2(1), pp. 1–12. doi: 10.1038/npjbcancer.2015.25.

Williams, C. and Lin, C. Y. (2013) 'Oestrogen receptors in breast cancer: Basic mechanisms and clinical implications', *ecancermedicalscience*. ecancer Global Foundation, p. 370. doi: 10.3332/ecancer.2013.370.

Winter, G. *et al.* (2003) 'Making Antibodies by Phage Display Technology', *https://doi.org/10.1146/annurev.iy.12.040194.002245*. Annual Reviews 4139 El Camino Way, P.O. Box 10139, Palo Alto, CA 94303-0139, USA , 12, pp. 433–455. doi: 10.1146/ANNUREV.IY.12.040194.002245.

Winters, S. *et al.* (2017) 'Breast Cancer Epidemiology, Prevention, and Screening', in *Progress in Molecular Biology and Translational Science*. Elsevier B.V., pp. 1–32. doi: 10.1016/bs.pmbts.2017.07.002.

Wong, F. Y. *et al.* (2018) 'Age exerts a continuous effect in the outcomes of Asian breast cancer patients treated with breast-conserving therapy', *Cancer Communications*. BioMed Central Ltd., 38(1). doi: 10.1186/s40880-018-0310-3.

Wong, N. K. *et al.* (2003) 'Characterization of the oligosaccharides associated with the human ovarian tumor marker CA125', *Journal of Biological Chemistry*. J Biol Chem, 278(31), pp. 28619–28634. doi: 10.1074/jbc.M302741200.

Wood, E. R. *et al.* (2004) 'A unique structure for epidermal growth factor receptor bound to GW572016 (Lapatinib): relationships among protein conformation, inhibitor off-rate, and receptor activity in tumor cells', *Cancer research*. Cancer Res, 64(18), pp. 6652–6659. doi: 10.1158/0008-5472.CAN-04-1168.

Wooster, R. *et al.* (1994) 'Localization of a breast cancer susceptibility gene, BRCA2, to chromosome 13q12-13', *Science*. American Association for the Advancement of Science, 265(5181), pp. 2088–2090. doi: 10.1126/science.8091231.

Xiao, H. *et al.* (2016) 'Precision glycocalyx editing as a strategy for cancer immunotherapy', *Proceedings of the National Academy of Sciences*. National Academy of Sciences, 113(37), pp. 10304–10309. doi: 10.1073/PNAS.1608069113.

Xiong, G. *et al.* (2014) 'Prolyl-4-hydroxylase α subunit 2 promotes breast cancer progression and metastasis by regulating collagen deposition', *BMC Cancer*. BMC Cancer, 14(1). doi: 10.1186/1471-2407-14-1.

Xiong, G. *et al.* (2018) 'Collagen prolyl 4-hydroxylase 1 is essential for HIF-1α stabilization and TNBC chemoresistance', *Nature Communications*. Nature Publishing Group, 9(1). doi: 10.1038/s41467-018-06893-9.

Xu, G. *et al.* (2019) 'Unveiling the metabolic fate of monosaccharides in cell membranes with glycomic and glycoproteomic analyses', *Chemical Science*. The Royal Society of Chemistry, 10(29), pp. 6992–7002. doi: 10.1039/C9SC01653H.

Xu, M. *et al.* (2022) 'Targeting the tumor stroma for cancer therapy', *Molecular Cancer 2022 21:1*. BioMed Central, 21(1), pp. 1–38. doi: 10.1186/S12943-022-01670-1.

Yang, L. *et al.* (2008) 'Abrogation of TGFβ Signaling in Mammary Carcinomas Recruits Gr-1+CD11b+ Myeloid Cells that Promote Metastasis', *Cancer Cell*. Cancer Cell, 13(1), pp. 23–35. doi: 10.1016/j.ccr.2007.12.004.

Yanmei, J. *et al.* (2014) 'The Clinical Significance of DC-SIGN and DC-SIGNR, which Are Novel Markers Expressed in Human Colon Cancer', *PLOS ONE*. Public Library of Science, 9(12), p. e114748. doi: 10.1371/JOURNAL.PONE.0114748.

Yin, X. G. *et al.* (2017) 'IgG Antibody Response Elicited by a Fully Synthetic Two-Component Carbohydrate-Based Cancer Vaccine Candidate with α-Galactosylceramide as Built-in Adjuvant', *Organic letters*. Org Lett, 19(3), pp. 456–459. doi: 10.1021/ACS.ORGLETT.6B03591.

Yip, B. *et al.* (1997) 'Organization of the human β-1,2-N-acetylglucosaminyltransferase I gene (MGAT1), which controls complex and hybrid N-glycan synthesis', *Biochemical Journal*. Portland Press Ltd, 321(2), pp. 465–474. doi: 10.1042/bj3210465.

Yoshimura, M. *et al.* (1995) 'Suppression of lung metastasis of B16 mouse melanoma by N-acetylglucosaminyltransferase III gene transfection', *Proceedings of the National Academy of Sciences of the United States of America*. National Academy of Sciences, 92(19), pp. 8754–8758. doi: 10.1073/pnas.92.19.8754.

You, N. *et al.* (2012) 'Swainsonine inhibits growth and potentiates the cytotoxic effect of paclitaxel in hepatocellular carcinoma in vitro and in vivo', in *Oncology Reports*. Spandidos Publications, pp. 2091–2100. doi: 10.3892/or.2012.2035.

Yu, M. *et al.* (2012) 'Production, characterization, and pharmacokinetic properties of antibodies with N-linked mannose-5 glycans', *mAbs*. MAbs, 4(4), pp. 475–487. doi: 10.4161/MABS.20737.

Zhang, L. *et al.* (2019) 'Combined effects of glycosylation precursors and lactate on the glycoprofile of IgG produced by CHO cells', *Journal of Biotechnology*. Elsevier B.V., 289, pp. 71–79. doi: 10.1016/J.JBIOTEC.2018.11.004.

Zhang, R. *et al.* (2022) 'D-mannose facilitates immunotherapy and radiotherapy of triple-negative breast cancer via degradation of PD-L1', *Proceedings of the National Academy of Sciences of the United States of America*. National Academy of Sciences, 119(8), p. e2114851119. doi: 10.1073/PNAS.2114851119/SUPPL_FILE/PNAS.2114851119.SAPP.PDF.

Zhang, S. *et al.* (1997) 'Selection of tumor antigens as targets for immune attack using immunohistochemistry: II. Blood group-related antigens.', *International journal of cancer*, 73(1), pp. 50–6. doi: 10.1002/(sici)1097-0215(19970926)73:1<50::aid-ijc9>3.0.co;2-0.

Zhang, X. *et al.* (2014) 'Discovery of Specific Metastasis-Related N-Glycan Alterations in Epithelial

Ovarian Cancer Based on Quantitative Glycomics', *PLOS ONE*. Public Library of Science, 9(2), p. e87978. doi: 10.1371/JOURNAL.PONE.0087978.

Zheng, K., Bantog, C. and Bayer, R. (2011) 'The impact of glycosylation on monoclonal antibody conformation and stability', *mAbs*. Taylor & Francis, 3(6), p. 568. doi: 10.4161/MABS.3.6.17922.

Zhou, G. *et al.* (2001) 'Role of AMP-activated protein kinase in mechanism of metformin action', *The Journal of clinical investigation*. J Clin Invest, 108(8), pp. 1167–1174. doi: 10.1172/JCI13505.

Zhou, Q. *et al.* (2008) 'Development of a simple and rapid method for producing non-fucosylated oligomannose containing antibodies with increased effector function', *Biotechnology and bioengineering*. Biotechnol Bioeng, 99(3), pp. 652–665. doi: 10.1002/BIT.21598.

Zuber, C. *et al.* (2017) 'Golgi Apparatus Immunolocalization of Endomannosidase Suggests Post-Endoplasmic Reticulum Glucose Trimming: Implications for Quality Control', *https://doi.org/10.1091/mbc.11.12.4227*. The American Society for Cell Biology , 11(12), pp. 4227–4240. doi: 10.1091/MBC.11.12.4227.